OPTIMAL OPERATION AND CONTROL FOR A HYBRID HFO-DLCO GAS TURBINE POWER GENERATING PLANT

By

Frank Kulor

Thesis submitted in fulfilment of the requirements for the degree

Doctor of Engineering in Electrical Engineering

In the Department of Electrical, Electronic and Computer Engineering

Faculty of Engineering, Built Environment and Information Technology

Central University of Technology, Free State

Bloemfontein

Supervisor: Prof. E.D. Markus

Co-supervisor: Prof. K. Kusakana

May 2022

DECLARATION

I, FRANK KULOR, with student number _________, do hereby declare that this research project, which has been submitted to the Central University of Technology Free State, for the degree: Doctor of Engineering in Electrical Engineering, is my own independent work and complies with the Code of Academic Integrity, as well as other relevant policies, procedures, rules and regulations of the Central University of Technology, Free State. This project has not been submitted before by any person in fulfilment (or partial fulfilment) of the requirements for the attainment of any qualification.

Frank Kulor Date: 20 April 2022

DEDICATION

This thesis is dedicated to my late wife, Mrs Mary Akogo-Kulor, for her encouragement and desire for me to obtain a PhD while she was still alive. May her soul find redemption.

ACKNOWLEDGEMENT

I am highly grateful to God Jehovah for his unmerited favour, protection, and guidance in bringing me to this point in my life. Professor E.D. Markus, my primary supervisor, has been incredibly patient and insightful throughout my research. I would also like to express my profound appreciation to my co-supervisor, Professor K. Kusakana for his advice before the start and end of my thesis.

I would like to express my humble appreciation to my primary sponsor, Ho Technical University under the leadership of the Vice-Chancellor, Professor Ben Quarshie Honyenuga for his esteem demand for PhD qualification of Staff.

To my lovely wife, I appreciate your understanding and support throughout my time studying to achieve this dream.

I would be doing an unpardonable injustice if I did not mention the following: my illustrious colleagues at the HTU Electrical/Electronic Engineering Department for taking most of my loads.

My final and most heartfelt thanks go to all the authors of the various works of literature that I referenced in this project work; they are the primary reason for this work's success.

Finally, but certainly not the least I would like to express my gratitude to Harrison Paul Adjimah for his unwavering support and encouragement.

ABSTRACT

Gas turbines (GT) are a critical and reliable part of modern power generation plants. They are required in aircraft engine propulsion and power generation for industrial and commercial applications where they serve as the primary mechanical power source for large pumps and compressors. These turbines typically comprise of dual nozzle gas/Heavy fuel oil – diesel light crude oil (HFO-DLCO) generators. Therefore, optimisation and control of their operation is crucial in maximising their performance and cost scaling. Significant research has been conducted, and a plethora of analytical and experimental models have been developed, to better understand that gas turbine systems exhibit nonlinear behaviour and complex dynamics. However, the requirement for accurate and reliable models of gas turbines for a variety of hybrid fuel applications, as well as for cost savings while minimising environmental impact, has been a strong incentive for researchers to continue working in this fascinating field of study. This thesis developed an intelligent control system for a hybrid dual nozzle fuel power plant to increase its energy conversion efficiency and reliability. To accomplish this, the study developed and integrated a dual nozzle power plant model and an optimal cost-effective fuel transition management into a comprehensive control system. The hybrid plant model is a novel modelling technique that combines the algorithms of PID and Model Predictive Controllers to extract plant parameters and uncertainties from operational data and to significantly improve the model's accuracy for subsequent and future analysis and research. To optimise plant efficiency, the MPC state estimator is used to generate optimal set points and PID control provides the final loop control action. By integrating heuristic MPC and PID, technologies, a nonlinear optimal control operation framework is developed.

Finally, the individual control systems are integrated into a comprehensive system that manages the dual nozzle fuel GT power plant as a whole. The integrated control system enabled the power plant to operate at normal fuel switching providing a smooth well-regulated system during low fuel pressure. As a result, an intelligent autonomous control system that can perform high-quality plant-wide control is achieved, ensuring efficiency, cost-effectiveness, and reliability. As a result, the hybrid dual nozzle GT power plant achieves an intelligent autonomous control system, allowing for high-quality plant-wide

fuel transition management that ensures fuel flow accuracy, efficiency, and reliability in fuel switching operation.

NOMENCLATURE

SYMBOL	MEANING	UNIT
M_a	Air mass flow	Kg/s
M_f	Fuel mass flow	Kg/s
m_e	Exhaust gas mass flow	Kg/s
V_{cc}	Volume of combustion chamber	m^3
ρ_{cc}	Combustion chamber air density	Kg/m^3
P_{cc}	Combustion chamber pressure	Pa
T_{cc}	Combustion chamber temperature	K
K_e	Exhaust gas constant	J/Kgk
C_{pe}	Specific heat	J/Kgk
T_a	Air temperature	K
H_f	Fuel lower heating value	J/Kgk
H_e	Enthalpy	J/Kg
Ui	Internal enthalpy	J/Kg
T_{amb}	Ambient temperature	K
P_{amb}	Ambient pressure	Pa
M_{ao}	Compressor air flow	Kg/s
η_c	Compressor efficiency	
m_a^*	Desired airflow	Kg/s
m_f^*	Desired fuelflow	Kg/s
K_{igv}	Static gain of inlet guide van	
K_{at}	Static gain of fuel valve	
T_{igv}	Inlet guide van time constant	S
T_{at}	Fuel valve time constant	S
η_t	Turbine adiabatic efficiency	
P_{gt}	Gas turbine power output	W
T_{exm}	Exhaust temperature	K
$\overline{q}$	Flow rate	Kg/s
q	Orifice coefficient	
ρ	Fluid velocity	Kg/s^2

Δp	Change in pressure drop across orifice	Pa
V_v	Orifice flow velocity	m/s^2
q_v	Volume flow rate	Kg/s^2
A	Flow channel cross section	m^2
f_m	Mass flow rate	Kg/s
CL	Coefficient of liquid leg	
ΔP_L	Change in liquid pressure	Pa
ΔV_L	Liquid volume rate of change	Kg/s^2
Δh	Change in height	m
P_{Lout}	Liquid pressure output	Pa
P	Pressure	Pa
H	Height	m
G	Gravity of flow	
CV	Liquid fuel valve coefficient	
Li	Liquid in flow	
K	Constant gain	
P_{gout}	Gas out flow	
ΔP_g	Change in gas pressure	
M	Molecular weight	
Δu	Change in input signal $(Umax - Umin)$	
Kc	Controller gain	
ti, td	Integral and derivative time constant	
e	Error signal	
Pc	Controller out pressure	
P_{vmin}, P_{vmax}	Upper and lower limit of pneumatic pressure	
Pi	Initial Pressure	
KL	Liquid control valve constant	
R_1	Universal gas constant	
Ps	Parallel and series controller	
Kcp, s	Configuration	
L	Transport delay time	
Pu, Ku	Ultimate period and ultimate gain	

Za	Geometry of GC and GV constant
Zb	Liquid flow calculation constant
Zc	Mass gas flow constant
Zd	Gas flow rate constant
Ze	Effect of pressure on liquid constant
Zf	Effect of liquid on pressure constant
Zg	Effect of pressure on gas flow constant
KT	Transmitter gain
D	Compressibility factor
t_1	Pneumatic line time constant
t_2	Valve time constant
L	Length of pneumatic line
u	Manipulated variable
y	Process out variable
x	State variable
P	Sample time
λ	Identity matrix
A	State space matrix model
B	Input matrix model
C	Output matrix model
D	Direct feed matrix model
T	Transpose matrix
Jc	Cost function
r(pi)	Setpoint signal at a time
R	Diagonal matrix
V_w	Tuning vector
Nc, Np	Control and prediction horizon
G, φ	Pair of matrix used in prediction control
ωp	Process disturbance white noise
Iqxq	Identity matrix
Q	Expectation
P1, P2	Minimum and maximum prediction limit
αj	Weight sequence

$\overline{R}$	Future trajectory	
Cmpc	Feedback control gain for MPC	
(A, B, C, D)	State space realization matrix	
X (pi + P/pi)	Predicted state variable vector at time P was given current	
$\hat{x}$	State variable	
Cob	State observer	
X (pi + m/pi)	Observer gain	
R_s	State variable prediction at a future time (pi + m)	
ε	Setpoint signal vector	
r	White noise	
P1	Reference trajectory	
P2	Pressure	
PR	Pressure	
φ_c	Pressure ratio	
φ_n	Cold end compressor specific heat	
ΔT_o	Hot end compressor specific heat	
M_{apu}	Coefficient of temperature rise	
M_{fpu}	Air mass flow rate per unit	
μ	fuel mass flow rate per unit	
Q_o	Thermodynamic cycle constnat	
V	Steady state mass flow out	
A_1	Specific volume	Kg/s
A_2	Active area	m^2/Kg
C	Effective area	
HDGT	Specific heat capacitor of shield	
Zc	Heavy duty gas turbine	
Qc	Characteristic impedance of injection line	
Pp	Pump flow capacity	
β	Pressure in the pump chamber	
ρ	Fuel bulk modulus	
C	Fuel density of pump hydraulic	
L	Length of injection line	

V	Kinetic viscosity
F_g^P	Primary fuel availability
C_g^P	Primary fuel cost
F_g^A	Auxiliary fuel availability
C_g^A	Auxiliary fuel cost
m_f^x, m_a^x	Desired air and fuel mass
$\dot{m}e$	High temperature exhaust mass gas flow
C_{pe}	Exhaust gas specific heat
ECR	Equal concern relaxation
X_{Lq}	Liquid fuel state equation
U_{Lq}	Liquid fuel input variable
Y_{Lq}	Liquid fuel output variable
Xgg	State variable LNG gas line
Kc	Controller gain
e	Error signal
Ti	Integral time
Td	Derivative time

CONTENTS PAGE

DECLARATION ii

DEDICATION iii

ACKNOWLEDGEMENT iv

ABSTRACT v

NOMENCLATURE vii

CONTENTS PAGE xii

List of Tables xviii

List of Figures xix

CHAPTER ONE: INTRODUCTION 1

1.1 Background 1

1.2 Problem statement 3

1.3 Research aims and objectives 3

1.4 Methodology and research design 4

1.5 Contribution to knowledge 5

1.6 Research Questions 7

1.7 Delimitation 7

1.8 Publications during the study 7

1.9 Organization of the thesis 8

1.10 Summary 8

CHAPTER TWO: LITERATURE REVIEW 9

2.1 Introduction 9

2.2 Performance of Gas Turbine 10

2.3 Classification of Gas Turbine 12

2.4 Configuration of Gas Turbines 12

2.5 Gas Turbine Modelling 13

2.5.1 Type of Gas Turbine 13

2.5.2 Gas Turbine Modelling Methods 14

2.5.2.1 Models, Linear and Nonlinear 14

2.5.2.2 Deterministic and Stochastic Model 15

2.5.2.3 Dynamic and Static Model 15

2.5.2.4 Discrete and Continuous Model 15

2.5.3 GT Control System Type and Configuration 16
2.5.4 Gas Turbine Modelling Objective 17
2.5.4.1 Fuel Control System 17
2.5.4.2 Fuel Nozzle Control 18
2.5.4.3 Temperature Control 18
2.5.4.4 System Identification 18
2.5.4.5 System Optimisation and Control 18
2.5.4.6 Acceleration Control 19
2.6 Design and Configuration Analysis of Hybrid Systems 19
2.7 Architecture for a Hybrid Solar-Gas Turbine 19
2.8 Architecture of a Hybrid Fuel–Cell Gas Turbine 21
2.9 Architecture of a Dual-Fuel Gas Turbine Control 23
2.9.1 LPG Dual-Fuel Gas Turbine (LDFGT) 25
2.10 AC Gas Turbine Generator Design 25
2.10.1 GT System with a Simple Cycle 25
2.10.2 Combine GT Cycle System 26
2.11 Conceptual design of Gas Turbine Power Plant 27
2.12 Gas Turbine cycle design Numerical Optimization Methodology 27
2.13 Controller Design Difficulties 28
2.14 Control system of the Gas Turbine Power Plant 29
2.15 Fuel flexibility in Gas Turbines 30
2.16 Design and performance of dual nozzles 31
2.17 Gas Turbine Plant combustion technology and pollution control 33
2.18 Design and optimisation of controllers 34
2.19 Dynamic simulation of the Gas Turbine power generator 36
2.20 Advantages and disadvantages of the hybrid GT design 36
2.21 Summary 40
CHAPTER THREE: GAS TURBINE (GT) POWER PLANT MODELLING 41
3.1 Introduction 41
3.2 Gas Turbine approximate model 41
3.2.1 Compressor modeling 42
3.2.2 Modeling of air and fuel system 44
3.3 Modeling dual fuel supply line for the Gas Turbine Plant 47

3.3.1 Liquid mass phase flow 50
3.4 External fuel line control model for GT 51
3.4.1 Pneumatic actuator delay line 52
3.4.2 Pneumatic control valve 53
3.5 Liquid fuel control loop of GT 53
3.6 Gas fuel control loop of GT 54
3.7 GT dual nozzle fuel control strategy and dynamic simulation 55
3.7.1 GT fuel line simulator development 55
3.7.2 Formulation linear models 57
3.7.3 Integrating liquid and gas control loop of GT 60
3.7.4 Mathematical evaluation of GT fuel supply model 62
3.7.4.1 Fuel tank level Control Valve 63
3.7.4.2 LNG Gas Control Valve Control Loop 66
3.7.4.3 Integrated GT LCV and LNGCV Control 68
3.8 Modelling of external fuel tank system without controller and onboard coupled 70
3.9 Simulation model for the dynamic GT fuel control 76
3.9.1 Valve positioner and fuel lag system 80
3.9.2 Time delays and discharge lag 82
3.9.3 Temperature measurement system 82
3.9.4 Turbine efficiency 83
3.9.5 Fuel system block 86
3.9.6 System discharge and time delay 87
3.9.7 Temperature measurement block 88
3.10 Simulation of GT internal Fuel System without Controller and external coupling 89
3.10.1 GT with liquid fuel line system without controller and external coupled 90
3.10.2 GT with NLG line system without controller and external coupled 92
3.11 GT LNG and Liquid fuel integrated with Combustion chamber flow 94
3.12 GT Liquid fuel line integrated with external tank fuel flow 96
3.13 GT LNG line integrated with external tank LNG flow 98
3.14 Integrated GT with Liquid fuel and LNG external tank flow 100
3.15 Summary 102

CHAPTER FOUR: DYNAMIC MODELLING AND DEVELOPMENT OF GT DUAL NOZZLE SYSTEM 103
4.1 Introduction 103
4.2 Liquid Nozzle Pump Line System 103
4.3 Nozzle Injection modelling system 105
4.4 Nozzle modelling design assumptions 106
4.4.1 Mathematical Modelling of Nozzle Pressure System 106
4.5 Nozzle Liquid Phase Delivery 110
4.5.1 Operation and Design of Dual Nozzle Fuel Engine 113
4.5.1.1 Modification of traditional Diesel Engine as Dual Fuel Nozzle 114
4.5.2 LPG–Diesel Dual Fuel Engine Combustion Process 114
4.6 Dual Fuel Gas-Phase Flow Modelling 117
4.7 Dual nozzle Simulink control modelling 118
4.7.1 Simulink design of automatic fuel selector pressure switch 118
4.7.2 Dual nozzle integration GT fuel combustion system 120
4.8 Summary 121
CHAPTER FIVE: DESIGN OF GAS TURBINE DUAL FUEL CONTROL LOOPS USING PID 122
5.1 Introduction 122
5.2 PID Model for the GT fuel control system 122
5.3 GT dual fuel system configuration 123
5.4 GT liquid fuel system 123
5.4.1 External liquid fuel tank 123
5.4.2 GT onboard fuel system 124
5.4.2.1 Acceleration Control 125
5.5 Simulation of GT liquid fuel system 126
5.5.1 GT liquid fuel model without PID Controller 126
5.5.2 GT liquid fuel model with PID Controller 127
5.6 GT LNG gas system 130
5.7 PID Controller Design for dual nozzle fuel control system 133
5.8 Optimisation of the PID Controller for Dual Nozzle GT Fuel Supply 136
5.8.1 Optimisation objective formulation 137
5.9 Summary 140
CHAPTER SIX: MODEL PREDICTIVE CONTROL 141

6.1 Introduction 141
6.2 GT Process Model Design 142
6.3 State Space Model with Embedded Integrator (SSMEI) 142
6.3.1 Single –Input and Single–Output (SISO) System 142
6.4 Prediction Control with one Optimal Window 144
6.4.1 Prediction of State and Output Variable 144
6.5 Optimisation Formulation 146
6.5.1 Cost function 146
6.6 Concept of Receding Horizon 148
6.6.1 Concept of Closed Loop Control (CCLC) 148
6.7 Multiple input and multiple output (MIMO) system prediction control 149
6.7.1 Model Development for MIMO 149
6.7.2 Principles of Observability and Controllability 151
6.7.3 Applying Prediction Control for GT MIMO dual fuel System 151
6.8 GT State Prediction Control Estimation 152
6.9 Tuning Model Predictive Controller 155
6.10 Gas Turbine Approximate Model 155
6.11 MPC Controller Design for a hybrid gas turbine system 157
6.12 Implementing MPC Controller 161
6.12.1 Model Horizon 161
6.12.2 Prediction Horizon 161
6.12.3 Weight Specification 161
6.12.4 Control Horizon 162
6.13 MPC Simulink Model Structure 162
6.14 MPC-PID controller design for dual fuel system 162
6.15 Summary 166
CHAPTER SEVEN: DISCUSSION OF RESULTS 167
7.1 Introduction 167
7.2 Results of external liquid fuel supply system modelling and simulation 168
7.3 Results of external Gas fuel supply system modelling and simulation 169
7.4 Dual nozzle modelling and simulation results 171
7.5 Results of GT dual nozzle fuel flow analysis with PID Controller 172

7.6 Result of PID controller design simulation of a combined dual fuel supply system 173
7.7 Results of PID-MPC Based Dual Fuel GT Control 175
7.8 Results of MPC State Space (SS) Values 178
7.8.1 MPC Liquid Model Plant 178
7.8.2 MPC LNG Model Plant 180
7.9 Tuning MPC Controller 182
7.10 Result of MPC-PID HFO GT Fuel Flow Control 182
7.11 Result of MPC-PID LNG GT Fuel Flow Control 183
7.12 Result of MPC-PID GT Dual-Nozzle Combustion Flow Control 184
7.13 Result of MPC-PID GT Dual-Nozzle Fuel Flow Optimal Control 186
7.14 Result of single and dual nozzle switching operation 188
CHAPTER EIGHT: CONCLUSION AND FUTURE WORKS 189
8.1 Conclusion 189
8.2 Future works 190
REFERENCES 192
APPENDIX A 204
APPENDIX B: EDITING CERTIFICATE 209

List of Tables

Table 2.1: Benefits and Downsides of Hybrid Gas Turbine Design Technology 37

Table 2.2: Controller Design Challenges..38

Table 3.1: LCV fuel level control parameter for modelling 62

Table 3.2: LNGCV liquid level control parameter for modeling 63

Table 3.3: Summary of LCV dynamic design parameter 66

Table 3.4: Summary of LNGCV dynamic parameters 67

Table 3.5: Integrated GCV liquid control of GT 68

Table 3.6: Summary of integrated fuel dynamic design parameter 69

Table 3.7: Selected data for modelling and analysis 83

Table 3.8: computational data for turbine and compressor efficiency 83

Table 3.9: Minimum fuel flow and no-load estimation 86

Table 3.10: Estimated operational data for fuel lag 86

Table 3.11: Compressor discharge operational data 86

Table 3.12: Radiation shield data 88

Table 3.13: HDGT model parameters for Figure 3.15 89

Table 5.1: GT liquid fuel control parameters of PID controller settings 128

Table 5.2: PID parameter for LNG GT fuel system control 131

Table 5.3: PID parameter for dual nozzle fuel system control 134

Table 5.4: Dual input parameters 135

Table 5.5: PID iteration for optimisation 139

Table 7.1: PID controller parameters for Liquid tank flow dynamics 168

Table 7.2: PID controller parameters for LNG tank flow dynamics 170

Table 7.3: PIDs parameters for GT dual nozzle fuel flow 172

Table 7.4: MPC Performance Test 175

Table 7.5: MPC – Constraint Assessment 177

Table 7.6: MPC Tunned Parameters 182

List of Figures

Figure 1.1: Schematic diagram for a hybrid dual fuel nozzle control concept 5

Figure 2.2: Typical Brayton cycle in pressure-volume and temperature-entropy frames 11

Figure 2.1: Typical single pool turbojet engine 16

Figure 2.2: a) open- loop control b) Closed-loop control system 17

Figure 2.3: Schematic of a Solar Hybrid GT Power Plant with Storage 20

Figure 2.4: General schematic of fuel cell 21

Figure 2.5: Power Generation in Fuel Cell Stacks 22

Figure 2.6: Schematic of the Dual-fuelled Gas Generator 24

Figure 2.7: Simple Cycle Gas Turbine Power Generation 26

Figure 2.8: Combined Power Gas Turbine Generation 26

Figure 2.9: Optimisation Problem Formulation Process 35

Figure 3.1: Typical heavy-duty gas turbine (GT) schematic layout 42

Figure 3.2: GT fuel supply model for dynamic control 55

Figure 3.3: Block diagram of a liquid fuel level control loop 56

Figure 3.4: Block diagram of LNG Level control loop 57

Figure 3.5: Linearised model of the fuel control loop of LFT 58

Figure 3.6: Linear Model of LNG control of GFT 59

Figure 3.7: Integrated dual fuel control of GT fuel supply tank 60

Figure 3.8: Linearised Model of integrated dual fuel control of GT fuel supply 61

Figure 3.9: Fuel flow rate without controller 70

Figure 3.10: Dynamic response of LFCV without the effect of the controller 71

Figure 3.11: LNGCV flow rate without controller 72

Figure 3.12: Dynamic response of LNGCV without controller 73

Figure 3.13: Combined LNG and Liquid fuel flow rate without controller action 74

Figure 3.14: Dynamic response of integrated fuel line without controller action 75

Figure 3.15: Rowen's model of HDGT for control system development 76

Figure 3.16: Brayton Cycle in temperature – entropy 77

Figure 3.17: Pneumatic valve positioner and valve actuator. (a) schematic view (b) internal feedback model……… 81

Figure 3.18: Linearised GT liquid fuel flow schematics 90

Figure 3.19: GT output response with liquid fuel without control action 92

Figure 3.20: Linearised GT LNG flow schematics.. 92
Figure 3.21: GT output response with LNG without control action.............................. 94
Figure 3.23: GT response of LNG-NLL dual fuel without controller 96
Figure 3.25: Dynamic response of integrated liquid-liquid fuel line without controller 98
Figure 3.27: Dynamic response of integrated LNG – LNG line without controller..... 100
Figure 3.29: Dynamic response of integrated synchronised GT LNG – LNG line without controller... 101
Figure A3.22: GT NLG-NLL Dual fuel simulation block diagram without controller 204
Figure 3.24: Dynamic simulation of integrated liquid-liquid fuel line without controller 204
Figure 3.26: Dynamic simulation of integrated LNG – LNG line without controller.. 205
Figure 3.28: Dynamic simulation of integrated synchronized GT LNG – LNG line without controller 205
Figure 4.1: Nozzle pump line schematic 104
Figure 4.2: The fundamentals of a dual-fuel engine's gasoline system for high natural gas nozzle injection... 105
Figure 4.3: Linear Operation of Nozzle... 110
Figure 4.4: Pressure wave arrival at the nozzle 112
Figure 4.5: Typical combustion pressure and pressure rise rate versus crank angle of LPG diesel fuel... 116
Figure 4.6: Heat release rate versus rank angle of dual-fuel combustion..................... 117
Figure 4.7: GT automatic dual pressure control switch... 118
Figure 4.8: Output response of automatic dual nozzle pressure-flow a) LNG flow.... 119
Figure 4.10: Response of integrated dual nozzle GT fuel Control 120
Figure 4.9: Simulink block diagram of integrated dual nozzle GT fuel Control.......... 206
Figure 5.2: Block diagram of external liquid fuel tank supply.................................. 123
Figure 5.3: PID control of liquid fuel tank 124
Figure 5.4: GT liquid fuel system... 124
Figure 5.5: Acceleration Control 125
Figure 5.6: GT Simulink model with Liquid fuel system without PID controller........ 126
Figure 5.7: Response of GT Liquid fuel system without PID controller...................... 127
Figure 5.9: GT liquid fuel flow control with PID controller 129

Figure 5.10: GT speed-torque characteristics response with liquid fuel flow control with PID 129
Figure 5.12: GT LNG gas flow control with PID controller 132
Figure 5.13: GT speed-torque characteristics response with LNG gas flow control with PID 132
Figure 5.14: Simulink Design for Dual Nozzle GT PID Controller 133
Figure 5.15: Response of fuel pressure control and combustion flow 135
Figure 5.16: Rotor speed and torque for the dual nozzle fuel system 136
Figure 5.17: Population generation for PID optimisation process 138
Figure 5.18: GT PID optimisation analysis with Bode plot 138
Figure 5.19: Optimal response for the GT PID dual nozzle plot 139
Figure 5.1: Modify GT model with dual fuel arrangement 206
Figure 5.8: GT Simulink model with Liquid fuel system without PID controller 207
Figure 5.11: GT Simulink model with LNG fuel system with PID controller 207
Figure 6.1: MPC GT model controller design 141
Figure 6.2: Block diagram of DMPC Observer 154
Figure 6.3: MPC Implementation of dual nozzle fuel system control 160
Figure 6.5: Optimisation of MPC-PID Controller 163
Figure 6.6: GT dual fuel MPC-PID tuning 163
Figure 6.7: MPC-PID controller response for dual fuel tank simulation 164
Figure 6.8: MPC-PID Controller response to dual fuel flow into the combustion chamber 165
Figure 6.9: MPC-PID response for fuel flow characteristics for dual nozzle 165
Figure 6.10: MPC-PID dual nozzle fuel control with measured turbine mechanical power 166
Figure 6.4: MPC -PID block diagram for complete GT system fuel control 208
Figure 7.1: Dynamic response of liquid tank flow 169
Figure 7.2: Dynamic response of LNG tank flow 170
Figure 7.3: Dynamic response of dual nozzle flow 171
Figure 7.4: Response of PID Controller design for GT dual nozzle fuel flow 173
Figure 7.5: Response of PID controller design for dual fuel GT control without external tank 174
Figure 7.6: GT fuel demand response for dual fuel PID control 174

Figure 7.7: MPC-PID Liquid Plant input response against Model internal parameters 179
Figure 7.8: MPC-PID Liquid Plant Output response against Model internal parameters 179
Figure 7.9: MPC-PID LNG Gas Plant Input response against Model internal parameters 181
Figure 7.10: MPC-PID LNG Gas Plant Output response against Model internal parameters 181
Figure 7.11: Response of GT MPC-PID Controller implementation for HFO -Fuel Flow 183
Figure 7.12: Response of GT MPC-PID Controller implementation for LNG -gas Flow 184
Figure 7.13: Response of GT MPC-PID Controller implementation for Dual-Nozzle Flow 184
Figure 7.14: Response of GT MPC-PID Controller for Dual-Nozzle Combustion Flow 185
Figure 7.15: Response of GT MPC-PID Controller Dual-Nozzle Optimal flow 186
Figure 7.16: Response of GT MPC-PID Controller Dual-Nozzle Cost function 186
Figure 7.17: Response of GT MPC-PID Controller Dual-Nozzle on (a) Speed, (b) Torque and (c) Combustion discharge 187

CHAPTER ONE: INTRODUCTION

This chapter contains several sections explaining the research process, including background study, problem statement formulation, research objective, methodological approaches, contributions to knowledge, research hypothesis, publications, and a comprehensive organisational outline of the thesis.

1.1 Background

In current power generation systems, gas turbines (GT) are a critical and reliable part of the process. Gas turbines also play a crucial role in the aeronautical industry and are the primary mechanical drivers for significant pumps and compressors for industrial and commercial applications. Optimal operation and control of hybrid HFO-DLCO gas turbine generation have been critical in maximising performance and cost scaling for this type of equipment. Significant research has been conducted, and many analytical and experimental models have been developed to understand better gas turbine systems' nonlinear behaviour and complex dynamics. However, the need for accurate and reliable gas turbine models for various hybrid fuel applications, as well as for cost reductions to encourage industry adoption while minimising environmental impact, has been a strong incentive for researchers to continue working in this research area. This area of research is concerned with the design of white-box and black-box models and their application in control systems.

MPC controller over the years has been demonstrated to be an efficient and dominant technique for data processing, modelling, and controlling highly nonlinear systems such as those found in gas turbine power plants. Additionally, due to the high electricity demand, power producers are constantly looking for new ways to optimise gas turbine plants' design, manufacture, operation, control, and maintenance.

Gas turbine plants are internal combustion engines that use positive work transfer to convert the chemical energy contained in the fuel and gaseous air into mechanical energy [1]. They are typically used to generate electricity. The compressor receives air from the atmosphere at high pressure in GT plants and compresses it using a negative shaft work transfer. Gas turbines operate on the Brayton cycle principle, employing both open and closed systems comprised of a compressor, combustor, and turbine connected in series. Compressed air from the compressor ignites the fuel in the combustion chamber, increasing the volume and temperature of the air. The hot air from the combustion chamber turns the turbine blade and provides the necessary thrust to operate the pre-mover of the electrical alternator [2].

Although the history of gas turbines dates back to the 1800s, it was not until the 1930s that Frank Whittle and his colleagues [3] in Britain developed the first practical GT for a jet aircraft engine. Following the Second World War, gas turbines advanced rapidly and became the primary choice for various applications. These were primarily due to advancements in different technological areas, including aerodynamics, cooling systems, and high-temperature materials, which significantly increased engine efficiency [1]. Each year, gas turbine applications and production expand in popularity and size - their ability to operate consistently and reliably. As a result, nearly all mechanical and electrical equipment and machinery in industrial plants such as petrochemical plants, oil field platforms, gas stations, and refineries, among others, are powered by gas turbines. Due to their reliability, availability, adaptability, quick-start capability, low initial cost, and short delivery time, GTs are widely used worldwide, particularly in electric utilities. They have flexible features such as silent mode operational capability which do not require cooling water and are compatible with various fuels. Gas turbines have a high capacity for load growth and a quick response time to load changes [4].

Recent years have seen a surge in research, particularly in gas turbine optimisation, modelling, and control. These demonstrate the necessity of gas turbines becoming more apparent in modern industrial applications. As a result, hybrid fuel models of gas turbines and their associated operation and control systems are beneficial for technical and cost-cutting strategies to optimise equipment performance throughout the design and manufacturing processes. Optimised operation and control models can forecast performance, monitor performance degradation, evaluate emissions, turbine creep life usage, and the engine control system [5]. Mathematical modelling is a broad term that refers to developing system models. This approach employs mathematical notation to define and visualise the dynamic properties. Researchers have made significant efforts to develop gas turbine models that overcome complex economic and technological challenges [6] and have a reliable and cost-effective design [7]. Hybrid dual fuel application is an intelligent strategy for optimising gas turbine fuel efficiency, maintenance, and reliability.

1.2 Problem statement

Hybrid gas/HFO-DLCO turbines encounter a series of operational constraints due to adverse effects caused by various components. This phenomenon affects the transition between fuel supply sources leading to poor combustion. Significant instability in the control operation occurs during fuel transition, causing an enormous surge in turbine inlet temperature since the fuel-to-air ratio reduces. Wave propagation is responsible for the flow instability associated with a decrease in compressor delivery pressure and the transmission of dangerous dynamic pulsation throughout the entire system. Surge prevention is therefore critical when the turbine operates, as it can destroy the plant and its surroundings. Due to these constraints, hybrid gas turbines cannot work at excessively high speeds when switching to different fuel sources.

During operation, the associated impact of surge reduces the electrical power output which might lead to islanding conditions. Advanced control technology is required for the hybrid dual fuel gas turbine generators for industrial power applications to overcome this phenomenon. Integrating an advanced control technique will improve the turbine's performance and efficiency, providing a smooth transition to suppress an islanding operation.

1.3 Research aims and objectives

This study will resolve the existing challenges mentioned above by utilising the MPC-PID control that predicts and monitors low fuel supply, which manages the switching operations with an optimal operational cost for optimal fuel application. The primary reason for optimising management is to ensure and achieve sustainable process operations by continuously monitoring and evaluating control parameters in constraints and disturbances.

Additionally, optimal process control assesses the performance of the hybrid gas turbine in the following areas:

- Develop and analyse the hybrid operation of a dual-fuel gas turbine to determine the most efficient and economical operation.
- Develop a dual-system MPC-PID controller.
- Compare performance to a conventional gas turbine operating on a single fuel source.

1.4 Methodology and research design

The methodology, which includes modelling and designing the GT dual fuel control system, is discussed in chapters three and four and is conceptualised in Figure 1.1. The dual nozzle hybrid gas turbine system incorporates input fuel control valves that a PID controller would control. MATLAB and Simulink software were employed to develop a mathematical model of the plant's control. Simulating PID controller equations requires the construction of the PID Simulink block and estimating various parameters. The parameters are determined using a mathematical model developed from the characteristics of the gas turbine power plant. The features of the plant necessitate constant tuning of the controller whenever the nozzle is maintained - these results in high operating costs, which become unfavourable when combined with plant downtime. An MPC controller shielded the PID controller from parameter deviation, as shown in figure 1.1, would allow a seamless transition from one fuel leg to the next. Thus, whenever the process's parameters change, the MPC controller can automatically adjust the parameters without affecting the PID controller. These provide resilience to the system and eliminate the need for frequent tuning in the presence of process disturbances.

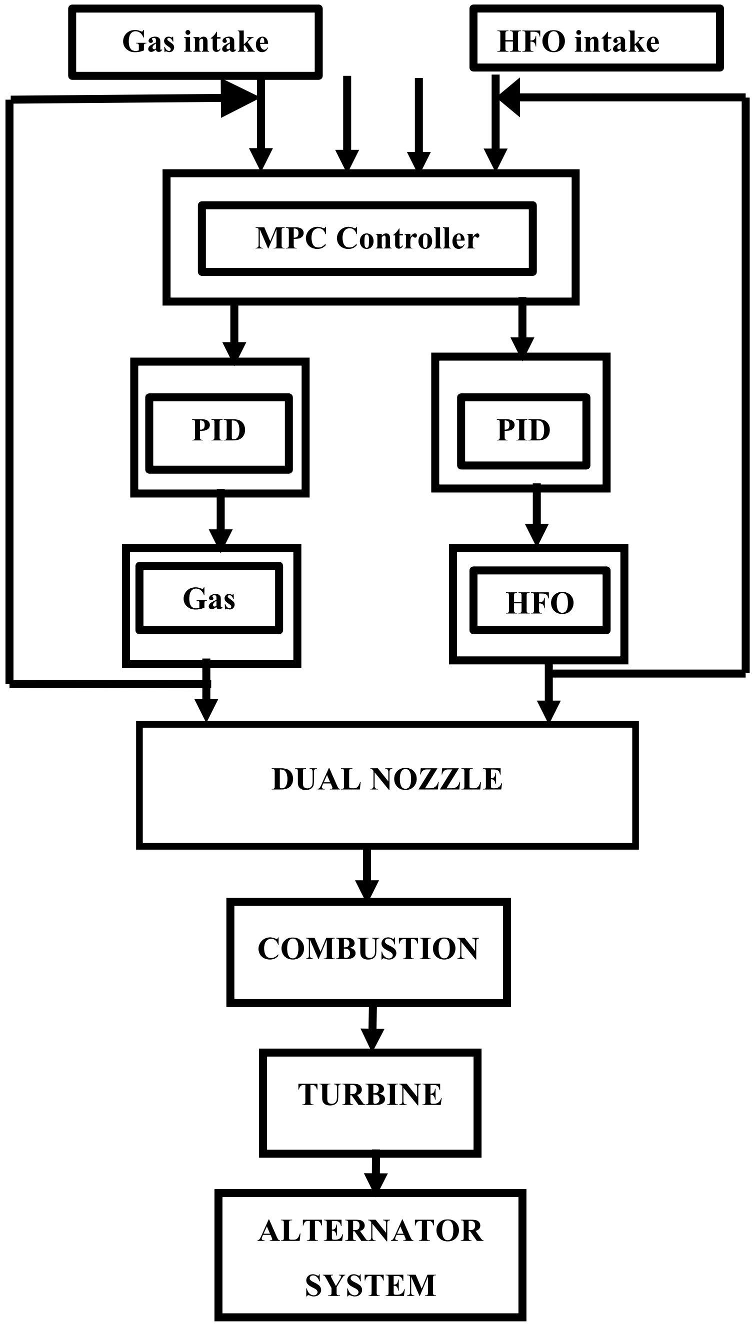

Figure 1.1: Schematic diagram for a hybrid dual fuel nozzle control concept

1.5 Contribution to knowledge

This thesis made the following contributions to the field of GT modelling, simulation, and control of hybrid dual fuel gas turbines:

This study provided an in-depth examination of hybrid dual fuel GT modelling, simulation, and control literature. The most pertinent research activities for various types of hybrid GTs, such as hybrid solid oxide fuel cell GTs and hybrid wind turbine GTs, were examined and discussed, including their methodologies, capabilities, and shortcomings. Despite extensive research in this area, still, additional research is necessary to address unanticipated challenges associated with single fuel operation in industrial applications.

This study developed a novel MPC-PID-based technique for controlling dual fuel nozzle GTs in an industrial GT model. The existing GT model parameters were processed using a Simulink model of a gas turbine running in a MATLAB environment. By combining the simulation algorithms for MPC and PID controllers in the Simulink environment, a resilient controller is created that overcomes the disadvantages of both controllers. When subjected to various fuel flow conditions during testing, the result is a smooth fuel switching logic for multi-fuel operation with no loss of combustion.

This research incorporated a new GT control model based on the Rowen single fuel model into the design and simulation of a multi-fuel control system. The modified model can adjust to optimal fuel price changes and select the most economically viable fuel for the GT's operation. Design of nozzle switching based on if-else condition operation with price as a deciding factor. The results were validated in the Simulink/MATLAB environment using operational data collected under various price conditions, including availability and effect on combustion.

This study aimed to investigate the design and application of conventional MPC-PID-based optimal dual fuel controllers for the fuel flexibility operation of a GT power plant. The GT plant's fuel mass flow rate and rotational speed were considered input and output for optimal function and control. When the fuel mass flow rate in a single fuel tank system decreases, the controller will ensure smooth fuel switching between multiple fuel sources while maintaining a constant rotational speed in response to changes in the plant control system's input. This is irrespective of the random reference, which is kept constant. After completing the system identification processes and developing the MPC-PID plant models, all controllers' associated parameters were tuned and set up to meet the controller design requirements for optimal GT operation.

1.6 Research Questions

The modelling and control of the dual hybrid GT fuel control system has the following research questions:

- Would the GT's dual-fuel power plant ensure a steady energy supply better than a single nozzle unit?
- Would fuel flexibility lead to efficient energy production costs compared with single-fuel power plants?
- Would the cost of producing energy be reduced due to fuel flexibility?
- Can optimal operation be achieved with fuel flexibility and optimal selection switching methods?

1.7 Delimitation

The following delimitation highlights future research and academic endeavours for potential researchers and academics:

- Parameterisation and operation of hybrid dual nozzle gas turbines interfacing with grid system for load flow analysis.

1.8 Publications during the study

Journal Paper(s)

- Kulor, F., Markus, E.D. and Kanzumba, K. 2021. Design and control challenges of hybrid, dual nozzle gas turbine power generating plant: A critical review. *Energy Reports*, *7*, pp.324-335.

- Kulor, F., Markus E.D. and Kanzumba, K. Dynamic analysis and design of a dual nozzle control system for gas turbine power plant efficient operation using parallel PID Controller (submitted).

- Kulor, F., Markus, E.D. and Kanzumba, K. Design and control of hybrid dual nozzle gas turbine power generating plant using model predictive control (submitted).

1.9 Organization of the thesis

Chapter Two discusses recent literature regarding gas turbine technologies, including their fundamental mechanisms and contemporary commercialisation techniques.

Chapter Three advances the methods used to improve the accuracy of the mathematical model of the GT power plant.

Chapter Four examines dual nozzle control of the power plant, heuristic dual nozzle operation, and dual fuel flow design.

Chapter Five examines PID controller design and Simulink extensively and used the control model to operate the dual nozzle developed in Chapter Four.

Chapter Six also examines MPC design to provide optimal setpoints and feedforward controls for dual nozzle gas turbine operations.
Chapter Seven presents the results for the various simulation models and further discusses them in detail.

Finally, Chapter Eight summarises the conclusion and anticipated future works.

1.10 Summary

This chapter discussed the general outlook of the entire thesis. The background of the thesis was presented. The problem statement, objectives of the study, a brief methodology and publications made during the study were highlighted. The chapter concluded with the hypothesis made for the study, delimitations, and general thesis outline.

CHAPTER TWO: LITERATURE REVIEW

2.1 Introduction

West Africa's power sector is currently facing one of its most daunting challenges of providing sustainable energy. Gas turbines have proven to be a reliable and sustainable source of thermal energy production processes. Despite technological advancements, modern gas turbine power plants continue to produce electricity at a high cost. Recent advances in gas turbine technology are necessary for thermal gas turbine power generation.

A hybrid dual nozzle gas turbine power plant may be a viable medium- to a long-term solution in this regard. It summarises and reviews design and control issues in developing a hybrid gas turbine, making recommendations for the most effective design and control approaches. With a 99 per cent plant availability, a hybrid combination of power plants combines multiple generation technologies to provide sustainable and reliable electricity with 99 per cent plant availability. A dual hybrid gas turbine design is the solar-gas turbine [8] and the hybrid fuel cell turbine [9], respectively.

The combination of gas turbines and other energy sources creates an appealing technological concept, and control operations are modelled, so that plant availability ensures constant power production [9]. Due to hybrid power plant commercialisation, there are now a variety of plant architecture and configuration options available to designers, innovators, and decision-makers. Economic analysis related to the plant uses various dynamic modelling and control operations. The mix logic dynamic (MLD) approach is adopted to develop a model for scheduling optimisation of combined-cycle cogeneration power plants [10, 15]. Although these approaches and measures are excellent, they cannot lower production costs and do not have the hybrid architecture necessary for success.

Papagiannakis et al. [11, 16], in their experiment, investigated and determined the effect of total air-fuel ratio on a high-speed compression-ignition engine's efficiency. When the chemical emissions of liquid diesel in the combustion chamber is replaced with natural gas fumigated into the intake air, the results indicate the effect on thermal brake efficiency, exhaust gas temperature, nitric oxide, carbon monoxide, unburned hydrocarbons, and soot emissions, with natural gas having a beneficial effect [11, 16].

The combustion and emission characteristics of dual-fuel engines that run on natural gas, biogas, producer gas, methane, liquefied petroleum gas, or propane were examined [12, 17]. The researchers found that increases in engine speed, injection timing advancements, and pilot fuel volume all contributed to higher thermal efficiency in dual-fuel engines. Their finding is evident in more research on the ignition characteristics of gaseous fuels in a long-term dual-fuel engine application. Design parameter optimisation in GT is critical in bridging the performance gaps between conventional diesel engines and so-called "gas-diesel engines." Hence the impact of hybrid GT fuel system design and configuration on control optimisation challenges coupled with a conceptual design of gas turbine power plants with recent control challenges emphasises the need for an improved dual-fuel gas turbine architecture in power generator design, cycle optimisation approach of a gas turbine and an evaluation of gas turbine power plants' performance

2.2 Performance of Gas Turbine

Gas turbines operate on the Brayton cycle's fundamental principles. The schematic diagram in Figure 2.1 depicts the arrangement of the GT's single shaft main components. It consists of a compressor, combustion chamber, and turbine, all mounted on the same shaft and thus rotated at the same speed [1- 2].

The Brayton cycle of constant pressure-volume (P-V) and temperature entropy is shown in Figure 2.2. The compressor produces atmospheric air via section 1 and the compressed hot air exits via section 2 to the combustion chamber. The combustion chamber reacts chemically with the hot compressed air and fuel to generate the necessary pressure and temperature to potentially exert thrust on the gas turbine [1, 13, 14]. The turbine serves as the prime mover for the alternator rotor shaft, driving both the compressor and alternator shaft at a constant speed simultaneously. The process generates a rotating magnetic field used by the stationary armature to create electrical energy.

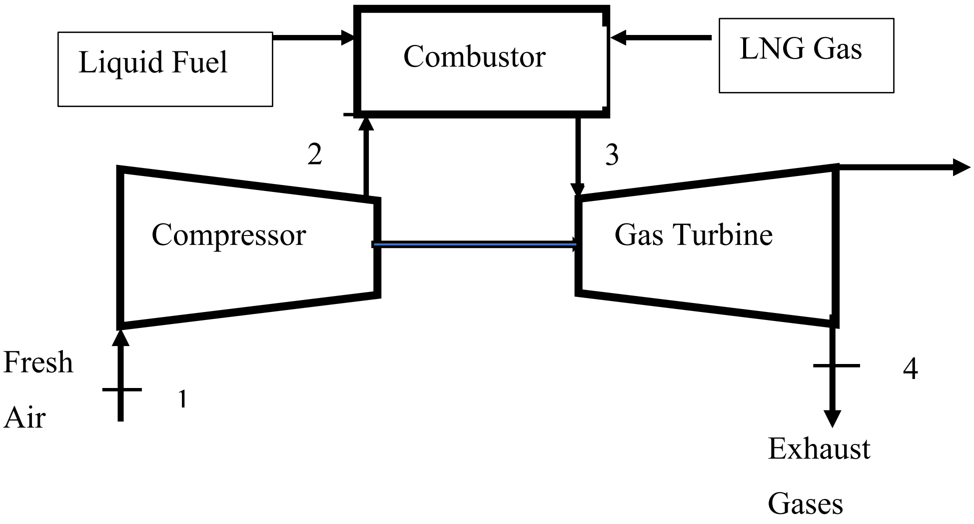

Figure 2.1: A typical gas turbine single-shaft Schematic

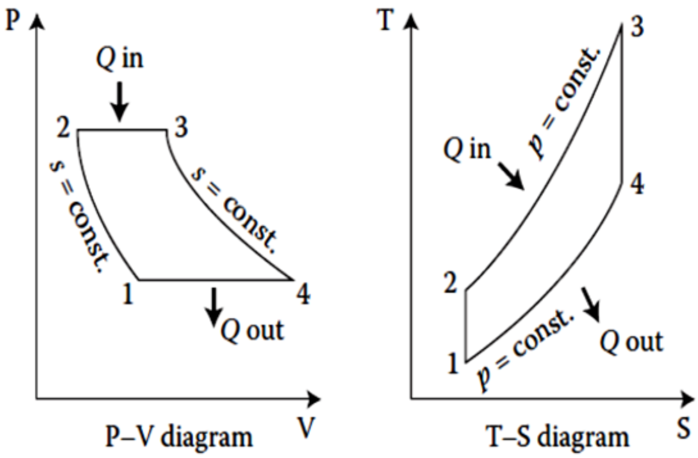

Figure 2.2: Typical Brayton cycle in pressure-volume and temperature-entropy frames

2.3 Classification of Gas Turbine

Fundamentally, the design, principles, and construction of GTs are similar in terms of the compressor, combustion chamber, and arrangement of the turbines. There are two categories of GTs: aero GTs and gas generators (GG) [5 & 13]. Aero GTs are designed for the propulsion system to generate the thrust required to propel the flight through the air at a significant speed and distance. Thrust is generated in aeronautical applications using Newton's third law of motion, which explains the principles of action and reactional forces. In the power industry, which is the focus of this research work, GTs are used to move the rotating part of the alternating current (AC) generator to produce a rotating magnetic field in generating the electromotive voltage (EMF) into the stationary conductor. The AC generator generates electromagnetic fields following Faraday's law of electromagnetic induction.

Additionally, according to their structure, application, and output power (MW), gas turbines can be classified into the following five categories [16]:

- Micro gas turbines (MGT) ranging in output from 20 to 350 KW
- Low-pressure turbines with output powers ranging from 0.5 to 2.5 MW for simple cycle applications
- Aero-derivative gas turbines with a power output of 2.5-50 MW and fuel efficiency of 35-45% for the aerospace industry.
- Heavy-duty gas turbines (HDGTs) with a power output range of 3-480 MW and an efficiency range of 30-46 per cent for large power generation units.
- Industrial-type gas turbines with a power output of 2.5-15 MW and 30–39% efficiency for use in petrochemical plants.

2.4 Configuration of Gas Turbines

It is critical to consider the architecture when designing and modelling the GTs control system. While the basic structure of compressors, combustion chambers, and turbines remains constant, the configuration is critical for thermodynamic analysis [1 & 15].

Although the thermodynamic cycle of various GTs is identical, there are significant differences between each GT depending on the application.

Two architectures of GT shaft systems are in use, single or twin shaft. In a single-shaft GT system, the output connects directly to the turbine rotor that drives the compressor. Most cases required a speed reducer between the rotor and the power output shaft. Nonetheless, the engine mechanical connection continues throughout the system. There is no mechanical connection between the Power Turbine (PT) and the gas generator turbine in a twin-shaft GT. PT is the component that performs the practical work. The gas generator turbine generates the necessary power to drive the compressor and associated equipment. The control output speed of this type of engine is by varying the gas generator speed. Additionally, the gas generator can operate at a reduced rotational speed under certain conditions while still providing the power turbine's maximum rotational speed. As a result, this configuration increases the life of the gas generator turbine while also improving fuel economy [5 & 13].

2.5 Gas Turbine Modelling

Certain fundamental factors must be thoroughly analysed when developing a gas turbine model. The most critical criteria at the start of the modelling process are the GT type, GT configuration, modelling methods, control system type and configuration, and modelling objectives [18].

2.5.1 Type of Gas Turbine

The first step in modelling GT is to collect sufficient data on the particular type of GT modelled. Although GTs come in various configurations depending on their industrial applications, the key components such as compressor, combustion chamber, and turbine remain the same. Figure 2.3 depicts a twin-shaft gas turbine engine, whereas Figure 2.4 depicts a typical single-spool aero gas turbine engine [17].

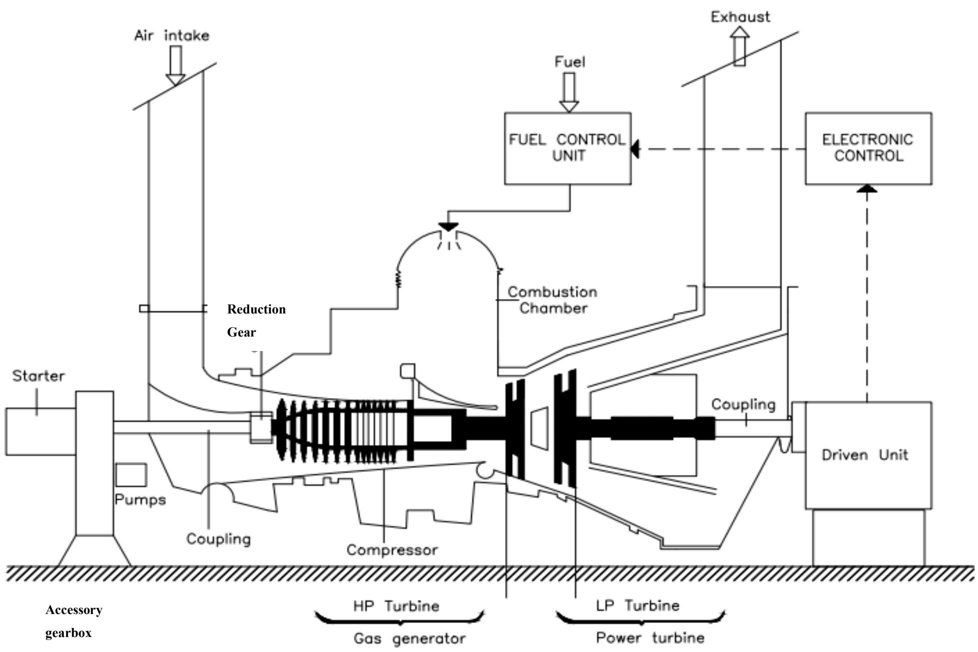

Figure 2.3: A typical twin-shaft gas turbine engine

2.5.2 Gas Turbine Modelling Methods

Generally, mathematical modelling approaches use mathematical language to describe and predict the dynamic behaviour of a system. Technological and scientific advancements have improved the quality and agreement of mathematical models with experimental data. Physics modelling is a subset of mathematical modelling, which implies that physical laws govern the system and, therefore, are physically realisable. Physics modelling is a technique that employs dynamic physics equations in conjunction with real-time data measurements to create operationally valuable models. In a physical system, the mathematical models can be classified as "linear and nonlinear," "deterministic and stochastic (probabilistic)," "static and dynamic," or "discrete and continuous" models [19].

2.5.2.1 Models, Linear and Nonlinear

If all of the system's objective functions and constraints defined are linear functions, the model is said to be linear. Unless explicitly stated, it is considered a nonlinear model.

While industrial GTs are nonlinear, the plant model is frequently simplified to allow linear analysis. Many techniques are available for the linearization of the nonlinear system. However, considering nonlinear dynamics is unavoidable when developing a model capable of accurately predicting the effects of complex and sensitive systems in gas turbines.

2.5.2.2 Deterministic and Stochastic Model

A model can be deterministic or stochastic from another perspective. In a deterministic model, all variable states are determined uniquely by the model's parameters and the sets of these variables' previous states. A deterministic model expresses itself without uncertainty due to the exact relationship between measurable and derived variables. In comparison, a stochastic model depicts quantities using stochastic variables or stochastic processes. As a result, stochastic models employ random probability distributions in modelling the state variable [18].

2.5.2.3 Dynamic and Static Model

Typically, the variables that define a system change over time. The system is said to be static if these variables are connected directly and instantaneously. When the values of variables in a design change independently with external influences and become dependent on previously applied signals, the system is said to exhibit dynamic behaviour [18].

2.5.2.4 Discrete and Continuous Model

A mathematical model that describes the interaction between continuous-time signals is called continuous-time. Continuous-time models employ time-varying functions f(t). Discrete-time models explicitly express the relationships between the values of discrete signals at discrete times in time. Differential equations characterise the relationship between signal values. Typically, during discrete-time measurements, signals are obtained in the sampled form [18].

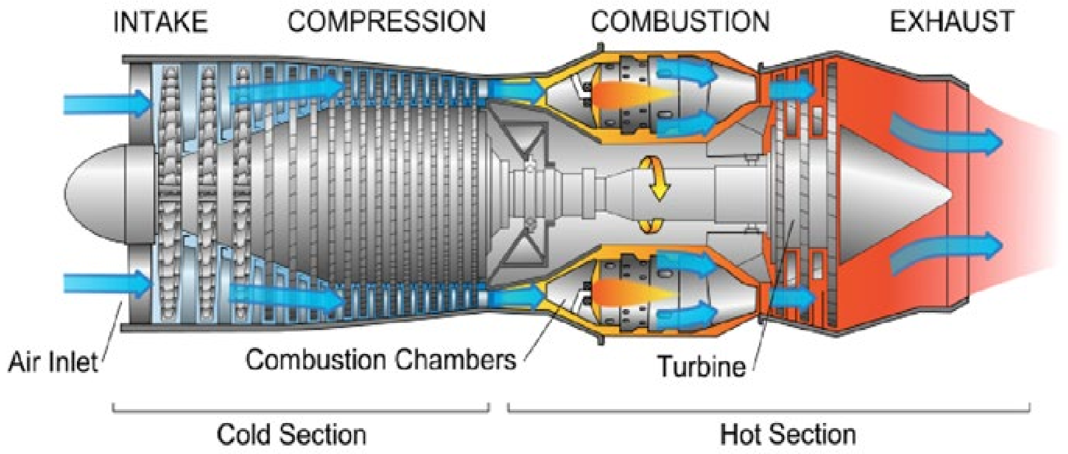

Figure 2.4 Typical single pool turbojet engine [17]

2.5.3 GT Control System Type and Configuration

The type and configuration of the gas turbine control system are critical factors in their modelling and control design. Control systems are essential components of industrial equipment. The style and structure are highly dependent on the complexity of the system dynamics and the defined tasks throughout the performance period. Without an adequate control system, serious problems such as compressor surge, overheating, and over speed can occur [19]. The final effect of these problems may be system shutdown and severe damage to the main components of GT.

All gas turbine control systems have three essential functions: "start-up and shutdown sequencing control," "steady-state or operational control," and "protection control for protection against overheating, over speed, overload, vibration, flameout, lubricant loss, and fuel switching current approach." Distributed control system (DCS) [16] refers to the control system of a power distribution network with multiple gas turbine topologies coupled to a central location.

Control systems for gas turbines (CSGT) can be either open-loop or closed-loop. The controlled variable is positioned manually or via a predetermined programme in an open-loop control system. However, in a closed-loop control system, one or more variables from the measured variable are used to adjust the manipulated variable for stable output.

The smooth, continuous, effective, and suitable operation of the closed-loop control system requires the controller to appropriately relate to the process parameters [16]. Figure 1.5a and Figure 1.5b illustrate open-loop and closed-loop control system block diagrams for a typical process.

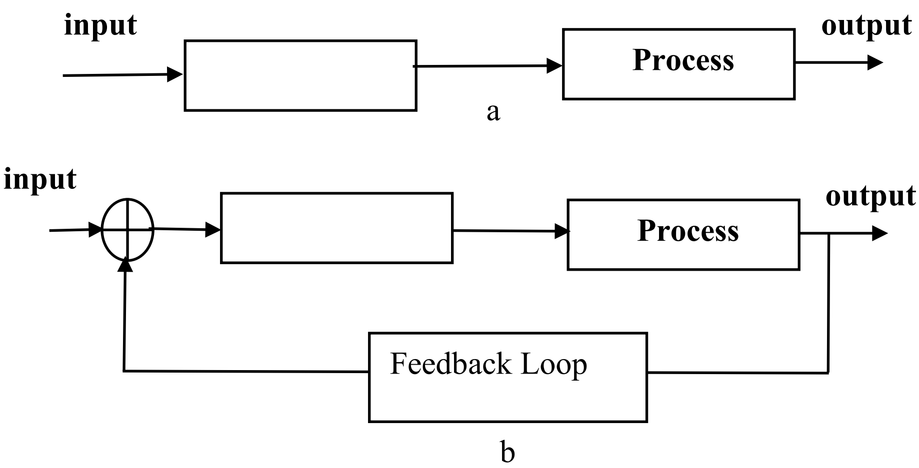

Figure 2.5: a) open- loop control b) Closed-loop control system

2.5.4 Gas Turbine Modelling Objective

The gas turbine model was developed for controller design functionalities, including fuel control, nozzle control, system identification, optimisation, acceleration control, and temperature control. As a result, a precise statement of the modelling objectives is to develop a successful GT model.

2.5.4.1 Fuel Control System

The objective of gas turbine engine's fuel control is to monitor the mass density of the fuel since it varies as the temperature and type of fuel changes. The fuel controller adjusts the initial mass density to a corrected value based on the most recent mass fuel flow measurement. Accurate mass fuel flow control enables gas turbine engine designers to reduce tolerances in moving parts and increase efficiency.

2.5.4.2 Fuel Nozzle Control

In the fuel nozzle control, the idea is to switch between two different types of multiple fuel sources to enable the gas turbine to operate on a hybrid fuel. The controller monitors flow pressure and switches over when the pressure drops in value. Switching logic or matrix is such that combustion does not stop in the process.

2.5.4.3 Temperature Control

When the output temperature exceeds the constant maximum, the temperature control expression regulates it. When a generator is operating normally or when the load demand on a gas turbine increases, the generator's output power and load frequency determine the controller's performance. This increased temperature above the setpoint has been monitored and controlled by the temperature controller. During the temperature control operation [20-21], the observed temperature is compared with the reference temperature to take remedial action.

2.5.4.4 System Identification

One of the primary objectives of gas turbine modelling is to establish the system's identity. From a series of system measurements, system identification generates a mathematical description of a dynamic system, which is a model [22-23]. Despite decades of research in this field, there is still a need for GT models with a higher degree of accuracy and reliability for system identification.

2.5.4.5 System Optimization and Control

The development of gas turbine models can aid in the design or optimisation of GT control systems. Any control system must be capable of measuring its output via sensing devices and taking corrective action if the measured data value deviates from the desired value [24]. Control engineering is concerned with the characteristics of dynamic systems. The installed sensors determine the output performance of the equipment and the control actions. These measurements provide feedback to the input actuators, which will adjust their performance to the desired level. There is an increasing demand for accurate dynamic models and controllers to study the system's response to disturbances and optimise existing control systems. Utilising novel modelling techniques as part of the optimisation process is always an option.

2.5.4.6 Acceleration Control

When the generator accelerates faster than is permitted, accelerating control attempts to control the fuel system by communicating with a dual controller, the injection process and startup can result in this condition. The acceleration control loop guard against shaft damage caused by excessive speed [5, 25–28].

2.6 Design and Configuration Analysis of Hybrid Systems

Renewable energy and efforts to reduce carbon emissions from the combustion of hydrocarbons that generate mechanical power are required to propel synchronous alternators to drive hybridisation. Solar-gas turbines, fuel cell gas turbines, liquefied natural gas turbines, combined cycle gas turbines, and wind turbines are all examples of typical design technology. This article discusses and synthesises control integration into a gas turbine power generation system employing dual nozzle technology. On the other hand, the alternative energy sector is working to develop more hybrid power plant combinations [29-30].

2.7 Architecture for a Hybrid Solar-Gas Turbine

The design incorporates a hybrid solar tower and a combined cycle gas turbine to maintain consistent power output. In this case, the turbine inlet temperature is constant throughout the operation, with a reduced fuel nozzle for the combustion chamber [29-30]. The solar tower converts solar energy into heat, whereas the gas turbine is built in accordance with the traditional architectural and engineering principles using the energy produced from the solar system [29-30].

The hybrid solar-gas turbine power plant under consideration includes a solar field and a tower. Hence, the power block is positioned on the top of the building. Natural gas (CH4) fuels a combustion chamber connected to an electrical power generator by a compressor. The HTF and working fluid are both pressurised air in this system. The thermal storage integration into the air stream with the solar receiver is shown in Figure 2.6.

The storage mode (idle, charging, or discharging) is determined by comparing the air temperature at the solar receiver outlet to the maximum temperature at the combustion chamber inlet (TCCh, min, max) and taking the storage status into account. When the average temperature of the storage reaches 110 per cent of the compressor outlet temperature or TCCh, in, max, the storage is empty/full. The compressor and combustion chamber maintains a constant air mass flow rate in all operating modes. When the storage unit discharges, the airflow circulates from point 1 to point 2 (or from point 2 to 1). (charged, respectively). In charging mode, a blower forces air through the storage, increasing the air mass flow rate in the solar receiver proportionately. A high-pressure drop via the solar receiver decreases the turbine's efficiency.

Consequently, the maximum airflow through the solar receiver is increased. A high-pressure drop through the solar receiver reduces the efficiency of the turbine. The receiver is bypassed wholly or partially in discharging mode, depending on the solar irradiation and the storage temperature [31]. This cost-effective green energy innovation lacks constant energy delivery, and the efficiency reduces when solar energy goes down notwithstanding a high cost of implantation.

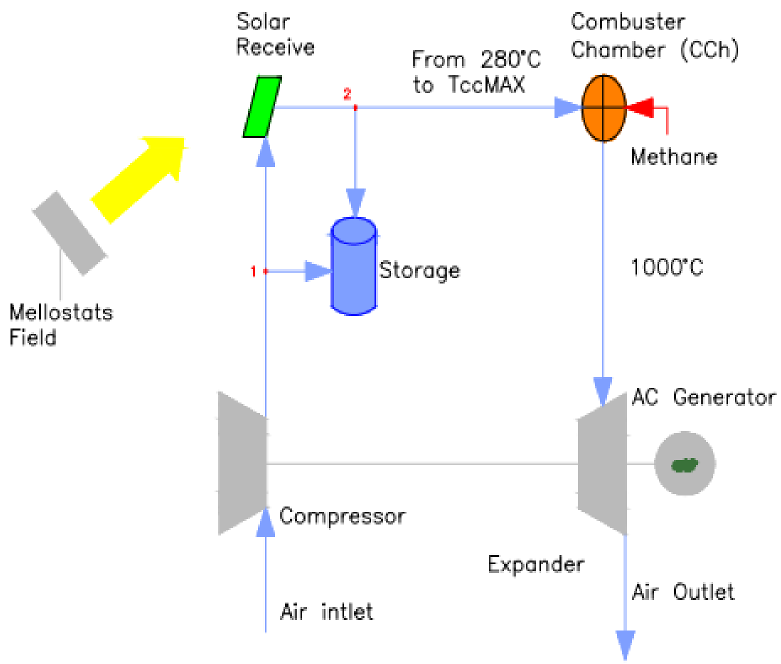

Figure 2.6: Schematic of a Solar Hybrid GT Power Plant with Storage

2.8 Architecture of a Hybrid Fuel–Cell Gas Turbine

In 1830s, Sir William Grove and Professor Christian Friedrich Schoenlein discovered fuel cell technology. The system uses a reversed water hydrolysis process with hydrogen and oxygen, producing water and electricity [29]. Fuel cells, like batteries, have electrodes and electrolytic materials that aid in generating electricity through electrochemical processes. Chemical energy is stored in an electrolyte in batteries and converted to electrical energy when needed. A secondary battery recharges using external power, but the primary battery needs replacement after some time. A fuel cell uses electricity to store chemical energy rather than keeping it in a battery cell. Fuel cells can produce electricity indefinitely since fuel and oxidants are never depleted [32, 33]. Figure 2.7 depicts the basic structure of a fuel cell. It consists of an anode, a cathode, and an electrolyte, in that order - anode (positive electrode) gets fuel while cathode (negative electrode) gets an oxidant (negative electrode). Using electrochemical oxidation and reduction of fuel on the anode surface of the cathode generates electricity. The electrolyte transports the ions generated by the electrochemical reactions between the anode and the cathode. The anode's developed electrons reach the cathode and complete the electrical circuit [29, 34].

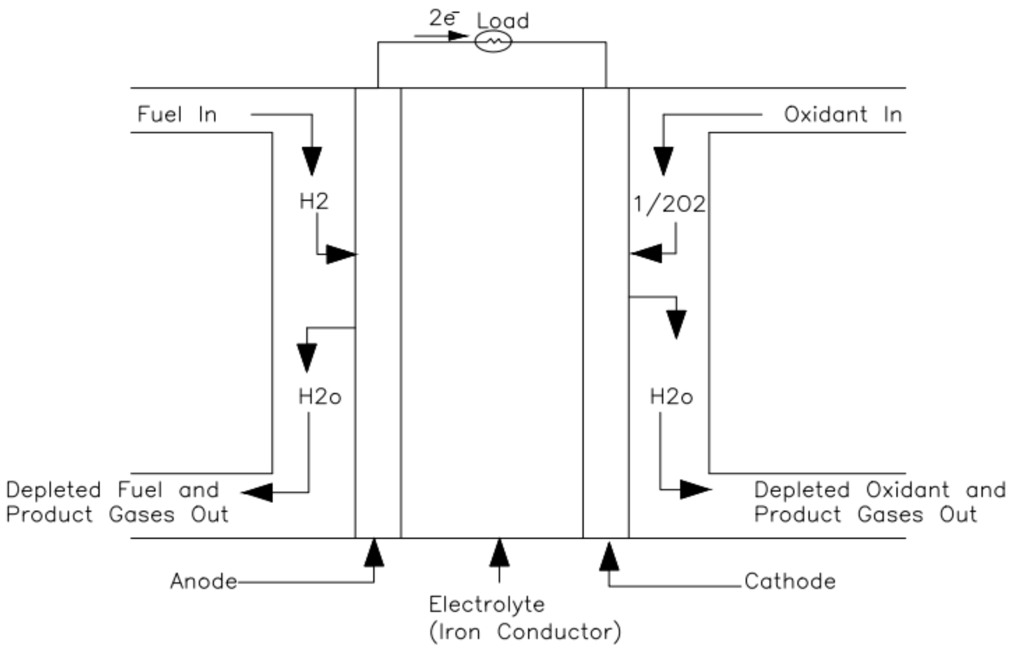

Figure 2.7: General schematic of fuel cell

Figure 2.8 illustrates the use of fuel cells in the generation and conditioning of electric power. Technology that incorporates both a fuel cell and a gas turbine has emerged that has the potential to increase the overall efficiency of a power plant significantly [34]. Fuel Cell Energy Inc. has developed a fuel cell and gas turbine hybrid system with an overall efficiency of 75 per cent based on this hybrid structure. Fuel cells integrate into a turbine system via gas and heat flow interactions, which is the primary characteristic of this structure [35]. The gas turbine-compressor-generator and fuel cell systems will simultaneously generate power. Before supplying the power network, a power conditioning system (PCS) [36] converts DC to asynchronous AC power and synchronises it with grid power.

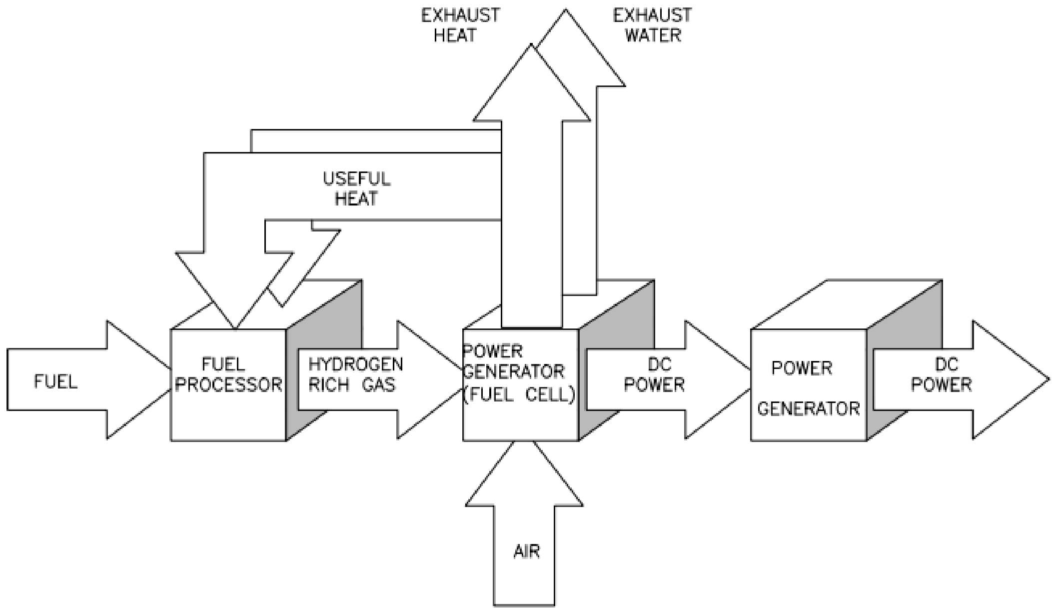

Figure 2.8: Power Generation in Fuel Cell Stacks

In a solid oxide fuel cell (SOFC), natural gas produces chemical-free, environmentally friendly electricity. The SOFC-gas turbine power plant is for domestic and commercial purposes. Compared with the traditional method, it has a minimal negative environmental impact. Yet research and analysis focus on energy production dynamic evaluation without control technique for parameter variation in perturbations. SOFC and gas turbine models in an independent power system with a comprehensive analysis developed for both systems.

The system used a dynamic tubular SOFC model distributed over a wide area for self-verification. There were several iterations before the simplified model was helpful in control implementation and operation [40]. The physical system with various load profiles is examined for control and operation procedures. By designing a part-load and full-load performance and analysing the hybrid system using the non-dimensional tubular model, investigated the hybrid system of SOFC was investigated. Because of this, the system has a drawback in that it stores energy for later use [37-39]. Energy supply availability and reliability became an issue because of this.

2.9 Architecture of a Dual-Fuel Gas Turbine Control

A dual-fuel diesel engine is equipped with a dual-fuel conversion kit that enables the engine to run on clean-burning alternative fuels such as compressed natural gas and other readily available fuels without modification or retrofit. Dual-fuel engines may offer several potential benefits, including increased fuel flexibility, reduced emissions, increased compression ratio, increased efficiency, and easy conversion of existing diesel engines without significant hardware modifications. Due to energy depletion and environmental pollution, researchers have identified dual-fuel technology as a viable option, especially given the increased availability of alternative fuels such as compressed natural gas (CNG). It is a green technology since it maintains diesel combustion efficiency while emitting less particulate matter and smoke.

Dual-fuel technology was historically prominent in big engines such as marine, locomotive, and stationary engines. The use of alternative fuels in gas turbine power plants and vehicle engines has been limited in the past due to a lack of alternative fuels and control-related obstacles.

The gas turbine can be designed to run on various fuels, including gaseous fuels, liquid fuels, atomised solid (coal) suspended in gas, and semi-solid fuels (biomass waste liquor). These different fuel types necessitate the development of customised fuel delivery systems with variable combustor residence times. However, most OEMs offer standard fuel systems for natural gas, liquid fuel (such as LNG or diesel), dual-fuel (gas or liquid), and, in the case of some manufacturers, bi-fuel (both gas and liquid at the same time). Refer to Figure 2.9.

The fundamental principle underlying most gas turbine power development is "temperature control." The fuel flow is controlled by a fuel control unit, which in earlier gas turbines was a mechanical device with several cams and contours. In more modern engines, the control is more akin to an electronic brain, with electronic functions replacing the mechanical cams depicted in Figure 2.9. Temperature control, in its simplest form, is as follows. Exhaust gas temperature readings inform the gas turbine's control system whether the gas turbine should be heated or cooled to meet a particular operational requirement. The reading is compared with the fuel flow setpoint, and the setpoint is increased or decreased according to the control logic requirements.

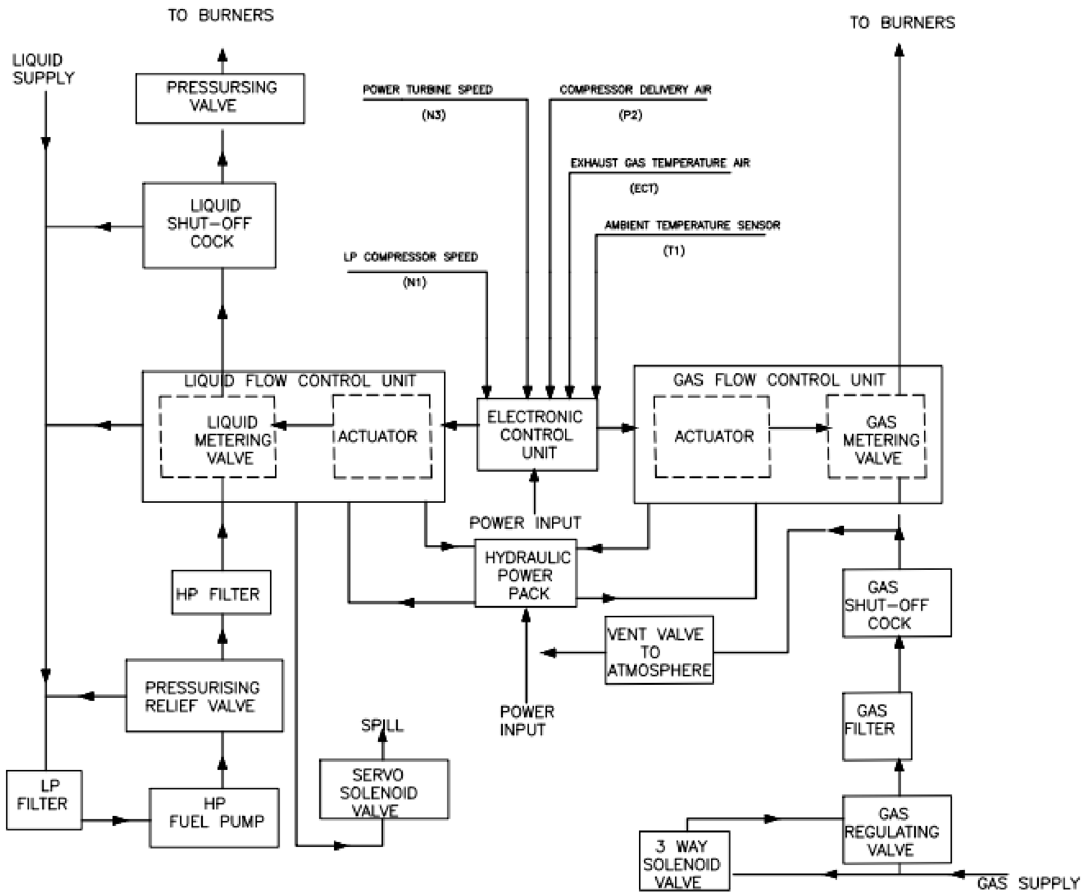

Figure 2.9: Schematic of the Dual-fueled Gas Generator

2.9.1 LPG Dual-Fuel Gas Turbine (LDFGT)

LPG dual-fuel engines are modified diesel engines that run on LPG as the primary fuel and diesel as the secondary fuel. While LPG dual-fuel engines have high thermal efficiency at high output, their performance is reduced during part-load conditions due to inefficient charge utilisation. This issue was resolved by adjusting variables such as pilot fuel quantity, injection timing, and the composition of the gaseous fuel and intake charge conditions to improve dual-fuel engine performance, combustion, and emissions [40-41].

The diesel model operates on the same principle as conventional diesel engines: diffuse combustion via fuel oil injection. In gas mode, the primary fuel source is natural gas. Additionally, a small amount of pilot fuel oil is injected via the diesel fuel oil injection mechanism. Premix combustion is accomplished using the pilot fuel oil as an ignition source [42]. The process is completed by designing a synchronous alternator that generates a voltage as an energy conversion device. (This is a reference to a power generator.)

2.10 AC Gas Turbine Generator Design

There are four main stages in designing a gas turbine: preliminary design, development and verification, system design and development, and finally, post-certification and in-service certification support (43). Based on system architecture, gas turbine power generation systems are divided into simple and combined cycle designs.

2.10.1 GT System with a Simple Cycle

A compressor describes the simple cycle, and a gas turbine powering an alternating current synchronous alternator makes up the simple cycle system depicted in Figure 2.10. Waste energy is released into the atmosphere in the form of hot exhaust gas.

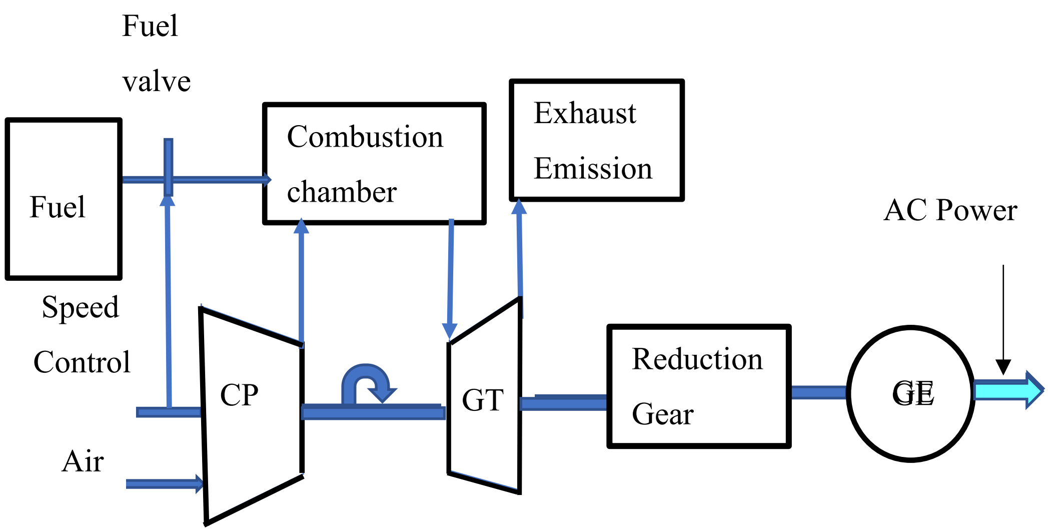

Figure 2.10: Simple Cycle Gas Turbine Power Generation

2.10.2 Combine GT Cycle System

The combined cycle plant in Figure 2.11 is designed for maximum performance by utilising the heat energy contained in the exhaust gas to generate steam that powers a steam turbine. Both turbines are then connected to a propeller-driven alternating current synchronous generator to generate electrical energy.

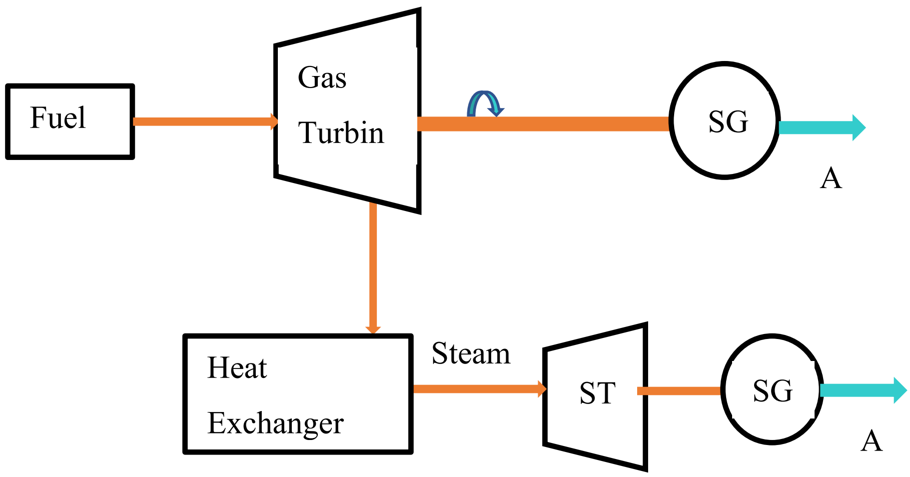

Figure 2.11: Combined Power Gas Turbine Generation

The two-design philosophy described above is appropriate for single nozzle fuel system operation. Essentially, it is all the same. As part of the combustion process, the high-intake air from the atmosphere is compressed and pressurised at high temperatures by the compressor. Fuel and compressed air from the compressor are mixed in the combustion chamber to produce the necessary energy for driving the gas turbine in the correct proportion.

2.11 Conceptual design of Gas Turbine Power Plant

Many engineering disciplines are involved in the conceptual design of gas turbine engines. An engine configuration is selected based on various factors, including physics and engineering, aerodynamics, heat exchange, materials engineering, component design, and structural analysis. Since the process is so complicated, it is essential to use a method that minimises engine options without sacrificing performance. There are several steps involved. A gas turbine's size and performance are influenced by many factors, including the design of the engine and its components, the flow path and weight prediction, and installation analysis [43].

The engine design process is non-linear because each step is dependent on the previous one. It is common for an engine configuration to be tweaked several times before a final decision. The inlet temperatures of gas turbines are increasing at an ever-increasing rate. A step-by-step, experience-based development process with validated design principles is required for all hot gas path components to meet lifetime requirements at this elevated temperature. Due to an exponential relationship between combustor flame temperature and NOx emissions, it becomes increasingly difficult to meet emission targets [44]. As a result, it is necessary to design an optimisation iteration to improve combustion performance.

2.12 Gas Turbine cycle design Numerical Optimization Methodology

This question frequently arises in gas turbine performance design simulations: "what is the best thermodynamic cycle point?" There are two ways to go about this optimisation task. Numerical optimisation algorithms produce a single cycle that meets all constraints, analyses multiple parameters, and finds the best solution. An engineering judgment-based approach to parameter selection yields helpful information across a wide range of parameter values [43].

Using numerical optimisation routines can speed up and improve the accuracy of finding the mathematical optimum when more than a few variables are involved. However, the traditional method of a new gas turbine's thermodynamic cycle selection involves many parameter variations. These variations can be time-consuming and require a unique logic optimum solution in a certain respect in a complex engine design.

In conjunction with an autonomous search, numerical optimization channels are applied to accelerate the design process. It is feasible to utilize a numerical optimization procedure to determine the optimal mathematical model instead of the physical model. The occurrence of an unusual cycle as a result of an optimization run often indicates a model error. The most probable design restriction may have been neglected during the problem specification phase. Additionally, it may be worthwhile to understand more about the region surrounding the optimal solution. In a parametric study, a restriction to the area of interest would disclose which design variables and constraints influenced the outcome [43].

2.13 Controller Design Difficulties

The steady state installed thrust and the Specific Fuel Consumption (SFC) required for a given application determine the type or cycle of a gas turbine engine. The performance aspects of an engine are considered in all aspects, including mass, noise, price, dimensions, and so on [43]. Open and closed-loop control strategies are used in gas turbines, similar to the primary control strategies found in the literature.

There are several reasons that open-loop control is not realistic for fuel flow, including the difficulty of measuring fuel mass flow rates, variations in fuel heating values; engine deterioration; and engine-to-engine scatter. Realistically, using multiple closed-loops increases the risk of control-loop interaction; if possible, each control loop should be kept separate to avoid cascading effects. A feedback parameter should not be affected by input. Many variable engine parameters can be used as feedback terms for variable geometry when the fuel flow increases in gas turbine engines, but this is not the case with reciprocating engines. Mathematical methods exist for reducing the amount of interaction.

On the other hand, interaction is kept to a minimum through the thoughtful selection of control parameters. This condition must be satisfied if the design strikes a balance between ideal performance requirements and the practicality of robustly implementing a specific control-loop combination with an adequate stability margin [44-47]. The complexity of the system dynamics and defined tasks over the performance period significantly affects the type and configuration of the control system. Proper control can result in compressor surges, overheating, and over speed.

Starting and shutting down the gas turbine, maintaining steady-state or operational control, and monitoring for overheating, over speeding, overloading, vibration, flameout, and lubrication loss are all part of the gas turbine control system's three primary duties. A central distributed control system (DCS) connects all gas turbine control systems in a power network [48, 49]. When it comes to gas turbine control, there are many different options. PID control, adaptive control, and neural networks with model predictive control are all common examples. Given the mathematical equations representing the model, the gas turbine system is highly non-linear. Therefore, it is necessary to carry out extensive analysis to obtain the system's transfer function when using a classical control technique. Non-linear control theory is also required to achieve a control loop because of this fact.

Using advanced control theory to control the system is a better alternative because advanced control methods can efficiently and effectively handle linear and non-linear systems [50-51].

2.14 Control system of the Gas Turbine Power Plant

Three significant controlled variables (VCs) exist in a gas turbine power plant: the rotor speed (N), the exhaust gas temperature (Te), and the turbine firing temperature (Tf). When the power plant is connected to the grid and synchronised, the power imbalance between the synchronous generator's output power and the connected load is likely to cause the grid frequency to deviate below the required frequency if it is not adequately controlled.

As a result, the gas turbine's rotor shaft rotating speed should be regulated and maintained at its nominal frequency throughout the operational period. The exhaust gas temperature of the turbine is kept lower than the reference temperature to avoid damage to the turbine while maintaining high efficiency. Nitrogen Oxide (NOx) emissions are controlled by turbine firing temperature, which must be kept lower than the specified upper limit. Two variables influence the turbine fuel demand (Fd) to vary the fuel flow, and compressor inlet guide vanes (IGVs) to schedule airflow. The ambient air conditions, such as temperature, pressure, relative humidity, and the connected load, are all possible disturbance variables (DVs) [52-53].

2.15 Fuel flexibility in Gas Turbines

The primary and inherent advantage of gas turbines is their fuel flexibility capability. A gas turbine can theoretically run on gaseous or liquid fuel. Natural gas, refinery gas, coke oven gas, low BTU coal gas, syngas, and biomass gas are gaseous fuels. Liquid fuels range from light distillates such as naphtha, kerosene, and diesel to heavier distillates such as crude oil. Trace elements including vanadium, salt, and potassium must be carefully removed due to their significant impact on hot corrosion on GT components.

Currently, natural gas is the standard fuel for land-based gas turbines. As a result, gas turbine components have the most extended lifespans. Although liquid fuels are declining, particularly for electricity generation, it remains popular in areas where these fuels are abundant, such as offshore locations, the Middle East, and West Africa.

Although gas turbines are fuel-flexible, additional fuel flexibility is required, particularly when carbon capture and storage (CCS) is used. In the CO_2 capture technologies, pre-combustion CO_2 capture will need the gas turbine to burn H2-rich gases. Current technologies developed by gas turbine manufacturers allow mixing a small amount of syngas with natural gas. However, there are currently no economically viable methods for using pure hydrogen-rich syngas with low NOx levels. This means that research on the combustion of H2-rich syngas in gas turbines is critical to enabling the use of coal gasification in conjunction with pre-combustion CO_2 capture. Another significant issue in power generation is operational flexibility. Solar and wind energy's growing share of electricity production necessitates a quick-response backup system to balance their intermittent nature and prevent an unstable grid. Gas turbines can and will play a critical role in ensuring the electricity system's flexibility and compensating for renewable energy sources' intermittent nature. However, this new requirement will significantly alter the operating mode of CCGT power plants in the coming years. In this case, the operation will transition from a baseload operation with 12 starts per year and 8000 hours of operation to a cyclic load following operation with as many as 250 or more starts and only 3000 h (or less) of operation per year, frequently at part load. This mode of operation, which includes the maintenance of a spinning reserve to provide backup during periods of reduced renewable energy production, results in decreased efficiency, increased costs, and increased CO_2 and NOx emissions per kWh produced. In the coming decades, gas turbine and power plant technology will need to evolve dramatically to meet these operational flexibility requirements. Transient behaviour, fatigue characteristics, part-load efficiency, and emission control will be critical in new development programs [49, 54–57]. GT fuel flexibility requires an efficient fuel nozzle design that can handle dual applications while also managing the combustion process to ensure the combustor's stability in achieving the necessary exhaust gas emissions and environmental pollution levels.

2.16 Design and performance of dual nozzles

GT fuel flexibility necessitated the design of a dual nozzle capability in combusting various fuel properties to generate the energy required to operate the GT engine. The fuel nozzle is an integral part of the GT combustor. Numerous experiments on the fuel nozzle have been conducted, and researchers are interested in resolving poor combustion processes by using an optimal nozzle design process.

Hongdae et al. [58] investigated the effect of dual fuel nozzle structures (EDFN) on the CRGT combustor's combustion flow field. These include the inner swirl nozzle, the double swirl nozzle, and the outer swirl nozzle, all of which were developed for the chemically recuperated gas turbine (CRGT) combustor. Based on the FLUENT simulation, the combustion characteristics of the combustor with the three nozzles were examined. They used a realizable k-model for turbulence flow and a PDF model for non-premixed reformed gas combustion. The three models' results agree with those obtained experimentally in the original oil combustor according to their structures.

Additionally, they investigated the effects of various dual fuel nozzle structures on the flow field, fuel concentration distribution, and temperature distribution in the combustor through simulation and analysis. They concluded that, compared to the inner swirl nozzle, the double swirl nozzle and outer swirl nozzle can create a more uniform flow field with an obvious central recirculation zone (CRZ), shortening the distance between the fuel and air mixing and achieving a more uniform outlet temperature distribution. However, when compared to the double swirl nozzle, the outer swirl nozzle can produce a more stable combustion flow field in the high-temperature region in the CRZ. Iyogun et al. [59] investigated the effect of nozzle geometry on the stability of swirling flames. They discovered that compared to an axisymmetric fuel nozzle, the non-axisymmetric fuel nozzle increased the size and dynamics of the flow recirculation zones and induced higher turbulence forces. Terasaki and Hayashi [60] pioneered using a dual swirl burner. The emission characteristics of the burner were compared to those of conventional swirl burners. The results of the experiments indicated that the double swirled burner could achieve the best fuel-air mixing and the lowest NOX emissions. Zhen et al. [61] conducted an experimental study to determine the effect of nozzle length on the emission of a multi-fuel-jet inverse diffusion flame on the emission of a burner. They discovered that nozzle length significantly affected the flame centre line temperature and CO/CO_2 concentrations. Lee and Yoon [62] invented a dimethyl ether-fuelled gas turbine nozzle.

The newly developed nozzle's performance was validated by comparison to the original nozzle. The new nozzle may eliminate flashback and significantly reduce NOX and CO emissions. Mansour and co-authors Li et al. [63] discovered that the nozzle diameter and arrangement of impinging premixed flames affected the heat transfer and CO emission. [64] developed a highly stabilised conical nozzle burner with the concentric flow. The flow field, temperature, and OH radicals were measured outside the cone. They discovered that this burner's flame was more stable than flames without a cone. Koyama and Tachibana [65] developed a low-swirl liquid fuel burner. Experiments were conducted to determine the effect of nozzle tip shape on flow patterns. They discovered that the chamfer dimensions had the most significant impact on the axial position of the flame. However, there is a shortage of published data on the design of dual-fuel nozzles for chemically recuperated gas turbine (CRGT) systems.

However, due to the rapid advancement of computers and numerical computation technology (CMNCT), computational fluid dynamics (CFD) now plays a significant role in combustor design. CFD technology reduces experimental costs and aids in creating the optimal structure. Numerous researchers used computational fluid dynamics to obtain information about the flow field. Liedtke and Schulz [65] developed a new type of lean combustion combustor. The commercial code CFD-ACE provided them with insight into the flow structures and information on the pilot's location and main flames within the combustor. Chui et al. [66] used CFD to evaluate burner and combustor design concepts. They discovered that computational fluid dynamics (CFD) could be an effective tool for assessing such burner and combustor designs. Koyama and Fujiwara [67] used computational fluid dynamics to predict the gas fuel concentration in the combustor using three different methods of gas swirl injection. They discovered that reverse swirl injection could produce a stable flame with adequate fuel-air mixing. Al-Attab and Zainal [68] optimised the design of the pressurised cyclone combustor using FLUENT. Finally, they determined the combustor's height, diameter, and outlet geometry. Arghode and Gupta [69] used FLUENT to calculate the combustor flow field. They discussed the effects of the diameter and confinement size of the air and fuel injection on gas recirculation and fuel/air mixing characteristics. Xing et al. [70] used CFD to investigate the effects of various cavity height-to-length ratios on the flow structure in a trapped vortex combustor.

2.17 Gas Turbine Plant combustion technology and pollution control

Gas turbine power plants are a significant source of environmental pollution due to exhaust gas emissions, and they also contribute to several health problems. Numerous policies have been implemented globally in recent years to mitigate the adverse effects of GT emissions on human health and the environment. Various studies on the emissions of GT exhaust gases and post-treatment emission control technologies were conducted.

GT exhaust gas contains four distinct types of pollutants. These include carbon monoxide (CO), which produced by incomplete combustion and unstable combustion, in which oxidation does not occur ultimately, and hydrocarbon (HC), produced by unburned fuel due to a lack of sufficient temperature at the cylinder wall.

Particulate matter (PM) is produced during the combustion process. It results from the agglomeration of very small particles of partially burned fuel, partially burned lube oil, the ash content of the fuel oil, and cylinder lube oil or sulphates and water. Finally, Nitrogen Oxide (NOx) is produced during the compression process in the adiabatic and Rankling cycles. Environmental management of GT exhaust gas emissions has become more humane over time due to technological advancement. The exhaust gas recirculation (EGR) system, the lean nitrogen trap (LNT), selective catalytic reduction (SCR), diesel oxidation catalyst (DOC), and particular diesel filter (DPF) are the most focused emission control technologies.

Stable combustion requires a sound design to minimise the acoustic propagation within the combustion cycle. Stability has been a significant issue in combustion design because the combustor is more prone to instability due to the unstable combustion process and acoustic disturbances within the combustion chamber. Stability in the combustion process require incorporating a variety of acoustic dampers into the design, such as perforated liners, Helmholtz resonators, baffles, half-and quarter-wave tubes, to control the perturbation and suppress the high-frequency waveform during the energy transfer process [70 & 71].

2.18 Design and optimization of controllers

In GT power plant optimisation, the subject drew the attention of several researchers, who presented various research findings and developed significant theoretical approaches over the last decade. Figure 2.12 evaluates and summarises the different methods suggested.
Implicitly, controller optimisation design (COD) necessitates extensive mathematical models of the target system, in this case, the GT model. In general, a control system's function can detect and measure the system's output and take the necessary corrective action. As an engineering discipline, control is concerned with the behaviour of plants and equipment monitoring is combined with the intelligence inherent in the dynamic

performance of the equipment detected through appropriate sensors that act as measuring devices. These measured parameters generate a feedback signal responsible for adjusting the input actuators toward the desired performance. Despite ongoing research in this field, there is a continuing demand for accurate dynamic models and controllers to investigate the system's response to disturbances and improve existing control systems for GTs. For examples of GT modelling for control, see Mu and Rees's research [72]. They investigated how to control the shaft speed of a gas turbine engine using a novel model predictive control strategy called approximate model predictive control (AMPC). The optimiser is responsible for selecting the process plant's performance indices. These include maximising fuel efficiency, minimising fuel costs, increasing total plant throughput, minimising downtime, maximising product quality, and minimising emissions. Depending on the complexity of the process plant, the optimisation process is classified as open-loop or closed-loop.

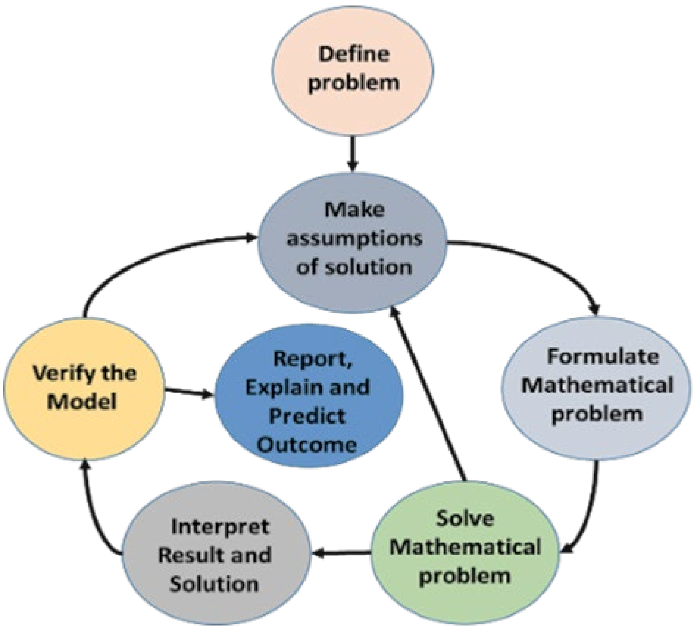

Figure 2.12: Optimization Problem Formulation Process

Optimisation for a given control horizon is solved offline in open-loop systems. The optimal set-points obtained are manually entered into the regulatory control system in closed-loop systems. The closed-loop systems optimisation model is solved using an online optimisation model, and the optimal set-points are automatically entered into the regulatory control system [73].

2.19 Dynamic simulation of the Gas Turbine power generator

It is difficult to model and manage the gas turbine because of its unique design and configuration. On the other hand, mathematical modelling simplifies the complex system by using defined differential equations to predict its dynamic behaviour. Models of physical systems are used to develop dynamic characteristics for use in developing plant models for control purposes. In the model system, the following dynamics exist; these include static and dynamic systems, stochastic and deterministic systems, linear and nonlinear systems, and continuous and discrete systems [74]. As with any other industrial plant, a gas turbine power plant needs a dynamic control system to keep it on track to meet its performance goals. Overheating, compressor surge, over speed, poor efficiency, and the subsequent breakdown of gas turbine components can result from improper control objectives.

2.20 Advantages and disadvantages of the hybrid GT design

Table 2.1 summarises the advantages, disadvantages, and related applications of hybrid gas turbine design technologies. To illustrate the trends, Table 2.2 identifies and presents the control challenges that these hybrid GT architectures face and a list of potential future control strategies.

Table 2.1: Benefits and Downsides of Hybrid Gas Turbine Design Technology

HYBRID TECHNOLOGY	CONTROL STRATEGY	DESIGN CHALLENGES	PROPOSED CONTROL STRATEGY	REFERENCE
Solar-Gas Turbine	PID	Part load disturbance	Multiple loop control with feedback integration	Jack Brouwer [29] and R.P. Merchant [30]
Fuel-Cell Gas Turbine	Multi-loop feedback	Poor performance at part load operation	Multi-loop feedback control with shielded MPC control	M. C. Camerata [32] and Yoshimasa Ando [33]
Liquid-Natural Gas	Servomechanism	Poor transition with load disturbance	Multi-loop feedback control with shielded MPC control	B. Ashok S. Denis Ashok [70]
Dual-fuel gas turbine	Adaptive control			These, K. P. Kavathekar [40] and B. Ashok [41]
Solid oxide fuel cell gas turbine	Multi-loop feedback	Poor performance at part load operation	Multi-loop feedback control with shielded MPC control	C. Stiller [76-78], K.P. Litzinger [78-81], and P. Costamagna [37]

Table 2.2: Controller Design Challenges

HYBRID TECHNOLOGY	BENEFITS	DRAWBACK	APPLICATION	REFERENCE
Solar-Gas Turbine	Less operating and running cost with solar energy availability	high-pressure drop through the solar receiver decreases the turbine efficiency	Powering Industrial boilers	Jack Brouwer [29] and R.P. Merchán [30]
Fuel-Cell Gas Turbine	highly efficient chemical-free electrical energy low environmental impact	Required constant replacement of batteries	Suitable for both domestic and commercial application	M. C. Camerettia [32]and Yoshimasa And[33]
Liquid-Natural Gas	Low operating cost when using LPG as the primary fuel	poor utilization of the LPG fuel at low and intermediate loads which results in poor engine performance	Suitable for both domestic and industrial power generating plants and other engines	B. Ashok S. Denis Ashok [68]
Combined cycle	High power output, Constant power production	High emission NOx	Suitable for grid power generation	Thipse, K. P. Kavathekar [40] and B. Ashok [41]
Dual-fuel gas turbine	High output power, Constant output	Low-efficiency High emission pollution and not environmentally friendly	Suitable for grid power production	Thipse, K. P. Kavathekar [40] and B. Ashok [41]
Solid oxide fuel cell gas turbine	Present economic power production strategy	Poor performance at part load operation and required sophisticated control design to overcome compressor surge or cell degradation	Power production at domestic and industrial level	C. Stiller and B. Thorud [62]

Extensive research on the hybrid application has discovered many architectural aspects to understand the nonlinear behaviour better. Even though the study in this field has produced satisfying results, efforts to address the design and control issues related to hybrid dual nozzle gas turbine power generating facilities will continue indefinitely as fuel types continuous evolve. However, the analytical and experimental models of control systems have been developed for gas turbines in multiple configurations. On the other hand, dual nozzle control is required for different control objectives and applications, providing a compelling reason for researchers to continue their work in this field.

Due to the negative impacts brought on by various components, as demonstrated in the analysis displayed in the tables above, hybrid gas/HFO-DLCO turbines experience some operational limitations. These impacts may affect, among other things, the maximum surge and the temperatures at the inlet of the turbine. When the compressor supply pressure drops, the flow becomes unstable, and the system begins to experience harmful dynamic pulsation. Surges cause this flow instability and hazardous dynamic pulsation transmission. Surge control is essential when the turbine is running since it might cause the plant and its surroundings.

Additionally, the turbine's maximum inlet temperature shouldn't be higher than the point at which the force is acting on the turbine rotor blade increases to an unacceptable level. Additionally, the control actuator restricts the valves, preventing them from entirely opening or closing. It is impossible to ignore a dual-nozzle gas turbine's performance when running part loaded.

These restrictions prevent hybrid gas turbines from operating at high speeds. Due to this, hybrid gas turbine generators must have a high-performance control system to provide electricity for industrial applications. It has been proven that implementing a cutting-edge control technique will enhance the turbine's functionality, effectiveness, and overall operation [41,82-86].

Hence, the study examined hybrid dual fuel GT modelling, simulation, and control literature. The most pertinent research activities for various types of hybrid GTs, such as hybrid solid oxide fuel cell GTs and hybrid wind turbine GTs, were examined and discussed, including their methodologies, capabilities and shortcomings. Despite extensive research in this area, still, additional research is necessary to address unanticipated challenges associated with single fuel operation in industrial applications.

2.21 Summary

This section provides a comprehensive review of research work from the literature on hybrid GT systems, including control challenges. It identifies some drawbacks associated with the operations and control optimization of the plant. It is obvious that much of the work on GT development has caught the attention of many researchers on the subject matter. A hybrid dual nozzle GT power plant may be an excellent long-term solution for West Africa's energy needs. However, the section also identified the fuel source for the hybrid dual nozzle GTs as natural gas, biogas, producing gas, methane, liquefied petroleum gas, or propane. Researchers have discovered that increasing engine speed, injection time, and pilot fuel volume improved thermal efficiency in dual-fuel engines and hence concluded that before gaseous fuels can be used in a long-term dual-fuel engine, much work must be done on their ignition characteristics. Standard diesel engines and "gas-diesel engines" behave very differently. Finally, the chapter discussed the impact of hybrid system design and configuration on optimization and control challenges in detail. Dual-fuel gas turbine architecture, power generator design philosophy, gas turbine cycle optimization approach, and evaluation of gas turbine power plant performance were also reviewed to kick start the methodology and mathematical model.

CHAPTER THREE: GAS TURBINE POWER PLANT MODELLING

3.1 Introduction

In this section, the application of the gas turbine (GT) model parameterisation to obtain a simplified model for both the design and simulation of the proposed dual nozzle GT control system is presented. The development will consider only the most essential components in modelling the exact GT model for feedback linear control applications [54, 55]. Also considered was tank level control for both GT fuel supply systems from external to onboard tank system with dynamic characteristics analysis for control system design simulation with dual nozzle effect.

3.2 Gas Turbine approximate model

Mathematically the GT systems are defined as three major components: the compressor, the combustion chamber (CC), and the turbine (or turbine generator). In Figure 3.1, the simplified schematic arrangement of the GT model [54] required for the approximation was established. The following underlining factor were considered in building the GT dual fuel model:

- In the CC a single volume control was assumed.
- It is hypothesised that two-state variables will accurately represent the liquid and natural gas thermodynamic behaviour in the CCP and the CCT, respectively.
- At any given time during operation, only one liquid or fuel source is allowed to flow into the CC with pilot fuel during LNG flow.
- The ideal gas law applies to the liquid contained within the CC. The inlet guide vanes (IGV), and fuel valves are modelled with a linear first-order dynamic approach for proper functionalities.
- Only one fuel rail nozzle would be activated during the fuel supply process.
- Discrete control logic is assumed for switching logic.

- It is possible to control the pressure of the fuel flow by using a differential pressure valve.
- This feedback element has the same fuel control and ignition control characteristics.

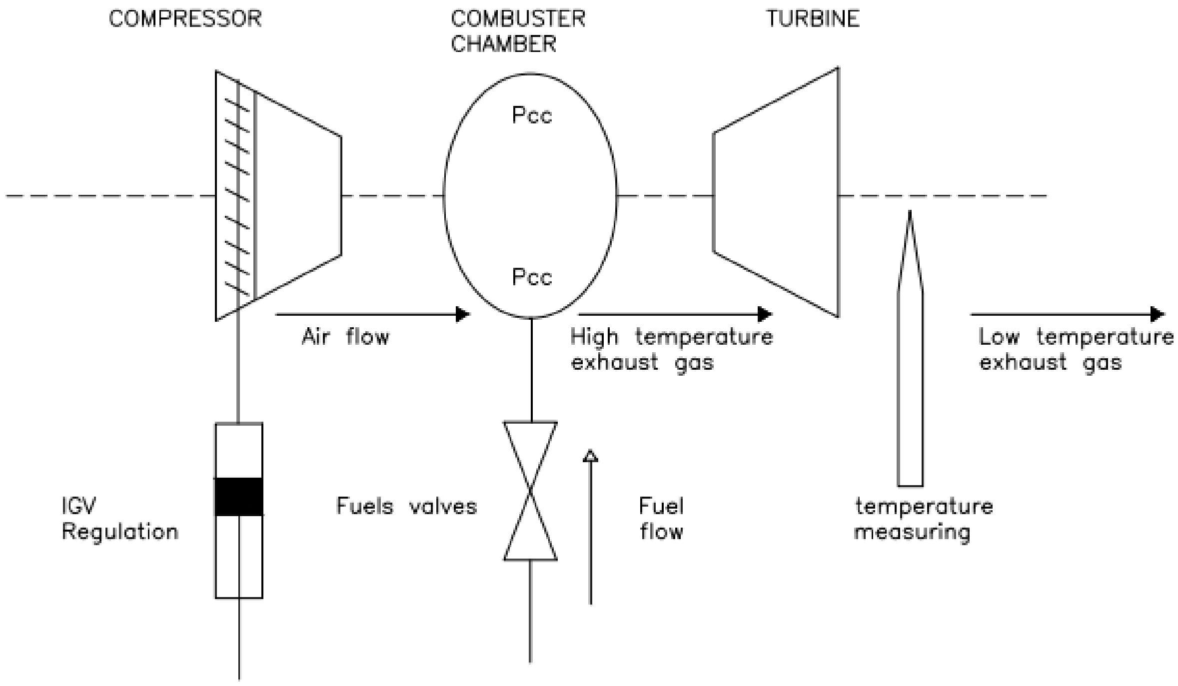

Figure 3.1: Typical heavy-duty gas turbine (GT) schematic layout

3.2.1 Compressor modeling

The first component of the model is a compressor, and the modelling is achieved by using a continuity equation to evaluate the volumetric flow in the CC to establish the mass balance equation. The continuity equation generally is obtained based on the principle that the difference between mass inflow into a CC and mass outflow from the CC is the equal time rate of change occurring in the CC. When this principle is applied to the compressor system of the GT, the result is expressed in equation (3.1) [54].

$$m_a + m_f - m_e = V_{cc}\left(\frac{d_{pcc}}{dt}\right) \qquad 3.1$$

m_a, m_f, and m_e represent the mass flows of air, fuel, and high–temperature exhaust gas in kilogrammes per second; Vcc represents the volume of CC in cubic metres, and *pcc* represents the density of CC air in kilogrammes per cubic metre. The ideal gas law, denoted by CC, can be expressed as:

$$\boldsymbol{\rho_{cc}(t) = \frac{P_{cc}\,(t)}{R_e\,T_{cc}(t)}} \qquad 3.2$$

P_{cc} denotes the compressor pressure in Pa, Tcc the compressor temperature in K, and Re the exhaust gas constant in J/KgK. This is obtained by differentiating equation (3.2) with respect to time and substituting the energy balance equation for the CC into equation (3.1).

$$m_a + m_f - V_{cc}\left(\frac{\frac{dP_{cc}\,(t)}{dt}}{R_e\,T_{cc}\,(t)} - \frac{P_{cc}\,(t)}{R_e\,T_{cc}\,\,(t)^2}\,\,\frac{dT_{cc}\,(t)}{dt}\right) \qquad 3.3$$

Using the principles of energy balance equation, to the CC,

$$m_a\,c_{pa}\,T_a + m_f H_f - \,m_e\,H_e = \frac{d}{dt}\,(V_{cc}\,\rho_{cc}\,(t)U\,(t)) \qquad 3.4$$

C_{pa}denotes the specific heat at constant pressure in J/kgK, Ta denotes the air temperature entering the CC in K, and Hf represents the lower heating value of the fuel. He describes the exhaust gas's enthalpy at the CC outlet in J/kgK, and U denotes the control volume's internal energy in J/kg.

The following relationship was obtained by applying the ideal gas law and considering equation (3.2):

$$\frac{d}{dt}\,(V_{cc}\,\rho_{cc}\,(t)U\,(t)) = \left(C_{pe} -\,R_e\right)T_{cc}\,(t)\,V_{cc}\,\frac{d\rho_{cc}\,(t)}{dt} + \frac{dT_{cc}\,(t)}{dt}\,\,\frac{P_{cc}\,(t)\,V_{cc}}{R_e\,T_{cc}\,(t)}$$
$$\left(C_{pe} -\,R_e\right) \qquad 3.5$$

C_{pe} is the specific heat of the exhaust gas at constant pressure in *J/kgK*.

When substituting equation (3.1) for equation (3.5) and taking into account equation (3.4), the equation of the CCT was obtained as follows:

$$\frac{dT_{cc}(t)}{dt} = \frac{T_{cc}(t)R_e}{P_{cc}(t)} \left\{ \frac{[(R_e - C_{pe})T_{cc}(t) + c_{pa}T_a]\, m_a}{V_{cc}(C_{pe} - R_e)} + \frac{[(R_e - C_{pe})T_{cc}(t) + H_f]\, m_f - R_e T_{cc}(t)\, m_e}{V_{cc}(C_{pe} - R_e)} \right\} \qquad 3.6a$$

Furthermore, by combining equations (3.3) and (3.6a), the dynamic equation of the CCP would be obtained:

$$\frac{dT_{cc}(t)}{dt} = \frac{R_e}{V_{cc}(C_{pe} - R_e)} \left(m_a c_{pa} T_a + m_f H_f - m_e c_{pe} T_{cc} \right) \qquad 3.6b$$

T_a and m_e can be expressed as:

$$\boldsymbol{m_e = Ma_0 \frac{\sqrt{T_{cc}N}}{P_{cc}N} \frac{P_{cc}}{\sqrt{T_{cc}}}} \qquad 3.7a$$

$$\boldsymbol{T_a = \frac{T_{amb}}{\eta_c} \left[\left(\frac{P_{cc}}{P_{amb}} \right)^{\frac{R_a}{c_{pa}}} + \eta_c - 1 \right]} \qquad 3.7b$$

T_{amb} and P_{amb} denote the ambient temperature and pressure, respectively; M_{a0}, $P_{cc}N$, and TccN denote the rated airflow, CCP, and temperature of the compressor in Kg/s, Pa, and K, respectively; and η_c represents the compressor efficiency.

3.2.2 Modeling of air and fuel system

This section considers and models the dynamic characteristics of the CC system's air and fuel flow intake. Air intake from Figure 3.1 is regulated and controlled by the inlet guide van (IGV), allowing about 60% (the allowable % provider better fuel to air ratio in the burning process) of the airflow into the CC for combustion. Fuel into the CC is controlled by a pressure valve which manages the pressure of the dual-fuel to select and allow the available fuel supply to the CC at a particular time. The fuel logic is pressure sensitive to prevent plant fluctuation during the transition.

The inlet system is modelled according to the following dynamics:

$$\begin{cases} \frac{dm_a}{dt} = \frac{K_{igv}}{\tau igv} m_a^* - \frac{1}{\tau igv}\, m_a \\ \frac{dm_f}{dt} = \frac{K_{at}}{\tau_{at}} m_f^* - \frac{1}{\tau_{at}}\, m_f \end{cases} \quad 3.8$$

m_{a^*} and m_{f^*} denote the desired air and fuel flow in kilogrammes per second. The static gains of the two intake channels are represented by K_{igv} and K_{at}, while the IGV and fuel valve time constants are denoted by τ_{igv} and τ_{at}. Additionally, the IGV has a maximum opening and closing speed that is modelled only at saturation, limiting the dm_a /dt ratio. The GT's control objective is to regulate generated power (i.e., maintaining a constant exhaust gas temperature (EGT) for optimal power plant operation) by following a programmed power reference in the primary external controller. The EGT is calculated by performing an adiabatic transformation on the expression.

$$T_{ex} = T_{cc}\,(t)\eta_t \left[\left(\frac{P_{amb}}{P_{cc}\,(t)} \right)^{\frac{R_e}{c_{pe}}} + \frac{1}{\eta_t} - 1 \right] \quad 3.9$$

η_t- the adiabatic efficiency of the turbine. It is essential to consider the instrument dynamics when designing a control architecture to estimate the EGT. This is because measuring the EGT can be difficult because of the large amount of mass flow and consequently slow meter time constant tc required for accurate measurement of the EGT. The following is a detailed description of the dynamics of the EGT measurement:

$$\frac{dT_{exm}}{dt} = \frac{1}{\tau_{at}} T_{ex} - \frac{1}{\tau_{tc}} T_{exm} \quad 3.10$$

Hence, the state equation defining the power measurement can be expressed as:

$$\frac{dT_{exm}}{dt} = \frac{1}{\tau_{tc}} \left[T_{cc}\eta_t \left[\left(\frac{P_{amb}}{P_{cc}(t)} \right)^{\frac{R_e}{C_{Pe}}} + \frac{1}{y_t} - 1 \right] T_{exm} \right] \quad 3.11$$

The actual power output from the gas turbine P_{gt} can be obtained by the principle of the energy balance equation.

$$P_{gt} = (P_t - P_c)\eta_{el} \qquad 3.12a$$

The parameters P_c and P_t are computed using:

$$P_c = m_a C_{pe}(T_a - T_{amb}) \qquad 3.12b$$

$$P_t = m_a C_{pe}(T_{cc} - T_{ex}) \qquad 3.12c$$

Electric power can also be estimated using the energy balance equation between the mechanical power available at the turbine shaft and the power generated and consumed by the compressor. The following accurately evaluates electric power output expressed as a function of the state variable:

$$P_{gt}(t) = M_{a0}\frac{\sqrt{T_{ccN}}}{P_{cc\,N}}C_{pe}\eta_t\eta_{el}p_{cc}\,(t)\sqrt{T_{cc}}\,(t)\left[1-\left(\frac{P_{amb}}{P_{cc}\,(t)}\right)^{\frac{R_e}{c_{pe}}}\right] - m_a c_{pa}(\,T_a - T_{amb}) - \eta \qquad 3.13$$

η - the efficiency with which the electric generator operates. According to the meter dynamics, the electrical power out is considered to have a negligible measurement time constant compared to the instrument's thermal dynamics. The approximate model of GT would result in the following fifth-order nonlinear system:

$$x = f(x) + G(x)u \qquad 3.14a$$

$$y = h(x)$$

where x is the state vector.

$$x = \begin{bmatrix} x_1 \\ x_2 \\ x_3 \\ x_4 \\ x_5 \end{bmatrix} = \begin{bmatrix} P_{cc} \\ T_{cc} \\ m_a \\ m_f \\ T_{exm} \end{bmatrix} \qquad 3.14b$$

u input vector

$$u = \begin{bmatrix} u_1 \\ u_2 \end{bmatrix} = \begin{bmatrix} \dot{m}_a \\ \dot{m}_f \end{bmatrix} \tag{3.15}$$

and y is the output vector

$$y = \begin{bmatrix} y_1 \\ y_2 \end{bmatrix} = \begin{bmatrix} P_{gt} \\ T_{exm} \end{bmatrix} \tag{3.16}$$

In particular, one has

$$f(x) = \begin{bmatrix} \frac{R_e}{V_{cc}\,(C_{pe} - R_e)} \left[x_3\, c_{pa}\, T_a(x_1) + x_4 H_f - c_{pe} x_2 m_e(x_1, x_2)\right] \\ \frac{x_2 R_e}{x_1} \frac{\left[\,(R_e - C_{pe})\, x_2 + c_{pa}\, T_a(x_1)\,\right] x_3 + \left[\,(R_e - C_{pe})\, x_2 + H_f\right] x_4 - R_e\, x_2 m_e(x_1, x_2)}{V_{cc}\,(C_{pe} - R_e)} \\ -\frac{1}{\tau igv}\, x_3 \\ -\frac{1}{\tau igv}\, x_3 \\ \frac{1}{\tau_{tc}} \left(x_2 \eta_t \left[\left(\frac{P_{amb}}{x_1}\right)^{\frac{Re}{cpe}} + \frac{1}{\eta_t} - 1 \right] - x_5 \right) \end{bmatrix} \tag{3.17}$$

$$G(x) = \begin{bmatrix} 0 & 0 \\ 0 & 0 \\ \frac{K_{igv}}{\tau igv} & 0 \\ 0 & \frac{K_{ta}}{\tau_{tc}} \\ 0 & 0 \end{bmatrix}$$

$$h(x) = \begin{bmatrix} h_1(x) \\ h_2(x) \end{bmatrix} = \begin{bmatrix} M_{a0} \frac{\sqrt{T_{cc} N}}{P_{cc}\, N}\, C_{pe} \eta_t \eta_{el} x_1 \sqrt{x_2} \left(1 - \left(\frac{P_{amb}}{x_1}\right)^{\frac{Re}{cpe}} \right) - x_3 c_{pa}\, (T_a(x_1) - \\ x_5 \\ T_{amb}) \eta_{el} \end{bmatrix} \tag{3.18}$$

3.3 Modeling dual fuel supply line for the Gas Turbine Plant

When modelling the fuel supply line, dynamics such as pressure and gas mass balance conditions were considered, to derive dynamic equations based on the liquid and gas pipeline [73], as described previously. This began by considering the pressure drops experienced by liquids.

$$P - P_{Lout} = \frac{C_L P_L q_{Lout}^2 - P_L gh}{gc} + \Delta P_L CV \quad 3.19$$

Where, P is liquid pressure, C_L is the liquid leg's overall coefficient, which can be calculated as follows:

$$C_L = \sum_{i=1}^{n} \frac{8 f_{Li} L_{Li}}{d_{Li}^5 \pi^2} + \sum_{j=1}^{m} \frac{8 K_{Li}}{d_{Li}^5 \pi^2} \quad 3.20$$

By evaluating the liquid control flow rate, the equation (3.2) can be used to determine the $\Delta P_L CV$ pressure drop across the liquid control valve

$$q_{Lout} = (0.002228) CV \sqrt{\frac{\Delta P_L CV}{\delta_L}} \quad 3.21$$

$$\Delta P_L CV = \frac{q_{Lout}^2 \delta_L}{(0.002228)^2 C_v^2} \quad 3.22$$

The total pressure drop across the liquid leg of the gas turbine's liquid supply line is calculated by substituting equation (3.24) into equation (3.21), as shown in the following equation:

$$P - P_{gout} = \frac{C_L P_L q_{Lout}^2}{gc} - \frac{P_L gh + q_{Lout}^2 \delta_L}{(0.002228)^2 C_V^2} \quad 3.23$$

The discharge flow rate was obtained by differentiating equation (3.25), which was done with respect to time.

$$\boldsymbol{\frac{dp}{dt} = \frac{C_L P_L (2q_{Lout}) \frac{dq_{Lout} - P_L g \frac{dh}{dt}}{dt}}{gc} + \frac{\left(2q_{Lout} \delta_L \frac{dq_{Lout}}{dt}\right)(0.002228)^2 C_V^2 - 2(0.002228^2) C_V q_{Lout}^2 \frac{dC_V}{dt}}{(0.002228^2 C_V^2)^2}} \quad 3.24$$

Taking into account the pressure drops in the gas line and can be obtained by:

$$P - P_{gout} = \frac{C_g P_g q_{gout}^2 - P_g g h}{gc} + \Delta P_g CV \tag{3.25}$$

C_g is the overall flow coefficient of the gas line in this case, which can be calculated as

$$C_L = \sum_{i=1}^{n} \frac{8 f_{gi} L_{gi}}{d_{gi}^5 \pi^2} + \sum_{j=1}^{m} \frac{8 K_{gi}}{d_{gi}^5 \pi^2} \tag{3.26}$$

The pressure drops across the gas line of the GT gas supply line denoted by $\Delta P_g CV$, can be calculated using equation (3.27) and obtained by evaluating as flow rate:

$$Q_{gout} = \frac{14.7}{3600} \sqrt{\frac{T}{(520)\delta g}}\, C_g sin \left[\frac{3417}{C_1}\right] \left[\frac{\Delta P_g CV}{P}\right] \tag{3.27}$$

From eq. (3.26) $\Delta P_g CV$ is obtained as follows:

$$\Delta P_g CV = \left[\frac{C_L}{3417}\right]^2 P \left[arc\ sin \left\{\frac{(3600) q_{gout}}{(14.7) C_g P} \sqrt{\frac{(520)\delta g}{T}}\right\}\right] \tag{3.28}$$

The total pressure drop across the gas line of the gas turbine gas supply line was calculated by substituting equation (3.29) for equation (3.26).

$$P - P_{gout} = \frac{C_g P_g q_{gout}^2 - P_g g h}{gc} + \left[\frac{C_L}{3417}\right]^2 P \left[arc\ sin \left\{\frac{(3600) Q_{gout}}{(14.7) C_g P} \sqrt{\frac{(520)\delta g}{T}}\right\}\right] \tag{3.29}$$

Under the assumption of constant liquid discharge pressure P_{gout} and operating temperature T, equation (3.31) is derivative with respect to time and yields an expression for the change in gas control valve position (GCV).

$$\begin{aligned}\frac{dp}{dt} = &\left(\frac{C_g q_{gout}^2 - gh}{gc}\right)\frac{dPg}{dt} + \frac{Pg}{gc}\left(2Cg q_{gout} \delta_g \frac{dq_{gout}}{dt} - g\frac{dh}{dt}\right) \\ &+ \left[\frac{C_L}{3417}\right]^2 \left[arc\ sin \left\{\frac{(3600) Q_{gout}}{(14.7) C_g P} \sqrt{\frac{(520)\delta g}{T}}\right\}\right] \frac{dP}{dt} + \left[\frac{C_L}{3417}\right]^2\end{aligned} \tag{3.30}$$

$$P\left[\frac{1}{\sqrt{1-\left\{\frac{(3600)q_{gout}}{(14.7)C_gP}\sqrt{\frac{(520)\delta g}{T}}\right\}^2}}\right]$$

$$\left(\frac{(3600)q_{gout}}{(14.7)C_g}\sqrt{\frac{(520)\delta g}{T}}\right)\left[\frac{\frac{dq_{gout}}{dt}C_gP - Q_{gout}P\frac{dC_g}{dt} + C_g\frac{dP}{dt}}{P^2C_g^2}\right] \qquad 3.31$$

The density of gas can be calculated using the equation of state given by:

$$P_g = \frac{PM_g}{DR1T} \qquad 3.32$$

To calculate the density rate of change, equation (3.32) is differentiated

$$\frac{dP_g}{dt} = \frac{M_g}{DR1T}\frac{dP}{dt} \qquad 3.33$$

3.3.1 Liquid mass phase flow

If only the liquid phase is considered, the mass balance for the liquid tank rate of liquid level can be calculated as:

$$\frac{dH}{dt} = \frac{4(dV_L)}{\pi d^2(dt)} \qquad 3.34$$

Additionally, the rate of change of liquid volume can be calculated using:

$$\frac{dV_L}{dt} = q_{Lin} - q_{Lout} \qquad 3.35$$

The mass balance equation for the rate of change in the gas phase of the gas tank is as follows:

$$\frac{dn_g}{dt} = (q_{gin} - q_{gout})\,\frac{P_g}{M_g} \qquad 3.36$$

By solving the derivate state equation $PV_g = n_g DRT$ with respect to time, the rate of change of storage tank pressure in a mole can be determined. As a result, the rate at which the volume of gas changes is equal.

$$V_g\frac{dP}{dt} = DR1T\frac{dn_g}{dt} - P\frac{dV_g}{dt} \qquad 3.37$$

The following equations establish a relationship between the rate of change of a gas and a liquid at a constant volume.

$$\frac{dV_g}{dt} = -\frac{dV_L}{dt} \qquad 3.38$$

By substituting equations (3.35), (3.36), and (3.37) into equation (3.38), the volumetric rate of change for both gas and liquid pressure can be determined.

$$V_g\frac{dP}{dt} = DR1T\frac{P_g}{M_g}(q_{gin} - q_{gout}) + P(q_{Lin} + q_{Lout}) \qquad 3.39$$

Hence, the volume of gas is $V_g = (h_{GL} - h)\ \frac{\pi}{4}d^2$

3.4 External fuel line control model for GT

External fuel control models are used to simulate the dynamic location of the gas and liquid loop control valves. Both setups include sensors, control valves, pneumatic transmission lines, and controllers. The controller compares the liquid level variable to the setpoint value of the error signal e(t) to estimate the control variable u(t) that drives the actuator (t). The MPC controller was used as a reference for the PIDs, while the PIDs controlled parameters in each fuel loop are protected against further disturbance signals. A PID controller's design will be evaluated by comparing the system's variables to the controller's equation.

$$\Delta u = Kc\left(e(t) + \frac{1}{t_i}\int edt + \frac{de}{dt}\right) \qquad 3.40$$

From equation (3.40), Δu is the controller output signal. The data sign indicates the difference between a controller output variable's initial and actual value. 4-20mA transducer signal is used to calculate the controller error, which is estimated using the equation (3.42) [47–43] based on u min and u_{min} $and\ u_{max}$.

$$e = e_s - e_r \qquad 3.41$$

$$e_s = 4 + 16\left(\frac{u_s - u_{min}}{u_{max} - u_{min}}\right) \qquad 3.42$$

$$e_r = 4 + 16\left(\frac{u - u_{min}}{u_{max} - u_{min}}\right) \qquad 3.43$$

Substituting equations (3.43 and 3.44) into equation (3.42), results in the following equation:

$$e = K_T(u_s - u) \qquad 3.44$$

$$K_T = \left(\frac{20-4}{u_{max} - u_{min}}\right) \qquad 3.45$$

Equation (3.46) is used to establish a relationship between the controller's output and the control of liquid level or pressure level by substituting into equation (3.42), and KT is the gain [73].

$$\Delta u = KcK_T(u_s - u) + \quad \frac{1}{t_i}\int (u_s - u)dt - \frac{d}{dt}(u_s - u) \qquad 3.46$$

3.4.1 Pneumatic actuator delay line

The output of the controller can be either current or voltage. Converting these values to liquid requires applying a scaling factor of 4-20mA to the current loop and 1-5V for Voltage [71].

$$P_c = P_{vmin} + P_{vmin} - P_{vmax}\left(\frac{e_c - 4}{20-4}\right) \qquad 3.47$$

The controller output pressure, Pc, and the upper and lower limits of the pneumatic pressure required to activate the valve, P_{vmin}, and P_{vmax}, are less than or equal to the controller output pressure, Pc. Pi will equal the initial control valve's (IPCV) pressure plus pneumatic pressure (Pn). If the initial pressure at the control valve is Pi, the available pneumatic pressure (Pn) can be calculated as follows:

$$P_n = P_c + (P_i - P_c)e^{-t/\tau_1} \qquad 3.48$$

3.4.2 Pneumatic control valve

A first-order model equation was used to simulate a pneumatic control system.

$$\frac{dx}{dt} = P_{vmax} - P_{vmin} - \left(\frac{(P_{vmax} - P_{vmin})}{100}\right)\frac{100}{(P_{vmax} - P_{vmin})\tau_2} \qquad 3.49$$

But

$$\tau_2 = \frac{t}{In\left(\frac{100}{100-x}\right)} \qquad 3.50$$

3.5 Liquid fuel control loop of GT

Equation (3.48) is implemented to obtain the dynamic model for the liquid loop. The controlled variable u is substituted for the liquid height h and solve for h, resulting in an expression for the dynamic model of the liquid control loop based on the valve characteristics used to control the liquid height.

$$C_v = K_L x \qquad 3.51$$

The derivative of equation (3.51) will yield the following expression:

$$\frac{dC_v}{dt} = K_L\left\{15 - P_{vL}\frac{12}{100}\left(\frac{C_v}{K_L}\right)\right\}\frac{100}{12\tau_{2L}} \qquad 3.52$$

The constant of the liquid control valve is denoted by K_L, and a pressure range of 3-15 psi is assumed for this application. P_{vL} is calculated with the help of the formula below.

$$P_{vL} = 3 + 12\left\{\frac{e_{0L} + K_{cL}K_{TL}\left(\Delta h + \frac{1}{t_i}\int \Delta h dt - t_{dL}\frac{dh}{dt}\right) - 4}{16}\right\}$$

$$+\left\{P_{wL}\left[3 + 12\frac{e_{0L} + K_{cL}K_{TL}\left(\Delta h + \frac{1}{t_i}\int \Delta h dt - t_{dL}\frac{dh}{dt} - 4\right)}{16}\right]\right\} e^{-t/\tau_{2L}} \qquad 3.53$$

But $\Delta h = h_s - h$

3.6 Gas fuel control loop of GT

Three configurations can be employed for modelling in the gas control loop system. The levels of the liquids can be manipulated, for example, to regulate the pressure of the gas, monitor the level of the liquid, or adjust the liquid's location. To manage the pressure, the generic expression may be as follows:

$$P_{vg} = 3 + 12\left\{\frac{e_{0g} + K_{cg}K_{Tg}\left(\Delta P + \frac{1}{t_i}\int \Delta P dt - t_{dL}\frac{dP}{dt}\right) - 4}{16}\right\}$$

$$+\left\{P_{wg}\left[3 + 12\frac{e_{0g} + K_{cg}K_{Tg}\left(\Delta P + \frac{1}{t_i}\int \Delta P dt - t_{dL}\frac{dP}{dt}\right) - 4}{16}\right]\right\} e^{-t/\tau_{2g}} \qquad 3.54$$

But $\Delta P = P_s - P$

If it is to be used to control level, g has to be replaced with L or, for displacement, replace g by x.

Similarly, $\Delta L = L_s - L$ or $\Delta x = x_s - x$

3.7 GT dual nozzle fuel control strategy and dynamic simulation

In Figure 3.2, the dynamic simulation model and control techniques are developed. This diagram depicts the entire GT control process, which includes signal conditioning and processing and the control instruments used to operate them. Additionally, the use of a combination of pressure control and gas control and integrated liquid level management via liquid and gas control valves is quite common.

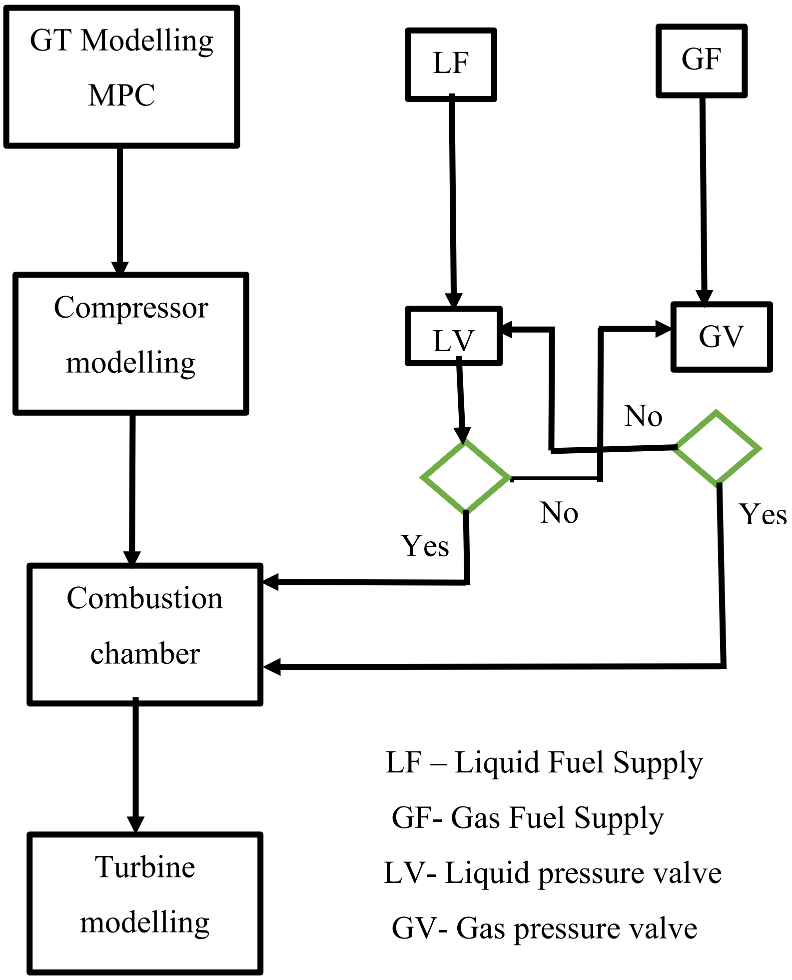

Figure 3.2: GT fuel supply model for dynamic control

3.7.1 GT fuel line simulator development

It is now easier to analyse and design a controller that can control the entire process. The dynamic modelling of various control devices considered in the previous articles, led us to build a Simulink/MATLAB design. Figures 3.3 and 3.4 show the physical system block diagrams for the liquid and pressure loops, respectively [73].

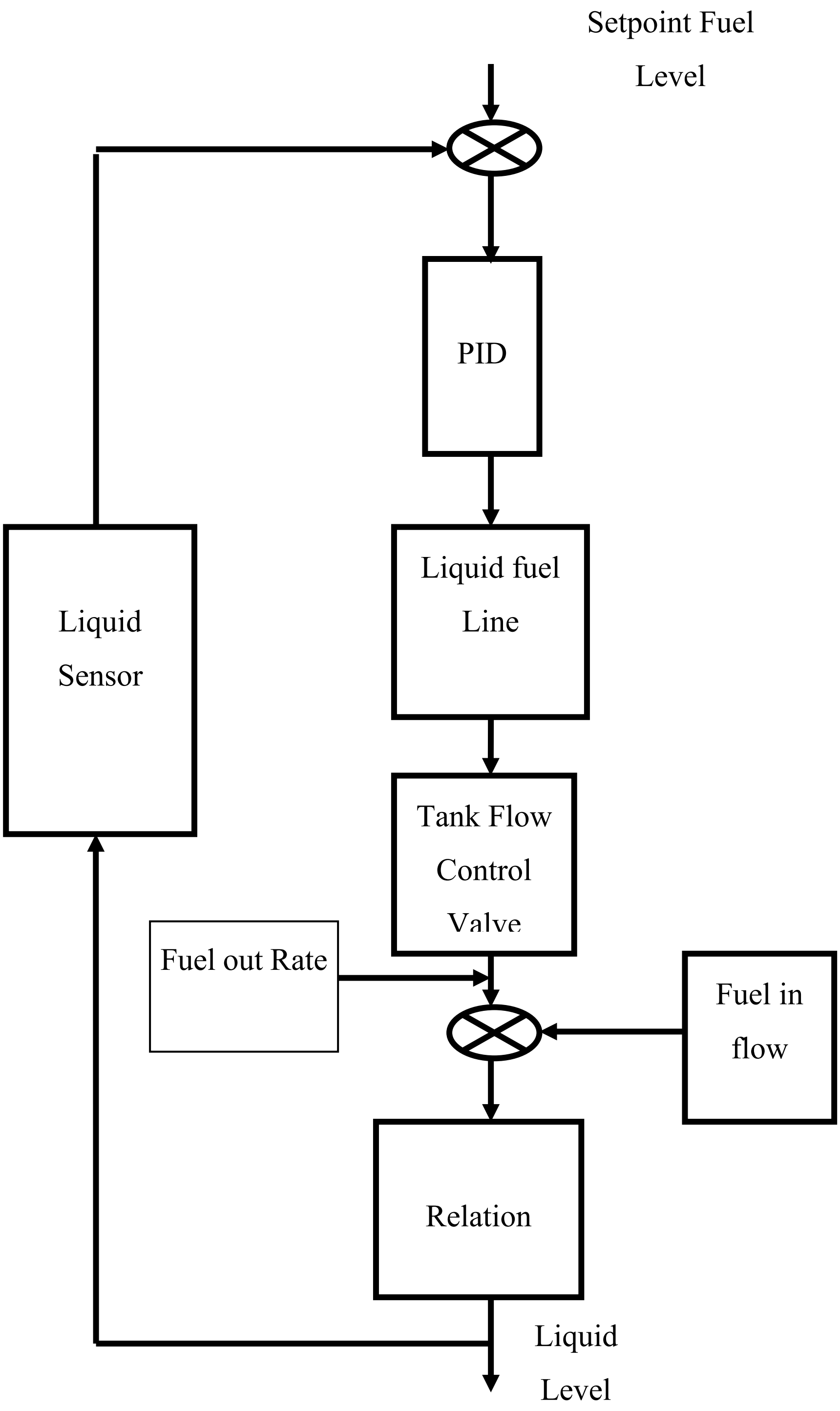

Figure 3.3: Block diagram of a liquid fuel level control loop

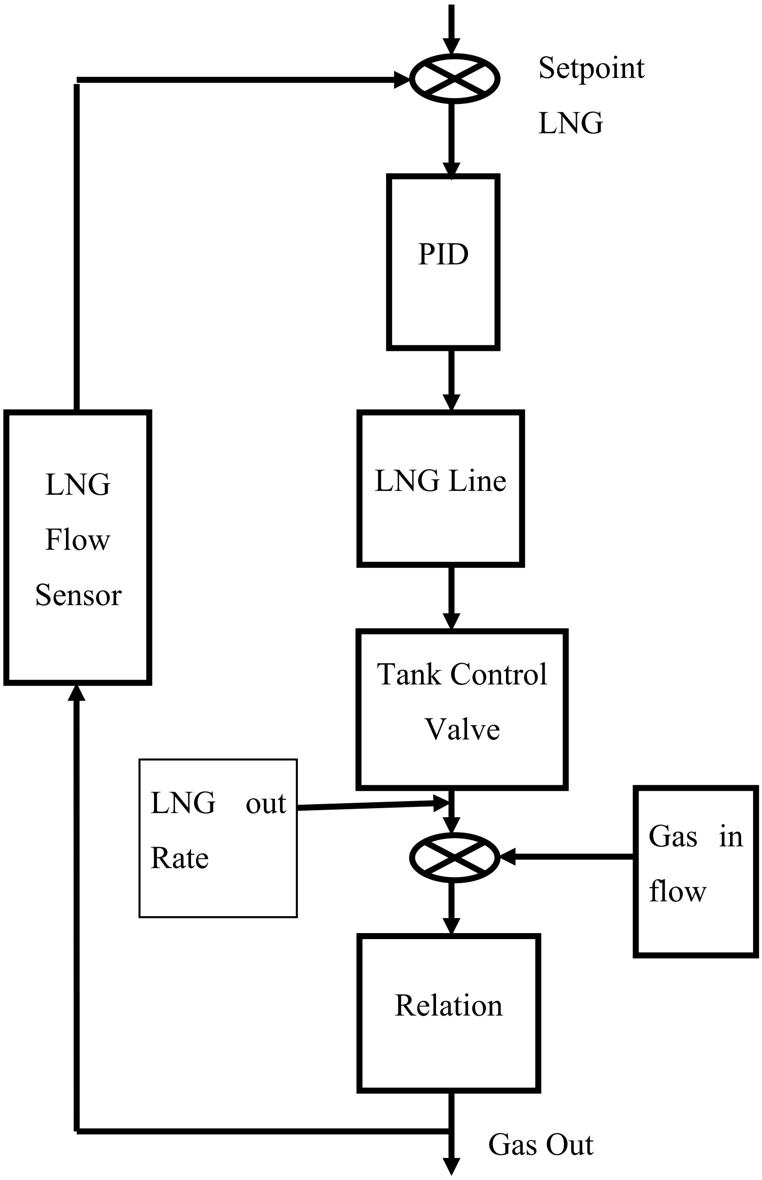

Figure 3.4: Block diagram of LNG Level control loop

3.7.2 Formulation linear models

It is appropriate to use a linearised model in Simulink/MATLAB to obtain the system equation and make complex mathematical manipulation to get the dynamic transfer function for various control loops more straightforward. Figures 3.5 and 3.6 depict the linear model shown in Figures 3.3 and 3.4.

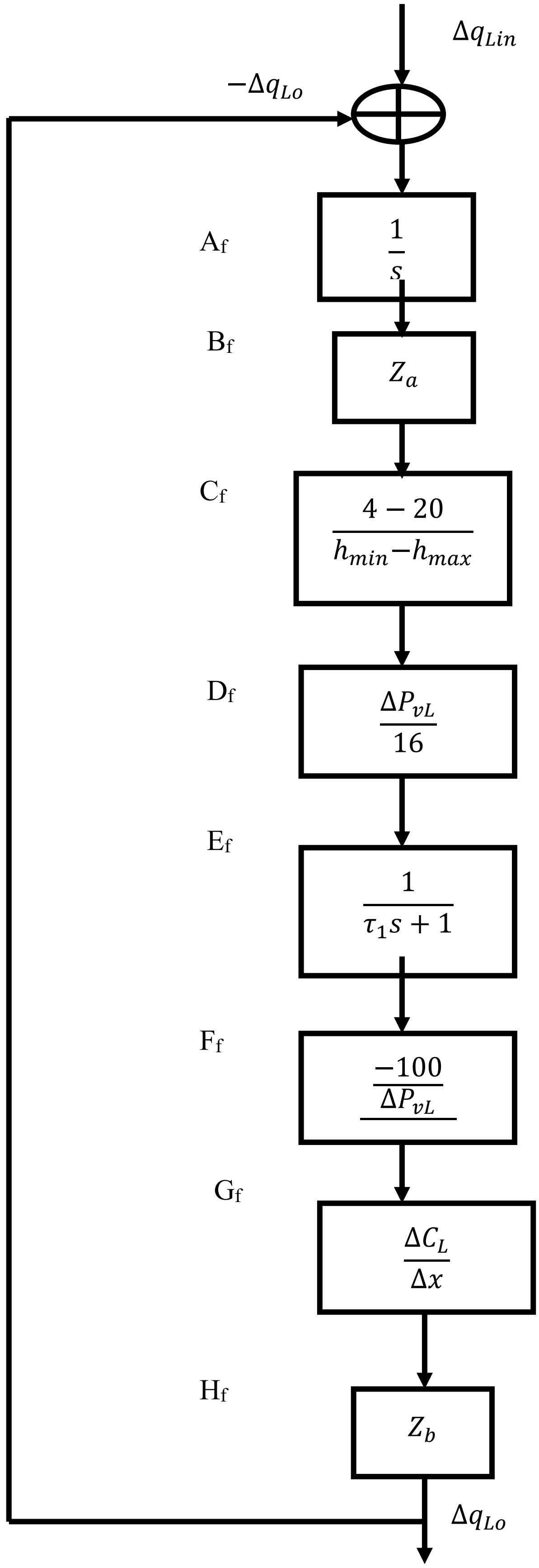

Figure 3.5: Linearized model of the fuel control loop of LFT

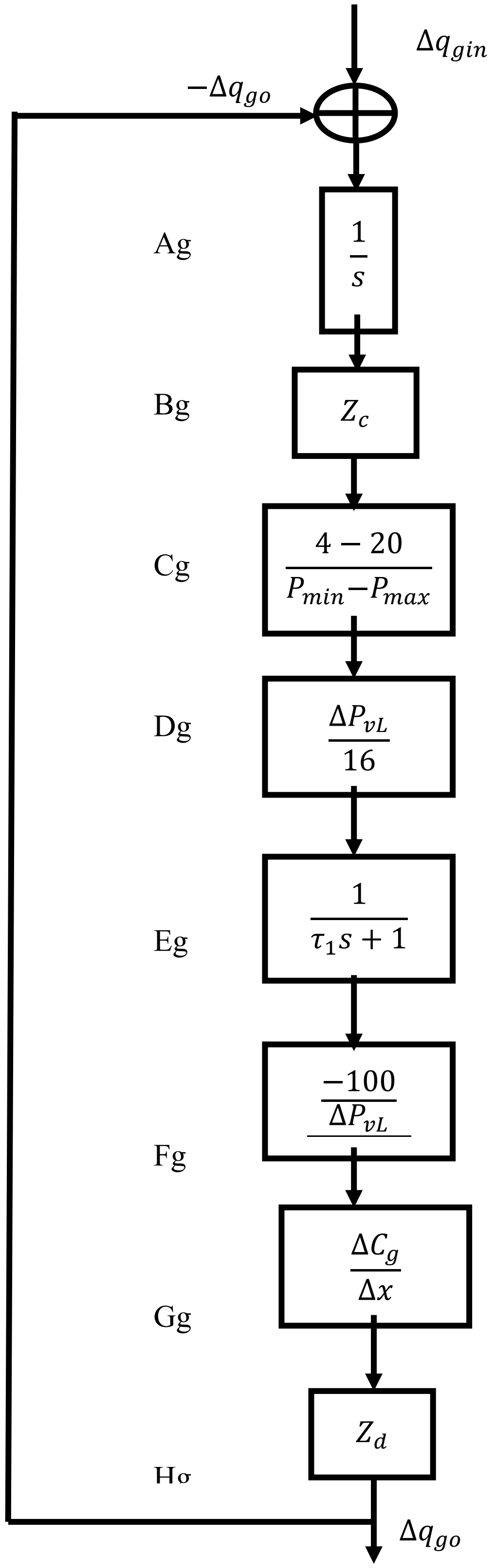

Figure 3.6: Linear Model of LNG control of GFT

3.7.3 Integrating liquid and gas control loop of GT

Because the multi-fuel line is supplied to GT input, the two systems are integrated to model a complete GT fuel management system. In the end, this results in a multi-input and multi-output system with various relationships, as illustrated in Figure 3.7. In addition, to make complex calculations of the transfer function, which will be used for controller design in the following chapter, the linear model of the multi-system shown in Figure 3.8 [73] is constructed, which simplifies the calculations.

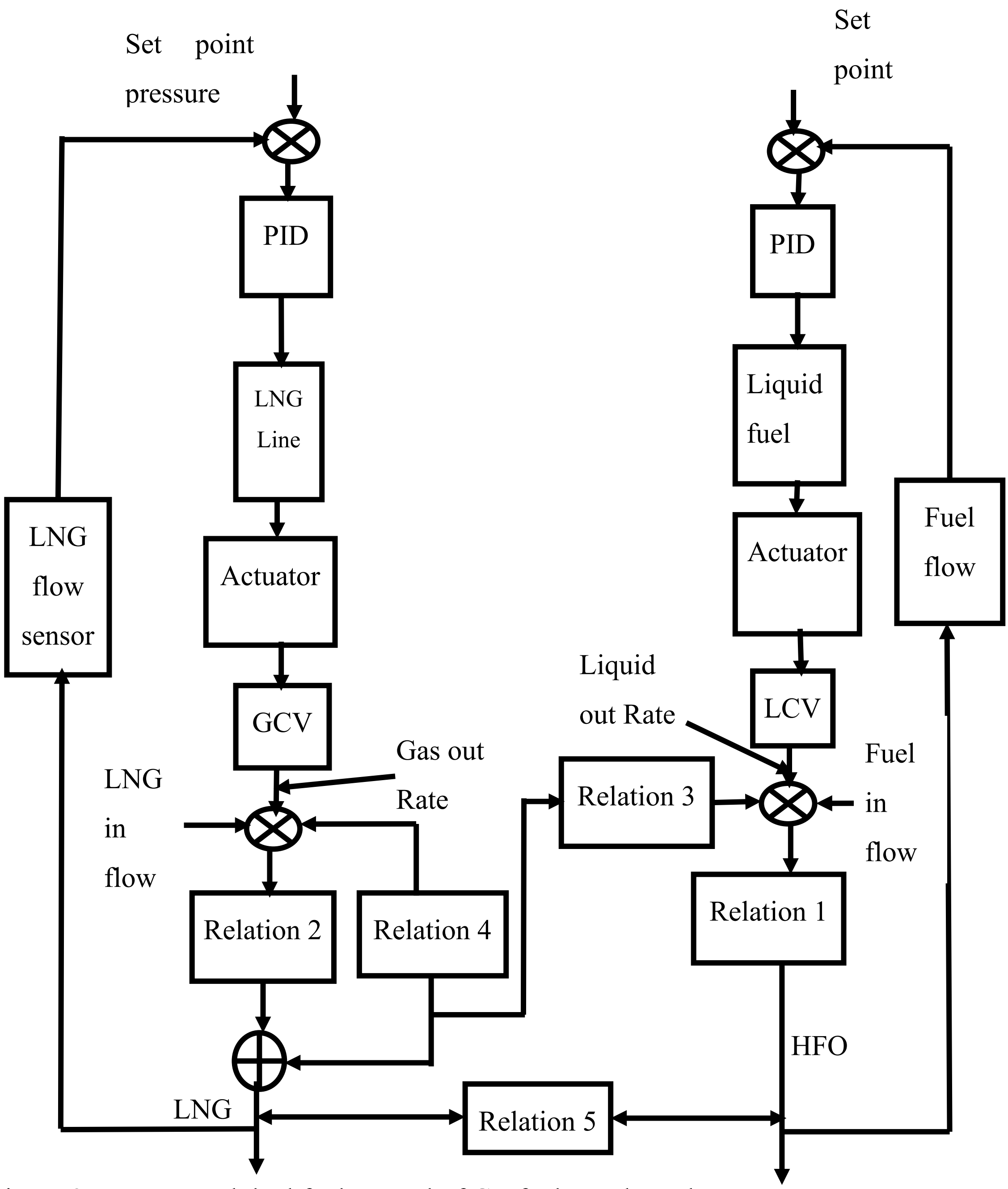

Figure 3.7: Integrated dual fuel control of GT fuel supply tank

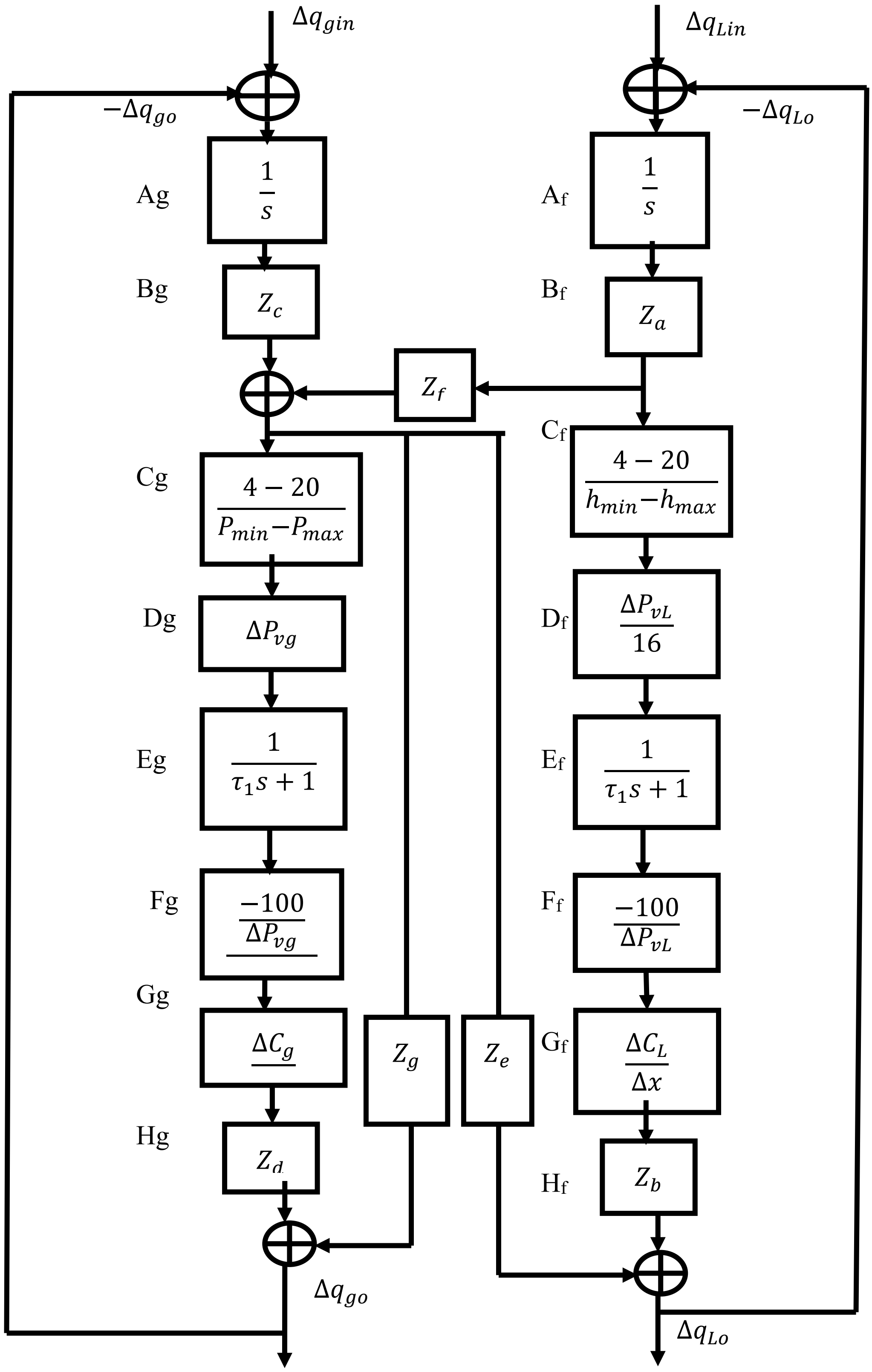

Figure 3.8: Linearized Model of integrated dual fuel control of GT fuel supply

3.7.4 Mathematical evaluation of GT fuel supply model

The GT fuel supply model design parameter are presented in Tables 3.1 and 3.2. A similar model for a different purpose was built by the University of Tulsa Chemical Engineering Department based on these requirements [73].

Table 3.1: LCV fuel level control parameter for modelling

SYMBOL	DESCRIPTION	UNITE	VALUE
P_{set}	Liquid Fuel Tank (LFT) set point pressure	psi	30
P_{Lout}	Liquid discharge pressure	psi	25
δ_L	Specific gravity of a liquid		1
h_{min}	Low fuel level	cm	2
h_{max}	High fuel level	cm	4
d_{LFT}	Fuel Tank size	cm	.25
Cv/x	The rate of change of the flow coefficient over the rate of change of the valve opening at the setpoint is the characteristic of the control valve.		0.5
τ_1	Valve time constant	s	2
τ_2	Actuator time constant	s	0.2
C_v			17.8

Table 3.2: LNGCV liquid level control parameter for modeling

SYMBOL	DESCRIPTION	UNITE	VALUE
P_{set}	LNG tank setpoint	psi	30
P_{gout}	LNG discharge	psi	28
δ_g	Specific gravity of a gas		1
T	Temperature	K	540
H_{set}	Setpoint gas level	cm	3
H_{GST}	LNG tank hight	cm	8
Vg	LNG Volume	Cub cm	0.25
d_{GST}	LNG tank size	cm	.25
Cl	Cg/Cv		15
Cg/x	The rate of change of the flow coefficient over the rate of change of the valve opening at the setpoint is the characteristic of the control valve.		8
τ_1	LNG control valve time constant	s	2
τ_2	LNG actuator time constant	s	0.2
C_g	LNGCV flow coefficient at setpoint		175

3.7.4.1 Fuel tank level Control Valve

The liquid tank level control model developed in Figure 3.5 has control components described with the letters A_f, B_f, C_f, D_f, E_f, F_f, G_f, and H_f. Dynamically, their parameters are obtained for the simulations with the following equations.

A_f - parameter

In this case, the integrator is responsible for relating the rate of liquid inflow to the volumetric flow rate. So, the inflow and outflow can be expressed in the following ways:

$$\Delta V_L = \frac{d\Delta V_L}{dt} \Delta q_{Lin} - \Delta q_{Lo} = q_{Lin} - q_{Lo} \qquad 3.55$$

Where ΔV_L change in liquid fuel volume. Taking the Laplace transform of equation (3.56), the integrator function previously discussed is obtained.

$$\frac{d\Delta V_L(s)}{V_L(s)} = \frac{1}{s} \tag{3.56}$$

B_f-parameter

In this block, fuel flow in volume is converted to height $\Delta h = h - h_s$ and calculated as follows:

$$Z_a = \frac{\Delta h(s)}{\Delta V_L(s)} = \frac{4}{\pi d^2} = \frac{4}{\pi (0.25)^2} = 20.372 \tag{3.57}$$

C_f-parameter

In this block, fuel level transmitter and gain are estimated with the current loop signal of 4-20mA.

$$\Delta \boldsymbol{e_L} = \frac{20-4}{h_{max}-h_{min}} x(-\Delta h) \tag{3.58}$$

The result by rearranging and taking the Laplace transform of equation (3.58):

$$\frac{\Delta e_L(s)}{\Delta h(s)} = \frac{-16}{h_{max}-h_{min}} = \frac{-16}{4-2} = -8 \tag{3.59}$$

D_f-parameter

This block is another gain converter that converts the controller output current into a pneumatic pressure signal between 3-15 psi that can be used to operate the control valve.

$$\frac{\Delta P_{cL}(s)}{\Delta E_{cL}(s)} = \frac{P_{max}-P_{min}}{20-4} = \frac{5}{16} = 0.3125 \tag{3.60}$$

E_f-parameter

The pneumatic line delay's transfer function is determined.

$$\frac{\Delta P_v(s)}{\Delta P_c(s)} = \frac{1}{\tau_1 s+1} = \frac{1}{0.2s+1} = \frac{5}{s+5} \qquad 3.61$$

F_f-parameter

In this block, the transfer function of the control valve characteristics is determined.

$$\frac{\Delta x(s)}{\Delta P(s)} = \frac{\frac{-100}{P_{vLim}}}{\tau_2 s+1} \qquad 3.62a$$

$$P_{vLim} = P_{vmax} - P_{vmin} \qquad 3.62b$$

The minus sign in equation (3.62) shows that the optimum valve acts opposite direction.

$$\frac{\Delta x(s)}{\Delta P(s)} = \frac{\frac{-100}{15-3}}{2s+1} = \frac{\frac{-100}{12}}{2s+1} = \frac{-16.6}{s+0.5}$$
3.322c

G_f-parameter

The dynamic characteristics of the control valve and its displacement are established. Linear elements are assumed to be present in this case.

$$\frac{\Delta C_v(s)}{\Delta x(s)} = \frac{\Delta C_v}{\Delta x} \qquad 3.63$$

This valve is given as $\frac{\Delta C_v}{\Delta x} = 0.50$

H_f-parameter

The transfer function of the fuel flow rate estimation control valve is shown in this formula. While the flow rate is always proportional to the flow coefficient, the pressure drop across the control valve is constant. This has been established in the following manner:

$$Z_b = \frac{\Delta q_o(s)}{\Delta C_v(s)} = 0.002228\sqrt{\frac{\Delta P_{Lcv}}{\delta L}} = 0.002228\sqrt{\frac{30-25}{1}} = 0.005 \qquad 3.64$$

For simplicity and quick visualisation, the liquid tank level control parameters in the dynamic flow control loop are tabulated in Table 3.3.

Table 3.3: Summary of LCV dynamic design parameter

BLOCK	DESCRIPTION	FUNCTION	PARAMETER/TRANSFER FUNCTION
A_f	flow rate to volume	Integrator	$\frac{1}{s}$
B_f	Volume to pressure	Gain	20.372
C_f	pressure to current	Gain	-8
D_f	current to pressure	Gain	0.3125
E_f	Pneumatic line delay	Model	$\frac{5}{s+5}$
F_f	Control valve response	Model	$\frac{16.6}{s+0.5}$
G_f	Coefficient of flow	Gain	0.5
H_f	Flow estimator	Gain	0.005

3.7.4.2 LNG Gas Control Valve Control Loop

In the LNGCV control loop, the block parameters similar to the LCV control loop is estimated.

Blocks A_f, C_f, D_f, E_f, F_f, and G_f of the GCV control loop are very similar to the LCV control blocks except for Bg and Hg, which are different. The transfer functions are evaluated as follows:

Bg-parameter

As gas pressure increases, the volume of the gas they contain decreases. If the gas column has a steady volume Vg and density is constant, the transfer function can be calculated as follows:

$$\frac{\Delta \boldsymbol{P_g}(\boldsymbol{s})}{\Delta \boldsymbol{Vg}(\boldsymbol{s})} = \boldsymbol{Z_c} \frac{\mathbf{1}}{\boldsymbol{s}} \quad 3.65$$

$$Z_c = \frac{\Delta P_g(s)}{\Delta Vg(s)} \cong \frac{P_s}{Vg_s} = \frac{30}{0.25} = 120 \quad 3.66$$

Hg-parameter

In addition, it provides the transfer function for the method of calculating of a gas flow rate of pressure.

$$Z_d = \frac{14.7}{3600}\sqrt{\frac{T}{(520)\delta g}}\,P_g sin\left[\frac{3417}{C_1}\sqrt{\frac{P_s - P_{go}}{P_s}}\right] \quad 3.67$$

$$= \frac{14.7}{3600}\sqrt{\frac{540}{(520)}}\,30 sin\left[\frac{3417}{15}\sqrt{\frac{30-28}{30}}\right] \quad = \quad 0.826$$

For simplicity and quick visualisation, the LNG gas tank level control parameters in the dynamic flow control loop are tabulated in Table 3.4.

Table 3.4: Summary of LNGCV dynamic parameters

BLOCK	DESCRIPTION	FUNCTION	PARAMETER /TRANSFER FUNCTION
Ag	flow rate to volume	Integrator	$\frac{1}{s}$
Bg	Volume to pressure	Gain	120
Cg	pressure to current	Gain	8
Dg	current to pressure	Gain	0.3125
Eg	Pneumatic line delay	Model	$\frac{5}{s+5}$
Fg	Control valve response	Model	$\frac{16.6}{s+0.5}$
Gg	Coefficient of flow	Gain	8
Hg	Flow estimator	Gain	0.826

3.7.4.3 Integrated GT LCV and LNGCV Control

All other blocks remain the same for LCV and LNGCV when considering the integrated system with relations Ze, Z_f and Zg. Table 3.5 outlines the specifications for the control parameters.

Table 3.5: Integrated GCV liquid control of GT

SYMBOL	DESCRIPTION	UNIT	VALUE
P_{set}	GST setpoint pressure	psi	30
P_{lout}	Fuel discharge pressure	psi	28
δ_L	The specific gravity of a fuel		1
δ_g	The specific gravity of a gas		1
T	Temperature	D	540
Cg	Gas sizing coefficient for normal operation		262
Cv	fuel sizing coefficient for normal operation		17.8
C1	Gas sizing constant		14.70
H_{set}	Setpoint fuel level	ft	3
H_{GST}	Total height of GST	ft	8
Vg	Volume of gas in GST	Cub ft	0.25
d_{GST}	Diameter of GST	ft	.25
Cl	Cg/Cv		15
Cg/x	The rate of change of flow coefficient over the rate of change of valve opening at the setpoint is a control valve characteristic.		4
τ_1	Parameter of control valve related to time response	s	2
τ_2	Time constant of actuator	s	0.2
C_g	LNGCV flow coefficient at set point		175

Z_e-parameter

If the LNGCV position or coefficient is assumed constant and fuel outflow is solely due to the LST pressure, this block shows the effect of the gas rate of flow through the LCV. Functions for the transfer of information are provided:

$$Z_e = \frac{\Delta q_{Lo}(s)}{\Delta P(s)} = \frac{0.002228C_{vs}}{\sqrt{\delta L}}\frac{1}{2}\frac{1}{\sqrt{P_S - P_{Lo}}} = \frac{0.002228 \ x \ 17.8}{1}\frac{1}{2\sqrt{30-28}} = 0.014 \tag{3.68}$$

Zf-parameter

This provides the impact of fuel level on the LNG inflow in the supply line.

$$\boldsymbol{Z_f} = \frac{\Delta \boldsymbol{P}(s)}{\Delta \boldsymbol{h}(s)} = \frac{\boldsymbol{P_s}}{\boldsymbol{h_{GLCC}} - \boldsymbol{h_s}} = \frac{\mathbf{30}}{\mathbf{8-3}} = \mathbf{6} \tag{3.69}$$

Zg-parameter

When the gas flow rate is constant, this block shows how the LNG control valve affects the fuel control valve's position or flow coefficient [83-87].

$$Z_g = \frac{\Delta q_{Lo}(s)}{\Delta P(s)} = \frac{14.7}{3600}\sqrt{\frac{T}{(520)\delta g}}C_g sin\left[\frac{3417}{C_1}\right]\sqrt{\frac{P_S - P_{go}}{P_S}} + cos\left(\frac{3417}{C_1}\sqrt{\frac{P_S - P_{go}}{P_S}}\right) \quad \left(\frac{3417}{C_1}\frac{1}{2}\sqrt{\frac{P_S}{P_S - P_{go}}}\right)\frac{P_{go}}{P_S^2} \tag{3.70}$$

$$= \frac{14.7}{3600}\sqrt{\frac{540}{(520)}}262\left|sin\left[\frac{3417}{15}\right]\sqrt{\frac{30-28}{30}} + cos\left(\frac{3417}{15}\sqrt{\frac{30-28}{30}}\right) \quad \left(\frac{3417}{15}\frac{1}{2}\sqrt{\frac{30}{30-28}}\right)\frac{28}{30^2}\right|$$

= 1.654 or 0.93

Hence, the values of Z terms in the control diagram have been arranged in Table 3.6.

Table 3.6: Summary of integrated fuel dynamic design parameter

BLOCK	DESCRIPTION	FUNCTION	PARAMETER /TRANSFER FUNCTION
Ze	Pressure to fuel outflow rate	Gain	0.014
Z_f	Height to pressure	Gain	6
Zg	pressure to gas	Gain	1.654/0.93

3.8 Modelling of external fuel tank system without controller and onboard coupled

This section models the fluid flow dynamics of the external fuel tank without the influence of controllers and the day tank fuel system. In this case, the valves are set to open at 50% in both cases (Figures 3.9 and 3.11), which equals 100%. A simple Simulink/MATLAB code is used to linearise the operation at the initial condition.

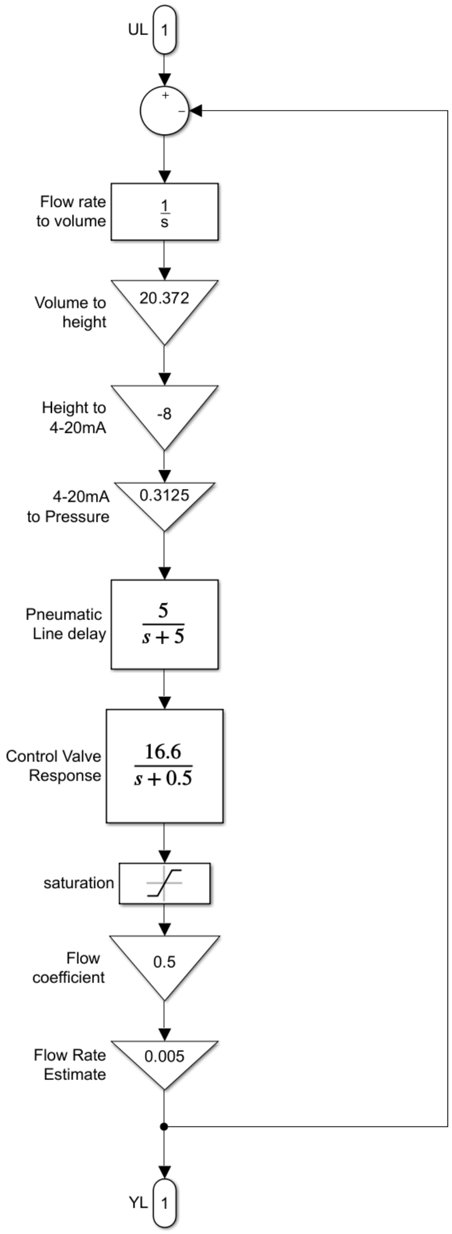

Figure 3.9: Fuel flow rate without controller

From the linearised Figure 3.9 the state equations of fuel control loop are obtained:

$$\begin{vmatrix} \dot{x_1} \\ \dot{x_2} \\ \dot{x_3} \end{vmatrix} = \begin{vmatrix} -5 & 0 & 5 \\ -0.0415 & 0 & 0 \\ 0 & -50.93 & -5 \end{vmatrix} \begin{vmatrix} x_1 \\ x_2 \\ x_3 \end{vmatrix} + \begin{vmatrix} 0 \\ 1 \\ 0 \end{vmatrix} u \qquad 3.71a$$

$$y = \begin{vmatrix} 0.0415 & 0 & 0 \end{vmatrix} \begin{vmatrix} x_1(t) \\ x_2(t) \\ x_3(t) \end{vmatrix} + |0|\, u \qquad 3.71b$$

Using equations (3.71), the dynamic characteristics of the liquid fuel control loop without a controller is estimated to investigate the dynamic factors which produce step response shown in Figure 3.10. The system exhibits a negative response, which indicates that the plant required a compensator design to regulate the flow.

$$G(s) = \frac{-10.57}{s^3+5.5s^2+2.5s-10.57} \qquad 3.72$$

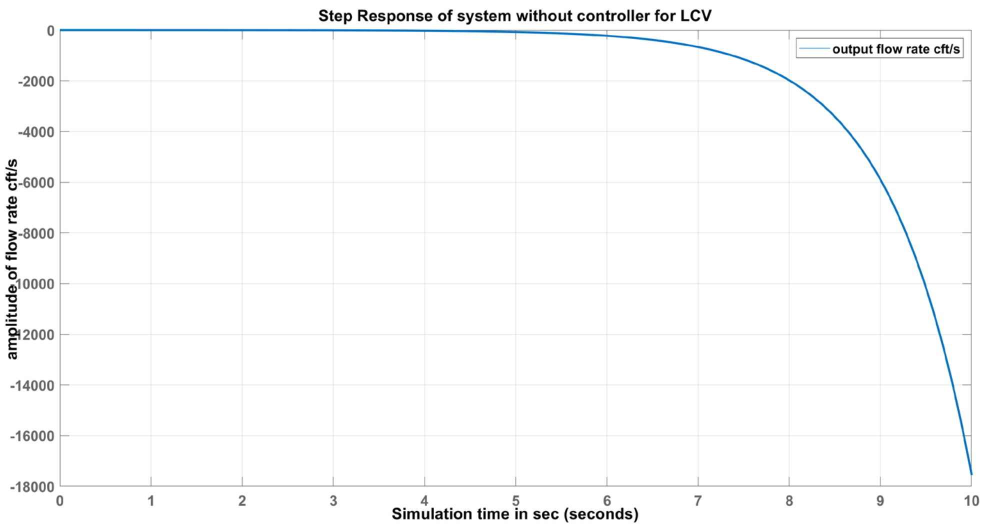

Figure 3.10: Dynamic response of LFCV without the effect of the controller

A linearised model for the GT LNG control loop is developed as shown in Figure 3.11 that enables one to obtain the control loop parameters dynamic study of the LNG flow system.

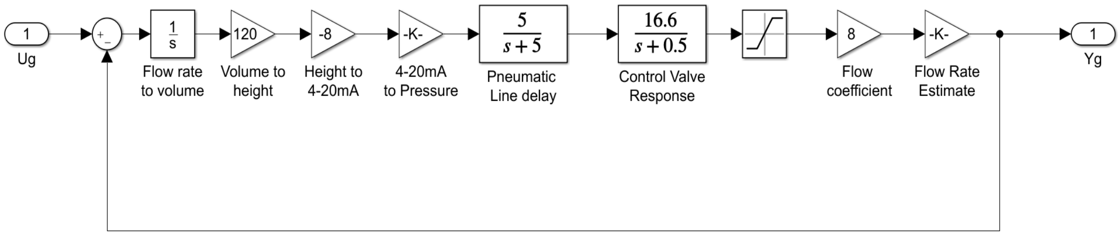

Figure 3.11: LNGCV flow rate without controller

The dynamic modelling of LNGCV produces the model equations modelled in the controller design section.

$$\begin{vmatrix} \dot{x_1} \\ \dot{x_2} \\ \dot{x_3} \end{vmatrix} = \begin{vmatrix} -5 & 0 & 5 \\ -109.6925 & 0 & 0 \\ 0 & -300 & -5 \end{vmatrix} \begin{vmatrix} x_1 \\ x_2 \\ x_3 \end{vmatrix} + \begin{vmatrix} 0 \\ 1 \\ 0 \end{vmatrix} u \qquad 3.73a$$

$$y = |109.6928 \quad 0 \quad 0| \begin{vmatrix} x_1(t) \\ x_2(t) \\ x_3(t) \end{vmatrix} + |0|\, u \qquad 3.73b$$

The transfer function obtained is as follows:

$$G(s) = \frac{-1.645e^{05}}{s^3+5.5s^2+2.5s+1.645e^{05}} \qquad 3.73c$$

Using equations (3.73), the dynamic characteristics of the LNG control loop without a controller is estimated to investigate the dynamic features which produce step response shown in Figure 3.11. The system exhibits a negative answer, indicating that the control required a compensator design to regulate the flow. Figure 3.12 demonstrates the same dynamic characteristics as Figure 3.11 with the overall gain of -1.645e^0.5.

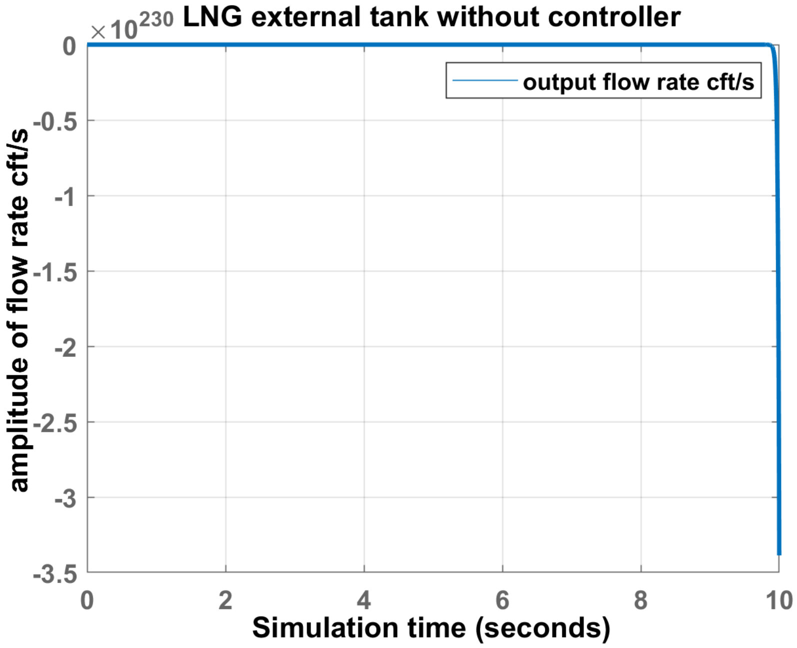

Figure 3.12: Dynamic response of LNGCV without controller

In Figure 3.13, the dual fuel tank system is developed and modelled to examine the dynamic relational characteristics of the two flow control loops. The plant was linearised at a specific operating point using MATLAB script developed to obtain the characteristics equations of the model.

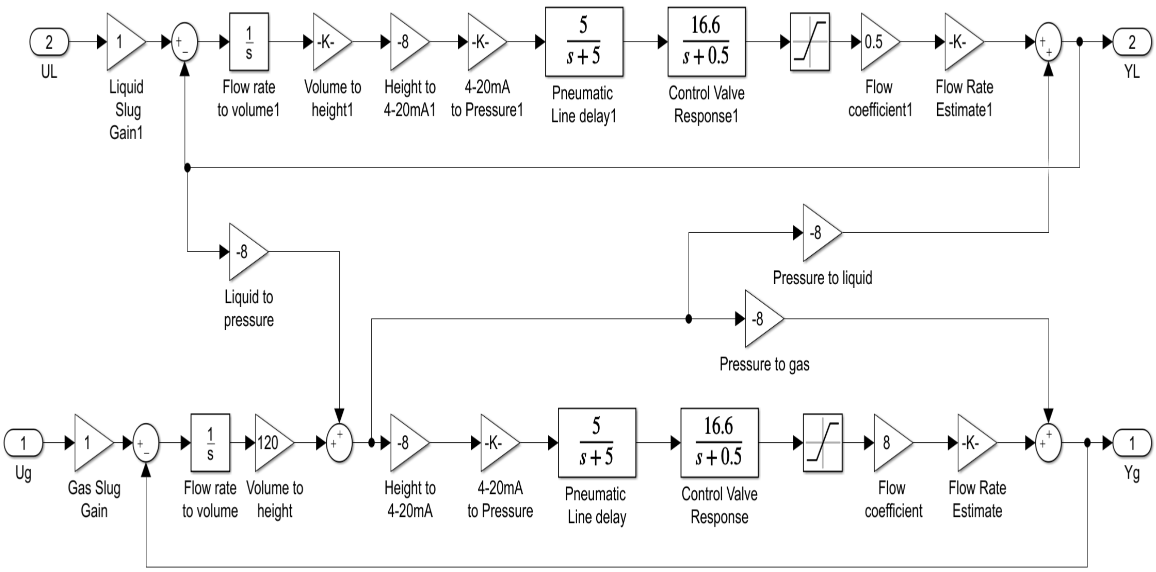

Figure 3.13: Combined LNG and Liquid fuel flow rate without controller action

The state-space variable extracted from the dynamic simulation of the combined fuel lines without the controller is as follows:

$$\begin{vmatrix} \dot{x}_1 \\ \dot{x}_2 \\ \dot{x}_3 \\ \dot{x}_4 \\ \dot{x}_5 \\ \dot{x}_6 \end{vmatrix} = \begin{vmatrix} -0.5 & 0 & 0 & 0 & 0 & 0 \\ -0.4472 & -215.5022 & -109.6928 & 0 & 0 & 0 \\ 0 & 0 & -0.5 & 0 & 0 & 5 \\ 0.0453 & -1.8341 & 0 & 0 & 0 & 0 \\ 0 & 0 & 0 & -50.93 & -50.93 & 0 \\ 0.6796 & -327.5109 & 0 & 0 & 0 & -5 \end{vmatrix} \begin{vmatrix} x_1 \\ x_2 \\ x_3 \\ x_4 \\ x_5 \\ x_6 \end{vmatrix} +$$

$$\begin{vmatrix} 0 & 0 \\ 0 & 1 \\ 0 & 0 \\ 1 & 0 \\ 0 & 0 \\ 0 & 0 \end{vmatrix} u1, u2 \qquad 3.74$$

$$\begin{vmatrix} y_1 \\ y_2 \end{vmatrix} = \begin{vmatrix} -0.0453 & 1.8341 & 0 & 0 & 0 & 0 \\ -0.4472 & 21.5022 & -109.6928 & 0 & 0 & 0 \end{vmatrix} \begin{vmatrix} x_1 \\ x_2 \\ x_3 \\ x_4 \\ x_5 \\ x_6 \end{vmatrix} +$$

$$\begin{vmatrix} 0 & 0 \\ 0 & 0 \end{vmatrix} u1, u2 \qquad 3.75$$

Transfer function

$$G1(s) = \frac{-11.541S^3 - 2341s^2 - 1.255e^{04}S - 1.904e^{\,06}}{s^6 + 226.5s^5 + 2406S^4 + 1.872e^{05}S^3 + 9.915e^{05}s^2 + 4.379e^{05}s - 1.904e^{06}} \qquad 3.76$$

$$G2(s) = \frac{-113.9s^3 - 626.3s^2 - 9.52e^{04}}{s^6 + 226.5s^5 + 2506s^4 + 1.872e^{05}s^3 + 9.915e^{05}s^2 + 4.379e^{05}s + 1.904e^{06}} \qquad 3.77$$

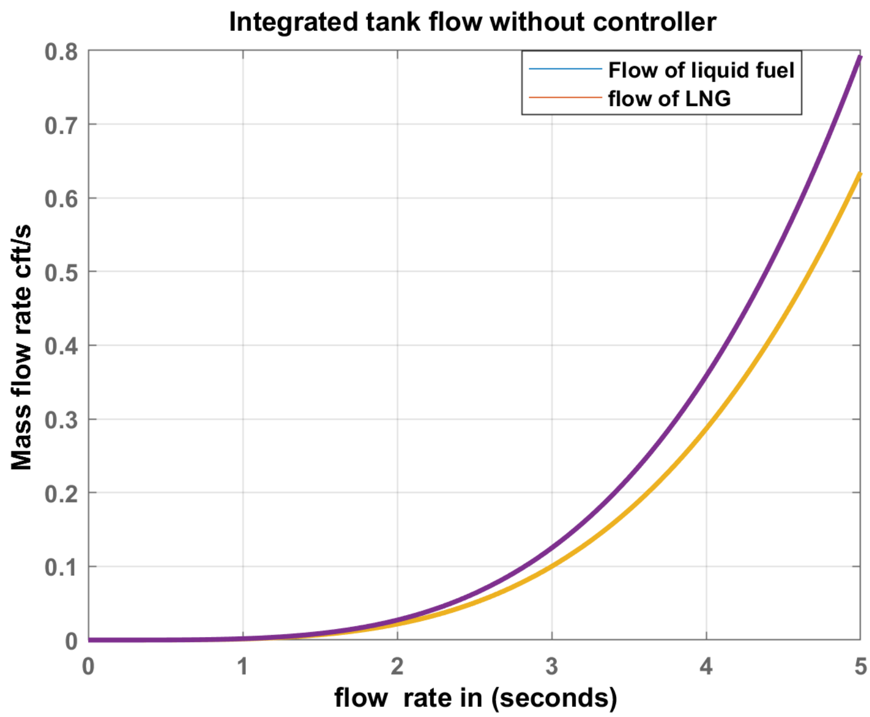

Figure 3.14: Dynamic response of integrated fuel line without controller action

LCV, LNGCV, and integrated dynamic performance are shown in Figures (3.11), (3.13) and (3.14) without the influence of a controller. Because the outflows are uncontrollable, they appear to be exponential. This design did not include GT onboard fuel flow to the combustion chamber. Therefore, the following will consider the design of the fuel system flow within the GT onboard before connecting to the external tank system. This approach required the study of the GT simulation model for the fuel control system.

3.9 Simulation model for the dynamic GT fuel control

The entire model is based on Rowen's educational iteration design by [70 - 71] model in Simulink for the various block for the control application. The setup includes fuel control, speed/load control, temperature control and gas turbine control block.

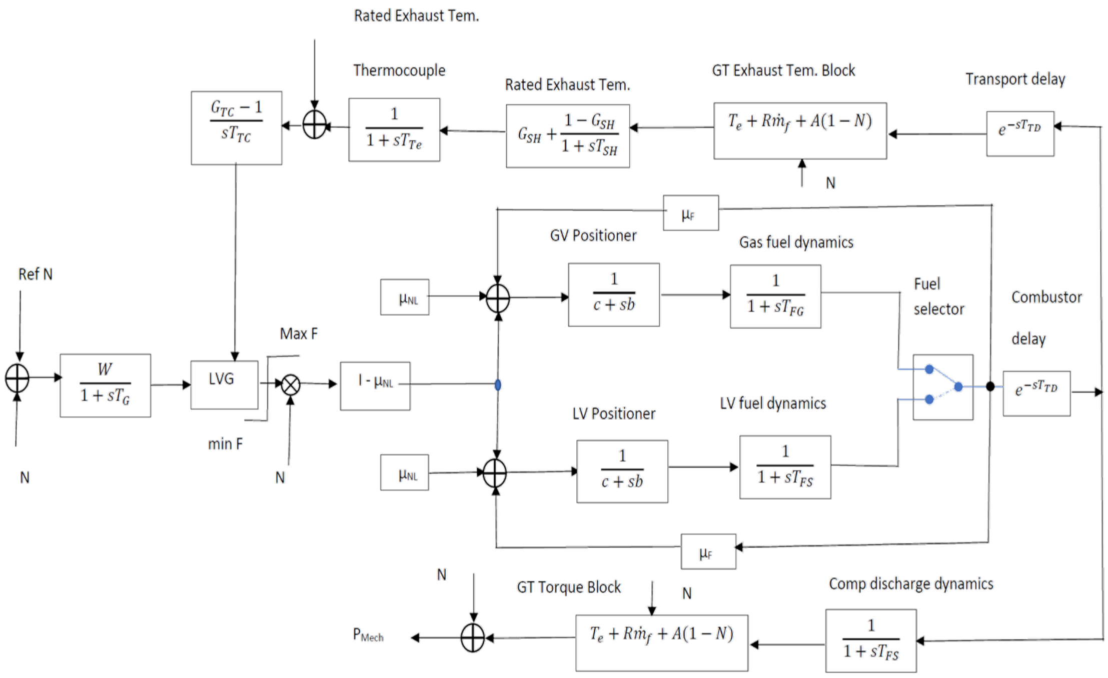

Figure 3.15: Rowen's model of HDGT for control system development

The blocks are developed based on the mathematical model in the previous sections. The modelling equations below, combined with the theoretical analysis above, are used to create the simulation models. The critical consideration is the Brayton temperature entropy cycle for turbine efficiency in analysing the generator parameters. When temperature against entropy was a plot for compressor operations during combustion mode, the process follows from point 1 through point 4, as shown in Figure 3.16.

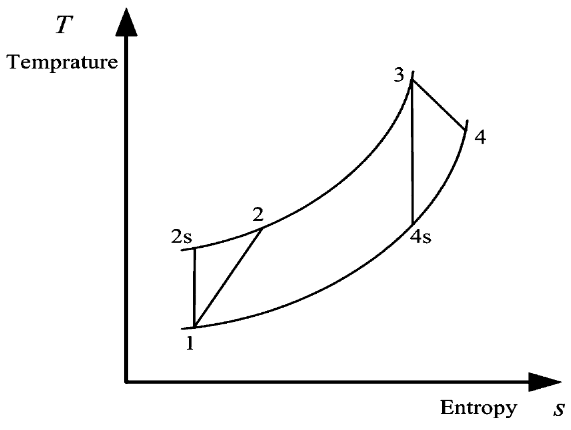

Figure 3.16: Brayton Cycle in temperature – entropy

Figure. 3.16 is used to evaluate the ideal compressor and turbine irreversible and adiabatic efficiency as follows:

$$\eta_c = \frac{h_{2s}-h_1}{h_2-h_1} \approx \frac{T_{2s}-T_1}{T_2-T_1} \qquad 3.78$$

$$\eta_t = \frac{h_3-h_4}{h_3-h_{4s}} \approx \frac{T_3-T_4}{T_3-T_{4s}} \qquad 3.79$$

In the Brayton concept, the fluid mixture entropy is in (kJ/kg), the absolute temperature in K, and h and T are all different aspects of the same concept, the cycle efficiency evaluation of the gas turbine plant. A subscript (s) after the word isentropic denotes that it is an isentropic process. Throughout the procedure, the efficiencies utilised are considered constant, and the turbine response is assumed to be approximate. Two factors govern the turbine output in the model depicted in Figure 3.16: output torque and exhaust temperature. In Figure 3.16, [20 & 93], the compressor and turbine isentropic efficiency is estimated with equation 3.80, and from Brayton cycle principles, the value must be within 1-2s.

$$\frac{T_{2s}}{T_1} = \left(\frac{P_2}{P_1}\right)^{\frac{\varphi_C-1}{\varphi_C}} = PR^{\frac{\varphi_C-1}{\varphi_C}} = x_c \qquad 3.80$$

$$\frac{T_3}{T_{4s}} = \left(\frac{P_3}{P_4}\right)^{\frac{\varphi_h - 1}{\varphi_h}} = PR^{\frac{\varphi_h - 1}{\varphi_h}} = x_h \qquad 3.81$$

$P_2/P_1 = P_3/P_4 = PR$, representing the cycle pressure ratio when the compressor pressure drop is assumed to be negligible. The cold and hot end compressor's specific heat ratios are φ_c and φ_h, respectively. In equations (3.80) and (3.81), the subscripts assigned to x are for reference only. The specific heat φ of air at a particular constant pressure volume is $\varphi = \frac{C_a}{C_v}$, and is measured at the hot and cold temperature points [88]. These values are established in this [58] experimental model for purposes of educational analysis.

$$C_{ah} = 1.1569\ \frac{kj}{kg}K, \quad \varphi_h = 1.33 \qquad 3.82$$

$$C_{vc} = 1.0047\ \frac{kj}{kg}K, \quad \varphi_c = 1.4 \qquad 3.83$$

Evaluating the temperature after the compressor processes the compressed air is essential. Equations (3.82) and (3.83) are used to establish this temperature as follows:

$$T_2 = T_1\left(\frac{x_c - 1}{\eta_c}\right) + 1 \qquad 3.84$$

$$T_4 = T_3\left[1 - \left(1 - \frac{1}{x_h}\right)\eta_t\right] \qquad 3.85$$

The process continues from the compressor to the combustion chamber, which also controls the GT. This process cannot be ignored. The combustor absorption and efficiency at a constant pressure process [20] is then evaluated.

$$\dot{Q}C = m_a.C_{ah}.(T_3 - T_2) \qquad 3.86$$

$m_a\ kg/s$ represents the air mass flow rate. During the process, heat is produced by energy extraction from the fuel and $\dot{Q}C$ in equation (3.86) becomes:

$$\dot{Q}C = \eta_{Com}.m_f.H \qquad 3.87$$

Again, η_{Com} combustor efficiency, $m_f\ kg/s$ fuel mass flow rate and H is the calorific value.

The combustor efficiency in equation (3.85) indicates the efficiency of unburn fuel in the combustion chamber; in reality, the combustor efficiency is higher and near unity. Using equations (3.84) and (3.85), the rise in temperature inside the combustion unit is established as:

$$T_3 = T_2 + \eta_{com}.\frac{m_f}{m_a}.\frac{H}{C_{ah}} = T_2 + \Delta T_0 \frac{m_f}{m_a} \qquad 3.88$$

ΔT_0 indicate the coefficient of temperature rise. The internal temperature change in the GT model affects the characteristics of the output response with varying speeds and makes it nonlinear. The mechanical power is estimated because system response is linear to speed deviation GT output is normal speed response. Hence, the per unit torque and mechanical power are given by:

$$P_G = m_f.[C_{ah}(T_3 - T_4) - C_{ac}(T_2 - T_1)] \qquad 3.89$$

The above equation is simplified and implemented in Figure 3.15 above, with equations (3.82), (3.83), and (3.87) becoming equation (3.90):

$$P_G = P + \dot{Q}.m_{fpu} \qquad (normal\ speed) \qquad 3.90$$

$$P = \frac{m_{apu}T_1}{P_{gn}}\left\{C_{ah}.\eta_t\left(1 - \frac{1}{x_h}\right) - \frac{x_c - 1}{\eta_c}\right\} \qquad 3.91$$

$$Q = \frac{\eta_{com}.\eta_t.m_{fpu}.H}{P_{Gn}}\left(1 - \frac{1}{x_h}\right) \qquad 3.92$$

P and Q are output torque coefficients, and the subscripts *n* and *pu* indicate normal and per unit parameters.

The exhaust temperature is established at normal speed using equations (3.82), (3.83) and (3.87).

$$T_4 = T_{en} - R.\left(1 - m_{fpu}\right) \qquad 3.93$$

$$R = \eta_{com} \frac{H}{C_{ah}} \frac{m_{fpu}}{m_{apu}} \left[1 - \left(1 - \frac{1}{x_h}\right) \eta_t\right] \qquad 3.94$$

R is the coefficient of exhaust temperature, and T_{en} is the average exhaust temperature show in Figure 3.15.

In the normal fuel operation mode of the GT, the torque is evaluated at 1pu open-loop response speed of the turbine.

$$T_{Gpu} = \frac{\mu - 1}{\mu} - \frac{1}{\mu} N_{pu} \qquad 3.95$$

μ is a thermodynamic cycle design constant and is also affected by thermo friction in the GT system. From the viewpoint of [57], the μ value is complicated to evaluate, and therefore, the design value varies between 1.5 and 2; hence, in the power block of figure 3.15, the $D = \frac{1}{\mu}$. Therefore, D also varies between 0.5 and 0.67 using the same principle for the exhaust temperature block in the same diagram, the coefficient of the exhaust temperature A with speed variation would be in the range of 0.55 to 0.65. GT fuel consumption is estimated to be very high even at the no-load operation as established by Rowen's model, which obtains the ratio of fuel demand signal and positioner into constant parts (μ_{NL}) and again multiplier is reduced by demand signal (block 1-μ_{NL} in Figure 3.15).

In figure 3.15, the fuel demand limiter is active, which implies that it prevents the maximum limit from being attained in typical operations. This means the exhaust gets hotter, and the temperature control mechanism is turned on, reducing the amount of gasoline supplied [20].

3.9.1 Valve positioner and fuel lag system

A valve positioner measures and response to the system fuel demand, thereby controlling the movement of the valve position. Except for GTs, which use liquid and gas fuels, models used to simulate fuel systems are the same regardless of the blocks used. The dual-fuel system uses inner loop feedback to regulate both fuels. Manufacturers' data sheets provide the time constant for the valve position. GT fuel system arrangement: Regardless of the setup, the bypass path for the fuel pump is always included. The feedback loop, including the feedback component μf, is also present in the Rowen model. To establish a feedback system with a unity gain, it is only necessary to estimate the value of the feedback component during operation [94].

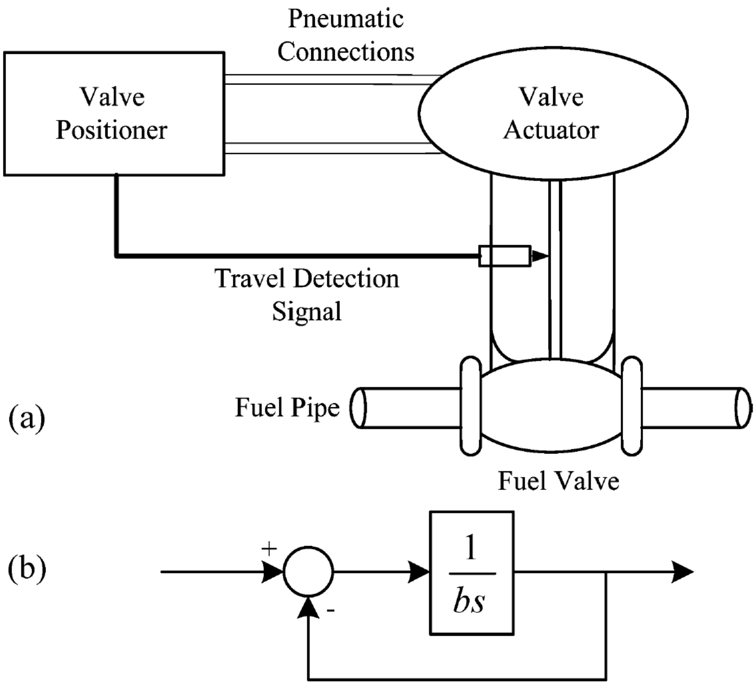

Figure 3.17: Pneumatic valve positioner and valve actuator. (a) schematic view (b) internal feedback model

From Figure 3.16, the fuel contained will have a lag associated with fuel travel through the pipes expressed in equation (3.96) with Tv time constant of the lag in seconds.

$$T_V = \frac{P_0}{Q_o} V \frac{\delta}{\delta P}\left(\frac{1}{v}\right)\Bigg|_{T_0} \qquad 3.96$$

Pa (kg/m.sec^2) is the average pressure, and Q_0 is the steady-state mass flow of the container in kilograms per second. The density change due to pressure changes at the same temperature is V's (Kg/m^3) function, where V is the specific volume. The lag constant for gas fuels is much longer because of the greater volume changes.

3.9.2 Time delays and discharge lag

The GT's characteristics make small delays and constant lag time possible. The system does experience a slight delay in the fuel injection and heat release in the combustor, known as the combustion reaction delay [58]. In this design, the value is expressed in ms. Rowen's model uses a time delay after the valve systems to implement this time delay. There is also a delay between the combustion of the fuel and the exhaust temperature measurement. The exhaust system and turbine are contributing factors to the delay in getting the fluid to the measuring point.

3.9.3 Temperature measurement system

GT temperature control requires a temperature measurement system, and a thermocouple device is introduced in the exhaust system. Temperature control is essential to avoid excessive heat, and where we rely on the radiation source obtained from the GT, which is likely to cause errors in the temperature measurement. The error associated with the radiation in the GT, a radiation shield is provided as a polished surface with a highly reflective material placed around the thermocouple. This effect results in the temperature model lagging and is neutralized with the heat transfer compensator model.

$$\frac{T_{measure}}{T_{exhaust}} \approx \frac{A_2}{A_1} + \frac{1-\frac{A_2}{A_1}}{\frac{C}{h-A_1}+1} \qquad 3.97$$

A_1 is the total active area of convection heat transfer to the shield head, A_2 is the effective area of convection heat transfer to the thermocouple tip, C (J/K) is the heat capacity of the shield head, and h (W/m^{2}K) is the convection heat transfer coefficient [90].

To model dual-fuel gas turbines and analyse fuel dynamics, HDGT data was used in Table 3.7. Table 3.8 lists the values used to calculate the turbine and compressor efficiency.

Table 3.7: Selected data for modelling and analysis

PARAMETER	SYMBOL	UNIT	VALUE
Gross electrical output	P_{Gn}	MW	172.2
Nominal frequency	F	Hz	50
Turbine speed	RPM	RPM	3000
Exhaust mass flow	m_n	kg/s	537
Exhaust gas temperature	Te	°C	522
Pressure ratio	P_R	-	15.4

Table 3.8: computational data for turbine and compressor efficiency

PARAMETER	UNIT	VALUE
Output power	MW	146.4
Turbine inlet temperature	°C	1100
Exhaust gas temperature	°C	532
Ambient temperature	°C	27.3
Exhaust mass flow	kg/s	438.1
Fuel	-	Gas/Diesel
Fuel flow	kg/s	8.34
The lower heating value of fuel	kJ/kg	43094

3.9.4 Turbine efficiency

Using equation (3.81) from Tables 3.7 and 3.8 above, the isotropic process T4s(oc) is calculated below.

$$x_{h(OD)} = (15.4\,x\,\frac{438.1}{537})^{\frac{1.33-1}{1.33}} = 1.87 \qquad 3.98$$

$$T_{4s(OD)} = \frac{T_{3(oc)}}{x_{h(oc)}} = \frac{1100+273}{1.87} = 734.22K = 461.22°C \qquad 3.99$$

The index OD represents the operating dynamics in Table 3.8, and the rated pressure ratio decreases when mass flow is reduced. Hence, the need to evaluate $T_{3(OD)}$ in K using equation (3.98) and thus turbine efficiency recall equation (3.79).

$$\eta_t = \frac{1100-532}{1100-461.22} = 0.89 \qquad 3.100$$

The efficiency of the compressor is evaluated based on the isotropic temperature process in the compressor equation (3.80).

$$x_{c(OD)} = (15.4\ x\ 438.1/537)^{\frac{1.4-1}{1.4}} = 2.06 \qquad 3.101$$

$$T_{2s(OD)} = T_{1(OD)}\mathrm{x}\ x_{c(OD)} = (27.3 + 273)\mathrm{x}\ 2.06 = 618.62\mathrm{K} = 345.62℃$$

Again, the compressor outlet temperature also is required and is computed using (3.86)

$$T_{2(OD)} = T_{3(OD)} - \eta_{comb}\frac{\dot{\mathrm{m}}_{f(OD)}}{\dot{\mathrm{m}}_{(OD)}}\frac{H}{C_{ph}} = 1100 - 0.99\ x\ \frac{8.34}{438.1}\ x\ \frac{43094}{1.1569} = 397.98℃ \qquad 3.102$$

Even though the combustor efficiency is nearly unit (0.99) during the combustion process, estimating the compressor efficiency at this stage is also essential. Hence, recall equation (3.86), compressor efficiency is evaluated.

$$\eta_c = \frac{345.62-27.3}{397.98-27.3} = 0.86 \qquad 3.103$$

Table 3.7 needs to be updated for regular operation with the computed data, and therefore there is need to evaluate the parameters x_h and x_c.

$$x_h = (15.4)^{\frac{1.33-1}{1.33}} = 1.97 \qquad 3.104$$

$$x_c = (15.4)^{\frac{1.4-1}{1.4}} = 2.18 \qquad 3.105$$

From the model block mentioned above, the parameters for mechanical power are extracted using equations (3.88) and (3.90).

$$P = \frac{537\text{x}\,(273+15)}{172200}\ \text{x}\ \left\{1.1569\ \text{x}\ 0.89\ \text{x}\ \left(1-\frac{1}{1.97}\right) - \frac{2.18-1}{0.86}\ \text{x}\ \left[1.0047 - 1.1569\ \text{x}\ 0.89\ \text{x}\ \left(1-\frac{1}{1.97}\right)\right]\right\}$$

$$P = -0.1580 \qquad 3.106$$

$$Q = \frac{0.99\ x\ 0.89\ x\ 43094\ x\ \dot{m}_{fn}}{172200}\left(1-\frac{1}{1.97}\right) = 0.1086\ \dot{m}_{fn} \qquad 3.107$$

And

$$\dot{m}_{fpu} = \frac{P_{Gpu} - P}{Q} \Rightarrow 1 = \frac{1+0.1580}{0.1086\ \dot{m}_{fn}} \Rightarrow \dot{m}_{fn} = 10.66kg/s$$

$$Q = 1.1580 \qquad 3.108$$

Since normal flow is needed to estimate the turbine exhaust temperature, from equation (3.92) parameter for exhaust temperature R is calculated below:

$$R = 0.99\ x\ \frac{43094}{1.1569}\ x\ \frac{10.72}{537}\left[1-\left(1-\frac{1}{1.97}\right)x\ 0.89\right] = 413.6°\text{C} \qquad 3.109$$

The sensitivity coefficient of speed (C and A) and selected to be C= 0.5 and A = $0.6T_e$ = 313^{O}C. During no-load operation, combustion flame must be maintained, and this is achieved by the minimum fuel flow rate from Table 3.9 hence:

$$\mu_{NL} \cong \frac{2.56}{10.66} = 0.24 \qquad 3.110$$

and

$$min\ F\ \cong \frac{\frac{1.5}{10.66}-0.24}{1-0.24} = -0.13 \qquad 3.111$$

Table 3.9: Minimum fuel flow and no-load estimation

No-load fuel flow (kg/s)	~2.56
Min fuel flow to maintain combustor flame (kg/s)	~1.5

Table 3.10: Estimated operational data for fuel lag

Fuel	Gas/Diesel
Fuel pressure (atm)	21
Average temperature (K)	320
Fuel piping approximate volume (m^3)	0.17 ~(15m x 6cm radius Equiv. cylinder)

Table 3.11: Compressor discharge operational data

Type of fuel	LNG
Average temperature K	~1050
Volume of discharge m^3	~16

3.9.5 Fuel system block

The time lag condition of the fuel system must be approximated when the dynamic state is well known. And for the dual fuel system, the same situation is assumed; hence approximation of methane dynamic characteristics for both gas and diesel is used to compute the density changes resulting from pressure variations with data established in Table 3.10.

$$\frac{\partial}{\partial P}\left(\frac{1}{V}\right)\Bigg|_{T_o} = \frac{\left(\frac{1}{0.07}\right)-\left(\frac{1}{0.1}\right)}{22-16.5}\Bigg|_{320K} = 0.78 \qquad 3.112$$

The data for the geometrical and operational parameters of the radiation shield needs to be established. In table 3.10 present the data for this purpose [72].

$$T_{FS} = \frac{21\ atm}{10.66\ kg/s}\ x\ 0.17m^3 x\ 0.78 \frac{kg/m^3}{atm} = 0.26\ s \qquad 3.113$$

The estimation is based on the normal flow, and the temperature is needed to establish a change in a specific volume of Methane. Manufacturer datasheet is used to develop the data based on GV and LV positioning at approximately 20ms. In steady-state analysis, the time constant is about five times the time constant and hence 'b' value, as shown in the model, is approximately 40ms.

3.9.6 System discharge and time delay

The following assumptions are made:

1. Delay of 5ms between fuel inject and combustor burning
2. Combustion reaction delay of 5ms
3. 40ms delay between air and combustion transfer to temperature point T_{TD} is approximately 40ms
4. There is a time constant during combustion discharge

Equation 3.96 approximates the time lag constant

$$\frac{\partial}{\partial P}\left(\frac{1}{V}\right)\Big|_{T_o} = \frac{\left(\frac{1}{0.14}\right)-\left(\frac{1}{0.2}\right)}{20-14}\Bigg|_{1050K} = 0.36 \qquad 3.114$$

The average temperature data presented in Tables 3.11 and (3.96) estimate the volume discharge time constant based on pressure change.

$$T_{CD} = \frac{15.4\ \mathrm{atm}}{537\ \mathrm{kg/s}}\ \mathrm{x}\ 16\mathrm{m}^3 \mathrm{x}\ 0.36 \frac{\mathrm{kg/m^3}}{\mathrm{atm}} = 0.16\ \mathrm{s} \qquad 3.115$$

Note pressure and mass flow are imported from Table 3.7.

3.9.7 Temperature measurement block

The radiation shield exhibits dynamic behaviour that needs to be accounted for, and equation (3.95) evaluates this characteristic. Table 3.12 accounts for the radiation shield parameters used to model the effect on temperature. The coefficients and heat energy capacity are obtained from [96]. The assumption is that thermocouple tip heat conversion, and transfer is taken as a cylinder having approximately twice the tip length in each thermocouple device.

Table 3.12: Radiation shield data

PARAMETER	SYMBOL	VALUE
Shield Alloy	-	
Shield Head Diameter (cm)	D_{SH}	3
Shield Head Length (cm)	L_{SH}	7.5
Shield Head Thickness (mm)	H_{SH}	0.08
Thermocouple Tip Length inside Shield (mm)	L_{tip}	16
Convection Heat Transfer Coefficient (W/^{m2} K)	H	250
Specific Heat Capacity per unit Volume (J/cm^{3}K)	C_{sp}	3.83

$$G_{SH} = \frac{A_2}{A_1} = \frac{\pi D_{SH} L_{tip}}{\pi D_{SH} L_{SH}} = \frac{4L_{tip}}{L_{SH}} = \frac{4 \; x \; 1.6}{7.5} = 0.85 \qquad 3.116$$

$$T_{SH} = \frac{C}{hA_1} = \frac{C_{sp} x \; \pi D_{SH} L_{SH} H_{SH}}{h \; x \; \pi D_{SH} L_{SH}} = \frac{C_{sp} H_{SH}}{h} = \frac{3.83\left(\frac{J}{cm^3 K}\right) x \; 0.08(cm)}{250 \; x \; 10^{-4}\left(\frac{W}{m^2 K}\right)} = 12.2s \qquad 3.117$$

According to [58] value for the thermocouple parameter obtained from the manufacturer datasheet is 1.7s. Hence, the time constant for the thermocouple block in Figure 3.15 is 1.7s. It is evident that the simulation parameters are based on the already existing HDGT plant for dual fuel control analysis and that controller parameters in the model are obtained from the controller set point. The data used for simulation is based on the HDGT model with a maximum power of 172MW. Parameters to be controlled are load frequency and exhaust temperature under two-speed scenarios. Hence, the parameters are reorganised in Table 3.13 for the model in Figure 3.15.

Table 3.13: HDGT model parameters for Figure 3.15

PARAMETER	SYMBOL	VALUE
Speed Governor Gain	W	25
Speed Governor Time Constant (s)	T_G	0.05
Fuel Demand Signal Max Limit	$maxF$	1.5
Fuel Demand Signal Min Limit	$minF$	-0.13
No Load Fuel Consumption	μ_{NL}	0.24
Valve Positioner Time Constant (s)	b	0.04
Fuel System Time Constant (s)	T_{FS}	0.26
Fuel System External Feedback Loop Gain	μ_F	0
Delay of Combustion System (s)	T_{CR}	0.005
Transport Delay of Turbine and Exhaust System (s)	T_{TD}	0.04
Compressor Discharge Lag Time Constant (s)	T_{CD}	0.16
Gas Turbine Torque Block Parameter	P	-0.158
Gas Turbine Torque Block Parameter	Q	1.158
Gas Turbine Torque Block Parameter	C	0.5
Gas Turbine Exhaust Temperature Block Parameter (°C)	R	413
Gas Turbine Exhaust Temperature Block Parameter (°C)	A	313
Radiation Shield Parameter	G_{SH}	0.85
Radiation Shield Time Constant (s)	T_{SH}	12.2
Thermocouple Time Constant (s)	T_{TR}	1.7
Rated Exhaust temperature (°C)	Te	522
Temperature Controller Parameter	G_{TC}	3.3
Temperature Controller Integration Constant (°C)	T_{Tc}	250

3.10 Simulation of GT internal Fuel System without Controller and external coupling

Again, we investigated the GT fuel dynamics system without external fuel supply to establish the mathematical model underpinning GT speed control behaviour and developed the control algorithms. The control parameters are obtained with a Simulink/MATLAB programme to linearise the operation at the initial conditions. The system would be simulated using liquid only, gas, and flow with the combined system with external supply lines. We shall proceed with the dual nozzle design and subject the integrated fuel system to the dual nozzle in order to study the characteristics of the system performance.

3.10.1 GT with liquid fuel line system without controller and external coupled

The block diagram in Figure 3.18 shows the Simulink arrangement of GT with only a liquid fuel control block for the traditional operation. In this respect, combustion takes place by spraying liquid fuel known as diesel fuel into the combustion chamber at the right proportion with compressed air.

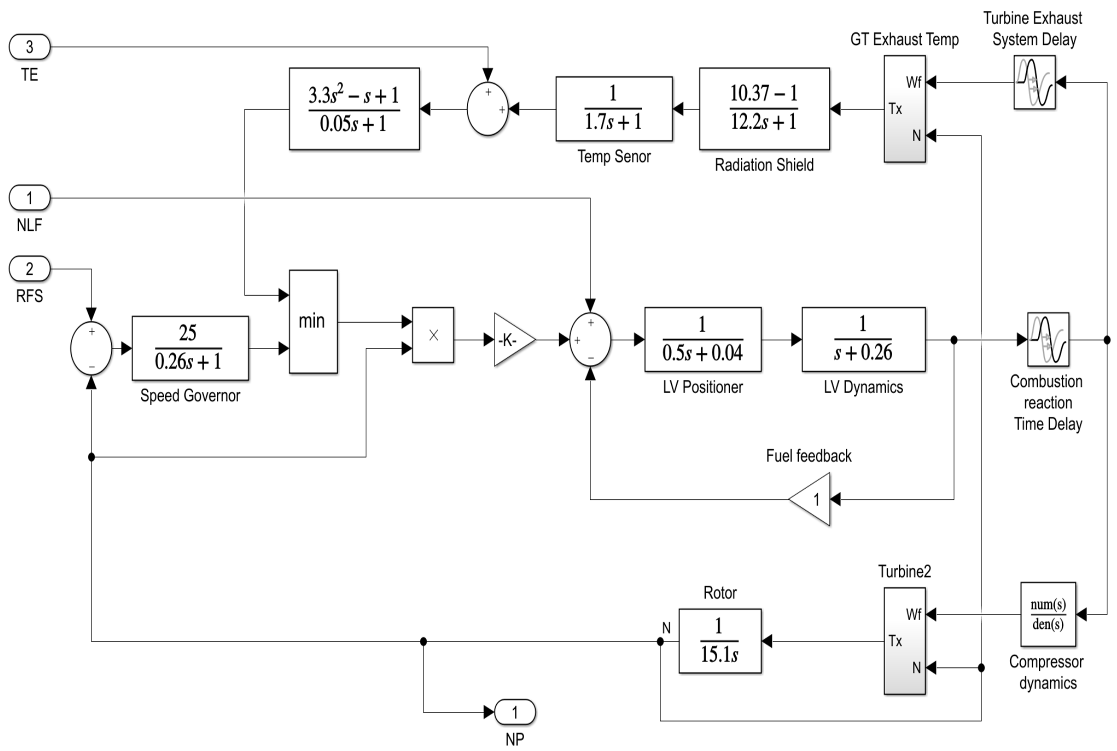

Figure 3.18: Linearized GT liquid fuel flow schematics

Using equations (3.115-3.117), the following parameters of the model is obtained.

$$x_{lq} = \begin{bmatrix} 0 & 0 & 0 & 0 & 0 & 0 & 0 & 0 & 0 & 0 \\ 0 & 0 & 0 & -1.2000 & 0 & 0 & 0 & 0 & 0 & 0 \\ 0 & 0 & -0.0060 & 0 & 0 & 0 & 0 & 0 & 0 & 0 \\ 0 & 0 & 0.0000 & 0 & 0 & 0 & 0 & 0 & 0 & 0 \\ 0 & 0 & -0.0120 & 0 & 0 & 0 & 0 & 0 & 0 & 0 \\ 0 & 0 & 0 & 0 & 0 & 0 & 0 & 0 & 0 & 0 \\ 0 & 0 & 0 & 0 & 0 & 0 & 0 & 0 & 0 & 0.0000 \\ 0 & 0 & 0 & 0 & 0 & 0 & 0 & -0.0000 & 0 & 0 \\ 0 & 0 & -0.0156 & 0 & 0 & 0 & 0 & 0 & 0 & 0 \\ 0 & 0 & 0 & 0 & 0 & 0 & 0 & 0 & 0 & -0.0000 \end{bmatrix} \quad 3.118$$

$$u_{lq} = \begin{bmatrix} 0 & 0 & 0 \\ 0 & 0 & 0 \\ 0 & 0 & 0 \\ 0 & 0 & 0 \\ 0 & 0 & 0 \\ 0 & 0 & 1 \\ 0 & 1 & 0 \\ 1 & 0 & 0 \\ 0 & 0 & 0 \\ 0 & 0 & 0 \end{bmatrix} \qquad y_{lq} = [0.0662 \quad 0 \quad 0 \quad 0 \quad 0 \quad 0 \quad 0 \quad 0 \quad 0 \quad 0] \quad 3.119$$

$$d_{lq} = [0 \quad 0 \quad 0] \quad 3.120$$

$$GS_{LC} = \frac{0.1722S^6 - 99.09S^5 + 1.815e^{04}S^4 + 4.97e^{05}S^3 + 1.915e^{06}S^2 + 1.089e^{06}S + 7.663e^{04}}{S^{10} + 6255S^9 + 1.351e^{05}S^8 + 3.072e^{06}S^7 + 1.307e^{07}S^6 + 1.862e^{07}S^5 + 3.326e^{07}S^4 - 9.414e^{08}S^3 - 3.948e^{08}S^2 - 7.00e^{08}S + 1.047e^{08}} \quad 3.121$$

Using equations (3.118, 3.119,3.120 and 3.121), the GT onboard liquid fuel control loop's dynamic characteristics are obtained without a controller to investigate the dynamic characteristics that produce the response shown in Figure 3.19. The system exhibits a negative response, indicating that the control required a compensator design to regulate the flow.

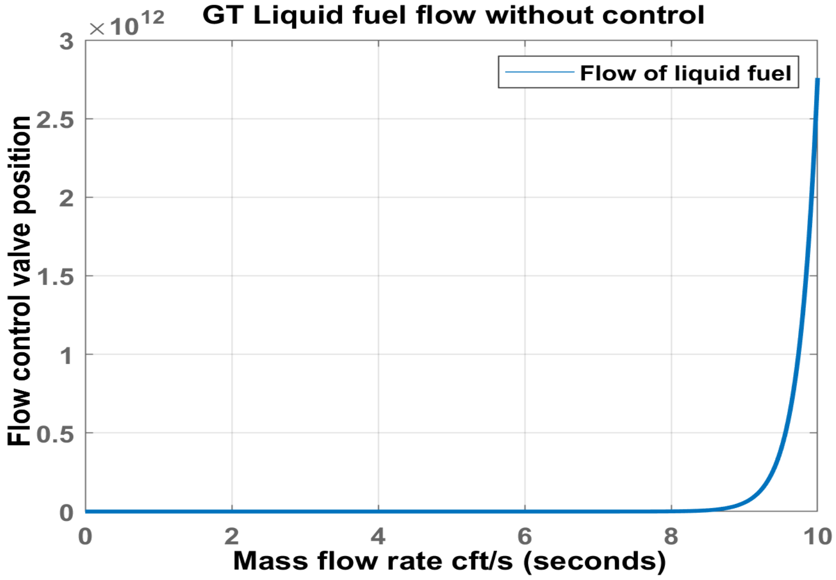

Figure 3.19: GT output response with liquid fuel without control action

3.10.2 GT with NLG line system without controller and external coupled

The GT model for both LNG and liquid fuel is the same except for the feedback element, which for LNG is assumed to be zero while the liquid fuel is always 1.

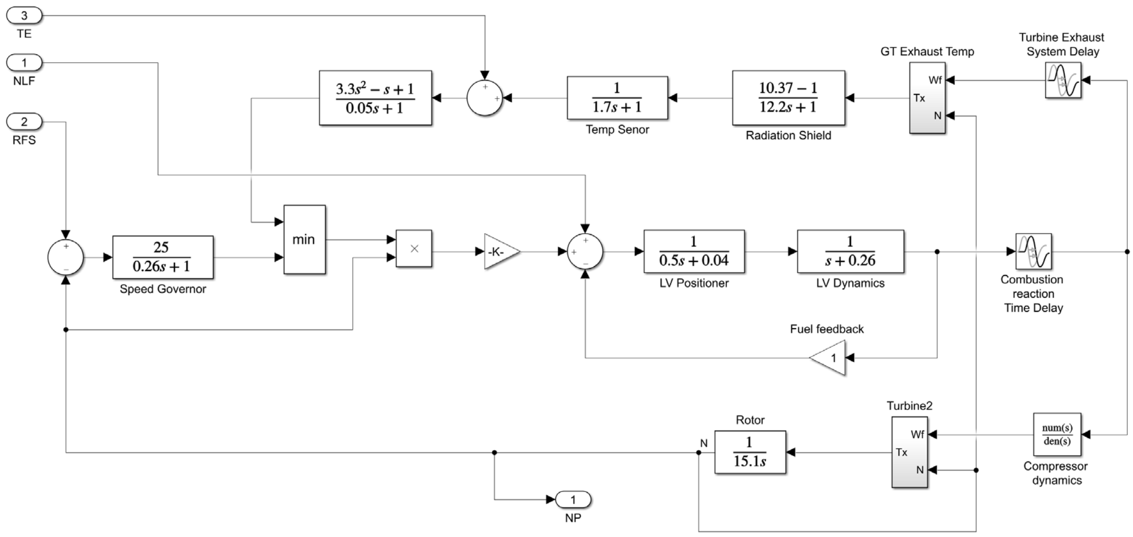

Figure 3.20: Linearized GT LNG flow schematics

Applying equations (3.115-3.117), the following parameters of the model is obtained.

$$x_m = \begin{bmatrix} 0 & 0 & 0 & 0 & 0 & 0 & 0 & 0 & 0 & 0 \\ 0 & 0 & 0 & -1.2000 & 0 & 0 & 0 & 0 & 0 & 0 \\ 0 & 0 & -0.0060 & 0 & 0 & 0 & 0 & 0 & 0 & 0 \\ 0 & 0 & 0.0000 & 0 & 0 & 0 & 0 & 0 & 0 & 0 \\ 0 & 0 & -0.0120 & 0 & 0 & 0 & 0 & 0 & 0 & 0 \\ 0 & 0 & 0 & 0 & 0 & 0 & 0 & 0 & 0 & 0 \\ 0 & 0 & 0 & 0 & 0 & 0 & 0 & 0 & 0 & 0.0000 \\ 0 & 0 & 0 & 0 & 0 & 0 & 0 & -0.0000 & 0 & 0 \\ 0 & 0 & -0.0156 & 0 & 0 & 0 & 0 & 0 & 0 & 0 \\ 0 & 0 & 0 & 0 & 0 & 0 & 0 & 0 & 0 & -0.0000 \end{bmatrix} \quad 3.122$$

$$u_n = \begin{bmatrix} 0 & 0 & 0 \\ 0 & 0 & 0 \\ 0 & 0 & 0 \\ 0 & 0 & 0 \\ 0 & 0 & 0 \\ 0 & 0 & 1 \\ 0 & 1 & 0 \\ 1 & 0 & 0 \\ 0 & 0 & 0 \\ 0 & 0 & 0 \end{bmatrix} \qquad y_n = [0.0662 \quad 0 \quad 0 \quad 0 \quad 0 \quad 0 \quad 0 \quad 0 \quad 0 \quad 0] \quad 3.123$$

$$d_n = [0 \quad 0 \quad 0] \quad 3.124$$

$$GS_{NC} = \frac{0.1722S^6 - 99.09S^5 + 1.815e^{04}S^4 + 4.97e^{05}S^3 + 1.915e^{06}S^2 + 1.089e^{06}S + 7.663e^{04}}{S^{10} + 625S^9 + 1.351e^{05}S^8 + 3.07e^{06}S^7 + 1.28e^{07}S^6 + 1.2562e^{07}S^5 + 9.724e^{07}S^4 - 9.584e^{08}S^3 - 3.951e^{08}S^2 - 7.005e^{08}S + 1.047e^{08}} \quad 3.125$$

Using equations (3.122, 3.123,3.124 and 3.125), the GT onboard liquid fuel control loop's dynamic characteristics are estimated without a controller to investigate the dynamic characteristics that produce the response shown in Figure 3.21. The system exhibits a negative response, indicating that the control required a compensator design to regulate the flow.

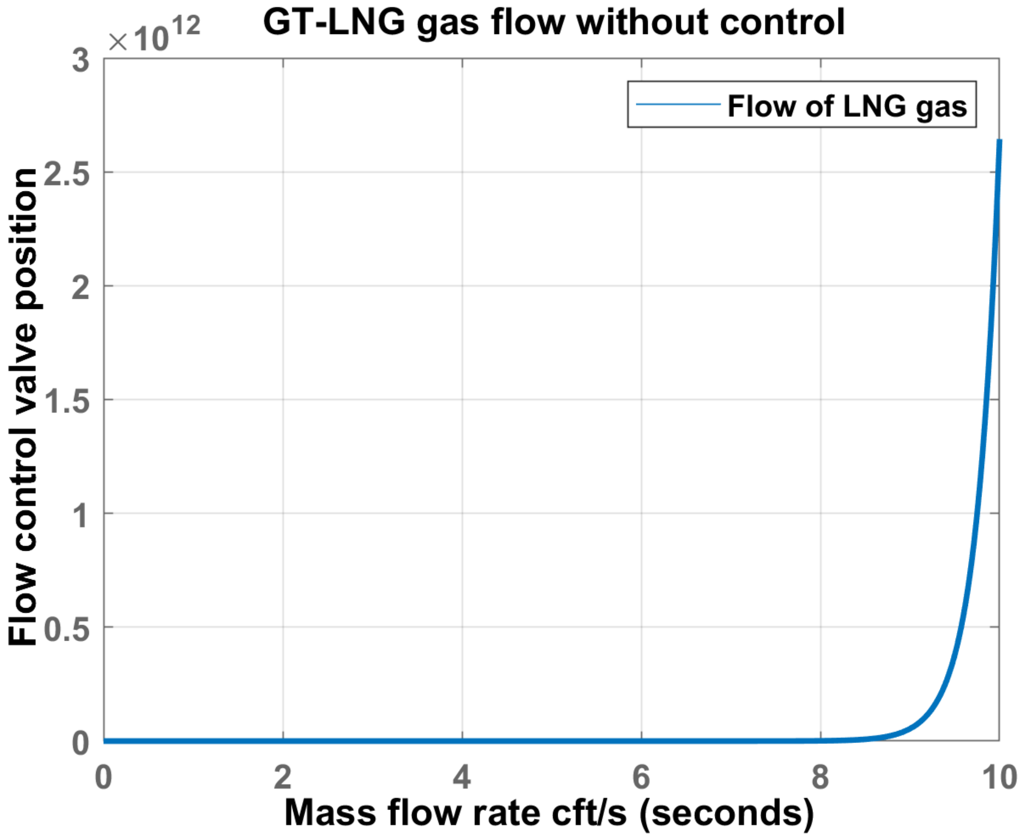

Figure 3.21: GT output response with LNG without control action

3.11 GT LNG and Liquid fuel integrated with Combustion chamber flow

In this section, the dynamic characteristics of the fuel rail system for dual engine supply with different injection systems for both LNG and liquid flow is investigated. The control objective is to stabilize the dynamic behaviour of the combined fuel system. In the simulation setup shown in Figure A3.22, the LNG and liquid fuel flow are designed so that the output minimum/maximum sensor will always select the high-pressure flow system.

$$x_C$$

$$= \begin{bmatrix} 0 & 0 & 0 & 0 & 0 & 0 & 0 & 0 & 0 & 0 \\ 0 & 0 & 0 & -1.2000 & 0 & 0 & 0 & 0 & 0 & 0 \\ 0 & 0 & -0.0060 & 0 & 0 & 0 & 0 & 0 & 0 & 0 \\ 0 & 0 & 0.0000 & 0 & 0 & 0 & 0 & 0 & 0 & 0 \\ 0 & 0 & -0.0120 & 0 & 0 & 0 & 0 & 0 & 0 & 0 \\ 0 & 0 & 0 & 0 & 0 & 0 & 0 & 0 & 0 & 0 \\ 0 & 0 & 0 & 0 & 0 & 0 & 0 & 0 & 0 & 0.0000 \\ 0 & 0 & 0 & 0 & 0 & 0 & 0 & -0.0000 & 0 & 0 \\ 0 & 0 & -0.0156 & 0 & 0 & 0 & 0 & 0 & 0 & 0 \\ 0 & 0 & 0 & 0 & 0 & 0 & 0 & 0 & 0 & -0.0000 \end{bmatrix} \quad 3.126$$

$$u_C = \begin{bmatrix} 0 & 0 & 0 \\ 0 & 0 & 0 \\ 0 & 0 & 0 \\ 0 & 0 & 0 \\ 0 & 0 & 0 \\ 0 & 0 & 0 \\ 0 & 0 & 1 \\ 0 & 1 & 0 \\ 1 & 0 & 0 \\ 0 & 0 & 0 \\ 0 & 0 & 0 \\ 0 & 0 & 0 \end{bmatrix} \quad y_C = [0.0662 \quad 0 \quad 0 \quad 0 \quad 0 \quad 0 \quad 0 \quad 0 \quad 0 \quad 0 \quad 0 \quad 0] \quad 3.127$$

$$d_C = [0 \quad 0 \quad 0] \qquad 3.128$$

GS_C =

1196 s^7 - 7.118e05 s^6 + 1.4e08 s^5 + 6.94e08 s^4 + 5.994e08 s^3 + 1.681e08 s^2 + 1.688e07 s + 5.536e05

----

s^12 + 625.4 s^11 + 1.354e05 s^10 + 3.117e06 s^9 + 1.411e07 s^8 + 2.311e07 s^7 + 3.985e07 s^6 - 9.297e08 s^5 - 4.267e09 s^4 - 2.062e09 s^3 - 2.154e08 s^2 + 2.105e07 s + 2.179e06 3.129

Using Equations (3.126, 3.127, 3.128 and 3.129), the dynamic characteristics of the GT onboard liquid fuel control loop combined with the external LNG tank control loop without a controller is simulated to investigate the dynamic characteristics, which produce the response shown in Figure 3.23. The system exhibits a negative response, indicating that the control required a compensator design to regulate the flow.

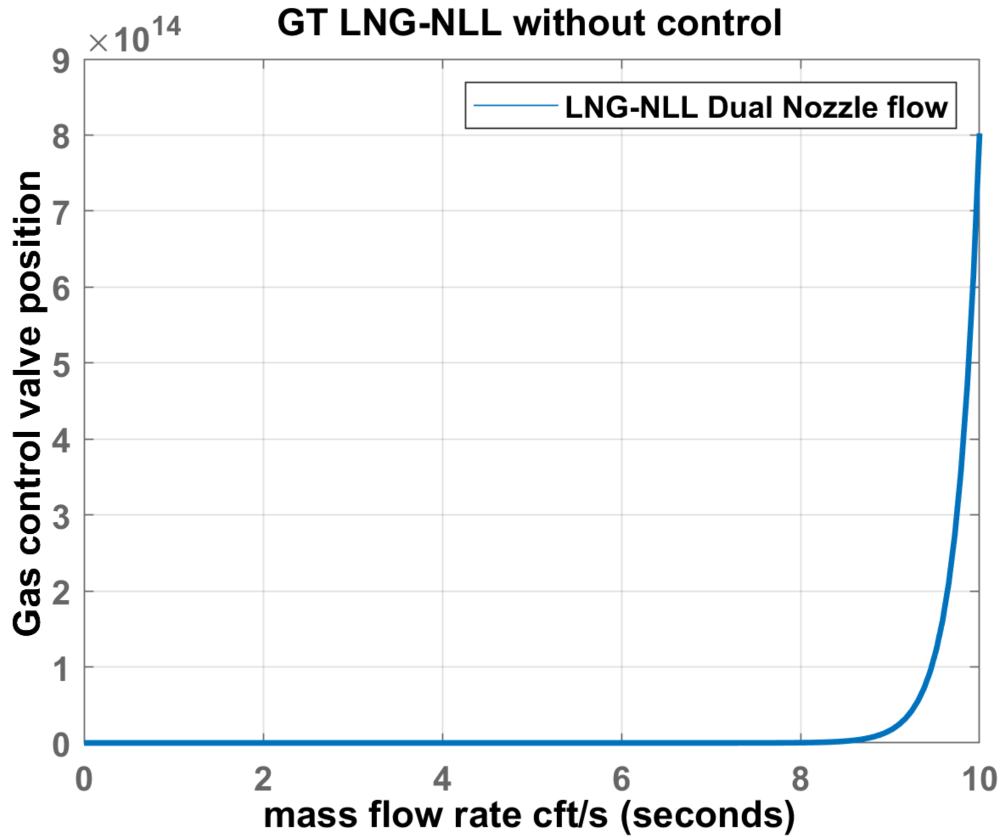

Figure 3.22: GT response of LNG-NLL dual fuel without controller

3.12 GT Liquid fuel line integrated with external tank fuel flow

This section investigates the dynamic characteristics of the GT fuel line system with an external liquid fuel tank system to study the flow dynamics. The control objective is to synchronize external flow with GT internal fuel flow dynamic. The setup is shown in figure A3.24, which is used to produce the state variable below for controller investigation.

$$x_{LL}$$

$$= \begin{bmatrix} 0 & 0 & 0 & 0 & 0 & 0 & 0 & 0 & 0 & 0 & 0 & 0 & 0 \\ 0 & 0 & 0 & 0 & 0 & 0 & 0 & 0 & 0 & 0 & 0 & 0 & 0 \\ 0 & 0 & -0.060 & -1.2 & 0 & 0 & 0 & 0 & 0 & 0 & 0 & 0 & 0 \\ 0 & 0 & 0 & 0 & 0 & 0 & 0 & 0 & 0 & 0 & 0 & 0 & 0 \\ 0 & 0 & -0.0120 & 0 & 0 & 0 & 0 & 0 & 0 & 0 & 0 & 0 & 0 \\ 0 & 0 & 0 & 0 & 0 & 0.02 & 0 & 0 & 0 & 0 & 0 & 0 & 0 \\ 0 & 0 & 0 & 0 & 0 & 0 & 0 & 0 & 0 & 0 & 0 & 0 & 0 \\ 0 & 0 & 0 & 0 & 0 & 0 & 0 & 0 & 0 & 0 & 0 & 0 & 0 \\ 0 & 0 & 0 & 0 & 0 & 0 & 0 & 0 & 0 & 0 & 0 & 0 & 0 \\ 0 & 0 & 00 & 0 & 0 & 0 & 0 & 0 & 0 & 0 & 0.01 & 0 & 0 \\ 0 & 0 & 0 & 0 & 0 & 0 & 0 & 0 & 0 & 0 & 0.01 & 0 & 0 \\ 0 & 0 & -0.0156 & 0 & 0 & 0 & 0 & 0 & -0.5 & 0 & 0 & 0 & 0 \\ 0 & 0 & 0 & 0 & 0 & 0 & 0 & 0 & 0 & 0 & 0 & 0 & 0 \end{bmatrix} \quad u_{LL} \begin{bmatrix} 0 \\ 0 \\ 0 \\ 0 \\ 0 \\ 0 \\ 0 \\ 1 \\ 0 \\ 0 \\ 0 \\ 0 \\ 0 \end{bmatrix} \qquad 3.130$$

$$y_{LL} = [0.0662 \quad 0 \quad 0 \quad 0 \quad 0 \quad 0 \quad 0 \quad 0 \quad 0 \quad 0 \quad 0 \quad 0 \quad 0 \quad 0] \qquad d_{LL}$$
$$= [0] \qquad 3.131$$

GS_{LL} =

-1.82 s^6 + 1047 s^5 - 1.918e05 s^4 - 5.252e06 s^3 - 2.024e07 s^2 - 1.15e07 s - 8.099e05

----

s^13 + 630.5 s^12 + 1.386e05 s^11 + 3.816e06 s^10 + 3.029e07 s^9 + 9.673e07 s^8 + 1.31e08 s^7 + 8.234e07 s^6 - 2.534e07 s^5 - 2.398e08 s^4 - 1.795e08 s^3 - 2.992e07 s^2 - 1.27e06 s - 2.348e05 *3.132*

Using equations (3.130, 3.131 and 3.132), the dynamic characteristics of the GT onboard liquid fuel control loop combined with the external liquid tank control loop without a controller is estimated to investigate the dynamic characteristics which produce the response shown in Figure 3.25. The system exhibits a negative response, indicating that the control required a compensator design to regulate the flow.

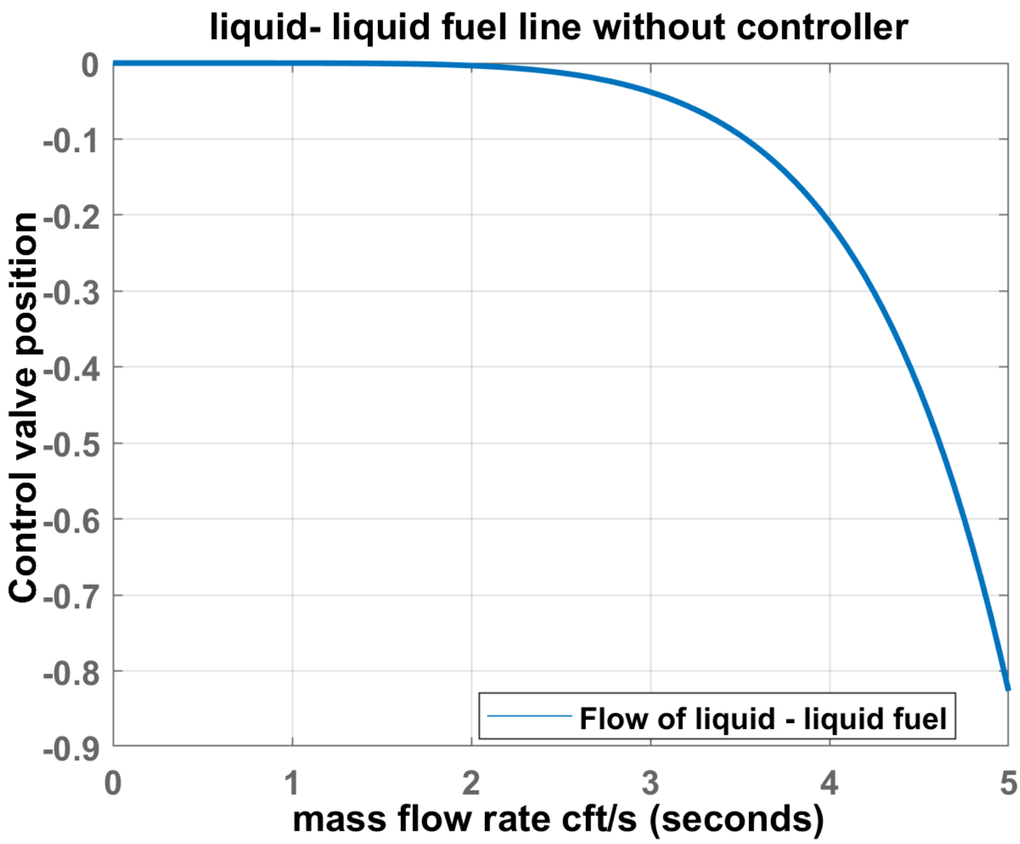

Figure 3.23: Dynamic response of integrated liquid-liquid fuel line without controller

3.13 GT LNG line integrated with external tank LNG flow

This section investigates the dynamic characteristics of the GT LNG line system with an external LNG fuel tank system to study the flow dynamics. The control objective is to synchronise external flow with GT internal LNG flow dynamic to investigate the dynamic response and produce state parameters for controller design. The complete architecture is presented in Figure A3.26.

$$x_{gg} = \begin{bmatrix} 0 & 0 & 0 & 0 & 0 & 0 & 0 & 0 & 0 & 0 & 0 & 0 & 0 \\ 0 & 0 & 0 & 0 & 0 & 0 & 0 & 0 & 0 & 0 & 0 & 0 & 0 \\ 0 & 0 & -0.060 & -1.2 & 0 & 0 & 0 & 0 & 0 & 0 & 0 & 0 & 0 \\ 0 & 0 & 0 & 0 & 0 & 0 & 0 & 0 & 0 & 0 & 0 & 0 & 0 \\ 0 & 0 & -0.0120 & 0 & 0 & 0 & 0 & 0 & 0 & 0 & 0 & 0 & 0 \\ 0 & 0 & 0 & 0 & 0 & 0.02 & 0 & 0 & 0 & 0 & 0 & 0 & 0 \\ 0 & 0 & 0 & 0 & 0 & 0 & 0 & 0 & 0 & 0 & 0 & 0 & 0 \\ 0 & 0 & 0 & 0 & 0 & 0 & 0 & 0 & 0 & 0 & 0 & 0 & 0 \\ 0 & 0 & 0 & 0 & 0 & 0 & 0 & 0 & 0 & 0.0011 & 0 & 0 & 0 \\ 0 & 0 & 00 & 0 & 0 & 0 & 0 & 0 & 0 & -0.0011 & 0.0001 & 0 & 0 \\ 0 & 0 & 0 & 0 & 0 & 0 & 0 & 0 & 0 & 0 & -0.0001 & 0 & 0 \\ 0 & 0 & -0.0156 & 0 & 0 & 0 & 0 & 0 & -0.003 & 0 & 0 & 0 & 0 \\ 0 & 0 & 0 & 0 & 0 & 0 & 0 & 0 & 0 & 0 & 0 & 0 & 0 \end{bmatrix}$$

$$u_{gg} = \begin{bmatrix} 0 \\ 0 \\ 0 \\ 0 \\ 0 \\ 0 \\ 0 \\ 0 \\ 1 \\ 0 \\ 0 \\ 0 \\ 0 \end{bmatrix} \qquad 3.133$$

$$y_{gg} = [0.0662 \quad 0 \quad 0 \quad 0 \quad 0 \quad 0 \quad 0 \quad 0 \quad 0 \quad 0 \quad 0 \quad 0 \quad 0 \quad 0] \qquad d_{gg} = [0] \qquad 3.134$$

GS$_{gg}$ =

-2.833e04 s^6 + 1.63e07 s^5 - 2.986e09 s^4 - 8.177e10 s^3 - 3.151e11 s^2 - 1.791e11 s - 1.261e10

----

s^13 + 630.5 s^12 + 1.386e05 s^11 + 3.65e06 s^10 - 7.283e07 s^9 - 2.214e10 s^8 - 5.05e11 s^7 - 2.105e12 s^6 - 2.068e12 s^5 - 8.001e11 s^4 - 1.19e11 s^3 + 9.537e10 s^2 + 1.867e10 s - 2.88e09

3.135

Modelling equations (3.133, 3.134 and 3.135), the dynamic characteristics of the GT onboard liquid fuel control loop combined with the external tank LNG control loop without a controller is estimated to investigate the dynamic characteristics which produce the response shown in Figure 3.27. The system exhibits a negative response, indicating that the control required a compensator design to regulate the flow.

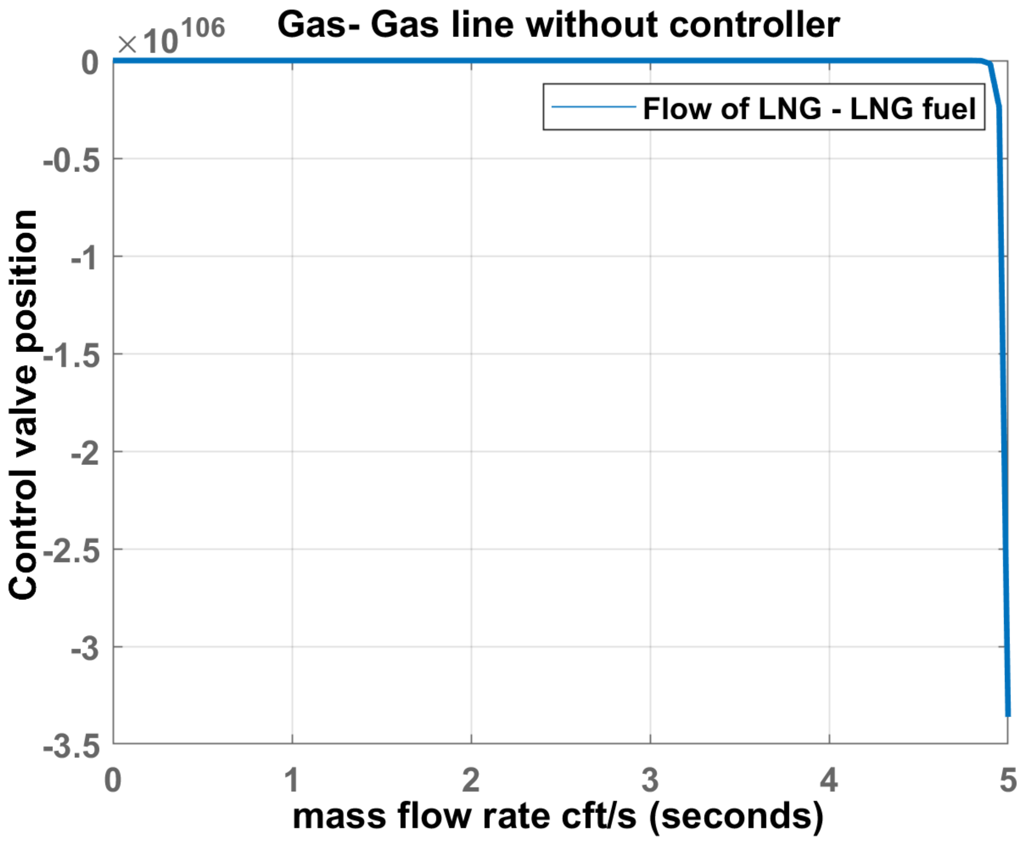

Figure 3.24: Dynamic response of integrated LNG – LNG line without controller

3.14 Integrated GT with Liquid fuel and LNG external tank flow

This section investigates the dynamic characteristics of the integrated GT fuel system with external liquid fuel and LNG dynamics flow. The control objective is to fully synchronise external dual flow with the GT internal flow system for dynamic study. In Figure A3.28, the state variables for the controller are obtained and result of show in state space form.

GS_{ILG} =

$$\frac{-2.833e04\ s^{11} + 1.614e07\ s^{10} - 2.891e09\ s^9 - 9.91e10\ s^8 - 8.117e11\ s^7 - 2.546e12\ s^6 - 3.191e12\ s^5 - 1.714e12\ s^4 + 9.558e11\ s^3 + 6.451e12\ s^2 + 3.807e12\ s + 2.693e11}{s^{18} + 636.4\ s^{17} + 1.423e05\ s^{16} + 4.463e06\ s^{15} - 5.062e07\ s^{14} - 2.255e10\ s^{13} - 6.348e11\ s^{12} - 5.196e12\ s^{11} - 1.762e13\ s^{10} - 2.707e13\ s^9 - 2.122e13\ s^8 - 1.023e12\ s^7 + 4.022e13\ s^6 + 4.31e13\ s^5 + 1.699e13\ s^4 + 2.894e12\ s^3 - 8.228e11\ s^2 - 1.874e11\ s + 2.961e10} \quad 3.136$$

Using equations (3.136) the GT onboard liquid fuel and LNG control loop combined with external liquid fuel LNG tank control loop without a controller is simulated to investigate the dynamic characteristics that produce step response shown in Figure 3.29. The system exhibits a negative response, indicating that the control required a compensator design to regulate the flow.

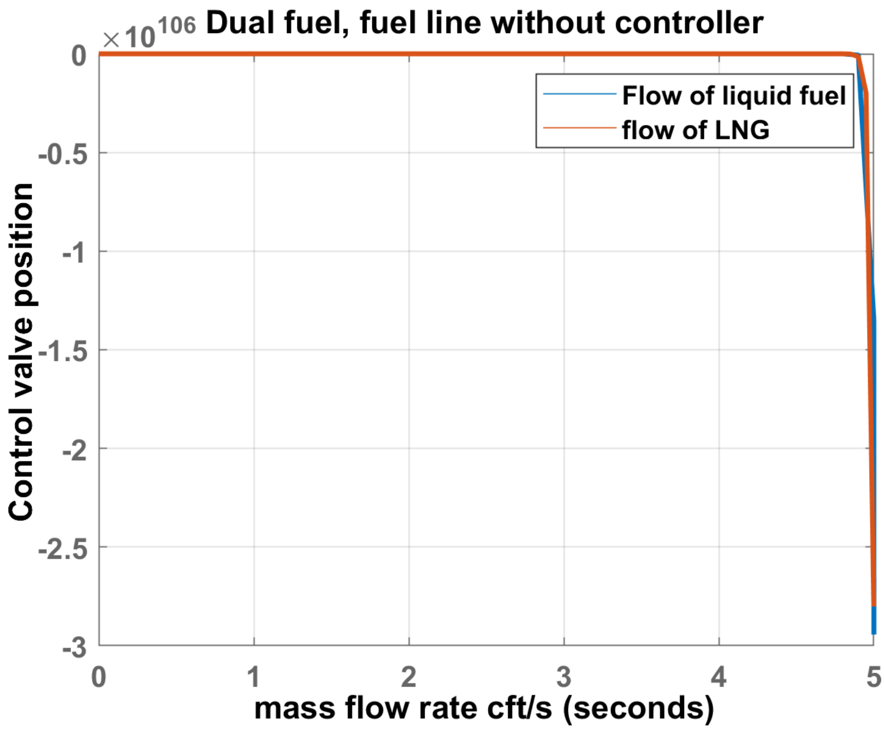

Figure 3.25: Dynamic response of integrated synchronised GT LNG – LNG line without controller

3.15 Summary

The GT model for a dual tank fuel system includes an external liquid fuel tank, an external LNG tank, an onboard liquid and LNG control loop, and an external and onboard fuel flow control loop. An integrated LNG and liquid control loop for dynamic response were also developed in this chapter. Step response characteristics were created with all the relevant state variables to understand the flow behaviour better. The system exhibits positive zeros and poles in all responses following the step input signal. A controller design is necessary to compensate for the flow valve's abnormal response and shape it appropriately with the error signal. The following section will concentrate on developing a thorough model of the nozzles, eventually resulting in dual nozzles for the flow of LNG and liquid fuel.

CHAPTER FOUR: DYNAMIC MODELLING AND DEVELOPMENT OF GT DUAL NOZZLE SYSTEM

4.1 Introduction

In this section, a dual nozzle fuel delivery system as depicted in the preceding section is modelled and developed. The mathematical model for dual-flow systems and control logic will help create nozzle architecture for the optimal controller design and simulation.

The nozzle is one of the essential components in the gas turbine system. It plays a significant role in the operation and efficient management of the gas turbine engine. The nozzle system consists of three elements that work simultaneously to enhance fuel delivery. These elements provide the necessary pressure required to move the fuel or gas through fuel lines. The fuel line also transports energy from the storage cylinder to the various fuel operating devices within the engine architecture. The nozzle dispenses the fuel into the combustion chamber following engine system fuel demand through the acceleration system.

According to [92], pump line fuel injection provides a high level of flexibility in the engine design and operation with an increase in performance by supplying other parts of the system. The liquid fuel nozzle modelling equation and delivery are considered when building the dual nozzle system, and the delivery of natural gas fuel is the second factor.

4.2 Liquid Nozzle Pump Line System

Irrespective of the type of nozzle for either fixed fuel or fuel flexibility system, there will always be a complete system described in Figure 4.1 as pump-line-nozzle injection system architecture. After closing the charge port, the pump's piston compresses the gasoline. The compression continues until the groove opens the discharge port in the pump piston's skirt. This relieves pressure in the pumping chamber and bring the pump's injection cycle close. The engine's demand determines the quantity of gasoline delivered for each stroke.

The governor changes the piston displacement at which the discharge port opens to vary the quantity of gas delivered.

The delivery valve (not illustrated) opens when the gasoline is compressed, allowing gas to flow into the injection line. When the injection cycle at the pumping process is complete, the delivery valve closes, trapping the fuel in the injection line.

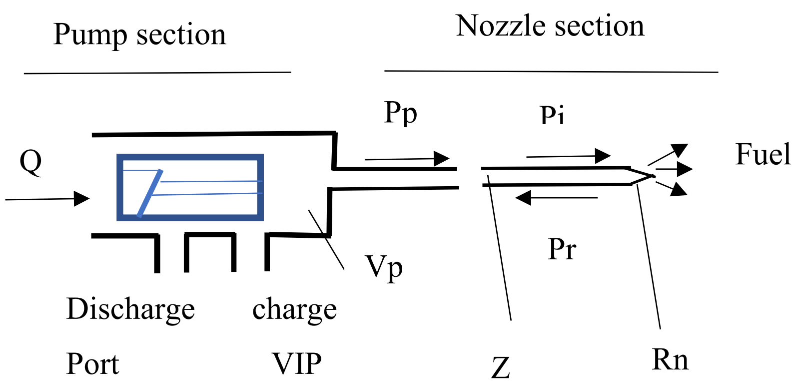

Figure 4.1: Nozzle pump line schematic

Gasoline is transported from the pump to the nozzle via wave propagation across the injection line. The pressure generated at the pump travels through the injection line, eventually arriving at the nozzle with a reduced amplitude due to viscous losses.

The pump reflects the pressure wave that reaches the nozzle and the remainder into the combustion chamber via the nozzle. Due to the brief injection duration, the injection line acts more like a waveguide than a flexible connecting rod.

The nozzle's valve (not shown) is spring-loaded and opens/closes when the nozzle's pressure reaches a predetermined value. The opening reassures typically twice the peak combustion pressure to prevent combustion gases from entering the nozzle chamber.

The injection line is a conduit for fuel transferred from the pump to the nozzle. The pressure generated at the pump propagates along the injection line and arrives at the nozzle with a reduced amplitude due to viscous losses a short time later.

The pressure wave reached the nozzle and reflected into the pump; due to the short injection time it behaves more like a waveguide.

4.3 Nozzle Injection modelling system

The technique associated with modelling and simulation related issues can be classified into three phases: complete system model, sub-systems model and Physical system processes. A proper modelling technique begins with the complete system defining the system's characteristics, dividing the system into manageable sub-systems, and identifying the physical processes involved. The challenges are recognised using this top-down process, and the basic modelling may begin at the bottom, developing the model block by block while establishing the mathematical relations. The high-pressure gaseous fuel injection system depicted in Figure 4.2 was designed and modelled in this project to demonstrate this technology. The system model is challenging because it requires the linkage of unsteady gas dynamics and servo oil flow to the operation of mechanical components in valves and injectors. As a result, this system is an example of coupling a lumped element model and a one-dimensional continuous flow model.

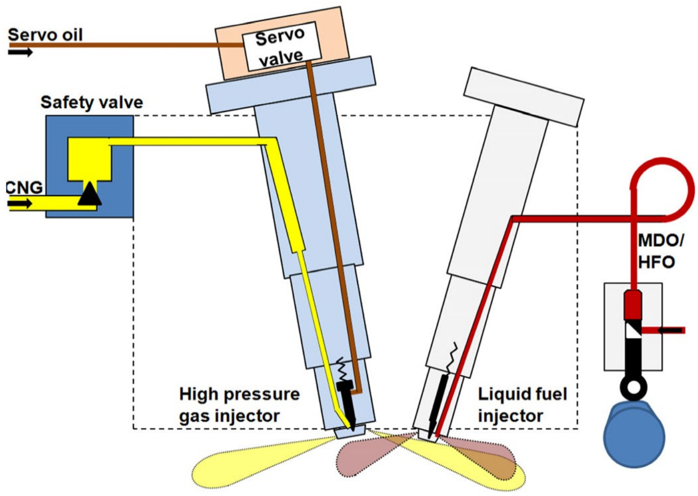

Figure 4.2: The fundamentals of a dual-fuel engine's gasoline system for high natural gas nozzle injection

4.4 Nozzle modelling design assumptions

During the design phase, the following assumptions were made:

1. The pump piston's velocity remains constant throughout the injection cycle. The system's velocity changes slightly during the pumping event.
2. The pump chamber volume remains virtually unchanged during the pumping event. This volume varies by approximately 13% during the pumping event.
3. The charge/discharge ports of the pump instantly close/open. These ports periodically close and reopen, altering the build-up and decay of pump pressure.
4. The deliver valve and snubber valve dynamics are negligible compared to the pressure forces.
5. Injection occurs due to pressure wave propagation along the injection line, and the amplitude of the pressure wave is reduced by viscous losses [95].
6. Because the injection line's outer diameter is approximately three times its interior diameter, the pressure wave propagates as a plane wave and is unaffected by its elasticity [95].
7. The resistance of the injection nozzle is linear. This result is a minor error, addressed in the following section.
8. The injector needle has a low dynamic range compared to the pressure forces, opening and closing instantly.

During the injection cycle, the velocity of the pump piston stays constant. During the pumping event, the speed of the system changes somewhat.

4.4.1 Mathematical Modelling of Nozzle Pressure System

The simplified design of the nozzle injection system from which the equations were derived is shown in Figure 4.2. Once the pump charge port is closed, the volume is trapped between the piston and the nozzle injection line. By ignoring the dynamics and resistance of the delivery valve, a first-order differential equation describes the pump cylinder pressure.

$$\frac{dP_p}{dt} + \frac{1}{\tau}P_p = \frac{Z_c}{\tau}Q_c \qquad 4.1$$

where Pp denotes the pump chamber pressure, Qc denotes the pump's flow capacity, Zc denotes the injection line's characteristic impedance and is the pump's time constant in the hydraulic system. The typical impedance of the line is:

$$Zc = \frac{1}{a_i}\sqrt{\beta\rho} \qquad 4.2$$

a_i is the inner area of the injection line, β is the fuel bulk modulus, and ρ is the fuel density. The time constant of hydraulic pump systems is given by

$$\tau = Z_c\frac{Vp}{\beta} \qquad 4.3$$

where Vp is the volume of compressed fuel. Hence, solution for equation (4.1) is modified as:

$$P_p = Z_c Q_c\left[1 - e^{-\frac{t}{\tau}}\right] \qquad 4.4$$

The pressure generated at the pump travels along the injection line gets to the nozzle in the form of incident wave Pi. Hence, the time it takes for the pressure to travel one line length is:

$$\eta = \frac{l_1}{C} \qquad 4.5$$

where l_1 is the length of the injection line, and c is the speed of the propagation wave. The magnitude of the propagated pressure wave is attenuated with viscous losses. The decay of the propagates pressure wave from the pump line to the injection nozzle is expressed as:

$$\frac{P_i}{P_P} = e^{-\sigma} \qquad 4.6$$

where σ is the loss parameter for the line

$$\sigma = 3.3\sqrt{\frac{v1}{r^2\,C}} \qquad 4.7$$

where V is the kinematic viscosity of the fuel and r is the inside radius of the injection line.

The magnitude of the first incident pressure wave that arrives at the nozzle is given by:

$$P_i^1 = Z_c Q_c\left[1 - e^{-(t-\eta)/\,\tau}\right]e^{-\sigma} \qquad 4.8$$

Some of the incident waves were reflected outside the nozzle, while others were transmitted through it. As a result, the proportion of incident wave reflected depends on the respective magnitudes of the nozzle resistance, Rn, and the line's characteristic impedance, Zc.

$$P_r^1 = P_i^1\left[\frac{R_n - Z_c}{R_n + Z_c}\right]^1 \qquad 4.9$$

The nozzle pressure of this initial wave equals the sum of the forces of the incident and reflected waves.

$$P_n^1 = P_i^1 + P_r^1 \qquad 4.10$$

The injection timing at the nozzle during the first transmitted wave is achieved by averaging equations (4.8, 4.9, and 4.10).

$$P_n^1\left[\frac{2\,R_n}{R_n + Z_c}\right]^1 Z_c Q_c\left[1 - e^{-(t-\eta)/\,\tau}\right]e^{-\sigma} \qquad 4.11$$

Equation (4.11) is used only if t > n and when nozzle pressure wave delays. Hence, the reflected pressure wave is expressed as:

$$P_n^1 \left[\frac{2\,R_n}{R_n+Z_c}\right]^1 Z_c Q_c\left[1-e^{-(t-\eta)/\,\tau}\right]e^{-\sigma} \qquad 4.12$$

The delay and losses as reflected wave return to the pump. This reaction gives rise to equation (4.13).

$$P_r^1 = \left[\frac{R_n-Z_c}{R_n+Z_c}\right]^1 Z_c Q_c\left[1-e^{-(t-\eta)/\,\tau}\right]e^{-\sigma} \qquad 4.13$$

The magnitude of the reflected wave to the pump is the function of the characteristic impedance of the injection and that of the pump given in equation (4.14).

$$P_r^P = P_i^P \left[\frac{Z_P-Z_c}{Z_P+Z_c}\right]^P \qquad 4.14$$

From equation (4.14), when the incident wave of the pump propagates back as Pi^2, equation (4.13) is modified as:

$$P_I^2 = \left[\frac{Z_P-Z_c}{Z_P+Z_c}\right]^P \left[\frac{R_n-Z_c}{R_n+Z_c}\right]^1 Z_c Q_c\left[1-e^{-(t-3\eta)/\,\tau}\right]e^{-3\,\sigma} \qquad 4.15$$

The equation (4.15) indicates the arrival of the second wave at the nozzle, and part will be reflected back while partly will flow through the nozzle for practical work. Hence, the nozzle carries pressure as a result of the sum. This is given as:

$$P_n^2 \left[\frac{2\,R_n}{R_n+Z_c}\right]^2 \left[\frac{Z_P-Z_c}{Z_P+Z_c}\right]^P \left[\frac{R_n-Z_c}{R_n+Z_c}\right]^1 Z_c Q_c\left[1-e^{-(t-3\eta)/\,\tau}\right]e^{-3\,\sigma} \qquad 4.16$$

Equation (4.16) is applicable only if t >3n. Hence, summing equations (4.11 and 4.16) give the total nozzle pressure.

$$P_n^t = P_n^1 + P_n^2 \qquad 4.17$$

4.5 Nozzle Liquid Phase Delivery

Effective fuel delivery per operating cycle depends on several factors such as load torque, frication torque and engine combustion efficiency. These variables are controlled by the engine governor that automatically regulates the movement of the pump piston between the discharge and charge port [92]. From the nozzle flow and pressure analysis, the initial injection is fixed from the start, but varies as the load is applied.

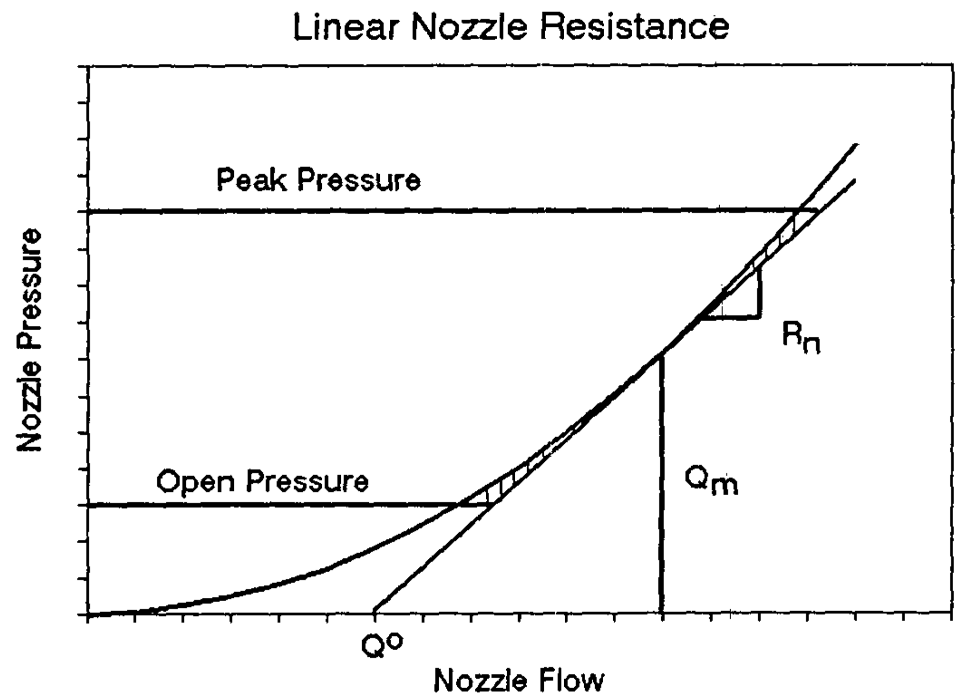

Figure 4.3: Linear Operation of Nozzle

From the graph, the injected fuel is the function of nozzle resistance and pressure at any instant of time. The linear nozzle resistance is defined by the expression below:

$$R_n = \frac{\rho Q_m}{\left(n C_d a_o\right)^2} \qquad 4.18$$

Where ρ is the fuel density, Q_m is the fuel flow through the nozzle and C_d discharge coefficient, a_o, area of an orifice in each nozzle, n number of orifices. The nozzle opening depends on the available pressure. The nozzle opening time t_0 for fluid flow is obtained using equation (4.19).

$$t_o = \eta + \tau 1n\left[\frac{2Z_c Q_c}{2Z_c Q_c - P_o e^{+\sigma}}\right] \qquad 4.19$$

Figure 4.3 clearly shows nozzle resistance crosses the flow axis at Qo at 0.5 of nozzle mean flow. Hence, total nozzle flow is given by:

$$Q_n = Q^o + \frac{P_n}{R_n} \qquad 4.20$$

And the fuel delivered by the injection is expressed as:

$$FD = \int_{t_o}^{t_c} Q_n \, dt \qquad 4.21$$

The nozzle injection wave's arrival time at various steps is shown in Figure 4.4. The figure illustrates the proportional delivery timings of the first and second waves at the nozzle. This diagram presupposes that the second wave arrives before the injection cycle is finished, which is typical for most injectors. When the trailing edge of the first pressure wave approaches the nozzle, as shown in Figure 4.4, the nozzle shuts. The fuel delivery is integrated into three intervals from the figure as shown in equation (4.22).

$$FD = \int_{t_o}^{3_{TL}} \left[Q^o + \frac{P_n^1}{R_n}\right] dt + \int_{3_n}^{t_o+2_{TL}} \left[Q^o + \frac{P_n^1 + P_n^2}{R_n}\right] dt + \int_{t_o+2_{TL}}^{t_c} \left[Q^o + \frac{P_n^1 + P_n^2}{R_n}\right] dt \qquad 4.22$$

In the equation (4.22), FD is fuel delivery, TL injection line time delay, n number of nozzle holes, R_n nozzle resistance, P_n nozzle pressure, to nozzle opening time, tc nozzle closing time, and Q^o half nozzle flow.

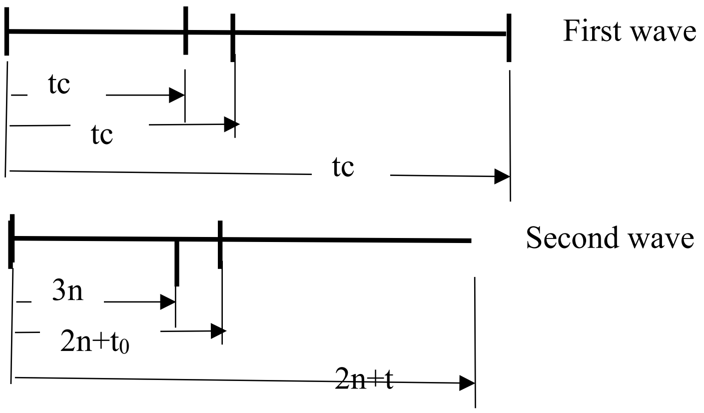

Figure 4.4: Pressure wave arrival at the nozzle

Hence, equation (4.22) is simplified by letting $\nabla t = tc - to.$

$$FD = Q^o(\nabla t) + \int_{t_o}^{t_c} \left[\frac{P_n^1}{R_n}\right] dt + \int_{3_{TL}}^{t_o+2_{TL}} \left[\frac{P_n^2}{R_n}\right] dt + \int_{t_o+2_{TL}}^{t_c} \left[\frac{P_n^2}{R_n}\right] dt \qquad 4.23$$

From equation (4.16), taken the third integral of Pn^2 with Zp approaches infinity, the fuel delivery is calculated with equation (4.24).

$$FD = Q^o(\nabla t) + \left[\frac{2\,R_n}{R_n+Z_c}\right]\left[\frac{Z_c}{R_n}\right] Q_p \tau [A + B + C] \qquad 4.24$$

A, B, C is calculated using the following

$$A = \left(\frac{\Delta t}{\tau} - \left[1 - e^{-\Delta t/\tau}\right] e^{-(t_o - TL)/\,\tau}\right)\, e^{-\sigma} \qquad 4.25$$

$$B = \left(\frac{t_o - TL}{\tau} - \left[1 - e^{-(t_o - TL)/\,\tau}\right]\right)\, e^{-3\sigma} \qquad 4.26$$

$$C = \left[\frac{R_n - Z_c}{R_n + Z_c}\right]\left(\frac{\Delta t - 2TL}{\tau} - \left[1 - e^{-(\Delta t - TL)/\tau}\right] e^{-(t_o - TL)/\,\tau}\right) \qquad 4.27$$

4.5.1 Operation and Design of Dual Nozzle Fuel Engine

All reciprocating internal combustion (IC) engines operate on the same principle. Crushing an explosive mixture in a small compartment between the piston's head and the surrounding cylinder begins. Following the ignition of the mix, the high-pressure combustion products propel the piston through the cylinder. Compression ignition (CI) and spark ignition (SI) are the two ignition technologies. The existing diesel engine operation method is compression ignition, in which the intake air is compressed alone. Then the diesel fuel is directly injected at high pressure over the compressed air inside the combustion chamber, causing it to ignite easily due to its ignition temperature. On the other hand, the LPG–diesel dual-fuel engine burns a mixture of primary gaseous (LPG) fuel and liquid pilot fuel via both compression and spark ignition [96–99].

In the case of an LPG–diesel dual-fuel engine, the intake air-to-LPG mixture is sucked into the cylinder, just as it is in a spark-ignited engine and compressed to increase the temperature and pressure. Following the compression stroke, a tiny amount of pilot diesel fuel is injected to ignite the mixture, as shown in Figure 4.5. This pilot injection acts as an ignition source. The LPG gas-air mixture ignites in various places close to the injected diesel spray, creating several flame fronts. As a result, combustion happens quickly and smoothly.

It is critical to note that combustion begins similarly to the CI engine but propagates via flame fronts similarly to the SI engine in a dual-fuel engine. Generally, the engine's power output is adjusted by varying the primary LPG gaseous fuel introduced into the intake manifold. The amount of diesel fuel required varies according to the engine's operating conditions and design characteristics. The amount of pilot diesel needed for ignition is typically between 10% and 20% of normal operating conditions on diesel fuel alone [104-105]. The mass fraction of LPG used in dual fuel mode is calculated using the following expression:

$$Z = \frac{m_{LPG}}{m_{Diesel} + m_{LPG}} x100\% \qquad 4.28$$

Where m_{LPG}, is for LPG mode and m_{Diesel} is for the diesel mode of operation. The Z varies from 10%, 20%, 30% etc, used in the mass flow dual mode.

4.5.1.1 Modification of traditional Diesel Engine as Dual Fuel Nozzle

Diesel engines can easily be modified to operate on an LPG–diesel dual fuel mode. LPG is blended with the air intake while the conventional diesel fuel injection system continues to supply a certain amount of diesel fuel at a reduced rate [101-102]. To operate the engine in dual fuel mode, the intake manifold must be modified by connecting an LPG line and an evaporator [103]. The regulating valve directs gaseous fuel into the intake manifold's gas mixer [104-106]. As mentioned in [107], when LPG is fed to the intake manifold via a tiny duct, the design of the gaseous fuel delivery system has a significant effect on HC emissions at a low load. LPG is injected into the engine in conjunction with mechanical or electronic management of the engine's loads and speed.

The combustion process and engine output vary according to the engine type (direct injection or port injection) and method of supplying gaseous fuel. When pressure is kept close to atmospheric, the mass flow rate of LPG is proportional to the pressure differential between the gas mixer and the evaporator. However, with LPG dual-fuel engines, it is critical to manage the flow rate of the primary LPG fuel and the pilot diesel fuel under a variety of engine operating conditions. Reduced LPG content may have little effect on soot emission reduction or engine performance improvement, whereas significantly increased LPG content is likely to cause rapid in-cylinder pressure to rise and engine damage [108]. Numerous researchers have researched LPG–Diesel dual-fuel engines, including modifications to single-cylinder [109-116] and multi-cylinder [107, 108, 118] diesel engines that use manifold injection [119-121] and manifold induction to supply LPG in the dual fuel mode [108, 110, 91, 122, 123, 124]. The combustion performance, and emission characteristics of an LPG–Diesel dual fuel engine are found to be highly variable depending on the engine type, LPG fuel supply system, and operating conditions.

4.5.2 LPG–Diesel Dual Fuel Engine Combustion Process

A pure diesel engine's soot is classified into four phases: spark delay, rapid combustion, regulated flame, and time after combustion. The same process in an LPG dual-fuel engine combines the characteristics of SI and CI engines and consists of five phases during the combustion process of the Ricardo E6 single cylinder, as illustrated in Figure 4.5. The phases are as follows: pilot ignition delay (AB), premixed pilot combustion (BC), principal fuel (LPG) ignition delay (CD), fast LPG fuel combustion (DE), and time after combustion (EF).

The pilot ignition delay period (AB) is more extended than for pure diesel fuel operation, partly due to a decrease in oxygen intake concentration caused by the addition of LPG to the air intake and partly due to a change in the compressed mixture's specific heat, resulting in a lower compression temperature. The premixed pilot combustion (BC) method generates a small flame initially ignited by a small amount of fuel, and the flame gradually increases the pressure. In the compression process, primary fuel (LPG) undergoes chemical pre-ignition reactions, resulting in prior ignition delay (CD), during which the pressure begins to decrease slowly. The fast combustion (DE) phase is volatile because it begins with flame propagation caused by pilot diesel fuel spontaneously igniting. Pressure is initially increased during this stage primarily due to the premixed combustion of a portion or all of the pilot diesel and the combustion of a small amount of the entrained LPG gas. The pressure is then increased to its maximum value as most of the LPG gaseous fuel and a trace of the remaining pilot diesel inside the cylinder are burned. After the burning stage (EF), which begins after the rapid pressure rise and continues well into the expansion stroke. This is because LPG fuel burns more slowly and contains pilot fuel substances. The length of the ignition delay dramatically influences the success of this phase.

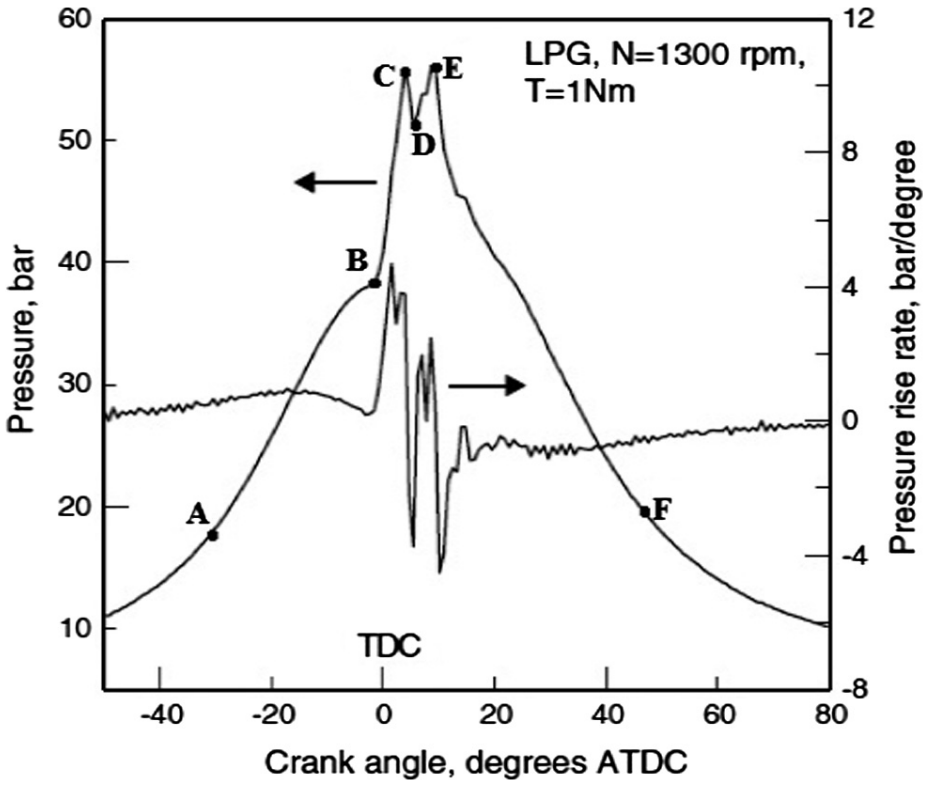

Figure 4.5: Typical combustion pressure and pressure rise rate versus crank angle of LPG diesel fuel

When the amount of LPG fuel injected increases, the combustion process frequently experiences banging and malfunctioning [126-128]. Knocking and misfiring are avoided by considering the mass of LPG used at higher loads. Increased diesel pilot fuel consumption reduces engine knock under high-output conditions. Due to the combustion and additional heat generated by gaseous fuel, the maximum pressure in an LPG dual-fuel engine is always more significant than the pressure in a diesel engine [125]. In dual-fuel vehicles, the increased LPG ratio has two consequences. First, premixed combustion and flame propagation speed increases while mixing-controlled liquid fuel combustion decreases. Second, the reduced pilot injection quantity results in fewer ignition sources, increasing the distance travelled by the flame to burn all the premixed mixtures in the chamber [128].

The three critical combustion phases of premixed combustion of the pilot diesel fuel, premixed combustion of the primary LPG fuel, and diffusion combustion of the primary

LPG fuel and any remaining pilot diesel fuel are shown in Figure 4.6. Rate of Heat Released (ROHR) of LPG diesel dual fuel for a single-cylinder constant speed engine.
The first phase is primarily due to the pilot diesel fuel, with a trace of LPG entrained by the diesel spray also burning concurrently with the diesel. The burning of diesel fuel accounts for most of the heat energy released during this period. Most of the LPG fuel and a minor portion of the residual pilot diesel fuel is burned during the second phase. The amount of pilot diesel replenished determines how much heat energy is produced during the premixed combustion phase of the LPG fuel. This suggests that as LPG consumption rises, energy emissions do as well. The second combustion phase uses more gaseous fuel than the first. The incorrect combustion of the two combined fuels results in the third phase.

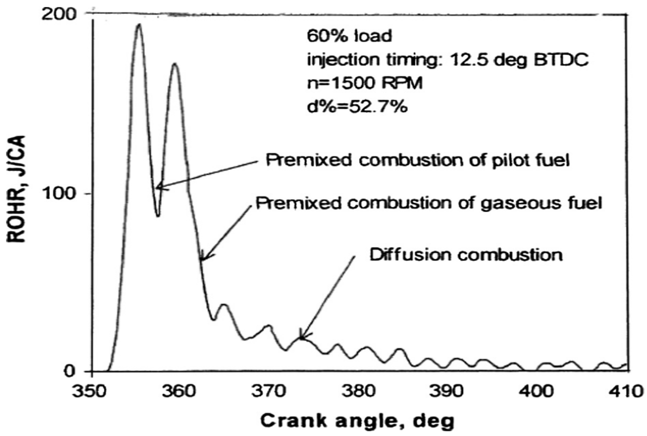

Figure 4.6: Heat release rate versus rank angle of dual-fuel combustion

4.6 Dual Fuel Gas-Phase Flow Modelling

In the traditional gas turbine system, liquid phase flow is established, and principles are clear, as described in section 4.5. However, the natural gas phase model requires mathematical model development that needs consideration for a complete system model, mechanical system, control system, and thermodynamic combination of hydraulic features. The most complicated aspect involved is the natural gas phase integrating thermo fluid and compressible fluid flow model. However, [109] establishes the principle of modelling thermo fluid systems as non-trivial since state equations in the domain are well-known. Hence, detailed calculations and design philosophy refer to the work [109].

4.7 Dual nozzle Simulink control modelling

4.7.1 Simulink design of automatic fuel selector pressure switch

The system model built in Simulink consists of liquid fuel phase flow and natural gas phase flow. The two-phase flow merges in the combustion chamber through the dual nozzle composed of three systems: liquid, gas, and air-fuel ratio. The model is developed using the existing thermodynamic principle found in the gas turbine block. The system is programmed such that when natural gas is available, it switches automatically to gas supply, and the turbine only runs on gas fuel supply. Liquid fuel supply only comes into operation when there is a gas shortage. Similarly, for economical operation, when the market price for gas rises above liquid fuel, the programming is flexible, and it will automatically switch to run on liquid fuel with the gas fuel operating as standby supply only.

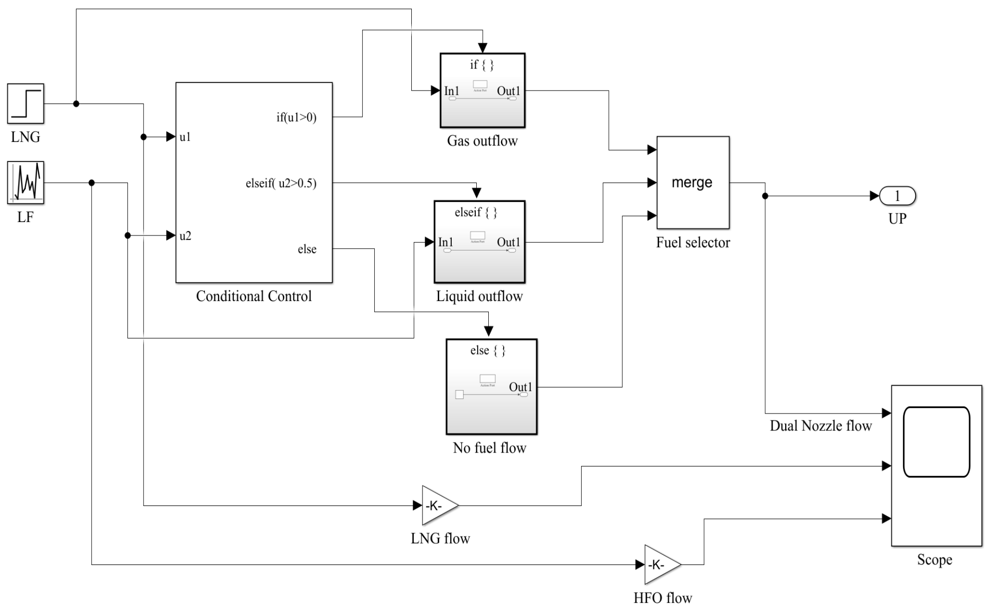

Figure 4.7: GT automatic dual pressure control switch

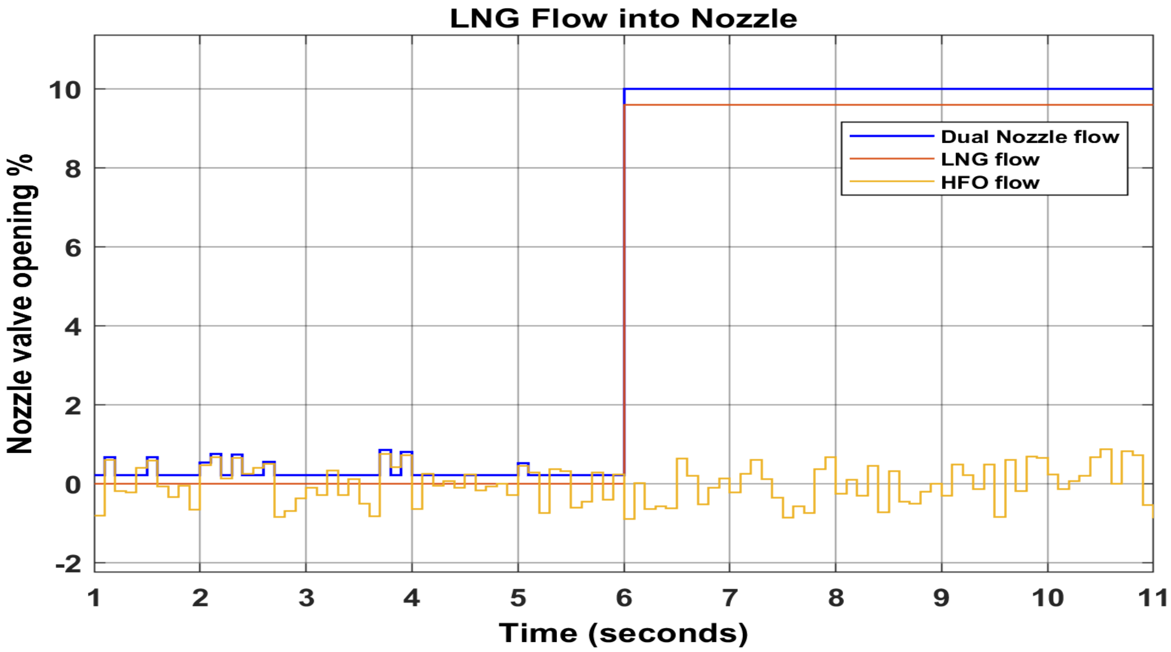

a

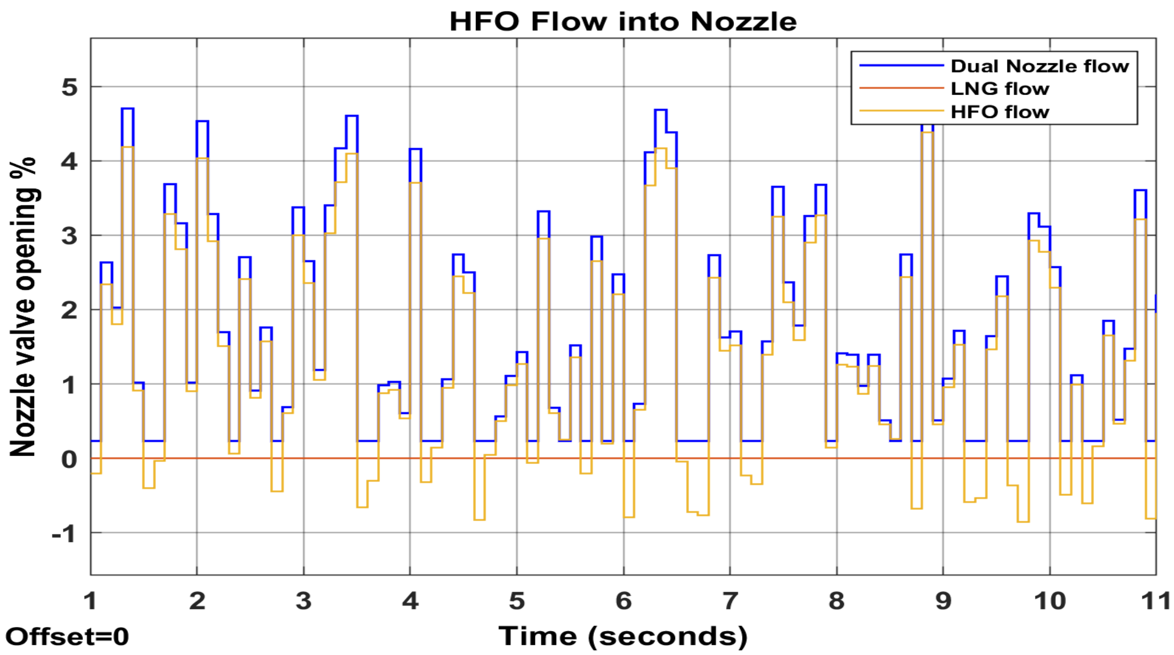

b

Figure 4.8: Output response of automatic dual nozzle pressure-flow a) LNG flow into nozzle b) HFO flow into the nozzle

Figure 4.8 shows a dual-nozzle simulation with LNG and HFO flowing through it. Figure 4.8a shows a dual nozzle with a pressure switch using LNG as the nozzle flow, while the

HFO valve is closed. When LNG pressure falls below expected, the HFO valve opens, allowing liquid fuel to flow into the nozzle, as shown in Figure 4.8b.

4.7.2 Dual nozzle integration GT fuel combustion system

The combustion chamber is designed with two nozzle systems for combusting the chemical energy. When the system starts on natural gas mode, the diesel fuel-air ratio comes into operation called pilot fuel supply which sparks ignite the turbine before the entire flow of natural gas. The simulated model built-in Simulink is shown in Figure A4.9. In the block diagram, the automatic pressure control switch monitors and selects the available fuel based on the pressure released from the tank. Due to economic reasons, LNG is given the higher priority and once available, the pressure switch cuts off liquid fuel. Further operational interlock is provided on the combustion chamber to implement the dual functionality using maximum/minimum block, allowing the high-pressure fuel flow into the combustion chamber. When simulated, the output response without control action is shown in Figure 4.10. The developed dual nozzle is applied to the GT system with external tanks connected to the onboard fuel system by the dual nozzle. The system is put through its paces with 5 litres of liquid fuel and 10 litres of LNG in the tank. The dual nozzle response indicates that only the LNG nozzle is in use because the pressure-flow limit is a minimum of 10 litres. However, the speed was set to 3000 rpm, but the engine revved to well over 6000rpm.

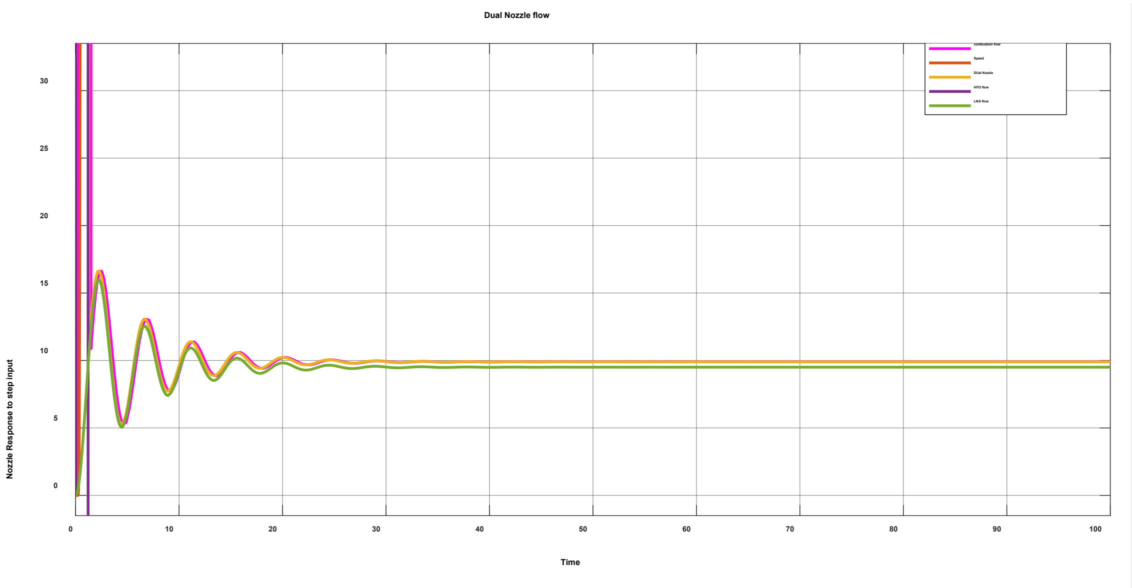

Figure 4.9: Response of integrated dual nozzle GT fuel Control

4.8 Summary

This chapter studied the dual nozzle design for the GT system using the single nozzle principles. The dual fuel model was designed with Simulink software and consisted of liquid fuel and natural gas flow. In the development, three systems in the combustion chamber are established: the two-phase flow, the gas flow, and the air-fuel ratio. The gas turbine block thermodynamic principle is applied to develop the nozzle model. The nozzle is programmed such that when LNG gas is available, the system is set up to automatically switch to gas supply, allowing the turbine to run solely on gas fuel. When the gas supply runs low, the liquid fuel supply kicks in. Programming is flexible enough to switch to liquid fuel if gas prices rise above liquid fuel's market price and the gas fuel as standby supply.

CHAPTER FIVE: DESIGN OF GAS TURBINE DUAL FUEL CONTROL LOOPS USING PID

5.1 Introduction

This chapter discusses the design of a PID controller for GT's dual-fuel control loops and its effect on the fuel flow system's dynamic performance. In chapter three, under gas turbine modelling, the dual-fuel nozzle system was extensively discussed using the Rowen model concept and modelling additional fuel lines for LNG fuel flow. Controllers are meant to work in tandem with the process to maintain the process's dynamics. These required meeting fundamental controller design goals and PID controllers to distribute the GT liquid and gas lines control.

The controller strategy maximises performance and optimises the switching process. The design ensures linearity between setpoint and output, but future constraints introduced by the process variable are also accommodated. Additionally, it will improve process safety and maximise operation, despite its ease of tuning, with a fast and stable response.

5.2 PID Model for the GT fuel control system

The mathematical model for the PID controller is expressed in equation (5.1) in the time domain. However, applying to the model, the equation converted and the model in the Laplace domain gives rise to equation (5.2) for the model.

$$U = Kc\left(e + \frac{1}{Ti}\int edt + Td\frac{de}{dt}\right) \qquad 5.1$$

Rewriting equation (5.1) in the Laplace domain gives equation (5.2).

$$G(s) = K_c\left(1 + \frac{1}{Tis} + Tds\right) \qquad 5.2$$

5.3 GT dual fuel system configuration

This diagram shows the GT block diagram with the modification of the fuel block loop shown in Figure A5.1. In the original Rowen mathematical model, only one fuel loop is required for the liquid fuel system [20]. The new block diagram for the GT control system design is built with the dual fuel nozzle model in Chapter 4.

5.4 GT liquid fuel system

The liquid fuel system of the GT is divided into two fuel loops, namely the external tank supply and the onboard fuel system. Each of these systems is controlled differently but connected to provide the complete fuel flow.

5.4.1 External liquid fuel tank

The PID control for the loop was developed using the liquid fuel line transfer function from the tank supply model in Chapter Three. The system's closed-loop transfer function is depicted in the diagram shown below. These plant dynamics are controlled with the PID controller design, as indicated in Figure 5.3.

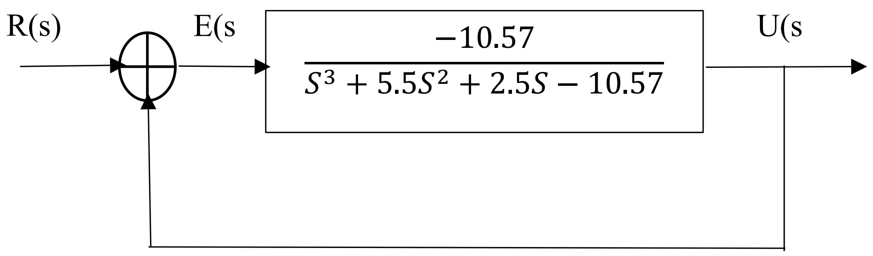

Figure 5.1: Block diagram of external liquid fuel tank supply

Figure 5.2 incorporates the PID model for controller design operation, as shown in Figure 5.3.

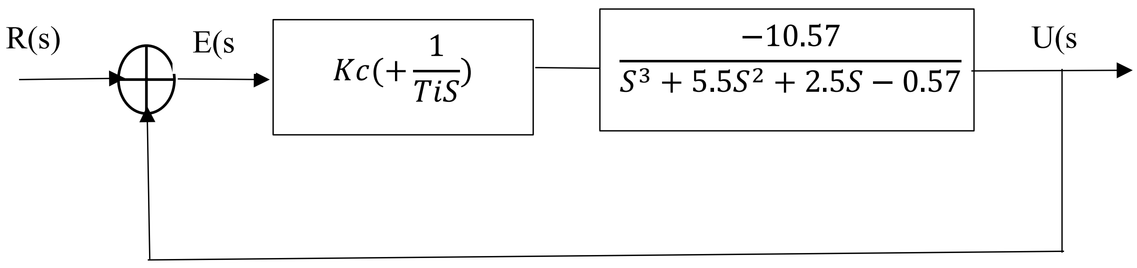

Figure 5.2: PID control of liquid fuel tank

5.4.2 GT onboard fuel system

The GT fuel system onboard consists of the fuel valve position and the fuel actuator dynamic shown in Figure 5.3. The flow out of the system depends on the inertia of the fuel actuator and the valve positioner.

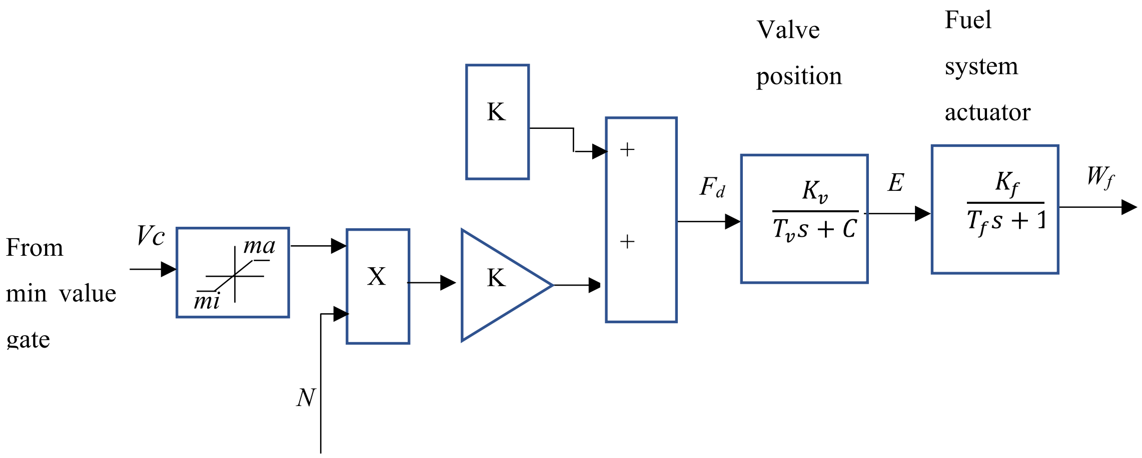

Figure 5.3: MATLAB block for GT liquid fuel system

From the diagram, K_v is the fuel valve positioner gain, T_v is the valve positioner time constant, Kf is the fuel actuator gain. At the same time, the Tf is the actuator time constant, Fd is the fuel demand from the system based on the engine's acceleration, and Wf is the fuel flow. At the same time, K_6 is the minimum value of fuel required, E_1 is the output from the valve positioner, and C is the constant.

The *Vc* minimum value output for this operating point is the lowest quantity of fuel required and is the input to the saturation of the product. The per-unit turbine speed *N* is another input to the system (limited by the acceleration control). Input to a fuel system *K6* is effectively the lowest quantity of fuel flow without loading and rated speed, and the gain *K3* scaled output fuel.

5.4.2.1 Acceleration Control

Figure 5.4 shows the acceleration control for the fuel system when the GT acceleration is above the limit. A speed control would prevent an over-speed gas turbine that might harm the shaft. The gas turbine speed is the input signal to the acceleration control. It passes a differential block to get the turbine speed. The acceleration is compared with an acceleration limit, which gives you an error signal. The error signal consists of an input for a control block with a minimum value gate output [5, 20-23].

Furthermore, when a rate higher than the acceleration limit increases the speed of the gas turbine, the integrator output decreases from an initial value of the maximum result. Because the gas turbine supplies less power, the speed control output delays to produce of the required speed by the controller. Furthermore, the speed controller output will be less efficient if the acceleration is significant and the gas turbine has high over-speed. The consequence is that the command signal would have tended to lower fuel usage rather than the acceleration control. Therefore, the integrator limit should be a little more significant than the actual power supplied by the gas turbine Figure 5.4.

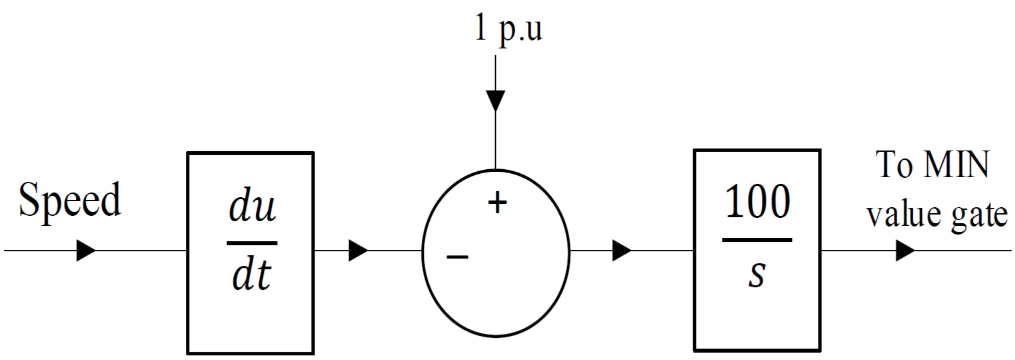

Figure 5.4: Acceleration Control

5.5 Simulation of GT liquid fuel system

This section applied the concepts developed in Chapter Three and Sections 5.1 to 5.3 to simulate the liquid fuel loop under various conditions. A system without a controller and a system with controller action.

5.5.1 GT liquid fuel model without PID Controller

Figure 5.5 shows a Simulink simulation model without a PID controller that combines the GT onboard fuel system with the external tank fuel system. Figure 5.6 captures the response when a step signal represents the fuel flow signal. A generator could not start at all because the flow is unstable, as shown by the response.

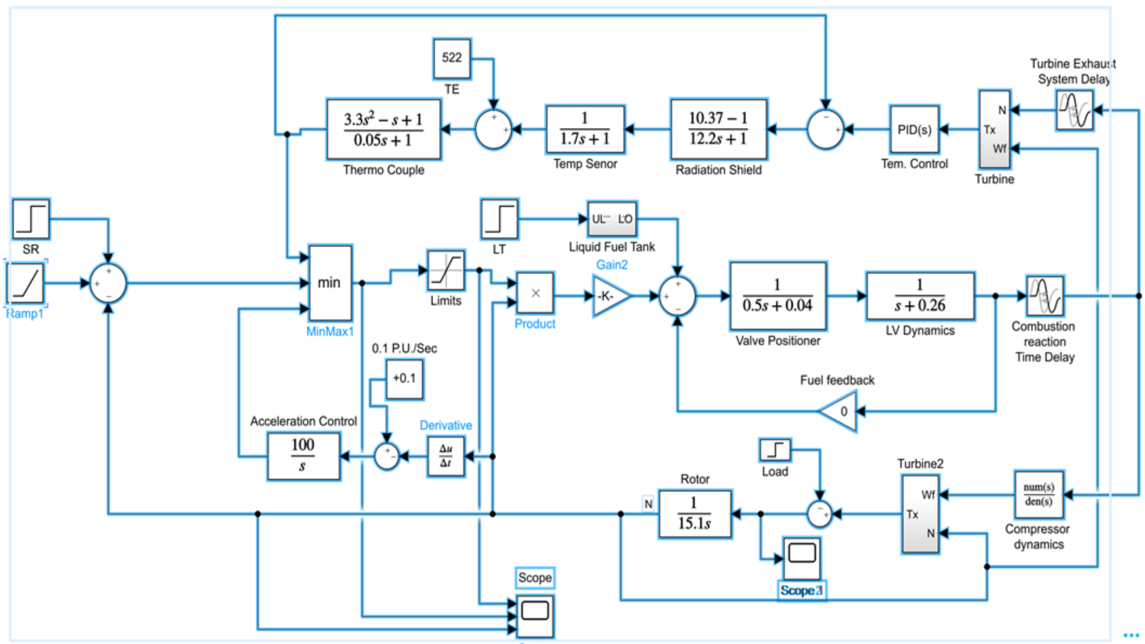

Figure 5.5: GT Simulink model with Liquid fuel system without PID controller

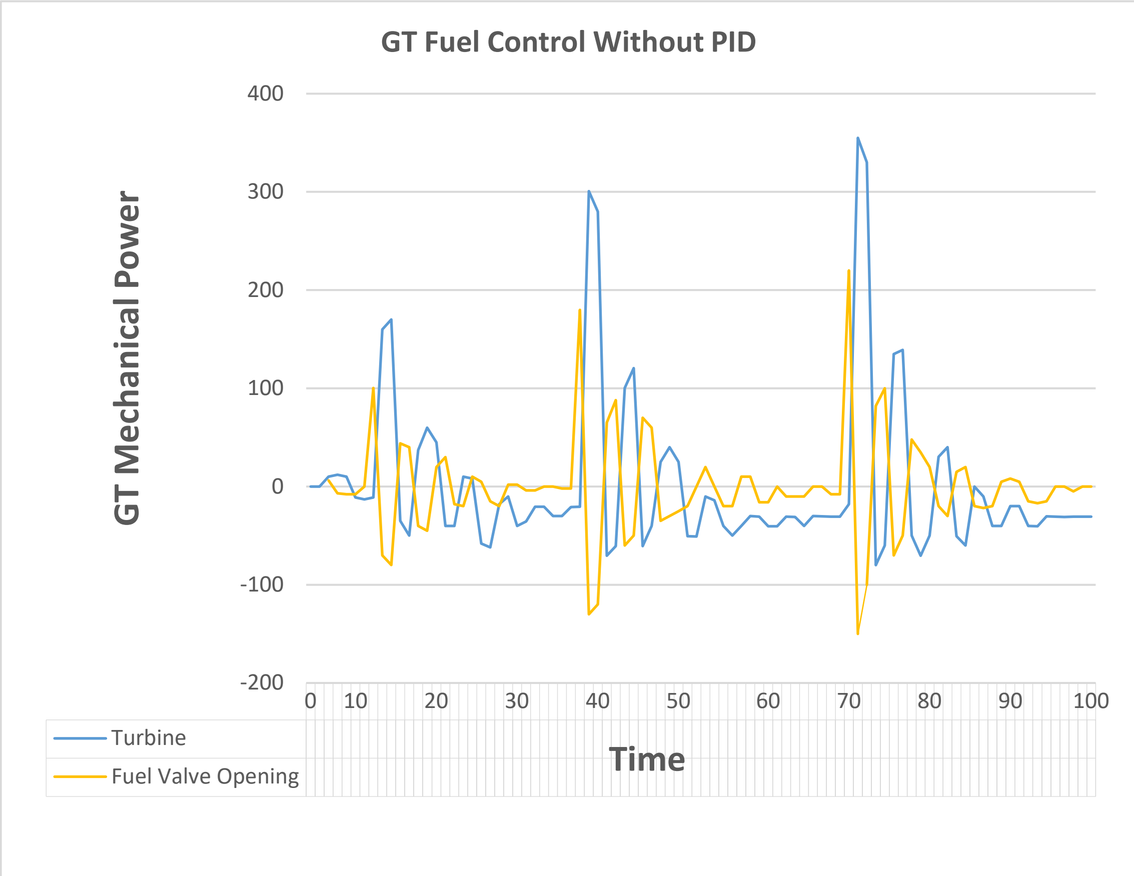

Figure 5.6: Response of GT Liquid fuel system without PID controller

5.5.2 GT liquid fuel model with PID Controller

Figure A5.8 shows a Simulink simulation model with a PID controller that combines the GT onboard fuel system with the external fuel tank system. Figure 5.7 captures the response when a step signal represents the fuel flow signal. A generator would be able to start because the flow is stable, which is evident from the simulation result.

The PID controller blocks Simulink and measures the fuel flow by varying the valve operation and the compressor pressure response. The GT rotor speed was set to 3000 rpm and kept constant. Table 5.1 displays the simulation parameter results, while Figures 5.7 and 5.8 depict the dynamic response for the rotor speed and compressor pressure flow, respectively.

Table 5.1: GT liquid fuel control parameters of PID controller settings

PID 1	CONTROLLER PARAMETER	TUNNED VALUE	PERFORMANCE AND ROBUSTNESS	VALUES
1	Proportional	0.6620	Rise time	4.47 seconds
2	Integral	0.0292	Settling time	46.2 seconds
3	Derivative	3.0905	Overshoot	15.1%
4	N (filter coefficient)	0,5166	Peak	1.15
5			Gain Margin	9.03dB @ 558 rad/s
6			Phase margin	55.7 deg @ 0.215 rad/s
7			Closed-loop stability	Stable
PID 2	**Controller parameter**	**Tunned value**	**Performance and robustness**	**Values**
1	Proportional	0.0759	Rise time	1.92 seconds
2	Integral	0.0021	Settling time	10.8 seconds
3	Derivative	0.4295	Overshoot	29.6% @ 4.9 sec
4	N (filter coefficient)	0.5841	Peak	1.3
5			Gain Margin	inf @ NaN rad/s
6			Phase margin	46.9 deg @ 584 rad/s
7			Closed-loop stability	Stable

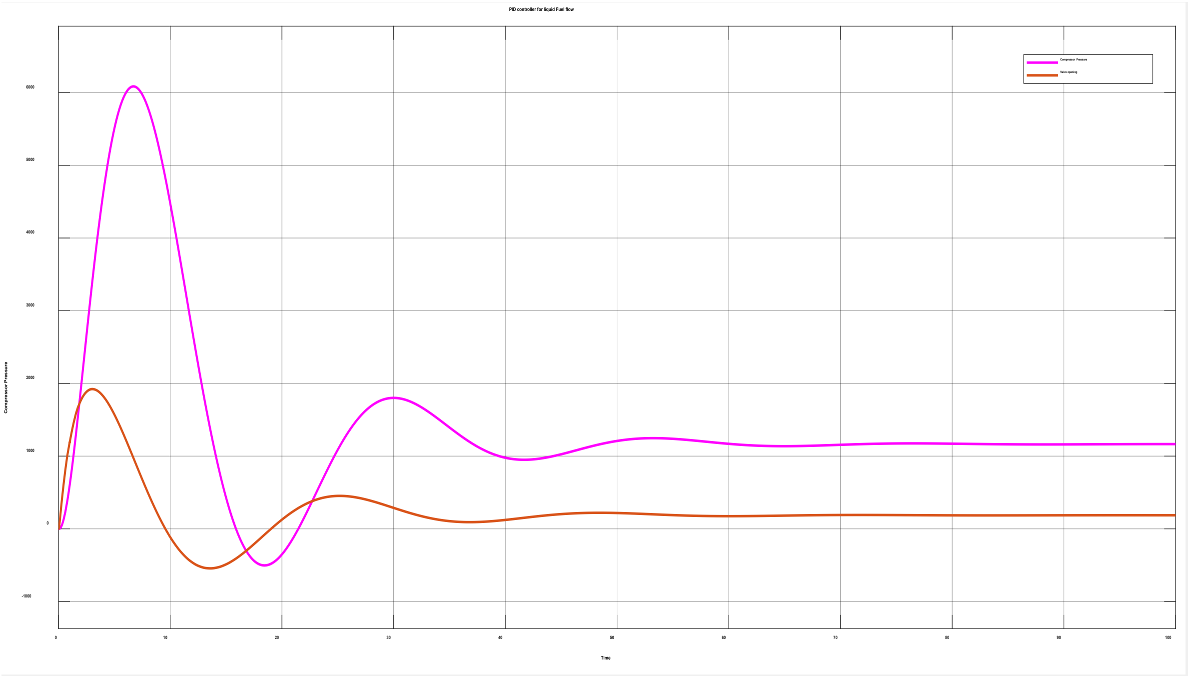

Figure 5.7: GT liquid fuel flow control with PID controller

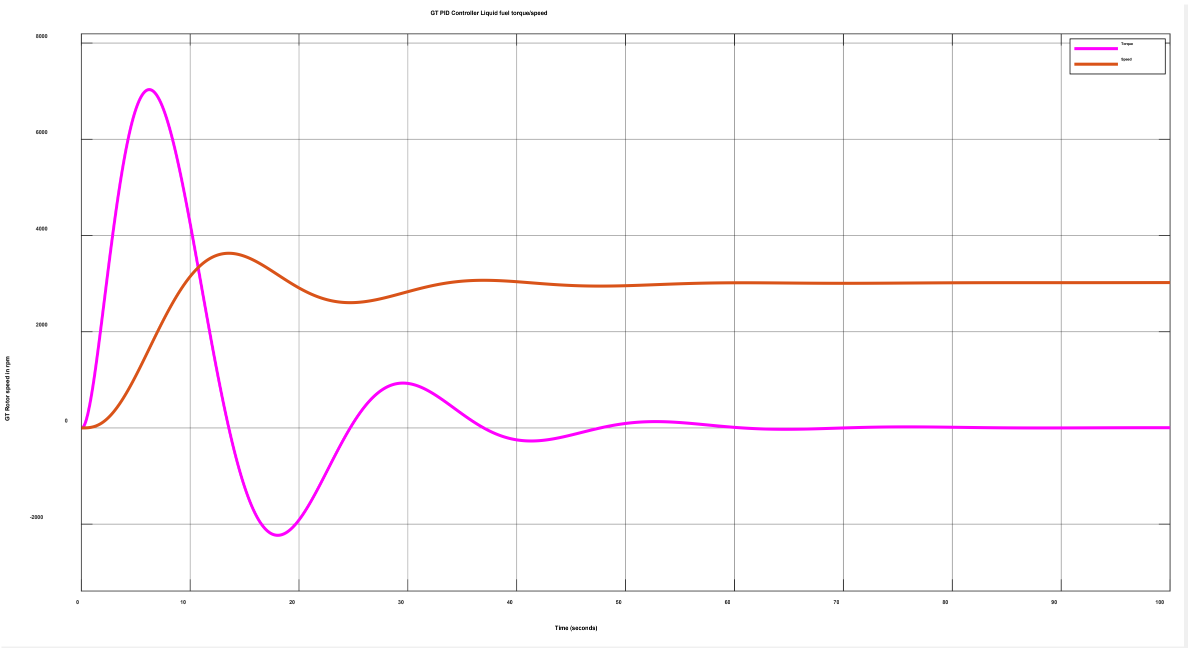

Figure 5.8: GT speed-torque characteristics response with liquid fuel flow control with PID

Figure 5.8 represent the torque-speed characteristics of the GT model. From the response, the torque decreases initially as the rotor speed increases until the maximum speed is attained and torque reduces to zero.

5.6 GT LNG gas system

The gas control system is evaluated using LNG flow from the external tank into the GT LNG control line. The fuel system was tested and evaluated using Simulink's PID controller design. The feedback is zero with the LNG supply system; all other functions remain the same as the liquid fuel system for the internal GT fuel control shown in Figure A5.11.
Table 5.2 presents the PID controller design's simulation parameters for the LNG flow control signal in the GT fuel system. The LNG gas nozzle's flow characteristics are dynamically observed as the speed demand increases from the acceleration block. The speed signal again was set constant at 3000rpm, and no changes in the speed of the rotor circuit were observed.

Table 5.2: PID parameter for LNG GT fuel system control

PID 1	CONTROLLER PARAMETER	TUNNED VALUE	PERFORMANCE AND ROBUSTNESS	VALUES
1	Proportional	1.0597	Rise time	2.8 seconds
2	Integral	0.023334	Settling time	19.8 seconds
3	Derivative	6.2563	Overshoot	10.7%
4	N (filter coefficient)	44.1654	Peak	1.11
5			Gain Margin	6.97dB @ 0.87 rad/s
6			Phase margin	65 deg @ 0.386 rad/s
7			Closed-loop stability	Stable
PID 2	**Controller parameter**	**Tuned value**	**Performance and robustness**	**Values**
1	Proportional	0.0049463	Rise time	1.52 seconds
2	Integral	8.8548e-06	Settling time	22.2 seconds
3	Derivative	0.16604	Overshoot	20.4%
4	N (filter coefficient)	24.9843	Peak	1.2
5			Gain Margin	12 dB @ 0.468 rad/s
6			Phase margin	44.7 deg @ 0.219 rad/s
7			Closed-loop stability	Stable

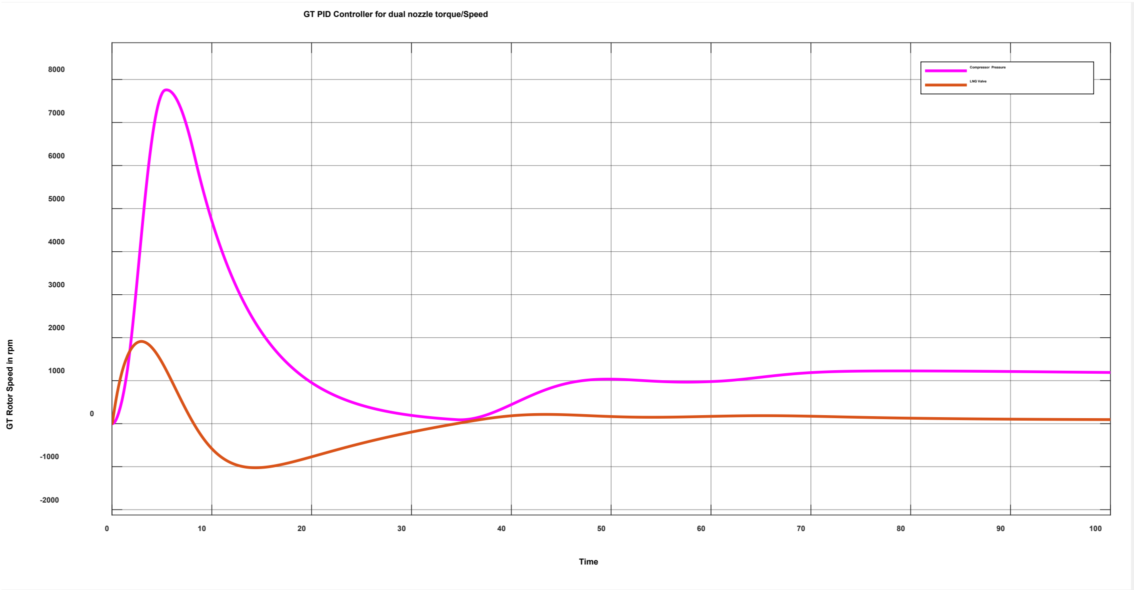

Figure 5.1: GT LNG gas flow control with PID controller

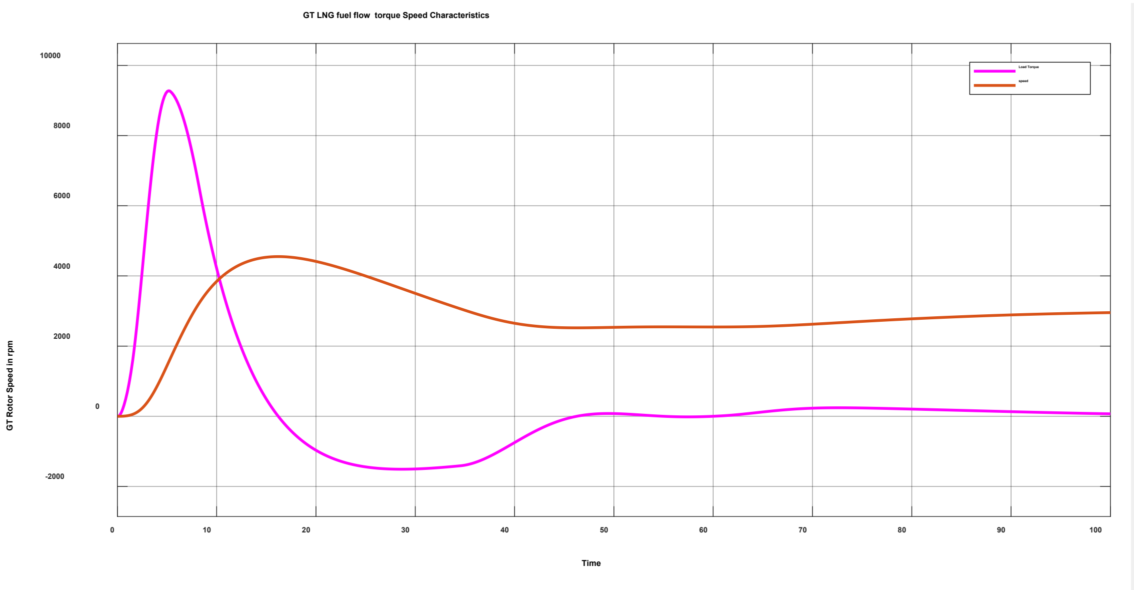

Figure 5.2: GT speed-torque characteristics response with LNG gas flow control with PID

When the torque-speed characteristics of both fuel systems are compared, the performance is the same, indicating that the two fuel nozzles can be combined on the same gas turbine without affecting the turbine rotor performance. The same dynamic effect with combustion ignition was observed. The following section will look at the dual nozzle, which will control both flows.

5.7 PID Controller Design for dual nozzle fuel control system

The dual-nozzle LNG and liquid fuel system for the GT operation includes a fuel pressure switch that uses the pressure from the external tank system to pick from the various fuel sources. Priority is given to the LNG fuel source for economic activities, and once it is available, the system immediately switches this source. Further control is provided at the output of the fuel dynamical control system using maximum block to select the required fuel into the combustion chamber. Figure 5.15 shows the PID Simulink controller design for the dual nozzle GT fuel system control and subsequent responses after the controller turning. The PID parameters obtained after the tuning are presented in Table 5.3, while Table 5.4 exhibits the simulation scenarios. It is clear from the table that the type of GT fuel depends on both availability and price at a given time.

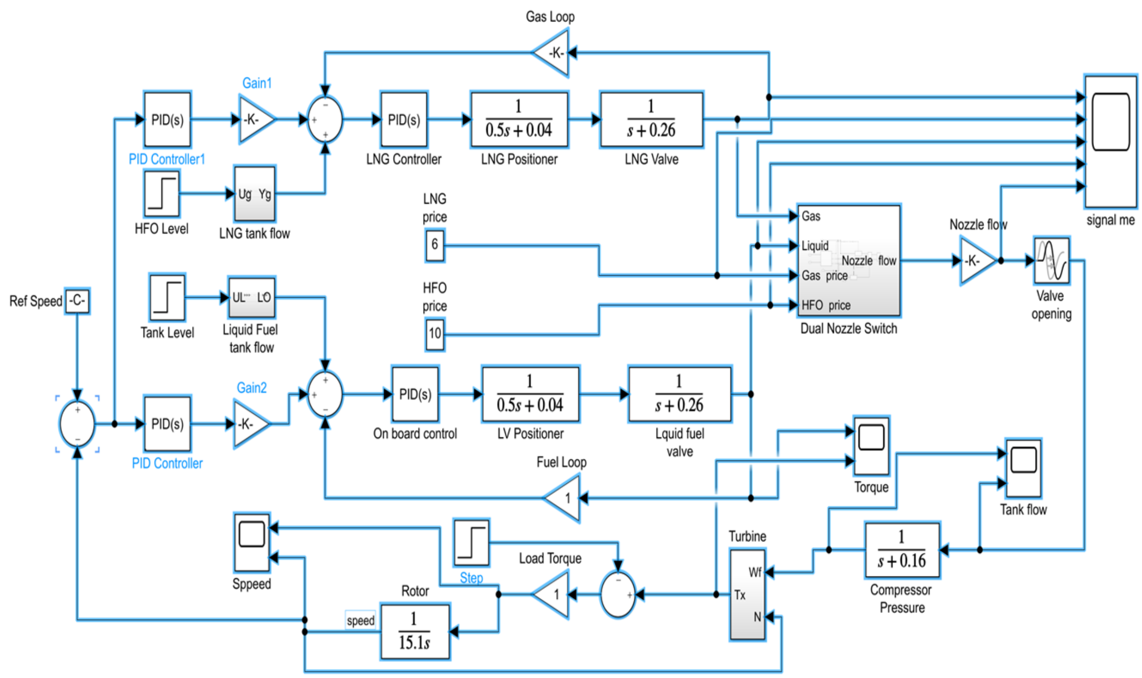

Figure 5.3: Simulink Design for Dual Nozzle GT PID Controller

Table 5.3: PID parameter for dual nozzle fuel system control

PID 1	CONTROLLER PARAMETER	TUNNED VALUE	PERFORMANCE AND ROBUSTNESS	VALUES
1	Proportional	1.0597	Rise time	2.8 seconds
2	Integral	0.023334	Settling time	19.8 seconds
3	Derivative	6.2563	Overshoot	10.7%
4	N (filter coefficient)	44.1654	Peak	1.11
5			Gain Margin	6.97dB @ 0.87 rad/s
6			Phase margin	65 deg @ 0.386 rad/s
7			Closed-loop stability	Stable
PID 2	**Controller parameter**	**Tunned value**	**Performance and robustness**	**Values**
1	Proportional	0.6620	Rise time	4.47 seconds
2	Integral	0.0292	Settling time	46.2 seconds
3	Derivative	3.0905	Overshoot	15.1%
4	N (filter coefficient)	0.5166	Peak	1.15
5			Gain Margin	9.03 dB @ 55.8 rad/s
6			Phase margin	55.7 deg @ 0.215 rad/s
7			Closed-loop stability	Stable

Table 5.4: Dual input parameters

SCENARIO	LNG TANK LEVEL	HFO TANK LEVEL	LGN PRICE	HFO PRICE	SPEED REF	DUAL NOZZLE FLOW
1	50	30	6	10	3000	Gas
2	100	50	10	7	3000	HFO
3	20	100	6	7	3000	HFO
4	5	4	6	7	3000	0

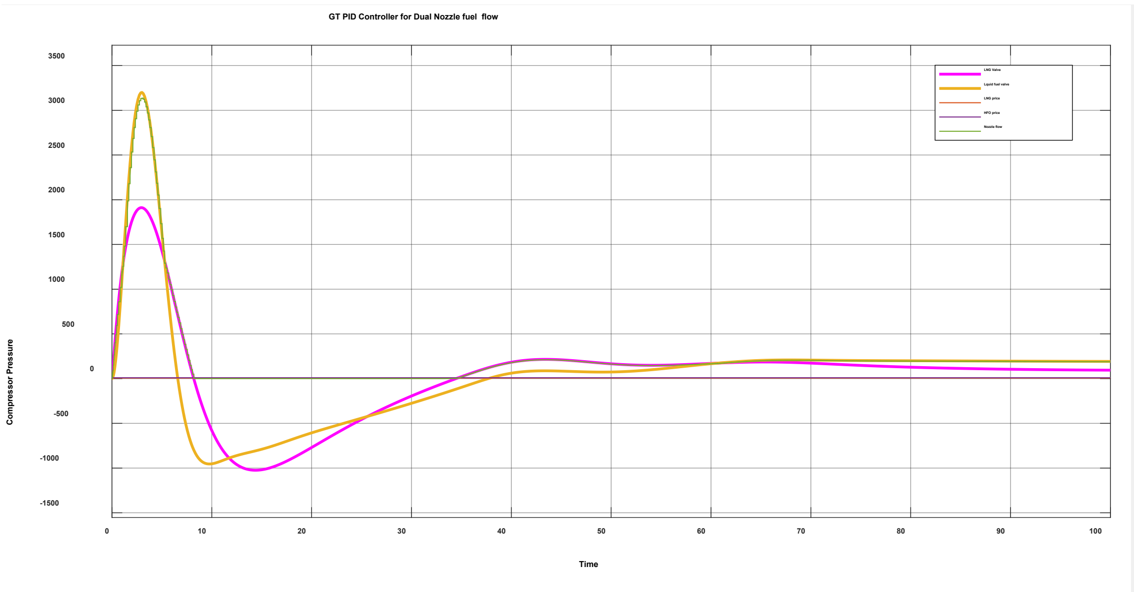

Figure 5.4: Response of fuel pressure control and combustion flow

Figure 5.16 shows the dual fuel nozzle flow with a PID controller response. The nozzle flow shows that the LNG gas valve is opened, and the gas flow produces combustion pressure into the combustion chamber. This indicates that the LNG price is lower than the liquid fuel price and is readily available.

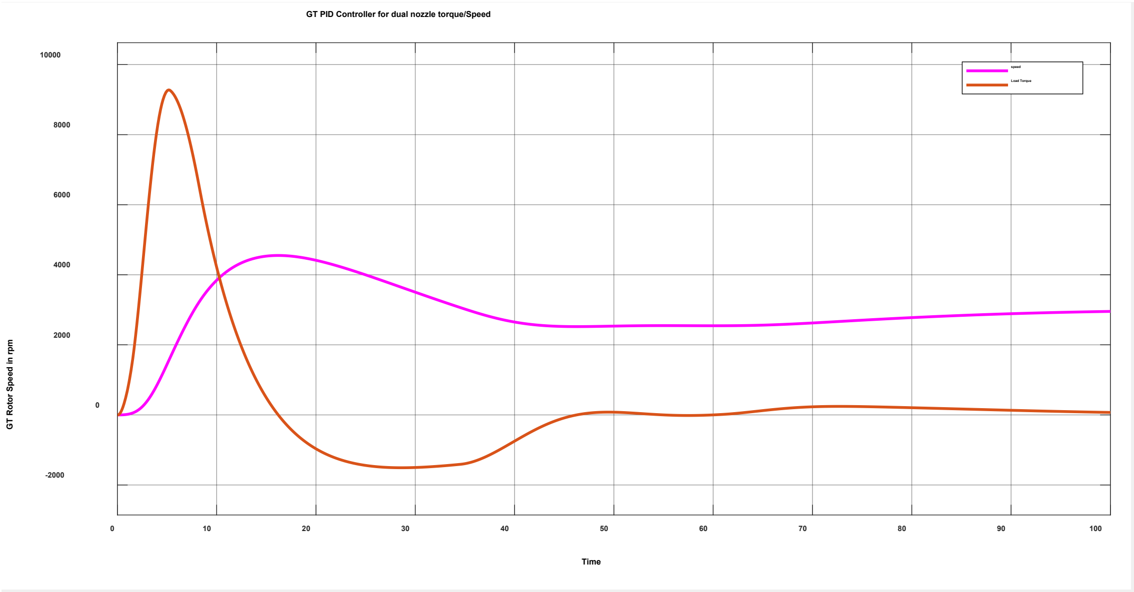

Figure 5.5: Rotor speed and torque for the dual nozzle fuel system

The performance of the turbine rotor speed with the load torque characteristics is evaluated. It is observed that initially, the torque was high, while the speed of the rotor was low. As the momentum begins to increase, the torque, however, reduces. The characteristics show the expected behaviour of the generator system.

5.8 Optimization of the PID Controller for Dual Nozzle GT Fuel Supply

The modified Rowen model's dual nozzle fuel supply system for the GT fuel system built in Simulink/MATLAB block diagram is illustrated in Figure 5.14. The block consists of LNG and HFO fuel supply tanks, a GT fuel valve positioner for both tanks, and their dynamics. The fuel tanks, filter, control valve, injectors, flow regulator valve, mixer, sensors, and the dual nozzle microcontroller unit make up the fuel delivery system. Once the engine is running, LNG outflows from the tank due to the somewhat high pressure that departs the tank. LNG enters the filter to ensure that the solenoid valve and regulator valve function properly. The liquid then passes via the solenoid valve and into the injectors, where it is vaporised and supplied to the air-fuel mixer. Finally, the gaseous mixture is burned in engine chambers. The dual control valve, located between the injectors and the engine throttle body, controls the amount of fuel that flows into the engine to maintain the stoichiometric air-fuel ratio.

The GT uses either HFO fuel or LNG gas for power generation. Hence, the cost associated with fuel systems varies, and also their reliability poses some level of challenge to the power generating industries.

5.8.1 Optimization objective formulation

The optimisation problem for the GT dual fuel nozzle is formulated as follows:

- Enhance smooth transition between dual fuel nozzle system without unit shutdown
- Using the availability of either HFO fuel and LNG fuel to manage the continuous operation
- The cost of each fuel supply also determines the selection criteria
- Combine the availability with the price to select the most efficient fuel supply to run the plant and reduce the energy production cost.

The algorithm selecting a specific fuel supply is described in the mathematical model of equations (5.3 & 5.4).

$$F_g^P(t) + C_g^P(t) \leq Q_g(t) \quad \left| F_g^P(t) > 0, C_g^P(t) > 0 \right. \qquad 5.2$$

$$F_L^A(t) + C_L^A(t) \leq D_L\ (t)\ |F_L^A(t) > 0, C_L^A(t) > 0 \qquad 5.3$$

$F_g^P(t)$ and $C_g^P(t)$ the primary fuel availability and cost of primary fuel, respectively. $Q_g(t)$ is the standard price limit while $F_g^A(t)$ and $C_g^A(t)$ are the auxiliary fuel supply with the limit $D_L(t)$, [136-139]. Applying the above function in the MATLAB/Simulink diagram for the PID controller, the control variable is optimized through iteration from 0 to 10 populations.

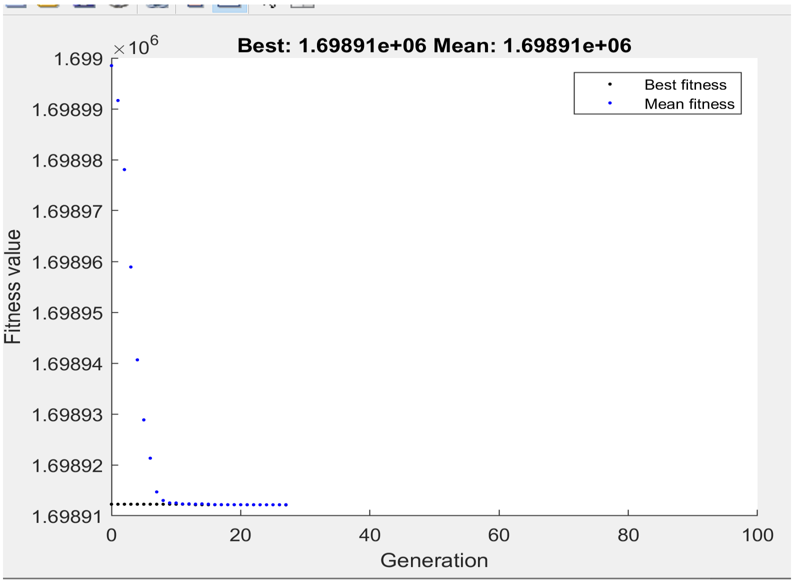

Figure 5.6: Population generation for PID optimization process

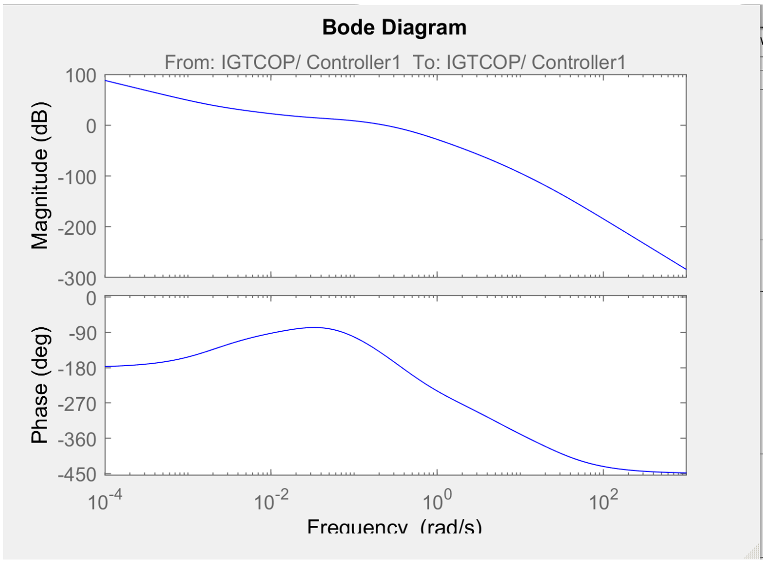

Figure 5.7: GT PID optimization analysis with Bode plot

Table 5.5: PID iteration for optimization

Optimization Progress

Iteration	Eval-Count	Cost function	Constraint vio...	Step size	Procedure
0	9	0	41.34		
1	11	0	41.34	0	
2	13	0	41.34	0	Hessian not ...
3	15	0	41.34	0	Hessian not ...
4	17	0	41.34	0	Hessian not ...
5	19	0	41.34	0	Hessian not ...
6	21	0	41.34	0	Hessian not ...
7	23	0	41.34	0	Hessian not ...
8	25	0	41.34	0	Hessian not ...
9	27	0	41.34	0	Hessian not ...
10	29	0	41.34	0	Hessian not ...
11	31	0	41.34	0	Hessian not ...
12	33	0	41.34	0	Hessian not ...
13	35	0	41.34	0	Hessian not ...
14	37	0	41.34	0	Hessian not ...
15	39	0	41.34	0	Hessian not ...

Constructing optimization problem...

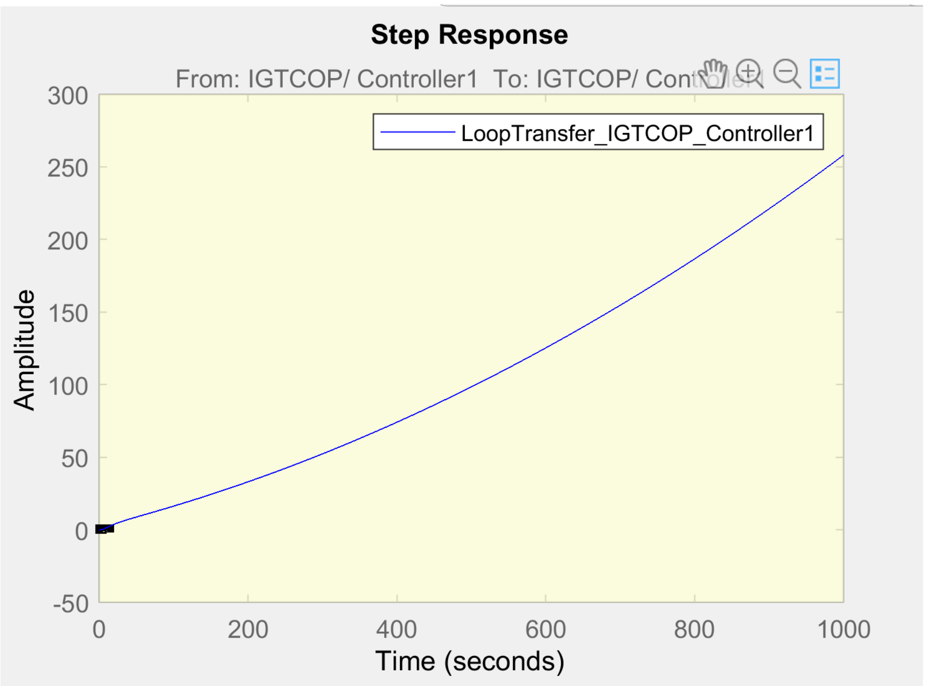

Figure 5.8: Optimal response for the GT PID dual nozzle plot

5.9 Summary

The chapter extensively discusses the design and simulation of the dual nozzle GT fuel control system model developed in chapters three and four. The controller is a proportional, integral and derivative (PID) control algorithm. System energizes with different simulation scenarios to the model with step signals representing fuel and LNG gas flow. While control scenarios include a dual nozzle without a PID control effect and an external fuel tank connection, the second scenario is coupling the external fuel tank and control with the PID controller.

Responses under different fuel conditions were observed, and the GT responds to the fuel pressure switch selector smoothly without combustion interference. GT performance plot shows the dynamic characteristics of the speed torque relation.

CHAPTER SIX: MODEL PREDICTIVE CONTROL

6.1 Introduction

The primary goal of MPC is to predict the manipulated variable's future trajectory and optimise the future process output to achieve the track set point as accurately as possible. A specific time frame of the optimal window completes this optimisation, which is dependent on the information provided to the plant at the beginning of that window. This process is summarised in Figure 6.1.

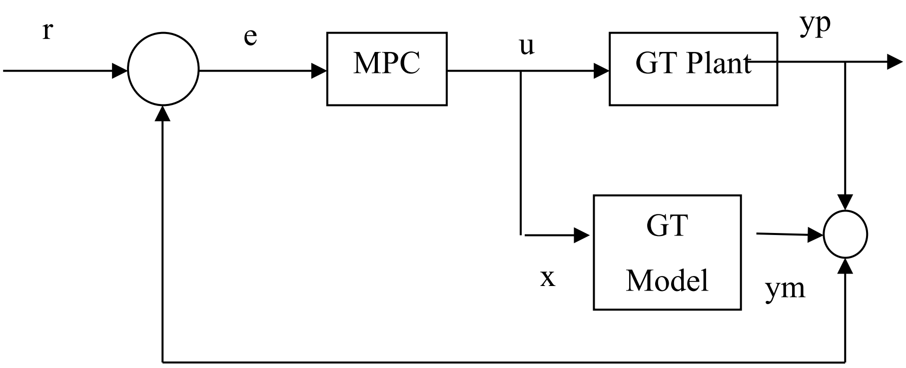

Figure 6.1: MPC GT model controller design

The structure outlines the overall goal of the MPC method, which is described in detail below. The GT model is placed in parallel with the plant model for the predictive control to use the dynamic model plant to predict the controlled variable, which is then fed back to the controller for the optimisation process to minimise the cost function and thus determine the manipulated variable.

The error signal, which represents the difference between the GT model output and the GT plant output, is fed back to the controller, which then uses this signal to eliminate the steady-state offset of the process to achieve a more consistent result. The cost function is dependent on the quadratic error between a future reference and a future control variable in the prediction window [142 and 143].

6.2 GT Process Model Design

There are three approaches to consider when developing the MPC model for the GT control process. Among these are finite impulse and response methods, the first methods on which the GT model formulation and design were based. The algorithms are based on either dynamic matrix control (DMC) or quadratic matrix control built in the MPC controller. The model was developed based on the transfer function of the process under consideration, which provides a suitable method for both stable and unstable systems. Transfer function approaches employ the general predictive control (GPC) algorithm. In contrast, the current model approach is based on state-space design [141, 144], which will be discussed in greater detail under the various sections of the control model.

6.3 State Space Model with Embedded Integrator (SSMEI)

For convenience, our MPC controller design is centred on the mathematical model of the GT. The GT plant model is first linearised, which is facilitated using MATLAB/Simulink software to obtain the state-space model. The MPC controller is then designed using this model, as is evident in the implementation article of the dual nozzle fuel model architecture [39]. The plant model could be either single–input, single-output (SISO) or multiple-input, multiple-output (MIMO). SISO and MIMO systems are considered in developing the GT control [144,145].

6.3.1 Single –Input and Single–Output (SISO) System

The following equation gives the SISO process's state-space design:

$$x_m(p+1) = A_m x_m(p) + B_m u(p) \quad 6.1a$$

$$y(p) = C_m x_m(p) \quad 6.1b$$

The parameter u denotes the manipulated or control variable, y represents the process output, and x_m denotes the state variable. The state-space model's general design must include an additional term defining the direct relationship between the process's input and output. Given this, equation (6.1b) is expressed more broadly as:

$$y(p) = C_m x_m(p) + \ D_m u(p) \qquad 6.1c$$

However, in many cases, D_m is assumed to be zero. Obtaining the derivative of equation (6.1a) yields the following result:

$$x_m(p+1) - x_m(p) = A_m x_m(p) - x_m(p+1) + B_m u(p) - u(p+1)$$

$$\text{Defining } \Delta_m(p+1) = x_m(p+1) - x_m(p)$$

$$\Delta_m(p) = x_m(p) - x_m(p-1)$$

$$\Delta u(p) = u(p) - u(p-1)$$

$$x_m(p+1) = A_m \Delta x_m(p) + B_m \Delta u(p) \qquad 6.2$$

According to equation (6.2), the state-space model has an input of $\Delta u(p)$ and the output of $y(p)$. This is accomplished by creating a new model of the state variable vector.

$$x(p) = [\Delta x_m(p)^T \ \ y(p)]^T$$

The transpose matrix is denoted by the superscript T.

$$y(p+1) - y(p) = C_m(x_m(p+1) - x_m(p) = C_m \Delta x_m(p+1)$$

$$= C_m A_m \Delta x_m(p) + C_m B_m \Delta u(p) \qquad 6.3$$

The model of the state-space vector is obtained by combining equations (6.2) and (6.3), which are denoted as:

$$\overbrace{\left|\begin{matrix}\Delta x_m(p+1) \\ y(p+1)\end{matrix}\right|}^{x(p+1)} = \overbrace{\left|\begin{matrix}A_m & om^T \\ C_m A_m & 1\end{matrix}\right|}^{A} \overbrace{\left|\begin{matrix}\Delta x_m(p) \\ y(p)\end{matrix}\right|}^{x(P)} + \overbrace{\left|\begin{matrix}B_m \\ C_m B_m\end{matrix}\right|}^{B} \Delta u(p) \qquad 6.4$$

$$y(p) = \overbrace{\left|\begin{matrix}O_m & 1\end{matrix}\right|}^{C} \left|\begin{matrix}\Delta x_m(p) \\ y(p)\end{matrix}\right| \qquad 6.5$$

In equation (6.5), $O_m = \overbrace{[\![0 \quad 0 \quad . \quad . \quad 0]\!]}^{n1}$ this define as the parameter (A, B, C) as an augmented model which will be used to design the predictive control for the dual fuel system.

6.4 Prediction Control with one Optimal Window

After developing the mathematical model, the next step is to design a model predictive control system that will predict future GT plant output based on the control variable that occurs within a single optimisation window, which will be implemented in the GT model.

6.4.1 Prediction of State and Output Variable

With the GT plant sample time interval $pi. with \ \ pi \geq 0$, the state vector $x(pi)$ value is taken from the measurement GT current state information at $x(pi)$. Hence, the future trajectory is determined as follows:

$$\Delta u(pi), \Delta u(pi+1) \ldots \ldots . . \Delta u(pi+Nc-1) \qquad 6.6$$

Nc implies the control horizon, which specifies the number of parameters required to derive the future control trajectory. Once *x(pi)* is obtained, the future state is predicted based on the prediction horizon's limit *(Np)*. Additionally, the prediction horizon specifies the time window and duration of the optimisation window. Given this, the sequence of our future state is expressed as:

$$x(pi+1|pi), x(pi+2|pi) \ldots \ldots . x(pi+m|pi) \ldots \ldots x(p1+Np|pi) \qquad 6.7$$

$x(pi+m|pi)$ is the predicted state variable at $pi+m$ based on current data about the GT plant at $x(pi)$, and the future state is expected using a state-space model and future control parameters as follows:

$$x(pi+1|pi) = Ax(p1) + B\Delta u(pi)$$
$$x(pi+2|pi) = Ax(pi+1|pi) + B\Delta u(pi+1)$$

$$= A^2x(pi) + AB\Delta u(pi) + B\Delta u(pi+1)$$

$$\vdots$$

$$x(pi+Np|pi) = A^{Np}x(pi) + A^{Np-1}B\Delta u(pi) + A^{Np-2}\Delta u(pi+1) + \cdots$$

$$+A^{Np-Nc}B\Delta x(pi+Nc-1) \qquad 6.8$$

From the above expression, the predicted output is calculated using the following:

$$y(pi+1|pi) = CAx(p1) + CB\Delta u(pi)$$

$$y(pi+2|pi) = CA^2x(pi) + CAB\Delta u(pi) + CB\Delta u(pi+1)$$

$$y(pi+3|pi) = CA^3x(pi) + CA^2B\Delta u(pi) + CAB\Delta u(pi+1) + CB\Delta u(pi+2)$$

$$\vdots$$

$$y(pi+Np|pi) = CA^{Np}x(pi) + CA^{Np-1}B\Delta u(pi) + CA^{Np-2}B\Delta u(pi+1) + \cdots$$

$$+CA^{Np-Nc}B\Delta u(pi+Nc-1) \qquad 6.9$$

The predicted state variable is constructed using the state variable's current data, and new sequence y is formulated utilising the output vector:

$$y = |y(pi+1|pi)y(pi+2|pi)y(pi+3|pi) \ldots.y(pi+Np|Np)|^T$$

$$\Delta u = |\Delta u(pi)\ \Delta u(pi+1)\ \Delta u(pi+2) \ldots.\Delta u(pi+Nc-1)|^T \qquad 6.10$$

Equations (6.8) and (6.9) are arranged into state matrix form as:

$$y = gx(pi) + \varphi\Delta u \qquad 6.11$$

$$g = \begin{vmatrix} CA \\ CA^2 \\ CA^3 \\ . \\ . \\ . \\ CA^{Np} \end{vmatrix};\ \varphi = \begin{vmatrix} CB & 0 & 0 & ... & 0 \\ CAB & CB & 0 & ... & 0 \\ CA^2B & CAB & CB & ... & 0 \\ . & . & . & ... & 0 \\ . & . & . & ... & 0 \\ . & . & . & ... & 0 \\ CA^{Np-1}B & CA^{Np-2}B & CA^{Np-3}B & ... & CA^{Np-Nc}B \end{vmatrix}$$

6.5 Optimization Formulation

The primary goal of our optimal control action formulation is to bring the GT plant output speed very close to the reference value when constraints occur within the optimal window. This is achieved during the design phase by selecting the most efficient parameter vectors in such a situation that the error between the setpoint and predicted output is minimised [141 & 143].

6.5.1 Cost function

The cost function or control objective Jc enables the determination of the process responsible for a specified prediction horizon (*Np*). After that, the setpoint signal encompasses a vector denoted by:

$$R_s^T = \overbrace{\lceil 1 \quad 1 \quad . \quad . \quad . \quad 1 \rceil}^{Np} r(pi) \qquad 6.12$$

Hence, Jc is calculated as follows:

$$Jc = (R_s - Y)^T(R_s - Y) + \Delta u^T \bar{R} \Delta u \qquad 6.13$$

The first term in equation (6.12) minimises the difference between predicted output speed following fuel demand by the acceleration unit and setpoint speed. In contrast, the second term denotes the value of Δu with the corresponding objective function reduced to its minimum value. $\bar{R}$ is a diagonal matrix obtained through the evaluation of equation (6.13).

$$\bar{R} = V_w I N_c \; X \; N_c \qquad (V_w \geq 0) \qquad 6.14$$

V_w is used as a tuning vector in this case to achieve the desired closed-loop performance. The value of V_w analysed under various scenarios; when $V_w = 0$, the value of Δu may be significant, and the control objective will minimise process error. If Vw becomes excessively large, the control objective becomes how large Δu should be to reduce the error. The following expression is used to optimise Δu while minimising the cost function Jc in equation (6.13).

$$Jc = (R_s - gx(pi)^T\big(R_s - gx(pi)\big) - 2\Delta u^T\varphi^T\big(R_s - gx(pi)\big) \qquad + \Delta u^T(\varphi\varphi^T + \bar{R})\Delta u \tag{6.15}$$

Taking the derivative of equation (6.14) gives:

$$\frac{\partial Jc}{\partial \Delta u} = -2\varphi^T\big(R_s - gx(pi)\big) + 2(\varphi^T\varphi + \bar{R})\Delta u \tag{6.16}$$

$\frac{\partial Jc}{\partial \Delta u} = 0$ produced the following condition for minimising the cost function and obtaining optimal control:

$$\Delta u = (\varphi^T\varphi + \bar{R})^{-1}Y^T\big(R_s - gx(pi)\big) \tag{6.17}$$

When $(\varphi^T\varphi + \bar{R})^{-1}$ exists, then the matrix $(\varphi^T\varphi + \bar{R})^{-1}$ represents the Hessian matrix in the optimisation technique, and Rs represents the vector containing data about the setpoint signal, evaluated using the expression below [144].

$$R_s = \overbrace{|1 \quad 1 \quad 1 \quad . \quad . \quad 1|}^{Np}{}^T\, r(pi) = \overline{R_s}r(pi) \tag{6.18}$$

Where

$$\overline{R_s} = \overbrace{|1 \quad 1 \quad 1 \quad . \quad . \quad 1|}^{Np}{}^T \tag{6.19}$$

Using the expression in equation (6.19), the setpoint signal (speed) r(pi) can now be connected to the optimal solution.

$$\Delta u = (\varphi^T\varphi + \bar{R})^{-1}\varphi^T\big(\overline{R_s}r(pi) - gx(pi)\big) \tag{6.20}$$

6.6 Concept of Receding Horizon

The MPC GT model that implements the receding horizon concept is as follows: the optimal vector Δu, which contains the control signal $\Delta u(pi)$, $\Delta u(pi+1), \Delta u(pi+2) \ldots\ldots \Delta u(pi+Nc-1)$ implements only the first sample and discards all subsequent predictions. After each set of receding horizons, a new measurement is taken to create an entirely new state vector of $x(pi+1)$ to calculate the following prediction sequence for the current speed signal [144].

6.6.1 Concept of Closed Loop Control (CCLC)

Using the principles of the closed-loop system, an optimal parameter of Δu at any given time (pi) can be obtained using the expression:

$$\Delta u = (\varphi^T\varphi + \bar{R})^{-1}\left(\varphi^T R_s - \varphi^T g x(pi)\right) \qquad 6.21$$

$\Delta u = (\varphi^T\varphi + \bar{R})^{-1}\varphi^T R_s$ represent setpoint change and $(\varphi^T\varphi + \bar{R})^{-1}\varphi^T \overline{R_s} g$

With the prediction control's state feedback, the receding horizon principle requires us to apply only the first prediction at a time (pi). The Δu at the time (pi) is obtained as;

$$\Delta u(pi) = |1 \quad 1 \quad . \quad . \quad 0|(\varphi^T\varphi + \bar{R})^{-1}\left(\varphi^T \overline{R_s} r(pi) - \varphi^T g x(pi)\right)$$
$$= C_y r(pi) - C_{mpc} x(pi) \qquad 6.22$$

Cy corresponds with the first row of $(\varphi^T + \bar{R})^{-1}\varphi^T \overline{R_s}$ while C_{mpc} characterise the first row of $(\varphi^T\varphi + \bar{R})^{-1}\varphi^T \overline{R_s} g$

Applying the state equation:
$x(pi+1) = Ax(p) + B\Delta u(p)$

From the state equation, the closed-loop system is modelled as:
$x(pi+1) = Ax(pi) + BC_{mpc}x(p) + BC_y r(p)$

$$= \left(A - BC_{mpc}\right)x(p) + BC_y r(p) \tag{6.23}$$

The characteristic equation can determine the closed-loop eigenvalue in equation (6.22).

$$det\left(\lambda I - \left(A - BC_{mpc}\right)\right) = 0 \tag{6.24}$$

6.7 Multiple input and multiple output (MIMO) system prediction control

While the previous system was supposed to be straightforward, the GT dual fuel systems currently being developed are MIMO systems

6.7.1 Model Development for MIMO

GT fuel control systems are considered to have m inputs, and q outputs with $q1$ states are treated analogously, with the number of outputs being equal to or less than the number of inputs. The GT model for the MIMO system is developed using a much more straightforward mathematical approach [141, 144].

$$x_m(p+1) = A_m x_m(p) + B_m u(p) + B_d w(p) \tag{6.25}$$

$$y(p) = C_m x_m(p) \tag{6.26}$$

$w(p)$, represents white noise generated during the process disturbance, and the noise sequence has been developed as:

$$\varepsilon(p) = w(P) - w(p-1) \tag{6.27}$$

By combining the principles of equations (6.26) and (6.24), the state equation (6.28) is formulated as:

$$x_m(p) = A_m x_m(p-1) + B_m u(p-1) + B_d w(p-1) \tag{6.28}$$

If a system is formulated as:

$\Delta x_m(p) = x_m(p) + x_m u(p-1)\ and\ \Delta u(p) = u(p) - u(p-1)$, by subtracting equation (6.28) from equation (6.24) which, results in the state equation below.

$$\Delta x_m(p+1) = A_m \Delta x_m(p) + B_m \Delta u(p) + B_d \varepsilon(p) \qquad 6.29$$

If the relationship is extended between the output $y(p)$ and the state variable $\Delta x_m(p)$, the following relationship can be derived:

$$\Delta y(p+1) = C_m \Delta x_m(p+1) = C_m A_m \Delta x(p) + C_m B_m \Delta u(p) + C_m B_d \varepsilon(p) \qquad 6.30$$

Again, if $\Delta y(p+1) = y(p+1) - y(p)$ then the state variable vector is obtained as:

$$x(p) = [\Delta x(p)^T\ \ y(p)^T]^T \qquad 6.31$$

$$\begin{vmatrix} \Delta x_m(p+1) \\ y(p+1) \end{vmatrix} = \begin{vmatrix} A_m & Om^T \\ C_m A_m & I_q xq \end{vmatrix} \begin{vmatrix} \Delta x_m(p) \\ y(p) \end{vmatrix} + \begin{vmatrix} B_m \\ C_m B_m \end{vmatrix} \Delta u(p) + \begin{vmatrix} B_d \\ C_m B_d \end{vmatrix} \varepsilon(p)$$

$$y(p) = |O_m \quad I_q xq| \begin{vmatrix} \Delta x_m(p) \\ y(p) \end{vmatrix} \qquad 6.32$$

Where $I_q xq$ is an identity matrix having a size of *q x q1*

As a result, the model obtained is given in equation (6.33).

$$x(p+1) = Ax(p) + B\Delta u(p) + B_\varepsilon \varepsilon(p) \qquad 6.33$$

Equation (6.33) includes two variables that aid in the GT model's interpretation. These are the eigenvalues of the 'augmented model' and the state-space model's realisation.

The characteristic system equation is used to determine the eigenvalue.

$$\rho(\lambda) = det \begin{bmatrix} \lambda I - A_m & Om^T \\ -C_m A_m & (\lambda - 1) I_q xq \end{bmatrix}$$

$$= (\lambda - 1)^q\ det(\lambda I - A_m) = 0 \qquad 6.34$$

6.7.2 Principles of Observability and Controllability

The MPC design is considered based on the performance of the GT augmented value of the state-space model, which must be controllable or observable to be feasible. In light of this, the GT controllability and observability is analysed in the following manner [143, 144]:

The Observability matrix is defined as:

$$rank = \begin{vmatrix} C_m \\ C_m A_m \\ . \\ . \\ C_m A_m^{n-1} \end{vmatrix} = n(full\,rank) \qquad 6.35$$

When n is greater than zero, the system is said to be completely observable.

$$rank = |B_m \quad A_m B_m \quad . \quad . \quad . \quad A_m^{n-1} B_m| = n\ (full\,rank) \qquad 6.36$$

6.7.3 Applying Prediction Control for GT MIMO dual fuel System

Predictive control is applied to GT MIMO system with the dimensions of the state, output, and control vectors. The vectors for $\Delta u\ and\ Y$ are formulated in this case as:

$$\Delta u = |\Delta x(pi)^T\ \Delta u(pi+1)^T \ldots \ldots \Delta u(pi+Nc-1)^T|^T$$
$$Y = |y(pi+1|pi)^T\ y(pi+2|pi)^T y(pi+3|pi)^T \ldots \ldots y(pi+Np|pi)^T|^T \qquad 6.37$$

The future state is estimated sequentially using the state-space representations of A, B, C, and D.

$$x(pi+1|pi) = Ax(p1) + B\Delta u(pi) + B_d \varepsilon(pi)$$
$$x(pi+2|pi) = Ax(pi+1|pi) + B\Delta u(pi+1) + B_d \varepsilon(pi+1|pi)$$
$$= A^2 x(pi) + AB\Delta u(pi) + B\Delta u(pi+1) + AB_\varepsilon \varepsilon(pi) + B_d \varepsilon(pi+1|pi)$$

$$\vdots$$

$$x(pi+Np|pi) = A^{Np}x(pi) + A^{Np-1}B\Delta u(pi) + A^{Np-2}B\Delta u(pi+1) + A^{Np-2}B_d\varepsilon(pi+1|pi) + \cdots + B_d\varepsilon(pi+Np-1|pi) \quad 6.38$$

In this, $\varepsilon(pi)$ denotes the white noise sequence, and the predicted variable $\varepsilon(pi+1|pi)$ (pi+1|pi) is assumed to be zero for subsequent sample. This implies that the predicted state and output variable comprises expected values.

$$Y = gx(pi) + \varphi\Delta u \quad 6.39$$

$$g = \begin{vmatrix} CA \\ CA^2 \\ CA^3 \\ . \\ . \\ . \\ CA^{Np} \end{vmatrix}; \ \varphi = \begin{vmatrix} CB & 0 & 0 & . & . & . & 0 \\ CAB & CB & 0 & . & . & . & 0 \\ CA^2B & CAB & CB & . & . & . & 0 \\ . & . & . & . & . & . & 0 \\ . & . & . & . & . & . & 0 \\ . & . & . & . & . & . & 0 \\ CA^{Np-1}B & CA^{Np-2}B & CA^{Np-3}B & . & . & . & CA^{Np-Nc}B \end{vmatrix}$$

$$\Delta u = (\varphi^T\varphi + \bar{R})^{-1}\left(\varphi^T\overline{R_s}r(pi) - \varphi^T gx(pi)\right) \quad 6.40$$

By applying the receding horizon concept, the control input is formulated as:

$$\Delta u(pi) = \overbrace{|I_m \quad Om \quad . \quad . \quad Om|}^{Nc}(\varphi^T\varphi\bar{R})^{-1}(\varphi^T R_s r(pi)) - \varphi^T gx(pi)) \quad 6.41$$

6.8 GT State Prediction Control Estimation

A prediction control design is used to compute the state since it is not easily measured. In many real-world systems, the state is not quantifiable, necessitating the need for calculation. This is accomplished through the application of the observer or controllable principle. This is a frequently used engineering principle for state measurement/estimation. Additionally, the approach acts as a filter, reducing the effect of noise on the controller output. [144] specifies the observer expression for state estimation.

$$\hat{x}(pi+1) = A\hat{x}(pi) + B\Delta u(pi) + C_{ob}\big(y(pi) - C\hat{x}(pi)\big) \qquad 6.42$$

To analyse and minimise the cost function Jc with the observer function $\hat{x}(pi+1)$ is substituted for the term $x(pi)$

$$Jc = \big(R_s - g\hat{x}(pi)\big)^T\big(\overline{R_s}r(pi) - g\hat{x}(pi)\big) - 2\Delta u^T\varphi^T\big(R_s - g\hat{x}(pi)\big) + \Delta u^T(\varphi^T\varphi + \bar{R})\Delta u \qquad 6.43$$

Based on the cost function obtained, the optimal solution of Δu is found:

$$\Delta u = (\varphi^T\varphi + \bar{R})^{-1}\varphi^T\big(R_s - g\hat{x}(pi)\big) \qquad 6.44$$

Using the receding horizon principle, the optimal value Δu at sampling time (pi) is obtained as:

$$\Delta u(pi) = C_y r(pi) - C_{mpc}\hat{x}(pi) \qquad 6.45$$

The eigenvalues and characteristic equation using the closed-loop system are as follows:

$$x(p+1) = Ax(p) + B\Delta u(p)$$
$$= Ax(p) + BC_y r(p) - BC_{mpc}\hat{x}(p) \qquad 6.46$$

When $\Delta u(p)$ is substituted in equation (6.45), it will give the observer error dynamic as:

$$\hat{x}(p+1) = \big(A - C_{ob}Q\hat{x}(p)\big) \qquad 6.47$$

let $\hat{x}(p) = x(p) - \hat{x}(p) and\ replace\ \hat{x}(p)\ with\ x(p) - \hat{x}(p)\ give$

$$x(p+1) = \big(A - BC_{mpc}\big)x(p) - BC_{mpc}\hat{x}(p) + BC_{mpc}r(p) \qquad 6.48$$

Combining equations (6.46 and 6.47) to obtain a state-space vector matrix as:

$$\begin{vmatrix}\hat{x}(p+1)\\x(p+1)\end{vmatrix}=\begin{vmatrix}A-C_{ob}Q & Onxn\\-BC_{mpc} & A-BC_{mpc}\end{vmatrix}\begin{vmatrix}\hat{x}(p)\\x(p)\end{vmatrix}+\begin{vmatrix}Onxn\\BC_y\end{vmatrix}r(p) \qquad 6.49$$

Therefore, the characteristic equation is as follows:

$$det\left|\lambda I-\begin{vmatrix}A-C_{ob}Q & Onxn\\-BC_{mpc} & A-BC_{mpc}\end{vmatrix}\right|=0 \qquad 6.50$$

This yielded two distinct characteristic equations:

$$det(\lambda I-(A-C_{ob}Q))=0 \qquad 6.51$$

$$det\big(\lambda I-(A-B_{mpc})\big)\ =0 \qquad 6.52$$

The above expressions were developed into the block diagram in Figure 6.2 [144].

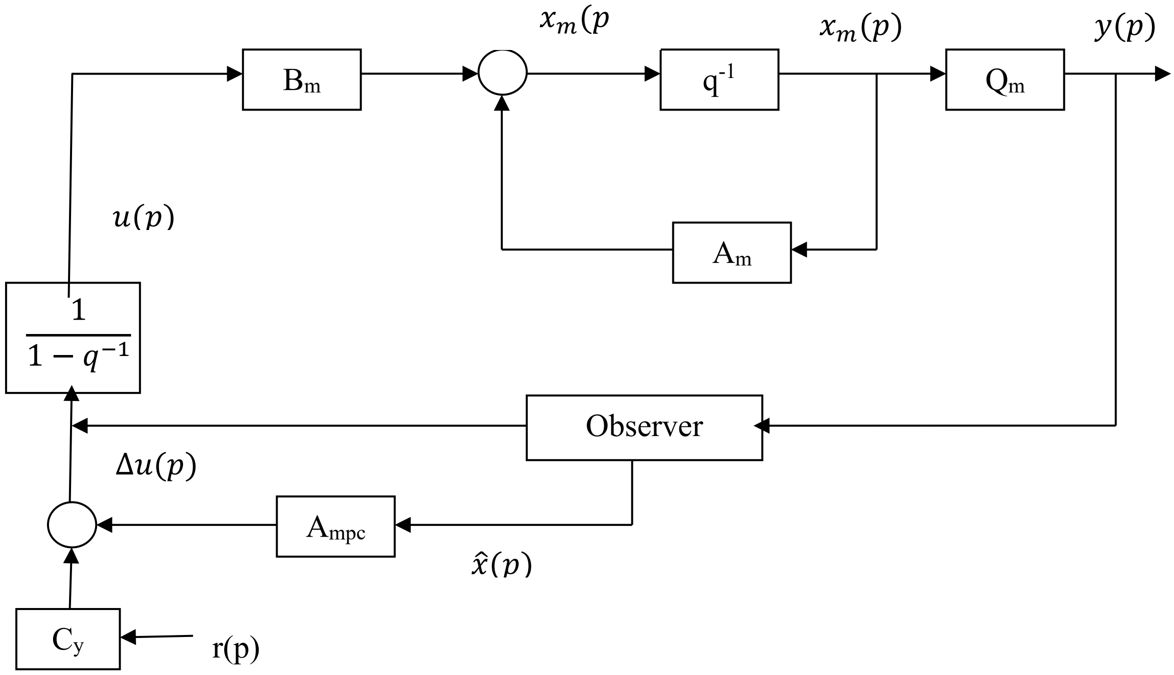

Figure 6.2: Block diagram of DMPC Observer

6.9 Tuning Model Predictive Controller

MPC tuning entails identifying four primary performance-related factors. A prediction horizon (*Np*), a control horizon (*Nc*), a weight matrix, and a moving suppression factor (sampling time) are used to generate an output that follows a set point in the current disturbance and maintains a balance between stability, robustness, and performance [144].

6.10 Gas Turbine Approximate Model

The gas turbine model used in the previous equations approximates the simplified MPC controller design and implementation model. These assumptions-based approximations are essential to effectively develop the mathematical model for the control algorithm of heavy-duty gas turbine power units. It is imperative to note that the assumptions are needed to build the MPC control laws, and the controller output will be checked using the actual GT model's control law.

Neglecting actuator dynamics:

$$u_1 = m_a^* = m_a \qquad 6.53$$

$$u_2 = m_f^* = m_f \qquad 6.54$$

$\dot{m}_a and\ \dot{m}_f$, air and fuel flow density in kg/s. The square root of the T_{cc} is included, equation (3.8) approximates with a simple inverse dependence, and the multiplier becomes proportional to the rated CCT:

$$m_e \cong k_1 \frac{x_1}{x_2} \qquad 6.55$$

$$k_1 = m_0 \frac{T_{cc\,N}}{P_{cc}N} \qquad 6.56$$

Concerning equation (3.6), it is worth noting that the lower heating value of the fuel is significantly greater than the product $x_2\left(C_{pe} - R_e\right)$; that is:

$$H_f >> x_2\left(C_{pe} - R_e\right) \qquad 6.57$$

This implies:

$$R_e x_2 \left(H_e - \ x_2 \left(C_{pe} - \ R_e\right)\right) \cong \ R_e H_e x_2 \qquad 6.58$$

The MPC controller regulates the desired quantities by utilising state measurement parameters to predict the desired output. In light of this, the simplified GT model is as follows:

$$\begin{aligned} \dot{x} &= f_a(x) + G_a(x)w \\ \psi &= h_a(x) \end{aligned} \qquad 6.59$$

Hence,

$$\text{x} \ = \begin{bmatrix} x_1 \\ x_2 \end{bmatrix} = \begin{bmatrix} P_{cc,a} \\ T_{cc,a} \end{bmatrix} \qquad 6.60$$

$$w \ = \begin{bmatrix} w_1 \\ w_2 \end{bmatrix} = \begin{bmatrix} m_a \\ m_f \end{bmatrix} \qquad 6.61$$

$$\psi \ = \begin{bmatrix} \psi_1 \\ \psi_2 \end{bmatrix} = \begin{bmatrix} P_{gt,a} \\ T_{ex,a} \end{bmatrix} \qquad 6.62$$

where $p_{cc,a}, P_{gt,a}, T_{cc,a}$, and $T_{ex,a}$ are respective approximations of p_{cc}, T_{cc}, P_{gt} and T_{ex}, Additionally,

$$f_a \text{ (x)} = \begin{bmatrix} f_{a1}(x) \\ f_{a2}(x) \end{bmatrix} = \begin{bmatrix} A_1 X_1 \\ B_1 X_2 \end{bmatrix} \qquad 6.63$$

$$G_a \text{ (x)} = \begin{bmatrix} A_2 T_a(X_1) & A_3 \\ \frac{x_2}{x_1} \left(B_2 X_2 + \ A_2 T_a(X_1)\right) & A_3 \ \frac{x_2}{x_1} \end{bmatrix} \qquad 6.64$$

$$h_a \text{ (x)} = \begin{bmatrix} h_{a1}(x) \\ h_{a2}(x) \end{bmatrix} = \begin{bmatrix} M_{a0} \frac{T_{cc} N}{P_{cc}\, N} \ C_{pe} \eta_t \eta_{el} x_1 \left(1 - \left(\frac{P_{amb}}{x_1}\right)^{\frac{R_e}{c_{pe}}}\right) - \ w_1 c_{pa} \left(T_a(x_1) - \ T_{amb}\right)\eta_{el} \\ x_2 \eta_t \left[\left(\frac{P_{amb}}{x_1}\right)^{\frac{R_e}{c_{pe}}} + \frac{1}{\eta_t} \ - \ 1\right] \end{bmatrix} \qquad 6.65$$

The constant parameters introduced as:

$$A_1 = -\frac{R_e}{V_{cc}\,(C_{pe} - R_e)}\,k_1 c_{pe} \quad 6.66$$

$$A_2 = -\frac{R_e}{V_{cc}\,(C_{pe} - R_e)}\,k_1 c_{pa} \quad 6.67$$

$$A_3 = -\frac{R_e}{V_{cc}\,(C_{pe} - R_e)}\,H_c \quad 6.68$$

$$B_1 = -\frac{R_e}{V_{cc}\,(C_{pe} - R_e)}\,R_e k_1 \quad 6.69$$

$$B_2 = -\frac{R_e}{V_{cc}\,(C_{pe} - R_e)}\,\left(R_e - c_{pe}\right) \quad 6.70$$

In Equation (6.59) model, the MPC controller design in a second-order dynamic system with even less nonlinearity

6.11 MPC Controller Design for a hybrid gas turbine system

The discrete-time system describes in equation (6.71).

$$x_k + 1 = Ax_k + Bu_k + d \quad 6.71$$

Here $x_k \in R^n and\ u_k \in R^m$ denotes input states at time Kts and ts being sample time. The MPC will respond to regulate the GT fuel reference signal by solving the quadratic constraint programming.

The heavy-duty GT's state dynamic Equation (6.59) can be rewritten as follows:

$$\text{x} = f_a\ (\text{x, w}) = \begin{bmatrix} f_{a1}(x) \\ f_{a2}(x) \end{bmatrix} \quad 6.72$$

The mathematical model for the prediction in equation (6.71) is performed with "successive linearisation" [147] at each sampling time step t*. This approach involves linearising Equation (6.71) around a point. Equation (6.71) is reduced to the form by applying the linearization process.

$$x = A^*x + B^*w + D^* \quad 6.73$$

The following definitions apply to the system matrices A*, B*, D* at the sampling time step t*:

$$A^* = \begin{bmatrix} \frac{\partial F_{a1}}{\partial x_1} & \frac{\partial F_{a1}}{\partial x_2} \\ \frac{\partial F_{a2}}{\partial x_1} & \frac{\partial F_{a2}}{\partial x_2} \end{bmatrix}_{t=\,t^*} \qquad 6.74$$

$$A^* = \begin{bmatrix} \frac{\partial F_{a1}}{\partial w_1} & \frac{\partial F_{a1}}{\partial w_2} \\ \frac{\partial F_{a2}}{\partial w_1} & \frac{\partial F_{a2}}{\partial w_2} \end{bmatrix}_{t=\,t^*} \qquad 6.75$$

$$D^* = \begin{bmatrix} F_{a1-} \frac{\partial F_{a1}}{\partial x_1} X_1 - \frac{\partial F_{a1}}{\partial x_2} X_2 - \frac{\partial F_{a1}}{\partial w_1} w_1 - \frac{\partial F_{a1}}{\partial w_2} w_2 \\ F_{a2-} \frac{\partial F_{a2}}{\partial x_1} X_1 - \frac{\partial F_{a2}}{\partial x_2} X_2 - \frac{\partial F_{a2}}{\partial w_1} w_1 - \frac{\partial F_{a2}}{\partial w_2} w_2 \end{bmatrix}_{t=\,t^*} \qquad 6.76$$

Due to the MPC control's discrete-time nature, Equation (6.71) must be discretised, and thus the zero-order hold discretisation is as follows:

$$X_{k+1} = (1_2 + T_s A^*) X_k + T_s B^* w_k + T_s D^* \qquad 6.77$$

At the sampling time kTs, the subscript k denotes discretised variables.

Two additional dynamic equations can be added to the equation to manipulate the physical limits of air and fuel flow inlet systems (6.75). The inputs are transformed into state variables and their derivatives. In the following manner, *Jma* and Jm_f are regarded as system control variables:

$$m_{a,k+1} = m_{a,k} + T_s J_{ma,k} \qquad 6.78$$

$$m_{f,k+1} = m_{f,k} + T_s J_{mf,k} \qquad 6.79$$

For the controller's prediction, the GT affine time-invariant discrete-time model is as follows:

Where $\tilde{X}_k$ is the discrete state variable

$$\tilde{X}_{k+1} = \tilde{A}^{*}{}_{d}\tilde{X}_{k} + \tilde{B}^{*}{}_{d}\tilde{w}_{k} + \tilde{D}^{*}{}_{d} \quad 6.80$$

$$\tilde{X}_{k} = \left[P_{cc,a,k} \;\; T_{cc,a,k} \;\; \dot{m}_{a,k} \;\; \dot{m}_{f,k}\right]^{T} \quad 6.81$$

$$\tilde{X}_{k} = \left[J_{ma,k} \;\; J_{mf,k} \;\; \right]^{T} \quad 6.82$$

$$\hat{A}_{d}^{*} = \begin{bmatrix} (I_2 + T_s A^{*}) & T_s B^{*} \\ 0_{2x2} & I_2 \end{bmatrix} \quad 6.83$$

$$\hat{B}_{d}^{*} = \begin{bmatrix} 0_{2x2} \\ T_s I_2 \end{bmatrix} \quad 6.84$$

$$\hat{D}_{d}^{*} = \begin{bmatrix} T_s D^{*} \\ 0_{2x1} \end{bmatrix} \quad 6.85$$

"The dynamic equation (6.80) is used to predict the next stage of the system in the MPC controller to satisfy the control objective of a particular power reference and keep the exhaust gas temperature constant. To meet control objectives, it is necessary to transform the system output references $P_{gt,a}^{ref}$ and $T_{ex,a}^{ref}$ into the state- variables references to calculate the state error for the quadratic optimisation problem described by equation (6.70). This is possible by implementing a look-up table which is calculated by solving an algebraic system for each combination of $P_{gt,a}^{ref}$ and $T_{ex,a}^{ref}$, in steady-state conditions as follows":

$$P_{gt,a}^{ref} = h_{a1}(X) \qquad \left[\begin{array}{l} 0 = F_{a1}(X, w) \\ 0 = F_{a2}(X, w \\ \\ T_{ex,a}^{ref} = h_{a2}(X) \end{array}\right. \quad 6.86$$

The system in equation (6.86) produces the following result:

$$\hat{X}^{ref} = \left[P_{cc,a}^{ref} \;\; T_{cc,a}^{ref} \;\; \dot{m}_{a}^{ref} \;\; \dot{m}_{f}^{ref}\right]^{T} \quad 6.87$$

Then, state and input limits can be defined for the heavy-duty GT's physical dynamic behaviour.

$$\dot{m}_{a,min} \leq \dot{m}_{a,k} \leq \dot{m}_{a,max} \qquad 6.88$$

$$\dot{m}_{f,min} \leq \dot{m}_{f,k} \leq \dot{m}_{f,max} \qquad 6.89$$

$$J_{ma,min} \leq J_{ma,k} \leq J_{ma,max} \qquad 6.90$$

$$J_{mf,min} \leq J_{mf,k} \leq J_{mf,max} \qquad 6.91$$

GT MPC controller regulator design block diagram – summarised model for the control system for the dual-fuel control using MPC controller formulation algorism.

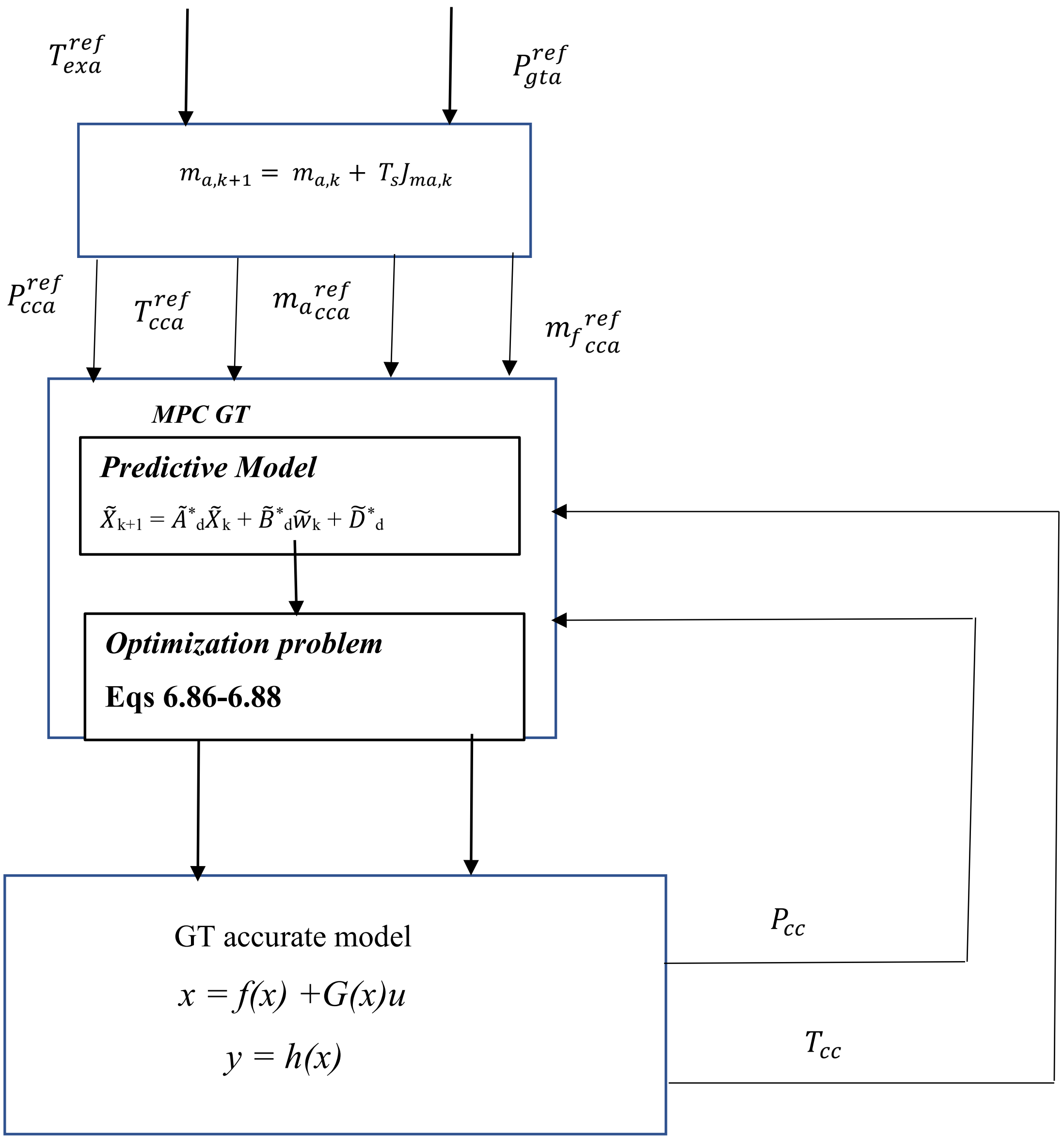

Figure 6.3: MPC Implementation of dual nozzle fuel system control

6.12 Implementing MPC Controller

The MPC controller is constructed based on the model equations developed earlier in this chapter. It should be emphasised that the MPC controller's accuracy is mainly determined by the model used. While the MPC controller can be configured to include an intrinsic action that compensates for the discrepancy between the state and model plants, this is not always the case. The model development and implementation process begin with the extraction of the plant's state-space model via linearisation using the system's initial conditions. The controller is designed using the linearised plant model [145].

6.12.1 Model Horizon

The model horizon is chosen to ensure that (nT) does not exceed 95% of the open loop settling time of the plant. The range for (n) is 20–70, and if it is set too low, a truncating phenomenon occurs during forecast estimation, resulting in poor controller response behaviour [146]

6.12.2 Prediction Horizon

The prediction horizon sets the upper and lower bounds of the controller's future time horizon for generating the desired output response. Typically, the upper limit is set to an infinite or finite value to ensure stability. The prediction horizon must be greater than the control horizon to provide a smooth prediction. The specification of the prediction horizon can be based on a variety of different rules [145].

6.12.3 Weight Specification

The weights assigned to the input and output parameters significantly impact the controller's robustness, making it either slow or aggressive. The less these factors are weighted, the less resilient the controller becomes, and vice versa [146].

6.12.4 Control Horizon

Additionally, the control horizon specifies the sample size over which the prediction horizon can affect the required control action. The MPC controller grows more aggressive as the control horizon increases. The amount usually is between 5 and 20, which must be specified to be less than the controller's prediction limit [144, 146].

6.13 MPC Simulink Model Structure

As illustrated in Figure A6.4, the model is developed using Simulink/MATLAB library blocks. The model is constructed using Simulink blocks and simple MATLAB code created to obtain the plant's linear behaviour and state-space model. The various responses are obtained as shown based on these parameters and by carefully selecting the performance weighting, control, and prediction horizons.

6.14 MPC-PID controller design for dual fuel system

This section combines the MPC and PID controller algorithms to design the dual fuel flow control. The dynamic performance of the PID controller was auto tuned to obtain the proportional, integral, and derivative parameters in controlling the fuel demand operations. The tunned parameters of the PID are dynamically protected by the shielding effect of the MPC controller, which is designed to safeguard the PID. The MPC can handle and predict the future transition from one fuel switching to another to limit the perturbation effect during the switching process. Figure 6.5 shows a Simulink design for dual fuel control with MPC-PID protected system. The diagram consists of a fuel tank dynamic system for LNG and HFO, GT fuel valve positioner and dynamics for the dual fuel flow and standard rail system. The switching characteristic for selecting the fuel type depends on availability and price variation at a given time limit. Programming of the selector is based on **if-else -if condition statement,** which requires the operator to enter both prices.

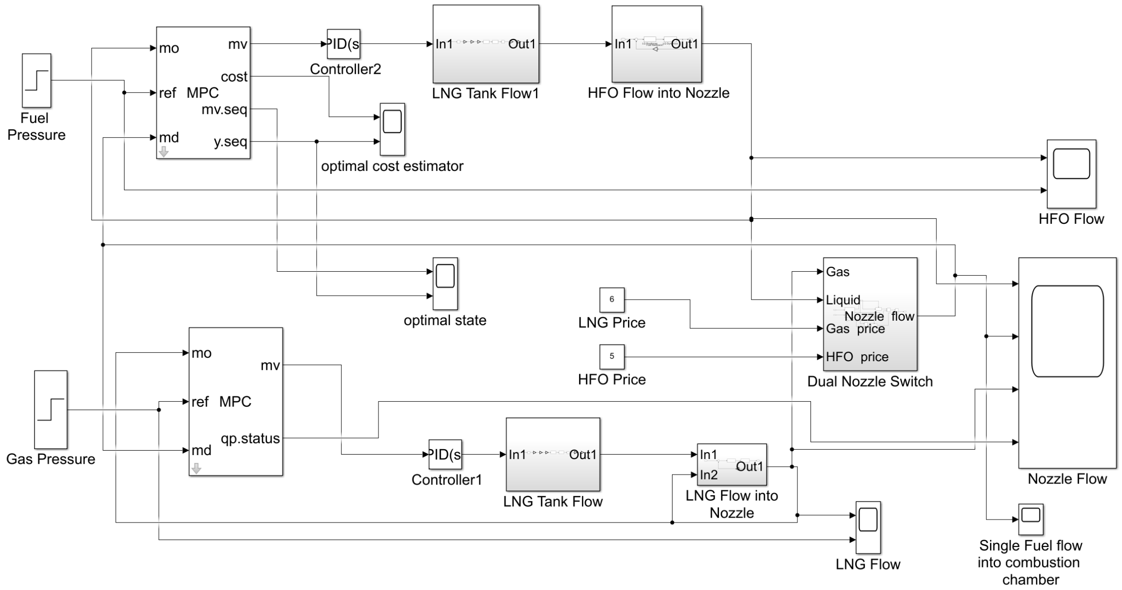

Figure 6.4: Optimization of MPC-PID Controller

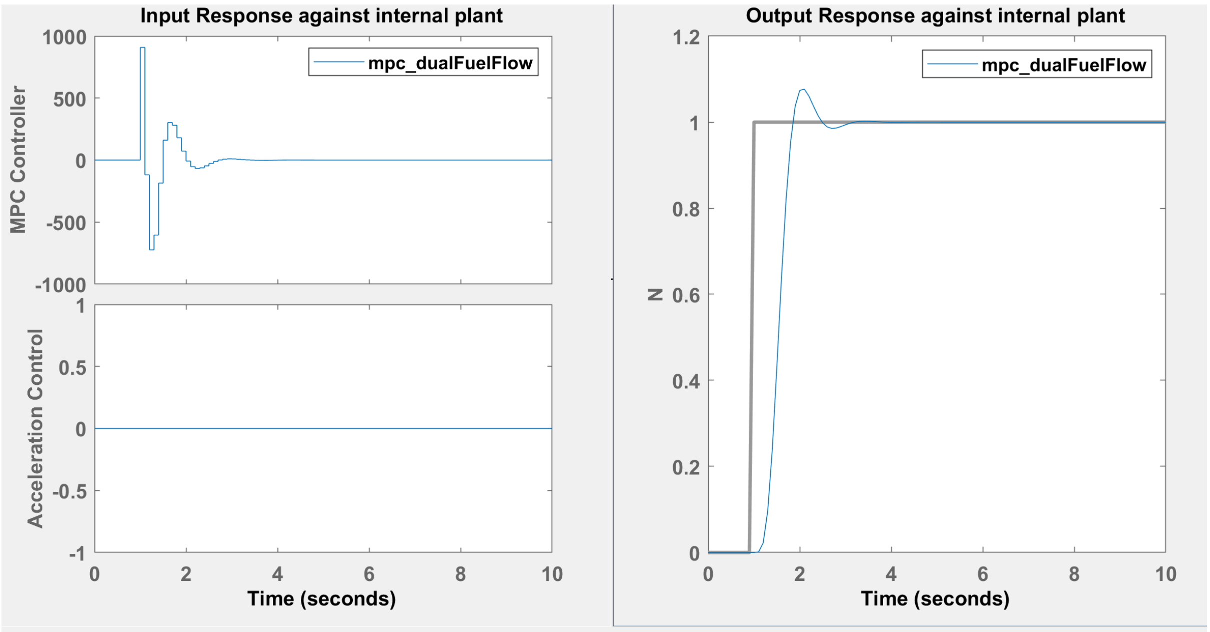

Figure 6.5: GT dual fuel MPC-PID tuning

Figure 6.6 shows the MPC controller design tuned to obtain the performance requirement for the fuel flow into the nozzle system. The prediction horizon setting, prediction control setting, weight matrix and input/output constraint are used to stabilise the model.

The MPC controller design was applied to the model in Figure 6.5, and a step signal is applied to both liquid fuel and LNG gas input with the turbine rotor speed set to a constant of 3000rpm. The system simulation performance. The system simulation performance is visualised on the scope for the various parameters shown in Figure 6.7 – 6.10.

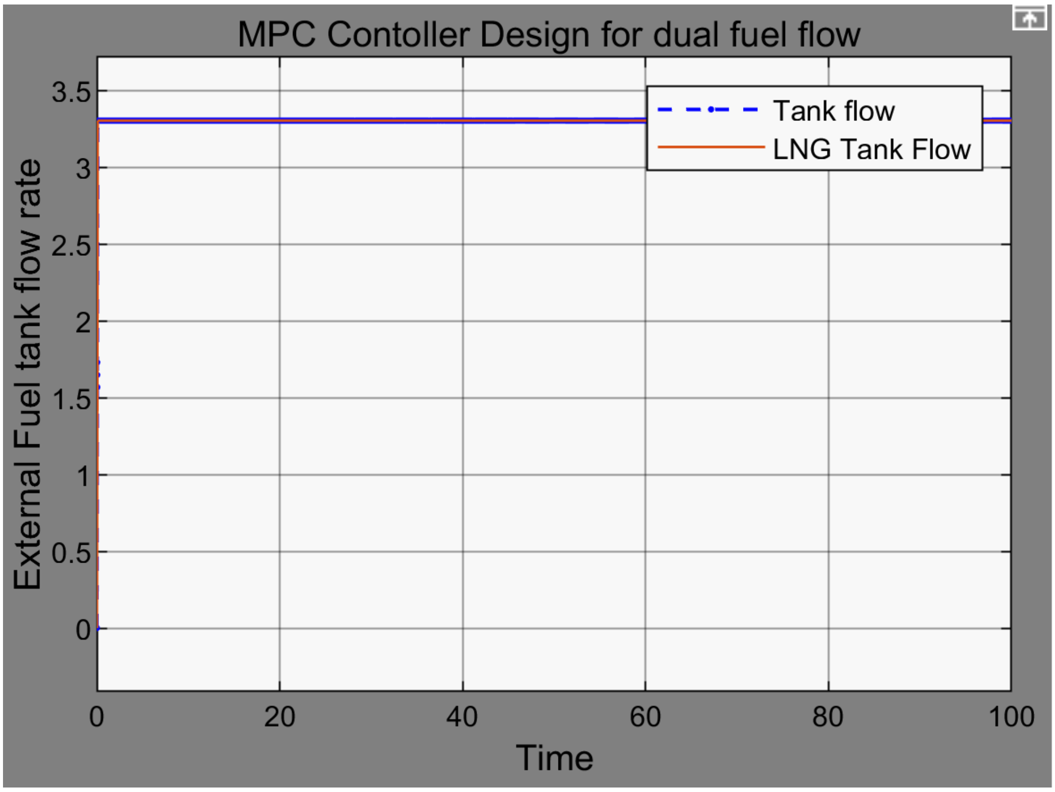

Figure 6.6: MPC-PID controller response for dual fuel tank simulation

Figure 6.7 observed the LNG gas tank flow into the onboard tank for the dual nozzle system. From the response, it can be seen that the valve position for the gas flow opened and settled within 10s. The flow after 10s the performance remains at a steady state over the entire period of operation. The system was simulated for 100s.

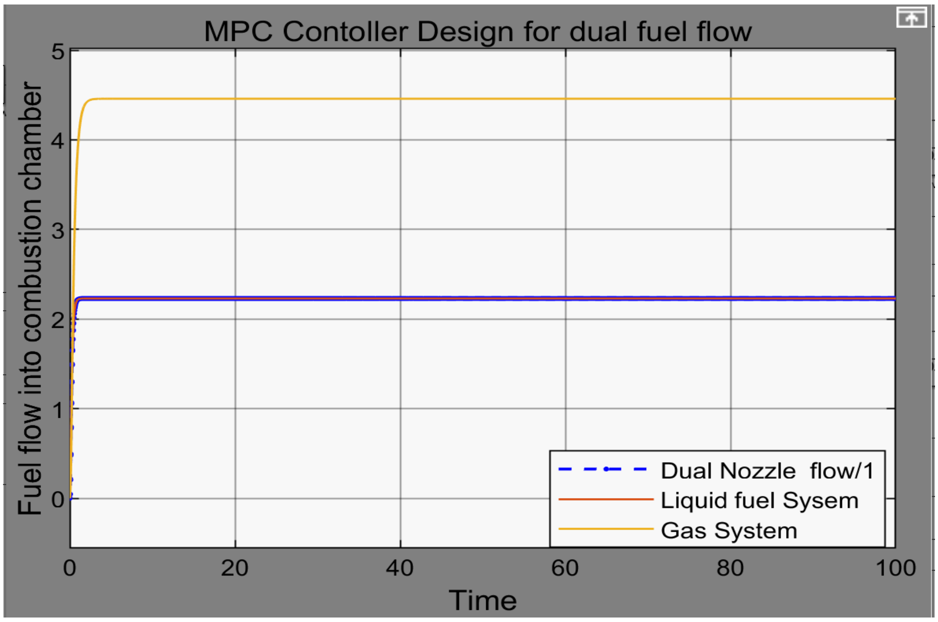

Figure 6.7: MPC-PID Controller response to dual fuel flow into the combustion chamber

In Figure 6.8, the dynamic performance of the nozzle flow into the combustion chamber for useful mechanical work by the turbine to turn the power generator rotor is observed. In the step response, the nozzle flow corresponds to the liquid fuel flow, which is an indication that the control system detects a price reduction in the liquid fuel compared to the LNG gas and shunts down the LNG nozzle.

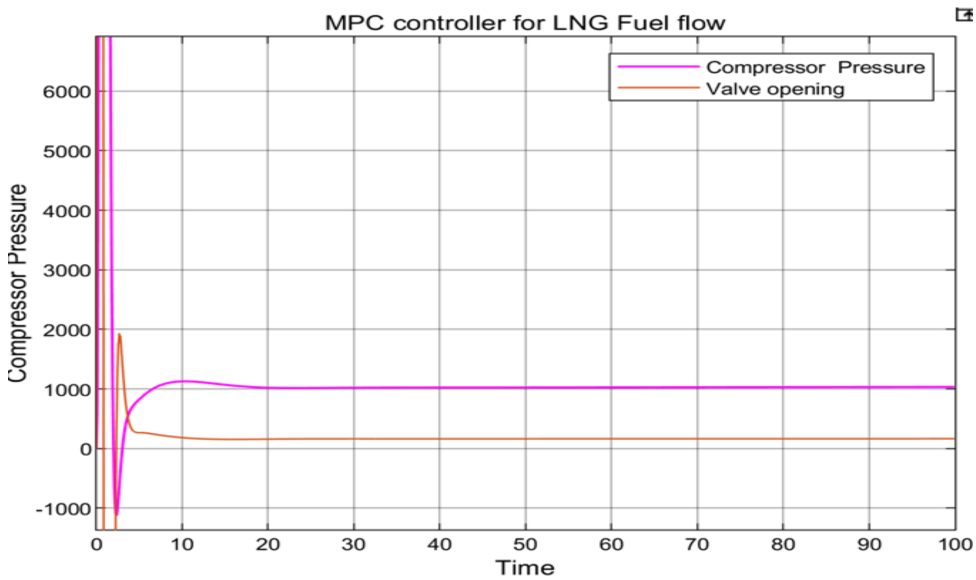

Figure 6.8: MPC-PID response for fuel flow characteristics for dual nozzle

Figure 6.9 shows the performance of the compressor characteristics as liquid fuel flow. From the graph, the initial opening of the fuel valve positioner against the compressor pressure system is evident. The valve opens with a high initial overshoot, which increases the pressure for the compressor very high and settles within 0–5 seconds. After 6 seconds, both flows stabilise and become stable over the operational period.

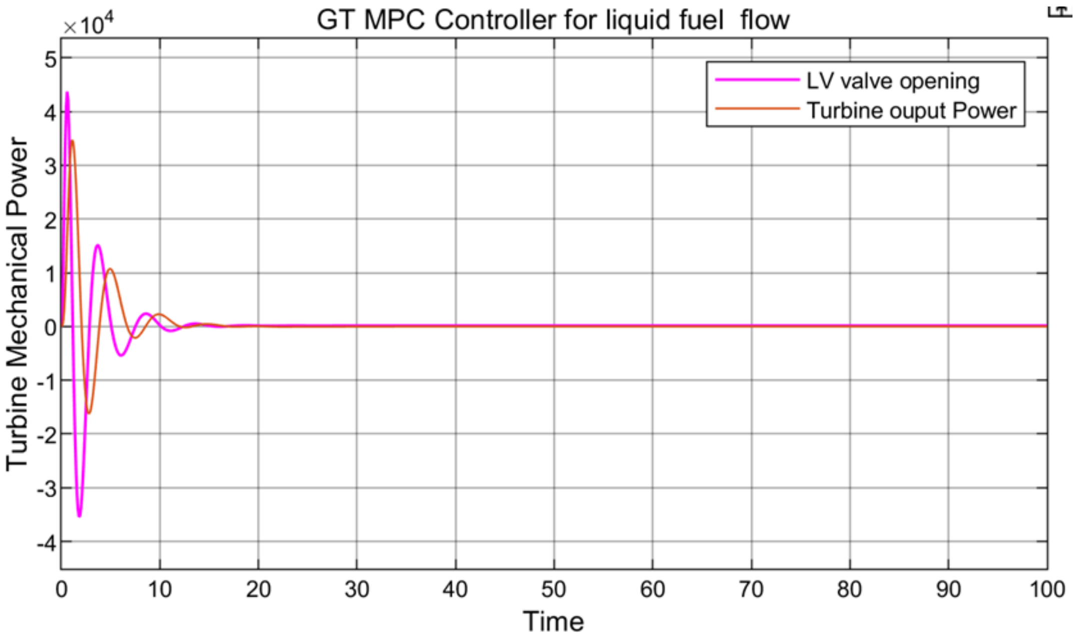

Figure 6.9: MPC-PID dual nozzle fuel control with measured turbine mechanical power

Figure 6.10 shows the turbine mechanical power against fuel flow for the dual nozzle system when only liquid fuel is available. As fuel flow became constant and steady over the period, the mechanical power was evaluated at about 500W.

6.15 Summary

In this section, the designed MPC controller is connected and placed in series with the PID controller design from the previous section, which protects the PID parameters in the respective dual control loops. The combined effect of the MPC-PID coupled with the gas turbine the fuel system to observe the fuel flow performance under various conditions. The resulting controller stabilised the fuel valve characteristics and fuel flow into the combustion chamber.

CHAPTER SEVEN: DISCUSSION OF RESULTS

7.1 Introduction

The results of the research work on the optimal operation and control for a hybrid dual nozzle HFO-DLCO gas turbine power generating plant have been subdivided and presented as described in the following captions. The design is not intended to compare the two controllers for optimal operation. Instead, it seeks to achieve a resilience controller by combining the algorithms of MPC and PID controllers to mitigate their respective drawbacks.

- External liquid fuel supply system modelling and simulation results
- External gas fuel supply system modelling and simulation results
- Dual nozzle modelling and simulation results
- PID controller design simulation of a combined dual fuel supply system results
- GT internal fuel line to the combustion chamber. PID controller design simulation of the external fuel supply system and GT inner fuel line to the combustion chamber
- PID-MPC controller design simulation results of the combined fuel system for GT operation

The design primarily studies GT's dual nozzle multi-fuel supply operation and management to improve performance. The system will also lower the GT's operational costs by selecting the cheapest fuel for continuous operation. The operation of GT in dual-fuel mode, where one fuel is saved as an auxiliary source, provides improved performance that will enhance continuous running for power generation. The study and model obtained from the research on the dual-fuel simulation for power generating plants operating at the optimal fuel cost provide the basis for multiple fuel design of a hybrid GT development within the renewable sector.

The research enables modification to the GT standard fuel system that has traditionally existed in the Rowen model by introducing an additional parallel fuel supply dynamic

system with an automatic fuel pressure detector selector switch. The switch uses the principle of the if-else-if condition—operator in the Simulink model.
Theoretical modelling and simulation are presented in Chapters Three to Six, and the results and discussions are presented in this chapter.

7.2 Results of external liquid fuel supply system modelling and simulation

The study investigated the dynamic characteristics of the external fuel system from the tank to the point of coupling into the GT fuel system. The mathematical model for liquid fuel was developed based on the first principles of thermodynamics. In this respect, the fuel flow performance is analysed to ensure a dynamic flow. The design is linearised in MATLAB scripts to obtain the designed transfer function equation for controller design. The dual fuel loop pressure flow is controlled with continuous proportional-integral-derivative control, for which the tuned parameters of the controller are tabulated in table 7.1.

Table 7.1: PID controller parameters for Liquid tank flow dynamics

S/N	CONTROLLER PARAMETER	TUNNED VALUE	PERFORMANCE AND ROBUSTNESS	VALUES
1	Proportional	-4.0188e^-06	Rise time	0.626
2	Integral	-5.2557e^-05	Settling time	9.82
3	Derivative	-6.954e^-05	Overshoot	7.72%
4	N (filter coefficient)	239.9599	Peak	1.08
5			Gain Margin	40.4 @ 34.4rad/s
6			Phase margin	64.5 deg @ 2.1 rad/s
7			Closed-loop stability	Stable

Figure 7.1 shows the response of the external liquid fuel tank flow for the dual fuel controller design characteristics. The fuel valve response has an initial delay of about 0.626secs during the step application with an overshoot of 7.72% with a settling time of

9.82 seconds. The results tabulated in Table 7.1 show that the closed-loop system is stable, making the design suitable for the intended purpose.

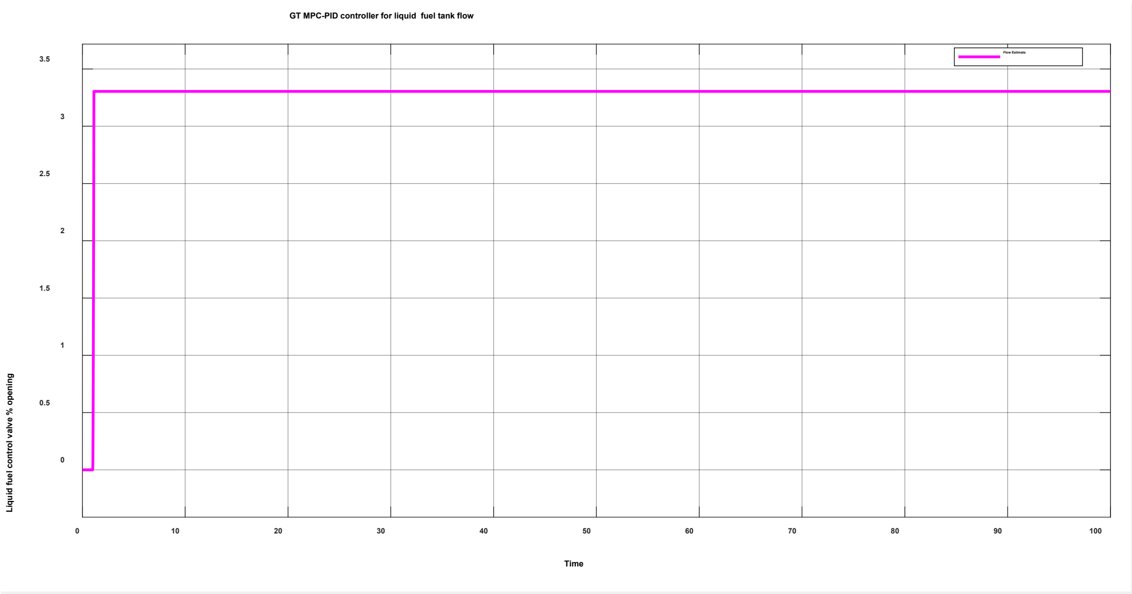

Figure 7.1: Dynamic response of liquid tank flow

7.3 Results of external Gas fuel supply system modelling and simulation

The dynamic characteristics of the external fuel system line from the tank to the point of coupling into the GT fuel system were investigated with the Gas fuel supply system. The mathematical model for Gas line and tank fuel was developed using thermodynamic first principles. In this regard, the fuel flow performance to ensure that flows are connected dynamically were analysed. The design in MATLAB scripts is linearised to obtain the designed transfer function equation for controller design and control the loop using continuous proportional-integral-derivative control.

Simulation results and system response are shown in Table 7.2 and Figure 7.2, respectively. The gas line and control valve characteristics are similar to the liquid line previously studied. The only difference is the valve saturation limit for the gas control signal.

Table 7.2: PID controller parameters for LNG tank flow dynamics

S/N	CONTROLLER PARAMETER	TUNNED VALUE	PERFORMANCE AND ROBUSTNESS	VALUES
1	Proportional	-6.6208e^-05	Rise time	0.18
2	Integral	-2.6855e^-06	Settling time	1.91
3	Derivative	-0.00036267	Overshoot	29.5%
4	N (filter coefficient)	794.582	Peak	1.29
5			Gain Margin	37.1 @ 65rad/s
6			Phase margin	37.8 deg @ 6.95 rad/s
7			Closed-loop stability	Stable

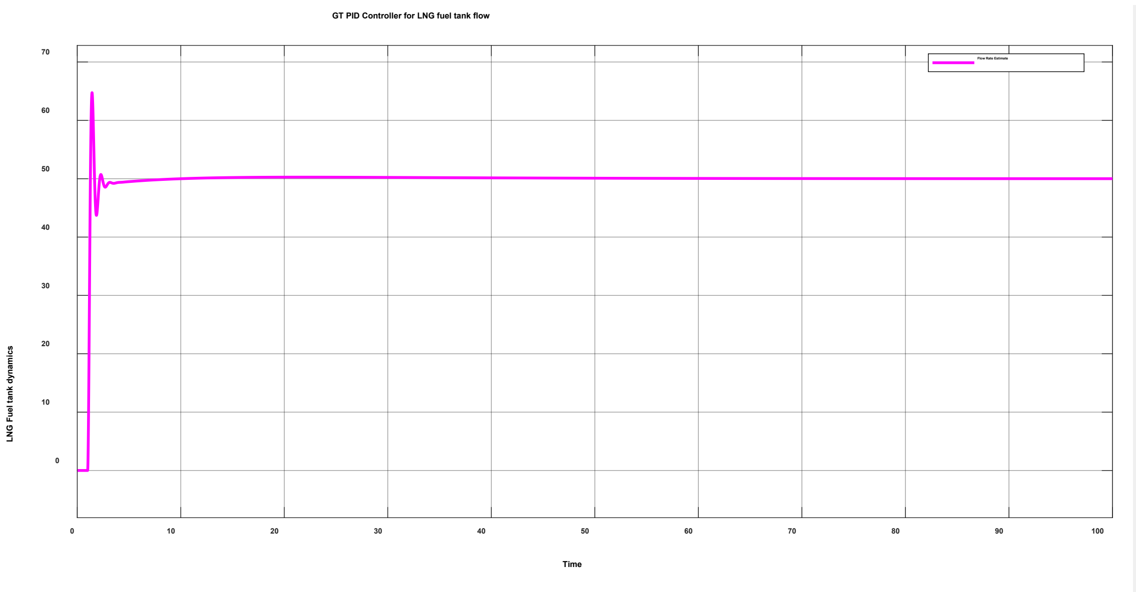

Figure 7.2: Dynamic response of LNG tank flow

The response of the external LNG fuel tank flow for the dual fuel system design is depicted in Figure 7.2. The fuel valve response time is approximately 0.18 seconds during step application, with a 29.5% overshoot and settling time of 1.91 seconds. According to Table

7.2, the closed-loop system is stable, indicating that the design is appropriate for the intended purpose.

7.4 Dual nozzle modelling and simulation results

The primary objective of dual nozzle modelling and simulation is to manage the transition of fuel flow from one nozzle to the next. The design formulation takes cost and availability into account to ensure optimal operation. The switching logic is synchronised with the combustion chamber's fuel burning rate, ensuring that the fuel chamber is never empty while the unit is operating. Online switching is accomplished via an **if-else – if** conditional block with price and fuel inputs as constraint parameters.

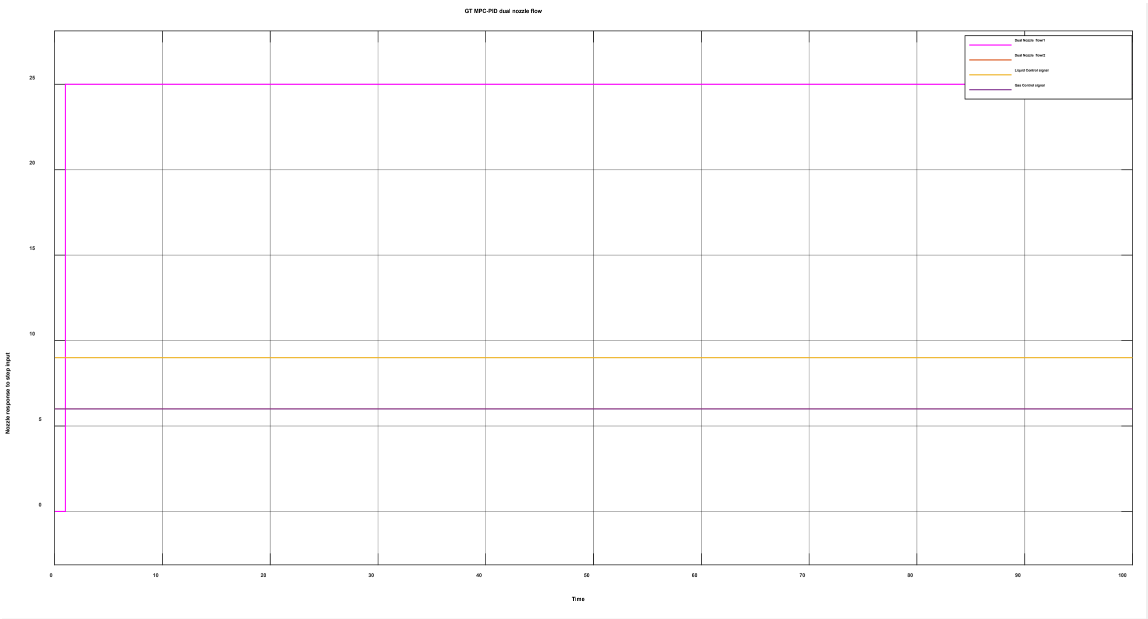

Figure 7.3: Dynamic response of dual nozzle flow

In Figure 7.3, selection of one particular nozzle (Liquid or LNG) for operation depends on the control signal applied to the control port of the nozzle in time t seconds. Currently, the selected fuel for operation is LNG since its price ranges from zero to a maximum of 5 cent per litre of fuel and is also available in the storage tank, and liquid fuel is available, but the price ranges between zero and 10 cents per litre.

7.5 Results of GT dual nozzle fuel flow analysis with PID Controller

The dual nozzle flow response is tested only on the GT fuel system without the combustion chamber dynamics. In the design, each loop has been controlled by loop control PID and the parameters are shown in Table 7.3, and Figure 7.4 show the dual nozzle response to the loop flow.

Table 7.3: PIDs parameters for GT dual nozzle fuel flow

S/N	CONTROLLER PARAMETER	TUNNED VALUE	PERFORMANCE AND ROBUSTNESS	VALUES
1	Proportional	18.327	Rise time	0.119 seconds
2	Integral	12.7487	Settling time	2.11 seconds
3	Derivative	6.5256	Overshoot	9.74%
4	N (filter coefficient)	1527.5737	Peak	1.1
5			Gain Margin	inf @ infrad/s
6			Phase margin	79 deg @ 13.4 rad/s
7			Closed-loop stability	Stable
S/N	**CONTROLLER PARAMETER**	**TUNNED VALUE**	**PERFORMANCE AND ROBUSTNESS**	**VALUES**
1	Proportional	0.17143	Rise time	2.16 seconds
2	Integral	0.016594	Settling time	12.3 seconds
3	Derivative	0.42709	Overshoot	4.05%
4	N (filter coefficient)	98.6168	Peak	1.04
5			Gain Margin	inf @ infrad/s
6			Phase margin	85.5 deg @ 0.863 rad/s
7			Closed-loop stability	Stable

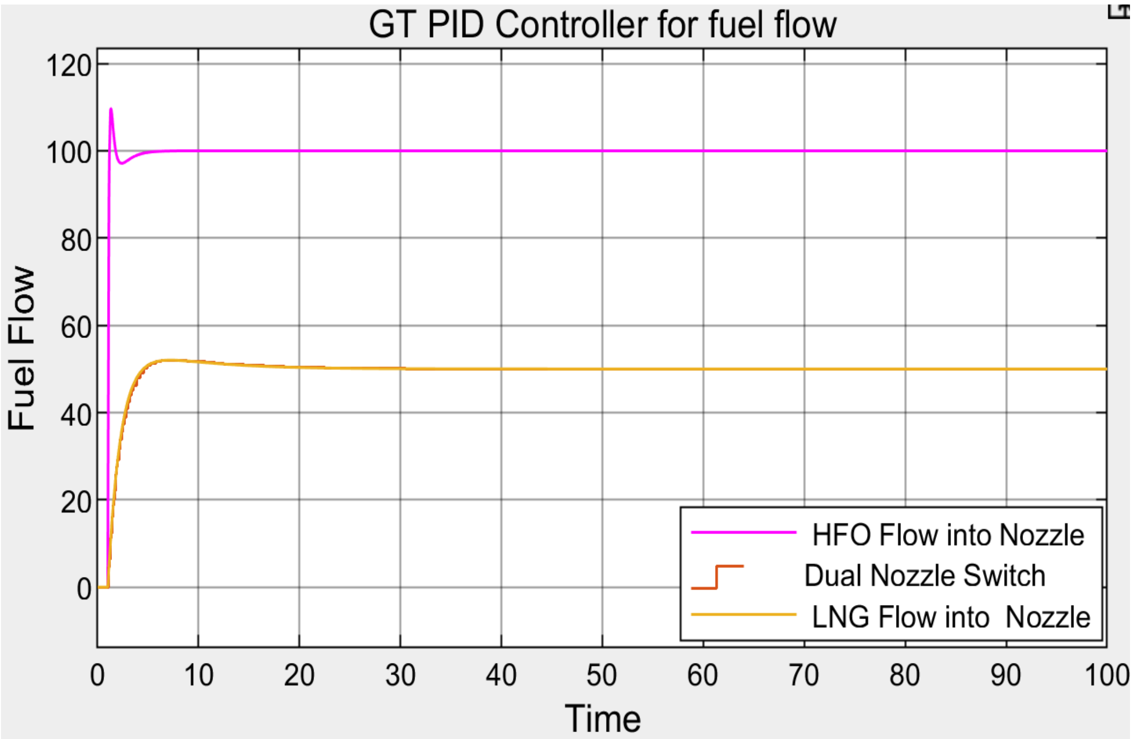

Figure 7.4: Response of PID Controller design for GT dual nozzle fuel flow

The response shows how GT fuel flows through the dual nozzle system with a PID controller in each loop regulating and stabilising the flow dynamic, which enhances smooth combustion. From the reaction, the outflow corresponds to LNG flow into the nozzle, which indicates its low price compared to liquid fuel. The controller performance recorded in Tables 7.3 (a) and (b) above shows the stable state of the fuel output flow in the respective loops.

7.6 Result of PID controller design simulation of a combined dual fuel supply system

The result of the GT dual fuel system response with the dual nozzle design is shown in Figure 7.5. PID controller is designed to control the opening and closing of the fuel control valve depending on the fuel demand by the acceleration throttle control and speed (N) increases. Clearly, from the response, the nozzle flow into the combustion chamber is linear and enhances the smooth combustion process in the GT system.

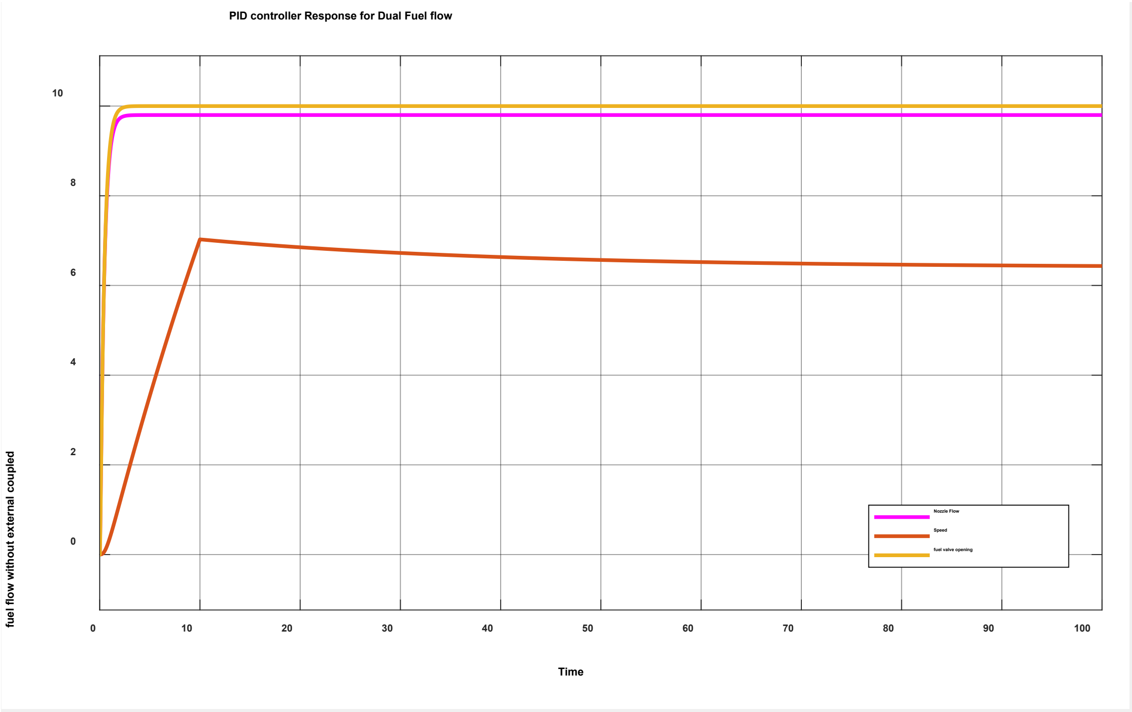

Figure 7.5: Response of PID controller design for dual fuel GT control without external tank

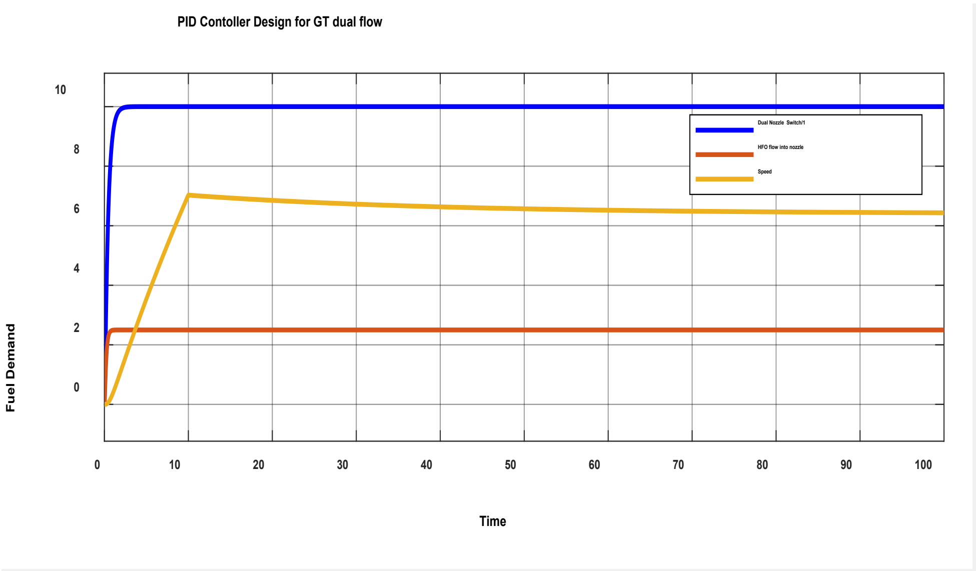

Figure 7.6: GT fuel demand response for dual fuel PID control

The response in Figure 7.6 shows the output speed characteristics, dual nozzle flow and liquid fuel valve opening when the GT demand more fuel for the output power. The nozzle outflow was limited to 9.5lb with a fast rise time of 0.001seconds which settled within 10 seconds, while the speed overshoot and settled at 50 seconds with a liquid fuel flow rate of 2lb per second.

7.7 Results of PID-MPC Based Dual Fuel GT Control

An MPC controller on top of the PID controller for the dual fuel system of GT fuel control is designed. The standard MPC's design parameters include penalty weights, a control horizon and a prediction horizon. These parameters can be fine-tuned using simulations and observations of the dual fuel nozzle operating at various flow rates. The MPC's control interval is set to 0.1 s in this simulation, the prediction horizon is set to forty steps, and the control horizon is set to eight to ten steps. The control rate has a weight factor of 40. The system outputs are regulated to step references to select appropriate output weight factors. The fuel demand specified a liquid tank flow of 200 bar and an HFO-LNG gas pressure of 50 bar. Each fuel loop is controlled by MPC- PID controller in the design, which is evaluated using performance criteria. All the MPC controller designs meet the performance test summarised below.

Table 7.4: MPC Performance Test

S/N	PARAMETER TESTED	TEST STATUS
1	MPC Objective	Pass
2	QP Hessian Matrix Validity	Pass
3	Closed – Loop Internal Stability	Pass
4	Closed -Loop Normal Stability	Pass
5	Closed – Loop Steady State Gains	Pass
6	Hard MV Constraints	Pass
7	Other Hard Constraints	Pass
8	Soft Constraints	Pass
9	Memory Size for MPC Data	Pass

7.7.1 Equal Concern Relaxation Parameter (ECR)

The test evaluates the ECR parameters associated with constraints to achieve the optimal balance of hard and soft constraints. An excessively permissive constraint may result in an unacceptable violation. If the task is too difficult, the controller may devote excessive time to it. Additionally, increasing the difficulty of a constraint does not guarantee that it will not be violated, which is fundamentally impossible.

Two arbitrary constraints in the simulation are defined. These are summarised in Table 7.5 as possible violations based on specified variable bounds and other factors.

This constraint violation increases the MPC cost function relative to the average increase caused by such violations. The rows are ordered by decreasing impact.

Sensitivity Ratio: the magnitude of the increase in the MPC cost function caused by this constraint violation relative to the magnitude of the typical cost function in the absence of violations.

The possibility of a constraint violation equal to 10% of the nominal output variable range is considered. The effect of the violation on the MPC objective function is then calculated compared to the impact of other violations. A high impact factor indicates a high-priority controller objective and vice versa.

Table 7.5: MPC – Constraint Assessment

MPC LIQUID			
CONSTRAINT	**ASSUMED VIOLATION**	**IMPACT FACTOR**	**SENSITIVITY RATIO**
Lower limit: HFO Flow into Nozzle	0.02	1	7.588
Upper limit: HFO Flow into Nozzle	0.02	1	7.588
MPC LNG GAS			
CONSTRAINT	**ASSUMED VIOLATION**	**IMPACT FACTOR**	**SENSITIVITY RATIO**
Lower limit: LNG Flow into Nozzle	0.14	1	16.89
Upper limit: LNG Flow into Nozzle	0.14	1	16.89

From Table 7.5, the two MPC controller design sensitivity assessment is acceptable for the GT fuel control system implementation on dual fuel flow simulations.

7.8 Results of MPC State Space (SS) Values

This section presents the results of the plant state-space estimation for the MPC controller design analysis for liquid and LNG fuel flow line into the GT using quadratic programming (QP) Hessian matrix.

7.8.1 MPC Liquid Model Plant

$$Plant\ A = \begin{bmatrix} 0.0709 & 0 & 0 & 0 & 0 & 0 & 0 \\ 0 & 1 & 0 & 0 & 0 & 0 & 0 \\ 0.4488 & -0.0249 & 0.9743 & 0.1966 & 1.0667 & -1.2237 & 0.1586 \\ 10.3136 & -0.6151 & 0 & 0.9920 & 10.6565 & -23.9542 & 2.2907 \\ 3.2992 & -0.2188 & 0 & 0 & 0.9512 & -6.2824 & 0.3830 \\ -0.9291 & 0.1000 & 0 & 0 & 0 & 1 & 0 \\ 16.1234 & -1.2784 & 0 & 0 & 0 & -23.6082 & 0.6065 \end{bmatrix}$$

$$Plant\ B = \begin{bmatrix} -6.5902e^{\wedge}-07 & 0 \\ -4.0027e^{\wedge}-12 & 0 \\ 3.188e^{\wedge}-07 & 0 \\ 7.3283e^{\wedge}-06 & 0 \\ 2.3447e^{\wedge}-06 & 0 \\ -6.6114e^{\wedge}-07 & 0 \\ 1.1463e^{\wedge}-05 & 0 \end{bmatrix} \qquad Plant\ C - \begin{bmatrix} 0 & 0 & 1 & 0 & 0 & 0 & 0 \end{bmatrix}$$

$$Pant\ D = \begin{bmatrix} 0 & 0 \end{bmatrix}$$

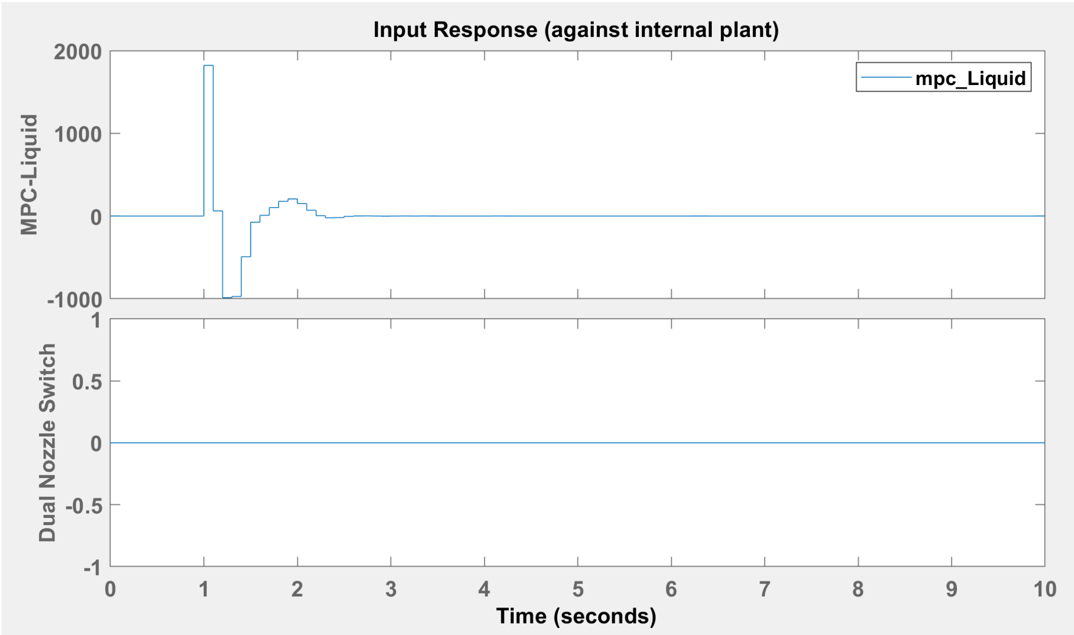

Figure 7.7: MPC-PID Liquid Plant input response against Model internal parameters

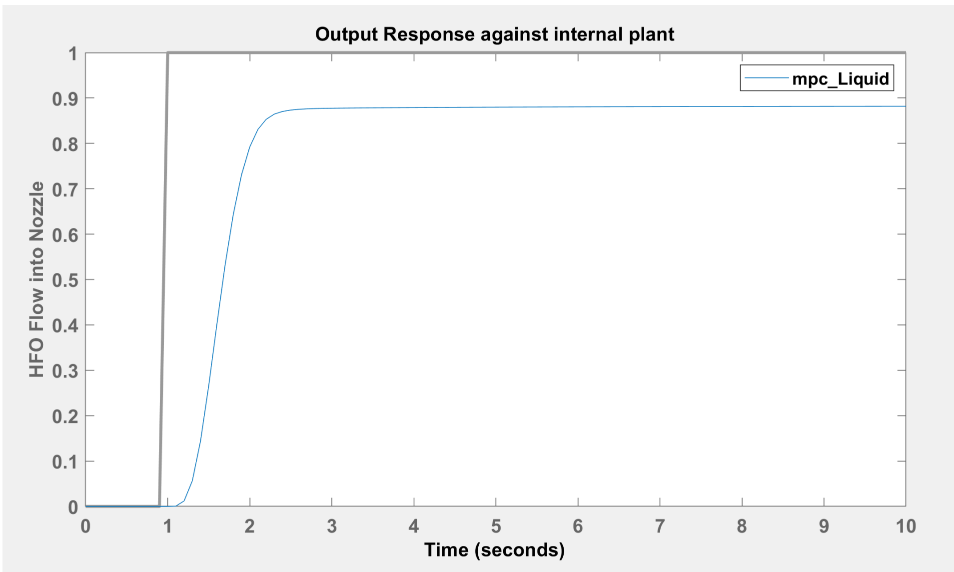

Figure 7.8: MPC-PID Liquid Plant Output response against Model internal parameters

7.8.2 MPC LNG Model Plant

$$Plant\ A = \begin{bmatrix} 0.0709 & 0 & 0 & 0 & 0 & 0 & 0 \\ 0 & 1 & 0 & 0 & 0 & 0 & 0 \\ 0.4488 & -0.0249 & 0.9743 & 0.1966 & 1.0667 & -1.2237 & 0.1586 \\ 10.3136 & -0.6151 & 0 & 0.9920 & 10.6565 & -23.9542 & 2.2907 \\ 3.2992 & -0.2188 & 0 & 0 & 0.9512 & -6.2824 & 0.3830 \\ -0.9291 & 0.1000 & 0 & 0 & 0 & 1 & 0 \\ 16.1234 & -1.2784 & 0 & 0 & 0 & -23.6082 & 0.6065 \end{bmatrix}$$

$$Plant\ B = \begin{bmatrix} -6.5902e^{\wedge}-07 & 0 \\ -4.0027e^{\wedge}-12 & 0 \\ 3.188e^{\wedge}-07 & 0 \\ 7.3283e^{\wedge}-06 & 0 \\ 2.3447e^{\wedge}-06 & 0 \\ -6.6114e^{\wedge}-07 & 0 \\ 1.1463e^{\wedge}-05 & 0 \end{bmatrix} \qquad Plant\ C - [0 \quad 0 \quad 1 \quad 0 \quad 0 \quad 0 \quad 0]$$

$$Pant\ D = [0 \quad 0]$$

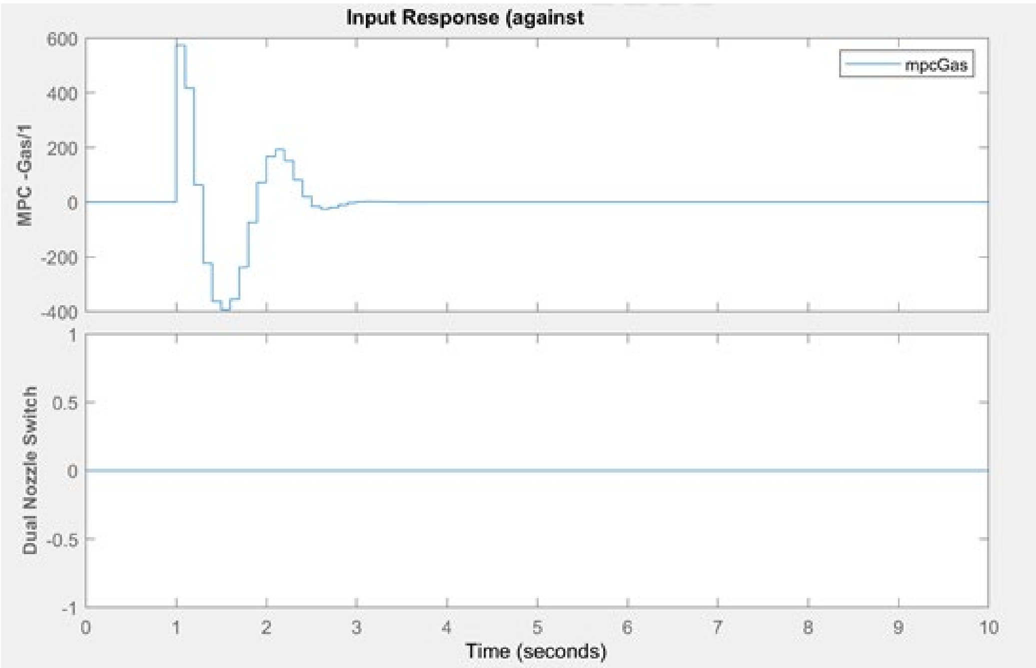

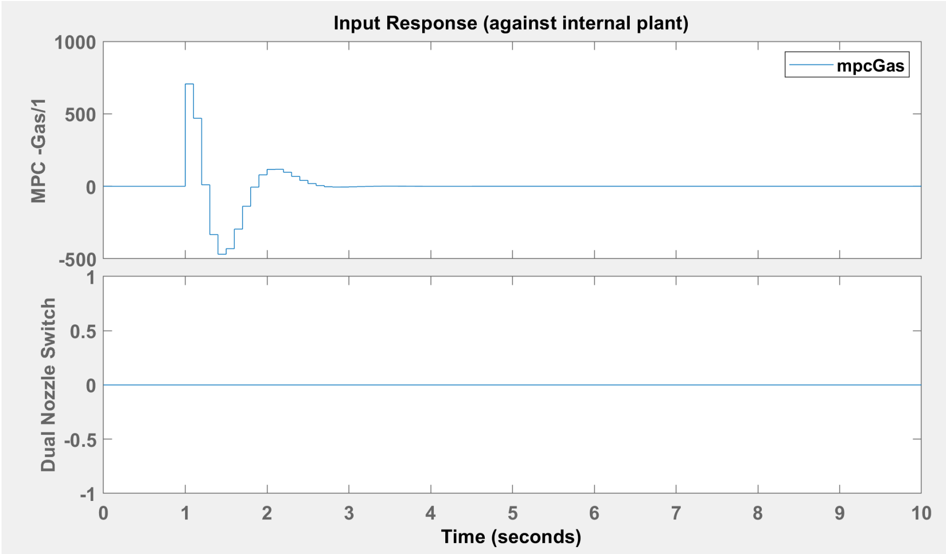

Figure 7.9: MPC-PID LNG Gas Plant Input response against Model internal parameters

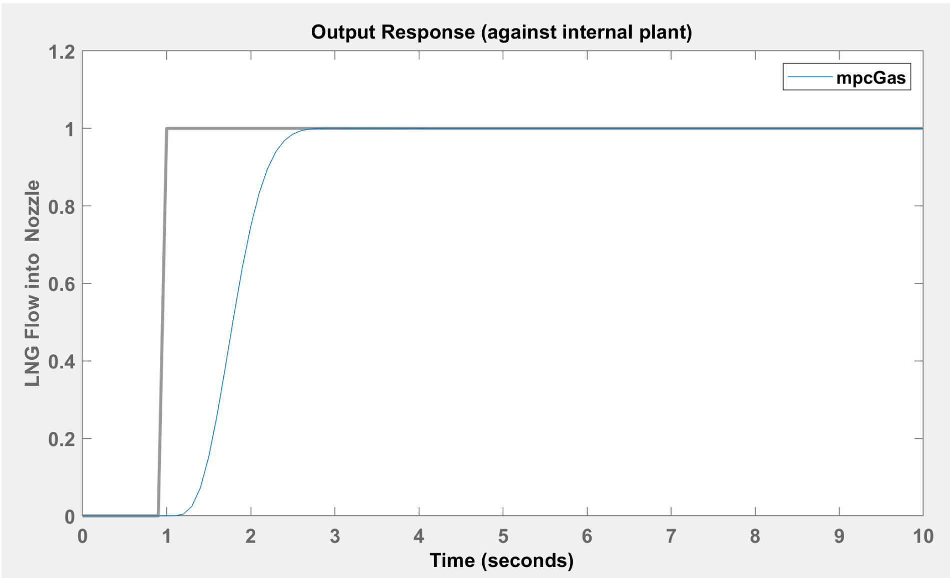

Figure 7.10: MPC-PID LNG Gas Plant Output response against Model internal parameters

Figure 7.7 to 7.10 shows the MPC-PID-based Simulink design for the respective fuel control for GT dual nozzle optimal operation. The responses show a correlation between the input/output plant model and its internal characteristics. The outputs are initially out of range and could be applied to the plant without tuning. The smooth performance is achieved by adjusting the plant parameter such as weight penalty, prediction horizon, and control horizon by imposing a hard and soft constraint on the outputs.

7.9 Tuning MPC Controller

The MPC was tuned in the time domain to define the controller bandwidth while satisfying each operating point region's robustness, stability, and performance criterion. This was accomplished by shaping the local MPC controller's control sensitivity function concerning the unconstrained case of the explicit solution. The small gain theorem was used to achieve the controller's robust stability during design, assuming a defined unstructured model output uncertainty level. The recursive feasibility of the MPC problem solution is ensured by treating output constraints as soft and assuming that the fuel actuators have only bound constraints. The tuning results for MPC-PID controller parameters which achieve the performance response are shown in Table 7.6. It is clear from the result that the LNG- fuel control system obtains its stabilised position in between controller performance for both aggressive and robustness. The constraint on the output is the exact value of ±0.1 for all the control loops, while the input has positive and negative infinity constraints defined function. The overall design is implemented on the model design with Simulink, and the responses with step input signal are shown below.

Table 7.6: MPC Tunned Parameters

MPC	**Prediction**	**Control**	**Weight**	**Construction**		**Performance**	
	Horizon	**Horizon**	**Factor**	**Input**	**Output**	**Aggressive**	**Robustness**
Liquid	40	5		±Inf	±0.1	√	
LNG	40	7	30	±Inf	±0.1	√	√

7.10 Result of MPC-PID HFO GT Fuel Flow Control

Figure 7.11 shows the response when the MPC-PID controller design is implemented on the HFO fuel flow control for the GT fuel system. The tank flow pressure is set to 60 bar/sec. The output response indicates that the controller response to the inflow rate causes the HFO actuating valve to open fully. The fuel gauge indicator spindly settled within 80 secs to stabilise the flow.

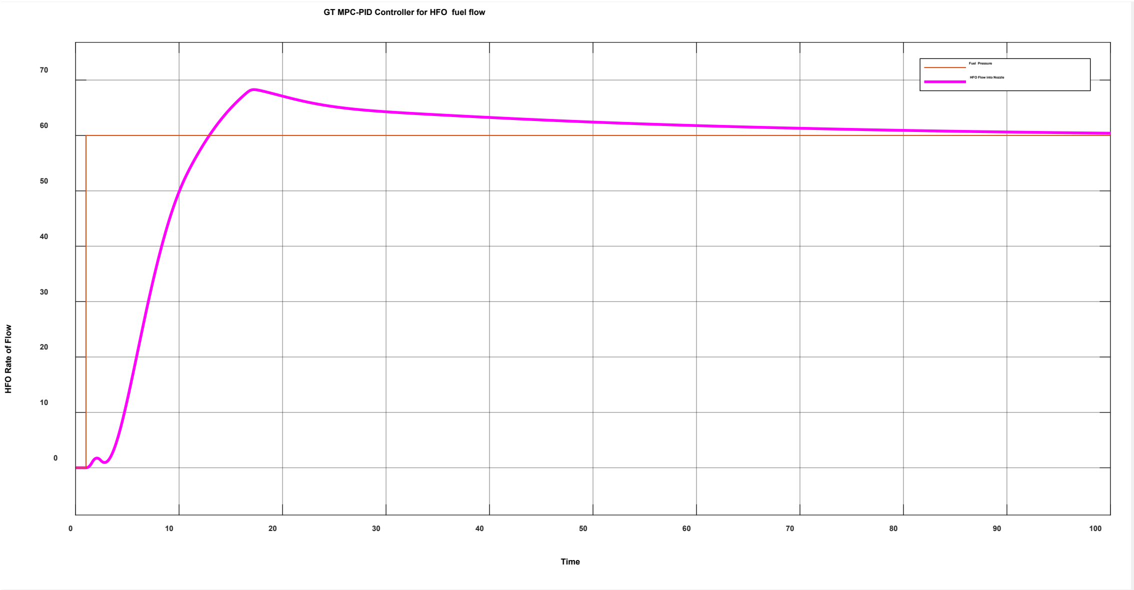

Figure 7.11: Response of GT MPC-PID Controller implementation for HFO -Fuel Flow

7.11 Result of MPC-PID LNG GT Fuel Flow Control

Figure 7.12 depicts the GT fuel system's LNG flow control response when the MPC-PID controller design is used. When the tank flow pressure is set to 80 bar/sec, and the controller responds to the inflow rate, the LNG actuating valve opens fully, and the fuel gauge indicator spins down to zero within 120 seconds, the flow is stabilised.

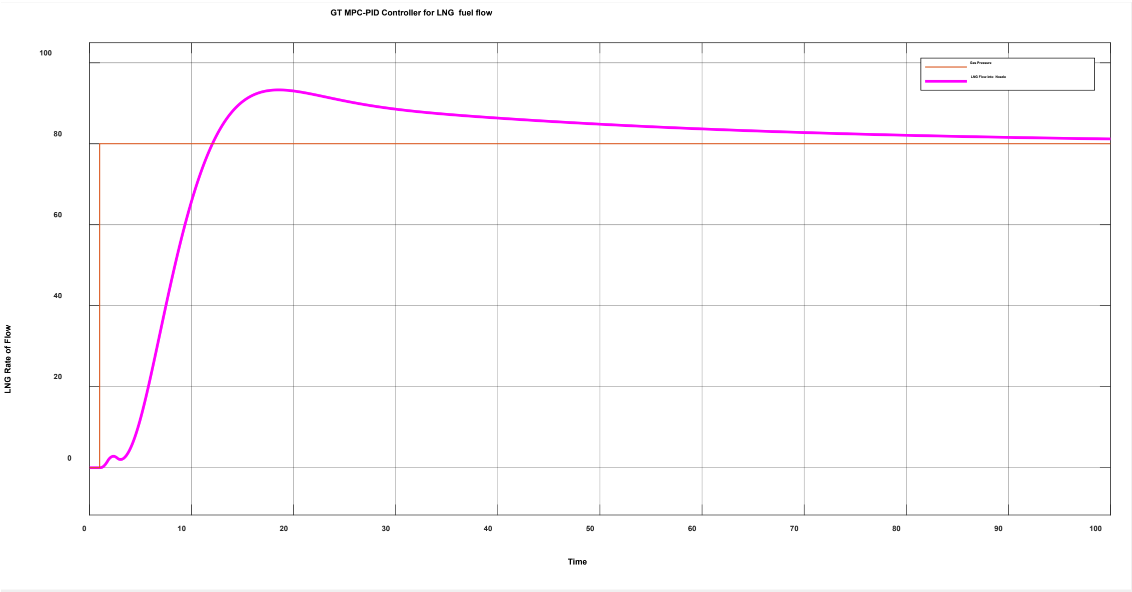

Figure 7.12: Response of GT MPC-PID Controller implementation for LNG -gas Flow

7.12 Result of MPC-PID GT Dual-Nozzle Combustion Flow Control

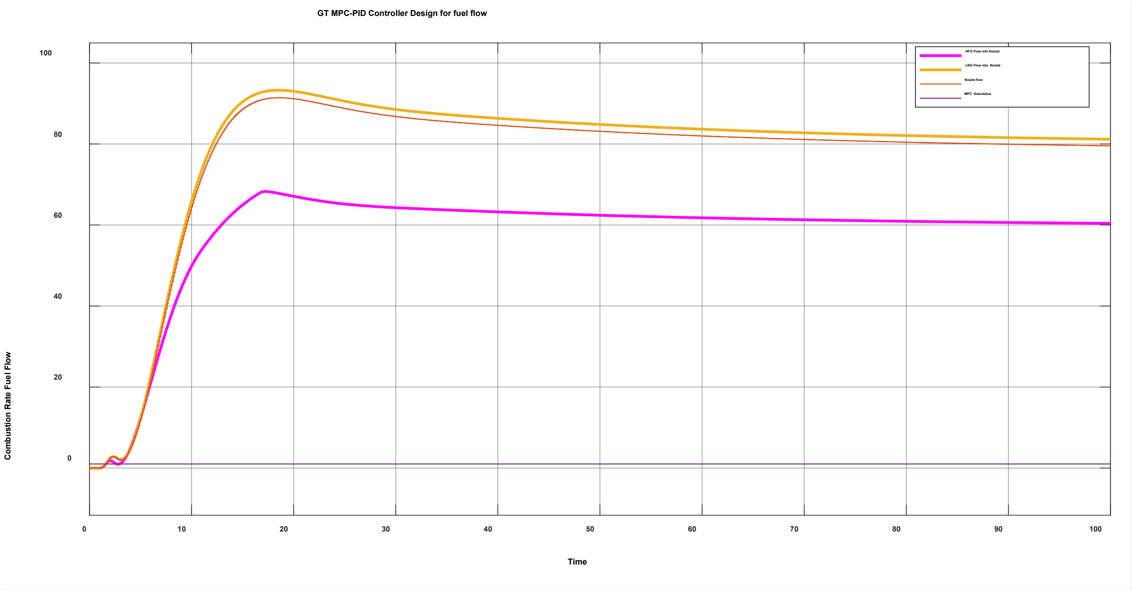

Figure 7.13: Response of GT MPC-PID Controller implementation for Dual-Nozzle Flow

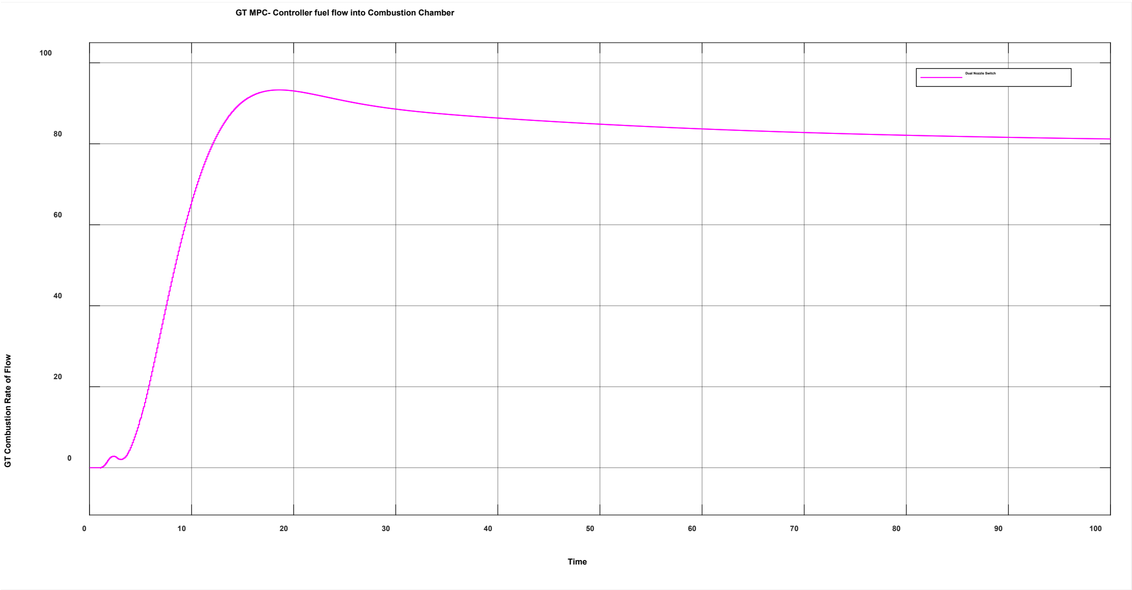

Figure 7.14: Response of GT MPC-PID Controller for Dual-Nozzle Combustion Flow

Figures 7.13 and 7.14 show the dual-nozzle combustion chamber flow response. The combustion chamber accepts single fuel only during operation. Although designed for alternate fuel consumption or applications, only single fuel is burned at a time. The switch logic will allow either LNG or HFO to flow into the combustion chamber depending on the fuel prince at a given time. However, during the fuel switching operation, the hybrid fuel function enables and limits the poor combustion process, which improves performance.

It could be observed from Figure 7.13 that even though LNG pressure was high, the switch logic allowed HFO fuel to flow into the chamber for burning, as indicated in the response in Figure 7.14.

7.13 Result of MPC-PID GT Dual-Nozzle Fuel Flow Optimal Control

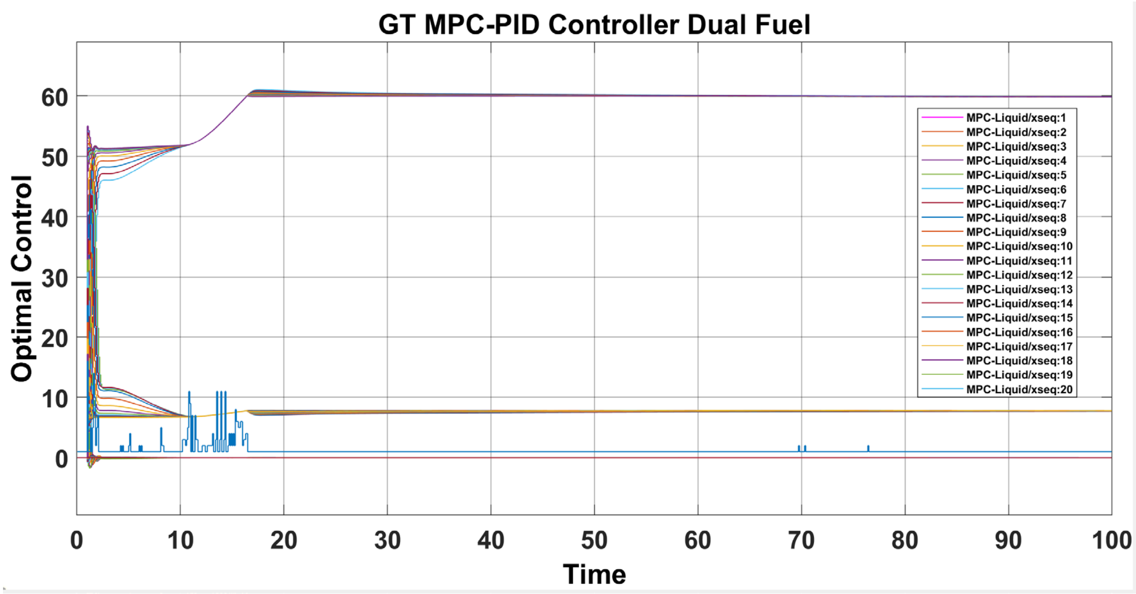

Figure 7.15: Response of GT MPC-PID Controller Dual-Nozzle Optimal flow

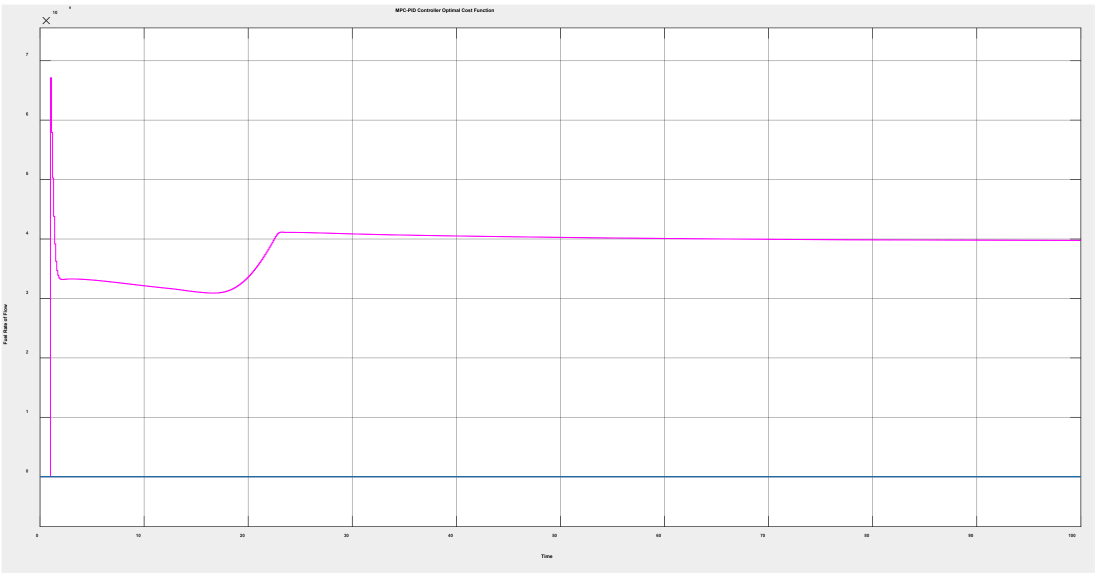

Figure 7.16: Response of GT MPC-PID Controller Dual-Nozzle Cost function

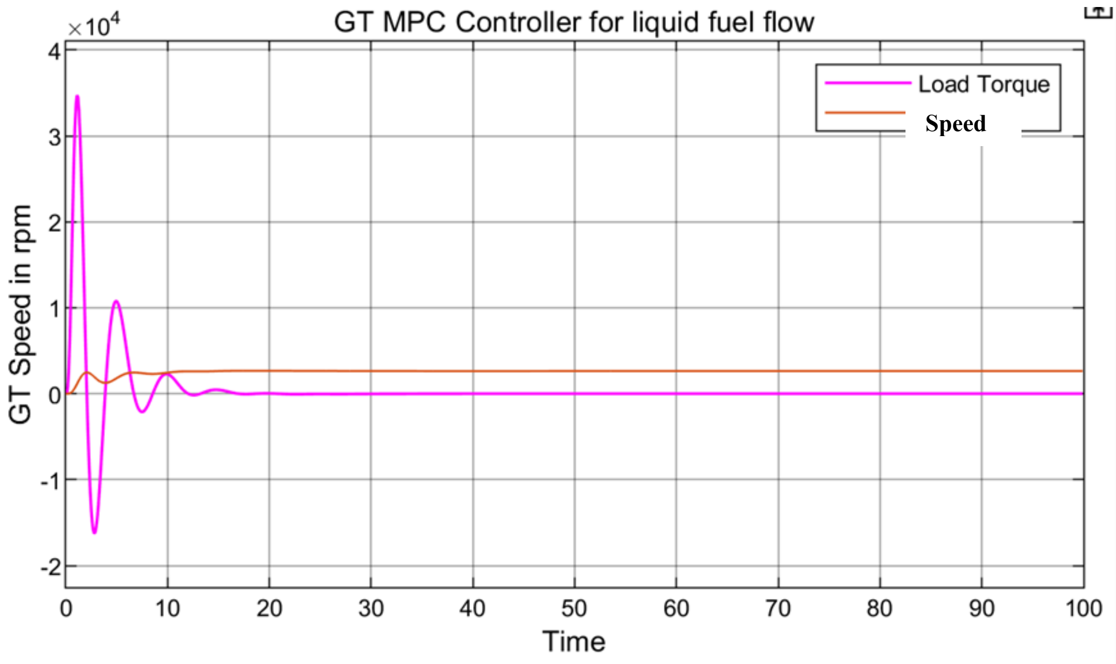

Figure 7.17: Response of GT MPC-PID Controller Dual-Nozzle on (a) Speed, (b) Torque and (c) Combustion discharge

In Figure 7.17, the dual fuel model is validated on the complete GT plant to evaluate the performance. From the response above, it is evident that the torque-speed characteristics showed that, while the torque was initially high, the speed was very low. As the speed increases, the torque reduces to a very low value. However, the combustion chamber fuel flow rate remains constant at 80 bars.

7.14 Result of single and dual nozzle switching operation

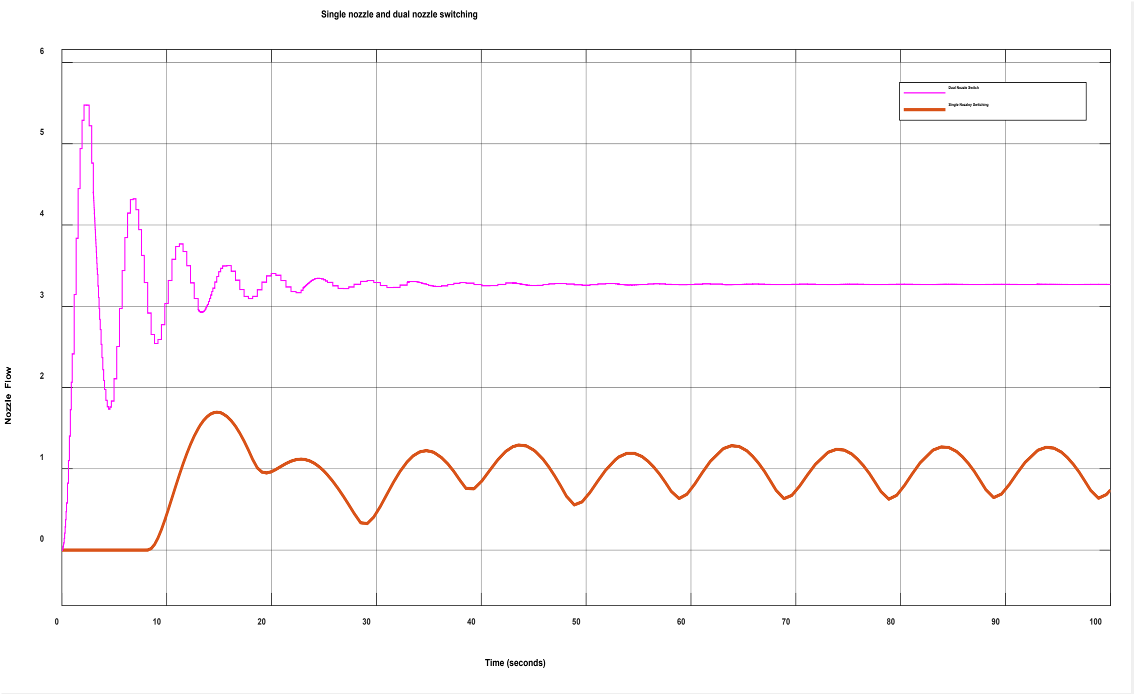

Figure 7.18. Response single and dual nozzle switching operation.

Figure 7.18 compares the fuel switching operation of the traditional single nozzle system and the fuel transaction in the combustion chamber that is performed by the dual nozzle system. In order to keep the power plant from falling into shut down mode, the operation is made more streamlined, quicker, and efficient thanks to the automated switching of fuel supply sources that is performed by twin nozzles. The switching process put the power plant into shutdown when it operated in single nozzle mode. During the first stages of the starter operation, the combustion is subpar due to this process.

CHAPTER EIGHT: CONCLUSION AND FUTURE WORKS

8.1 CONCLUSION

The study discussed three phases of development in gas turbine fuel control scheme modelling for optimal operations. A dual nozzle (hybrid) fuel system model based on Rowen's traditional gas turbine model is developed and proposed. The new model structure provides an improved version of Rowen's model for academic study in multi-layer fuel sources for modern gas turbine industrial operation and control. Under the gas turbine mathematical modelling, the fuel model to include a fuel storage tank system coupled directly to supply the GT fuel line system is considered. Two fuel systems were modelled in the process: liquid fuel (HFO-DFO) and LNG gas fuel were the main considerations in the simulation's mathematical formulation.

Dual nozzle model for liquid and LNG gas flow model was controlled with dual nozzle automatic selector switch developed using conditional statement block in MATLAB/Simulink software. The transition from one fuel to another largely depends on the availability of fuel in individual fuel tanks and the fuel price at the time of the operation. Indeed, gas turbine power plants have demonstrated their remarkable application potential in electrical power generation due to increased energy demand efficiency and low emissions. Significant research efforts have been made into system modelling and developing intelligent control systems for power plants, laying the groundwork for this thesis, which sought to address model accuracy, fuel efficiency, and plant reliability.

To enhance the efficiency and optimal fuel switching in dual-fuel power plants and provide a solid foundation for subsequent and additional research, this thesis developed an improved dual fuel dynamic model whose operational principles were deduced from a single fuel nozzle by extension. Additionally, the MPC-PID combined algorithm compensates for errors and disadvantages each other in performance to improve the model's accuracy. The hybrid fuel model presented in this thesis is a sophisticated dynamic system modelling technique that allows for identifying both model parameters and uncertainties from operational data. The hybrid fuel model's update capability enables it to remain valid even as the dynamics of the actual plant change.

This hybrid modelling technique is effective for dual-fuel power plants, but it can also be applied to most dynamic physical systems, providing a reliable podium for exploring and analysing. Additionally, the thesis developed a framework for model predictive based multi-objective nonlinear optimisation for a dual nozzle GT power plant operating as a base-load power source. Fuel efficiency and availability are the primary concerns for continuous plant operations. The core optimisation algorithm and state estimator were implemented using MPC- PID optimisation algorithms. The optimisation framework presented is a combination and extension of the heuristic optimisation of model predictive technologies. The framework is validated through simulations of the power plant model's dual-fuel logic. It can also be used to solve optimisation problems for power plants of various types of configurations. Meanwhile, when applied to the combined GT plant fuel line, the dual-fuel system exhibits the combined controller algorithm well. The MPC model can correctly identify and forecast a drop in fuel pressure for large-scale power plant systems and effectively prevent the power plant from entering shut-down mode local failures.

Additionally, the integrated system is a prototype for a comprehensive plant-wide control system in which local controllers, optimisers, and plant models operate efficiently. The overall control system is not a simple amalgamation of the individual control systems but a cohesive system in which each component works in concert. The intelligent control system significantly improves the efficiency and reliability of the dual-fuel GT power plant, and the entire control system's performance can be upgraded. Finally, an intelligent autonomous control system was achieved for the hybrid dual nozzle GT power plant, allowing for high-quality plant-wide fuel transition management that ensures fuel flow accuracy, efficiency, and reliability in fuel switching.

8.2 Future works

Future improvements to the intelligent control system may be made by examining the overall control system on a real-world dual nozzle GT power plant and collecting additional operational data for system improvement. If operational pressure data is available, the pressure model's parameters on fuel flow can be refined. Further optimisation analysis will identify the bottleneck in the power plant's path to higher efficiency in the presence of fuel transition during operation. Then, the plant's configuration, structure, or hardware can be optimised to achieve the desired fuel efficiency.

Other critical aspects of the control system that necessitates future investigation includes:

- Interfacing a dual fuel nozzle GT power plant with the utility grid to reduce the impact on power line protection devices and improve their effectiveness at the point of interconnection.
- optimization and control of exhaust temperature in the dual fuel nozzle plant to improve the performance and efficient operation of the physical model.
- Smart combustion used in the dual fuel flow detection in the liquid and gas injection nozzles to balance air to fuel ratio control for better fuel flexibility and the best way to cut down on fuel consumption.
- The incorporation of hydrogen gas into the operation of a dual-fuel GT plant and its impact on dual nozzle injection control
- Fuzzy-based fault detection control in a dual nozzle fuel GT power plant with economic setpoint failure to enhance plant availability and operation.

REFERENCES

1. H. Asgari and X. Q. Chen, Gas Turbine Modelling, Simulation and Control using artificial neural network. Boca Raton: CRC Press, 2016.
2. L. Tsai. Design and Performance of a Gas-Turbine Engine from an Automobile Turbocharger, Thesis (S.B.), Massachusetts Institute of Technology, Dept. of Mechanical Engineering, 2004.
3. G. G. Kulikov and H.A. Thompson, Eds., Dynamic Modelling of Gas Turbines. London: Springer, pp. 336, 2010.
4. J. W. Sawyer, Ed., Sawer's Gas Turbine Engineering Handbook, Gas Turbine Publications, pp. 552, 1966.
5. A. M. Y. Razak, Industrial Gas Turbines: Performance and Operability, First ed., Cambridge, England: Woodhead Publishing Limited, pp. 602. 2007.
6. H. Asgari, X. Q. Chen and R. Sainudiin, "Modelling and Simulation Approaches for Gas Turbine System Optimization," in Engineering Creative Design in Robotics and Mechatronics, Hershey, PA: IGI Global, 2013, pp. 240-264.
7. G. V. Beard and M. R. Rollins, "Engineering Economics," in Power Plant Engineering, V. Black, Ed., Springer Science & Business Media Inc., 1996.
8. R. D. Geertsma, R. R. Negenborn, K. Visser, J. J. Hopman, "Design and Control of Hybrid Power and Propulsion Systems for Smart Ships, A Review of Developments," *Applied Energy,* vol. 194, pp. 30-54, 2017.
9. Duk, "Wikimedia Commons Webpage," 2013. [Online]. Available: http://en.wikipedia.org/wiki/File:Brayton_cycle.svg
10. H. Cohen, G. Rogers and H. Saravanamut, Gas Turbine Theory, 5th ed., Pearson Education, 2001.
11. M. P. Boyce, Gas Turbine Engineering Handbook, 4th ed., Oxford: Butterworth-Heinemann Ltd, ELSEVIER Science & Technology, pp. 1000, 2011.
12. H. Asgari and X. Q. Chen, Senior Member, IEEE, and Raazesh Sainudiin- Considerations in Modelling and Control of Gas Turbines – a Review- ICCIA, 2011.
13. H. Asgari, X. Q. Chen and R. Sainudiin, "Considerations in Modelling and Control of Gas Turbines - A Review," in The 2nd International Conference on Control, Instrumentation, and Automation (ICCIA 2011), Shiraz, Iran, 2011.
14. M. D &. T. Co., THM Gas Turbine Basic Training, Turbo Training catalogues, 2009.

15. L. Ljung and T. Glad, Modelling of Dynamic Systems, Englewood Cliffs, New Jersey: PTR Prentice Hall, Prentice Hall Information and System Sciences Series, pp. 361, 1994.
16. L. C. Saikia, N. Sinha, and J. Nanda, Maiden application of bacterial foraging based fuzzy IDD controller in AGC of a multi-area hydrothermal system, Electric. Power Energy Syst., vol. 45, pp. 98–106, Feb 2013.
17. W. de Paepea, M. M. Carrerro, S. Bram, A. Parente, and F. Contino, Advanced humidified gas turbine cycle concepts applied to micro gas turbine applications for optimal waste heat recovery, Energy Procedia, vol. 105, pp. 1712–1718, May 2017.
18. M. Eslami, M. R. Shayesteh and M. Pourahmadi, Optimal Design of PID-Based Low-Pass Filter for Gas Turbine Using Intelligent Method, IEEE Access March 5, 2018.
19. M. Norgaard, O. Ravn, N. K. Poulsen, and L. K. Hansen, Neural Networks for Modelling and Control of Dynamic Systems: A Practitioner's Handbook, New York: Springer-Verlag Inc., pp. 246, 2003.
20. R. S. Burns, Advanced Control Engineering, Oxford, UK: ButterworthHeinemann Publications, 2001.
21. W. I. Rowen, "Simplified mathematical representations of heavy-due gas turbines," J. Eng. Power, vol. 105, no. 4, pp. 865–869, 1983.
22. L. M. Hajagos and G. R. Berube, "Utility experience with gas turbine testing and modeling," in Proc. IEEE Power Eng. Soc. Winter Meeting, Columbus, OH, USA, Jan, pp. 671–677, 2001.
23. A. Bagnasco, B. Delfino, G. B. Denegri, and S. Massucco, "Management and dynamic performances of combined cycle power plants during parallel and islanding operation," IEEE Trans. Energy Convers., vol. 13, no. 2, pp. 194–201, Jun. 1998.
24. M. Korlu, J. Pirkandi, and A. Maroufi, "Thermodynamic analysis of a gas turbine cycle equipped with a non-ideal adiabatic model for a double acting Stirling engine," *Energy Conver. Manage.,* vol. 147, pp. 120-134, Sep 2017.
25. J. James, D. Spelling, Hybrid Solar Gas-Turbine Power Plants. Doctoral Thesis, KTH Royal Institute of Technology, 10044 Stockholm, Sweden, 2013.
26. F. Giancarlo, G. Eduardo, L. Paolo, S, Matteo, M. Manfred, M. Antoine, Modelling and Control of Cogeneration Power Plants, A Hybrid System Approach, Google Scholar, 2002.

27. R. G. Papagiannakis, C. D. Rakopoulos, D. T. Hountalas, D. C. Rakopoulos, Emission Characteristics of High Speed, Dual Fuel, Compression Ignition Engine Operating in a Wide Range of Natural Gas/Diesel Fuel Proportions, Elsevier Fuel Journal, 2009.
28. B. B. Sahoo, N. Sahoo, U. K. Saha, "Effect of Engine Parameters and Type of Gaseous Fuel on the Performance of Dual-Fuel Gas Diesel Engines," *A Critical Review Renewable and Sustainable Energy Reviews,* vol. 13, pp. 1151-1184, 2009.
29. J. Brouwer, PhD Associate Director; Hybrid Fuel Cell system, National Fuel Cell Research Center University of California, Irvine, CA 92697-3550. www.nfcrc,uci.edu
30. R. P. Merchán, M. J. Santos, I. Reyes-Ramírez, A. Medina, A. Calvo Hernández, "Modelling Hybrid Solar Gas-Turbine Power Plants: Thermodynamic Projection of Annual Performance and Emissions," *Int. J. of Pow. Ene. Conv. and Managt,* vol. 134, pp. 314-326, 2017.
31. B. Grangea, C. Daleta, Q. Falcoza, F. Sirosb, A. Ferrièrea, "Simulation of a Hybrid Solar Gas-Turbine Cycle with Storage Integration," *Science Direct Energy Procedia,* vol. 49, pp. 1147-1156, 2014.
32. M. C. Camerettia, G. Langellaa, S. Sabinoa, R. Tuccilloa, "Modeling of A Hybrid Solar Micro Gas-Turbine Power Plant," *Science Direct Energy Procedia*, vol. 82, pp. 833-840, 2015.
33. A. Yoshimasa, O. Hiroyuki, M. Masahiro, I. Hiroki, U. Yasutaka, I. Takuo, "Demonstration of SOFC-Micro Gas Turbine (MGT) Hybrid Systems for Commercialization". *Mitsubishi Heavy Industries Technical Review*, vol. 52, pp. 4, 2015.
34. Y. Wenli, An Intelligent Control System for a Hybrid Fuel Cell with Gas Turbine Power Plant.
35. Fuel Cell Energy, Inc.. "Thrust Area: Hybrid Fuel Cell/Turbine Power Systems" [online]. Available: http://www.fuelcellenergy.com
36. T. I. Choi and K. Y. Lee, Interface of a Fuel Cell Distributed Generator with Distribution System Network. In Proceedings of the IEEE PES GM, July 26-30, 2009.
37. P. Costamaga, L. Magistri, A. F. Massardo, "Design and Part-load Performance of Hybrid System Based on Solid Oxide Fuel Cell Reactor and Micro Gas Turbine", *Int. J. of Pow. Sou.,* pp. 96, 2000.

38. C. Stefano, "Full Load and Part-Load Performance Prediction for Integrated SOFC and Micro-turbine Systems." *Int. J. of Eng. for Gas Turb. and Pow,* vol. 122, pp. 239, 2000.
39. A. Gaeta, R. Fabrizio, C. Fabio, P. Massoli, "A Dynamic Model of a 100 kW Micro Gas Turbine Fuelled with Natural Gas and Hydrogen Blends and its Application in a Hybrid Energy Grid." *Energy,* 129, pp. 299-320, 2017.
40. K. P. Thipse, S. D. Kavathekar, A. A. Rairikar, N. V. Tyagi, Development of Environment-Friendly Diesel-CNG Dual Fuel Engine for Heavy Duty Vehicle Application, India 2013-26-0015, 2013.
41. B. Ashok, A. S. Denis, K. C. Ramesh, LPG Diesel Dual Fuel Engine – A Critical Review – March 2015.
42. Dual Fuel Engine Gas Fuel Conversion Technology; JFE TECHNICAL REPORT No. 19, Mar. 2014.
43. Performance Prediction and Simulation of Gas Turbine Engine Operation for Aircraft, Marine.
44. J. Peter, Modern Gas Turbine Systems, High Efficiency, Low Emission Fuel Flexibility, Power Generation. Woodhead Publishing Limited, 2013.
45. H. H. Vahab, F. Afef, "Concepción Alicia Monje, Ramin Fakhri Asfestani, H2, H∞, H2/H∞, and μ-synthesis controllers for the speed and temperature control of a real gas turbine unit in a combined cycle power plant", *Energy Sci Eng,* vol. 7, pp. 2205–2222, 2019.
46. Z. M. Qusai, Design Criteria and Performance of Gas Turbines in Combined Power and Power Plant for Electrical Power Generation. Doctor of Philosophy Thesis, University of Hertfordshire, Hertfordshire, AL10 9AB Hatfield, UK, June 2002.
47. B. S. Choi, J. H. Ahn, J. H. Lee and T. S. Kim, "A comparative performance analysis of a solid oxide fuel cell and gas turbine combined cycles with carbon capture technologies," *Journal of Mechanical Science and Technology,* vol. 33, no. 3, pp. 1463-1475, 2019.
48. M. P. Boyce, Gas Turbine Engineering Handbook, 4th edition, Oxford: Butterworth-Heinemann Ltd, ELSEVIER Science & Technology, pp. 1000, 2011.
49. A. Hamid, Modelling, Simulation, and Control of Gas Turbines Using Artificial Neural Networks, Thesis Doctor of Philosophy in Mechanical Engineering, University of Canterbury, Christchurch, New Zealand, 2014.

50. S. Y. Munzer, A. Al-Fahoumb, “Design of Fuel Control System Using Fuzzy Logic for a Pre-Designed Radial Gas Turbine Driving Directly High-Speed Permanent Magnet Alternator”. *Int. J. of Mod. and Sim.*, vol. 36, no. 4, pp. 145-161, 2016.
51. S. K. Jong, M. P. Kody, T. F. Edgar, Nonlinear Model Predictive Control for a Heavy-Duty Gas Turbine. American Control Conference (ACC) Washington, DC, USA, June 17-19, 2013.
52. A. Bonfiglio, Member, IEEE, S. Cacciacarne, M. Invernizzi, D. Lanzarotto, Student Member, IEEE, A. Palmieri, Student Member, IEEE, R. Procopio Senior Member, IEEEA; Sliding Mode Control Approach for Gas Turbine Power Generators. IEEE DOI 10.1109/TEC.2018.2879688
53. Ghazal, G and Hamid, K, “Modelling and Control of a Single Shaft Heavy Duty Industrial Gas Turbine Based on Operational Data,” *Int. J. on Cont. Sys. and App. (IJCS)*, vol. 1, pp. 1, 2014.
54. R. Alessandro, P. Alessandro, L. Damiano, P. Renato, B. Andrea, B, A Model Predictive Control Design for Power Generation Heavy-Duty Gas Turbines. Article of Energies, June 2019.
55. H. Naimul, N. R. Jitendra, B. A. Bharat, Optimization of the CCGT Power Plant and Performance Analysis Using MATLAB/Simulink With Actual Operational Data; Springer Plus, 2014.
56. A. K. Ghazi, Dual-Fuel Diesel Engines-CRC Press, 2015.
57. GE Powering the World 2016 edition; www.gepower.com
58. H. Zheng, G. Pan, X. Chen and X. Hu, “Effect of Dual Fuel Nozzle Structures on Combustion Flow Field in CRGT Combustor Hindawi Publishing Corporation,” *Mathematical Problems in Engineering*, pp. 11, 2013.
59. C. O. Iyogun, M. Birouk and J. A. Kozinski, “Experimental investigation of the effect of fuel nozzle geometry on the stability of a swirling non-premixed methane flame,” *Fuel,* vol. 90, no. 4, pp. 1416–1423, 2011.
60. T. Terasaki and S. Hayashi, “The effects of fuel-air mixing on NOx formation in non-premixed swirl burners,” in Proceedings of the 26th Symposium International on Combustion, pp. 2733–2739, The Combustion Institute, 1996.
61. H. S. Zhen, Y. S. Choy, C.W. Leung, and C. S. Cheung, “Effectsof nozzle length on flame and emission behaviours ofmulti-fuel-jet inverse diffusion flame burner,” *Applied Energy,* vol. 88, no. 9, pp. 2917 2924, 2011.

62. M. C. Lee and Y. Yoon, "Development of a gas turbine fuel nozzle for DME and a design method thereof," *Fuel,* vol. 102, pp. 823–830, 2012.
63. H. B. Li, H. S. Zhen, C. W. Leung, and C. S. Cheung, "Nozzle effect on heat transfer and CO emission of impinging premixed flames," *International Journal of Heat and Mass Transfer,* vol. 54, no. 1–3, pp. 625–635, 2011
64. M. S. Mansour, A. M. Elbaz, and M. Samy, "The stabilization mechanism of highly stabilized partially premixed flames in a concentric flow conical nozzle burner," *Experimental Thermal and Fluid Science,* vol. 43, pp. 55–62, 2012.
65. M. Koyama and S. Tachibana, "Technical applicability of lowswirl fuel nozzle for liquid-fueled industrial gas turbine combustor," *Fuel,* vol. 107, pp. 766–776, 2013.
66. E. H. Chui, A. J. Majeski, M. A. Douglas, Y. Tan, and K.V. Thambimuthu, "Numerical investigation of oxy-coal combustion to evaluate burner and combustor design concepts," *Energy,* vol. 29, no. 9-10, pp. 1285-1296, 2004.
67. M. Koyama and H. Fujiwara, "Development of a dual-fuel gas turbine engine of liquid and low-calorific gas," *JSME International Journal B*, vol. 49, no. 2, pp. 224-229, 2006.
68. K. A. Al-attab and Z. A. Zainal, "Design and performance of a pressurized cyclone combustor (PCC) for high and low heating value gas combustion," *Applied Energy,* vol. 88, no. 4, pp. 1084–1095, 2011.
69. V. K. Arghode and A. K. Gupta, "Development of high intensity CDC combustor for gas turbine engines," *Applied Energy,* vol. 88, no. 3, pp. 963-973, 2011.
70. F. Xing, P. Wang, S. Zhang et al., "Experiment and simulation study on lean blow-out of trapped vortex combustor with various aspect ratios," *Aerospace Science and Technology,* vol. 18, no. 1, pp. 48-55, 2012.
71. I. Aslan Res¸itog˘lu, K. Altinis, A. Keskin, "The pollutant emissions from diesel-engine vehicles and exhaust after treatment systems," *Clean Techn Environ Policy,* pp: 15-27, 2015.
72. J. Mu, D. Rees, Approximate Model Predictive Control for Gas Turbine Engines, Proceedings of the 2004 American Control Conference Boston, Massachusetts, 5704-5709, 2004.
73. F. Kulor, E. Markus and W. M. Apprey, "MPC-PID Control of a Gas-Liquid Cylindrical Cyclone", *International Journal of Mechanical and Robotics Research,* vol. 8, July 2019.

74. D. S. Ewens, J. R. Huey, System and Method for Gas Turbine Operation. US 2014/01565A1 – 2014.
75. B. P. Numbi, X. Xia, "Systems Optimization Model for Energy Management of a Parallel HPGR Crushing Process". *Science Direct Applied Energy*, vol. 149, pp. 133–147, 2015.
76. C. Stiller, B. Thorud, O. Bolland, R. Kandepu, I. Imland, "Control Strategy for a Solid Oxide Fuel Cell and Gas Turbine Hybrid System", *J. of Pow. Sou.*, vol. 158, pp. 303-315, 2006.
77. C. Stiller, B. Thorud, S. Seljebo, Q. Mathisen, H. Karoliussen, O. Boland, "Finite-Volume Modeling and Hybrid-Cycle Performance of Planar and Tubular Solid Fuel Cell", *J. of Pow. Sou.*, vol. 141, pp. 227-240, 2005.
78. D. Rao, G. S. Samuelsen, A Thermodynamic Analysis of Tubular SOFC Based Hybrid Systems, ASME paper 2001-GT-2522.
79. S. H. Chan, H. K. Ho, Y. Tian, "Modeling for the Part-load Operation of Solid Oxide Fuel Cell-Gas Turbine Hybrid Power Plant," *J. of Pow. Sou.*, vol. 114, no. 9, pp. 213-22, 2003.
80. P. Palsson, A, Selimovic, L, Sjunnesson, "Combined Solid Oxide Fuel Cell and Gas Turbine System for Efficient Power and Heat Generation," *J. of Pow. Sou.*, vol. 86, pp. 442-448, 2000.
81. S. E. Veyo, W. L. Lundberg, S. D. Vora, K. P. Litzinger, Tubular SOFC Hybrid Power System Status, ASME paper 2003 - GT-38943.
82. S, Campanari, "Full load And Part Load Performance Predictions for a Combine SOFC and Micro-Turbine Systems," *J. of Ener. Gas Turb. Pow.* Vol. 122, pp. 239-246, 2000.
83. B. Prabodh, D. Vaishalee, "Hybrid Renewable Energy Systems for Power Generation in Stand-Alone Applications: A review", *Renewable and Sustainable Energy Reviews*, vol. 16, pp. 2926-2939, 2012.
84. Y. Liu, X. Sun, V. Sethi, D. Nalianda, Y. Li, L. Wang, "Review of modern low emissions combustion technologies for aero gas turbine engines" – Elsevier, *Science Direct*, pp: 1-34, 2017.
85. O. Mohamed and A. Khalil, "Progress in Modeling and Control of Gas Turbine Power Generation Systems: A Survey." *Energies* vol. 13, pp. 2358, 2020.

86. O. Mohamed, M. E. Za'te, "Comparative Study Between Three Modeling Approaches for a Gas Turbine Power Generation System", *Arabian Journal for Science and Engineering*, pp. 369-019-04274, 2019.
87. F. Kulor, Advanced Control System for Offshore Oil Production Platforms, University of Strathclyde UK, September, 2011.
88. M. Reza, "Bank Tavakoli, Behrooz Vahidi, Wolfgang Gawlik: An Educational Guid to Extract the Paramters of Heavy-Duty Gas Turbines Model in Dynamic Studies Based on Operational Data." *IEEE Transactions on Power System,* vol. 24, no. 3, August 2009.
89. G. J. Van Wylen, R. E. Sonntag, and C. Borgnakke, Fundamentals of Classical Thermodynamics, 4th ed. New York: Wiley, 1998.
90. J. V. Nicholas and D. R. White, Traceable Temperatures, 2nd ed. New York: Wiley, 2001.
91. P. P. Walsh and P. Fletcher, Gas Turbine Performance, 2nd ed. Oxford, U.K.: Blackwell Science, 2004.
92. R. D. Strunk, The Dynamics of Pump-Line-Nozzle Fuel Injection Systems; Dept. of Mechanical Engrg, University of Wisconsin-Platteville Platteville, WI sept. 1991.
93. V. Aesoy, E. Pedersen. Modelling and Simulation for Design and testing of Direct Injection Gaseous Fuel Systems for Medium Speed Engines, SAE International 20211.
94. B. E. Romig, R. D. Strunk and M. S. Weinert, Performance Comparison of Unit Injector and Pump-Line-Nozzle Systems, SAE Paper 840274,1984
95. N. Ahmad, M. K. G. Babu, A. Ramesh. Experimental Investigations of Different Parameters Affecting the Performance of a CNG – Diesel Dual Fuel Engine. SAE 2005-01-3767, 2005.
96. W. Chatlatanagulchai, S. Rhienprayoon, K. Yaovaja, K. Wannatong, Air/Fuel Ratio Control in Diesel-Dual-Fuel Engine by Varying Throttle, EGR Valve, and Total Fuel. SAE 2010-01-2200, 2010.
97. Y. J. R da Costa, A. G. B. de Lima, C. R. B. Filho, L. D. A. Lima, "Energetic and exergetic analyses of a dual-fuel diesel engine," *Renew. Sustain. Energy Rev.* vol. 16, pp. 4651–4660, 2012.

98. A. Pal, A. Tiwari, “An investigation of the combustion and emission characteristics of compression ignition engines in dual-fuel mode,” *Int. J. Adv. Res. Innovation,* vol. 3, pp. 98–106, 2013.

99. L. Goldsworthy, “Combustion behavior of a heavy-duty common rail marine diesel engine fumigated with propane,” *Exp. Thermal Fluid Sci.*, vol. 42, pp. 93–106, 2012.

100. A. T. Ergenc, D. Koca, “PLC controlled single cylinder diesel– LPG engine,” Fuel*,* pp. 273–278, 2014.

101. R. Sproat, A. M. Hassan, A. Waldie, G. Jay, D. Holland, The Risk Posed to Vehicle Occupants and Rescue Personnel by Dual-Fuelled Vehicles Fitted with Liquid Petroleum Gas (LPG) Tanks. SAE 2006-01-1274, 2006.

102. B. J. Bora, B. K. Debnath, N. Gupta, U. K. Saha, N. Sahoo, “Investigation on the flow behavior of a venturi type gas mixer designed for dual fuel diesel engines,” *Int. J. Emerging Technol. Adv. Eng.* Vol. 3, no. 3, 2013.

103. G. A. Rao, A. V. S. Raju, K. G. Rajulu, C.V. M Rao, “Performance evaluation of a dual fuel engine (diesel+LPG),” *Indian J. Sci. Technol.* vol. 3, no. 3, 2010.

104. A. Paykani, R. K. Saray, A. M. Kousha, M. T. S. Tabar, “Performance and emission characteristics of dual fuel engines at part loads using simultaneous effect of exhaust gas recirculation and preheating of inlet air,” *Int. J. Automotive Eng.*, vol. 1, no. 2, 2012.

105. C. J. T. Renald, P. Somasundaram, V. Sateeshkumar, Investigation of LPG Induction Jet Angle with Injector Nozzle Angle in a Dual Fuel Diesel Engine Using CFD Technique. 2009-28-0040, 2009.

106. D. Jian, G. Xiaohong, L. Gesheng, Z. Xintang, Study on Diesel–LPG Dual Fuel Engines. SAE 2001-01-3679, 2001.

107. K. Murthy, N. Madhwesh, B. R. ShrinivasaRao, “Influence of injection timing on the performance of dual fuel compression ignition engine with exhaust gas recirculation,” *Int. J. Eng. Res. Dev.*, vol. 1, no. 11 pp. 37–42, 2012.

108. S. Kaleemuddin, G. A. Rao, Study on Single Cylinder Engine for Performance and Exhaust Emission with Diesel, Bio Diesel, LPG and CNG. SAE 2009-32-0048, 2009.

109. M. Selim, S. Al-Omari, A. Al-Aseery, "Effects of Steam Injection to Dual Fuel Engine on Performance, Noise and Exhaust Emission," [online] SAE Technical Paper 2009-01-1831, 2009, Available: https://doi.org/10.4271/2009-01-1831

110. H. S. Tira, J. M. Herreros, A. Tsolakis, M. L. Wyszynski, "Characteristics of LPG–diesel dual fuelled engine operated with rapeseed methyl ester and gas-to-liquid diesel fuels," *Energy,* vol. 47, pp. 620–629, 2012.

111. S. Ganesan, A. Ramesh, Investigation on the use of Water– Diesel Emulsion in a LPG–Diesel Dual Fuel Engine. SAE 2001-28-0032, 2001.

112. P. Vijayabalan, G. Nagarajan, "Emission and combustion Vijaya Balan of LPG diesel dual fuel engine using glow plug," *Jordan J. Mech. Ind. Eng.*, vol. 3, no. 2, pp. 105–110, 2009.

113. K. Wattanavichien, Visualization of LPG-PME Dual Fuel Combustion in an IDI CI Engine. The Second TSME International Conference on Mechanical Engineering, 2011.

114. G. A. Rao, A. V. S. Raju, C. V. M. Rao, K. G. Rajulu, "Effect of LPG content on the performance and emissions of a diesel– LPG dual-fuel engine," *Bangladesh, J. Sci. Ind. Res.,* Vol. 46, no. 2, pp. 195–200, 2011.

115. C. A. J. Leermakers, B. Van den Berge, C. C. M. Luijten, L. P. H. de Goey, S. Jaasma. Direct Injection of Diesel-Butane Blends in a Heavy-Duty Engine. SAE 2011-01-2400, 2011.

116. J. Stewart, A. Clarke, R. Chen, "An experimental study of the dual-fuel performance of a small compression ignition diesel engine operating with three gaseous fuels", *J. Automobile Eng.,* Part: D 221, 2007.

117. L. Raslavicius, A. Kersys, S. Mockus, N. Kersiene, M. Starevicius, Liquefied petroleum gas (LPG) as a medium-term option in the transition to sustainable fuels and transport, *Renew. Sustain. Energy Rev.*, vol.32, 513–525, 2014.

118. K. Wattanavichien, Spray and combustion visualization of LPG-PME dual fuelling an IDI compression ignition engine. 3rd Regional Conference on Mechanical and Aerospace Technology, 2011.

119. C. Arapatsakos, A. Karkanis, G. Katirtzoglou, I. Pantokratoras, Liquid Petroleum Gas (LPG) and Natural Gas (NG) as fuels on Diesel engine–Dual fuel engine. Recent Advances in Fluid Mechanics and Heat & Mass Transfer. ISBN: 978-1-61804-183-8.

120. S. Luft, A. Michalczewski, Analysis of Choosen Parameters of Dual Fuel CI Engine Fuelled with Propane- Butane Gas as a Main Fuel. SAE 2002-01-2234, 2002.

121. M. P. Poonia, A. Ramesh, R. R. Gaur, Experimental Investigation of the Factors Affecting the Performance of a LPG – Diesel Dual Fuel Engine. SAE 1999-01-1123, 1999.

122. C. V. Sudhir, V. Desai, S. Y. Kumar, P. Mohanan, Performance and Emission Studies on the effect of Injection Timing and Diesel Replacement on a 4-S LPG–Diesel Dual-Fuel Engine. SAE 2003-01-3087, 2003.

123. Y. E. M. Selim, "Sensitivity of dual fuel engine combustion and knocking limits to gaseous fuel composition," *Energy Convers. Manage.* Vol. 45, pp. 411–425, 2004.

124. H. Ogawa, N. Miyamoto, C. Li, S. Nakazawa, K. Akao, Low Emission and Knock-Free Combustion with Rich and Lean Biform Mixture in a Dual- Fuel CI Engine with Induced LPG as the Main Fuel Low Emission and Knock-Free Combustion with Rich and Lean Biform Mixture in a Dual-Fuel CI Engine with Induced LPG as the Main Fuel. SAE 2001-01-3502, 2001.

125. A. C. Polk, C. D. Carpenter, Kalyan Kumar Srinivasan, Sundar Rajan Krishnan, "An investigation of diesel–ignited propane dual fuel combustion in a heavy-duty diesel engine", *Fuel,* vol. 132, pp. 135–148, 2014.

126. Polk, Andrew C., Chad D. Carpenter, E. Scott Guerry, U. Dwivedi, Kalyan Kumar Srinivasan, Sundar Rajan Krishnan, and Zach L. Rowland. "Diesel-ignited propane dual fuel low temperature combustion in a heavy-duty diesel engine." Journal of Engineering for Gas Turbines and Power 136, no. 9, 2014.

127. A. Bilcan, O. Le Corre, M. Tazerout, A. Ramesh, S. Ganesan. Characterization of the LPG – Diesel Dual Fuel Combustion. SAE 2001-28-0036, 2000.

128. D. Xue, Y. Chen and D. P Atherton, Linear Feedback Control Analysis and Design with MATLAB ISBN 978-0-878716-38-2.

129. K. Astrom and T. Hagglund, PID Controller design and Tuning, 2nd Edition ISBN 1-55617-516-7.

130. K. Ogata, Moden Control Engineering Fouth Edition-ISBN 0-13-043245-8

131. J. Michael. Grimble: University of Strathclyde Glasgow UK. Industrial control system design-ISBN 9780471492252: ISBN 0471472256.

132. S. Shhiu and S. Hwang, "Sequential Design Method for Multivariable Decoupling and Multiloop PID controllers." *Chem.Res.* vol. 37, pp. 107-119, 1998.

133. A. P. Loh, C. C. Hang, C. K. Quek, and V. U. Vasnani. "Autotuning of Multiloop Proportional-Integra1 Controllers Using Relay Feedback Chem." *Res.*, vol. 32, pp. 1102-1107, 1993.

134. K. J. Astrom, T. Hagglund, "Automatic tuning of simple regulators with specification on phase and amplitude margin," *Automatica*, pp. 645–651, 1988.

135. K. J. Astrom, T. Hagglund, PID Controller, 2nd ed., Instrument of Society of America, Research Triangle Park, NC, 1995.

136. C. Scali, G. Marchetti, D. Semini, "Relay and additional delay for identification and autotuning of completely unknown processes," *Ind. Eng. Chem. Res.*, vol. 1, no. 38, pp. 1987–1997, 1999.

137. J. J. Di Stefano, A. R. Stubberud, I. J. Williams, Feedback and Control Systems, McGraw-Hill, New York, 1975.

138. G. Marchetti, C. Scali, D. R. Lewin, Identification and control of open-loop unstable processes by relay methods. Automatica, 2001.

139. MPC controller Chemical Engineering Department King Sand University, 2002.

140. R, Fischer, Downstream pressure control: Calculation of the transfer function and optimization of control parameters leading to a new controller design.VAT AG, 9469 Haag, Switzerland.

141. Prof Mike Grimble and Dr. Hong Yue: EE905 Lecture Note Control of Industrial Processes. University of Strathcylde Glasgow UK-Scotland

142. E. F. Camacho and C. Bordons, Model Predictive Control in the Process Industry-Advances in Industrial Control Springer ISBN 3-540-19924-1.

143. A. V. Okpanachi, Developing Advanced Strategies for a 4-Tank Laboratory Process. Master's Thesis 2010 Telemark University College of technology.

144. P. S. A. Cristea, and A. Imre-Lucaci, Model Based Control

145. A. Oliveri, M. Lodi, M. Storace, High-speed explicit nonlinear model predictive control. In Proceedings of the 2017 European Conference on Circuit Theory and Design (ECCTD), Catania, Italy, 4–6 September 2017, pp. 1–4.

APPENDIX A

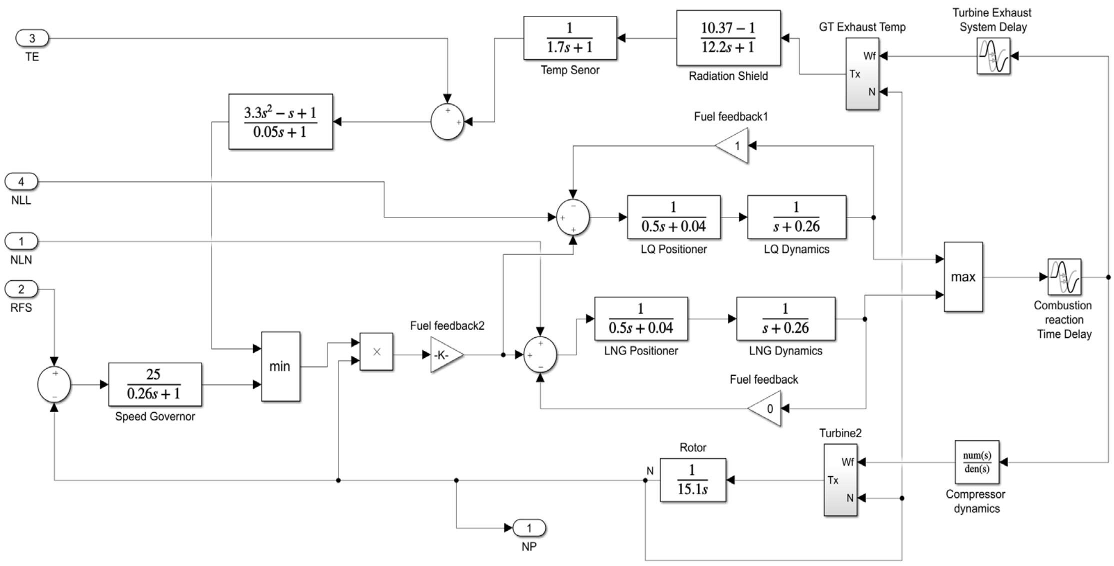

Figure A3.26: GT NLG-NLL Dual fuel simulation block diagram without controller

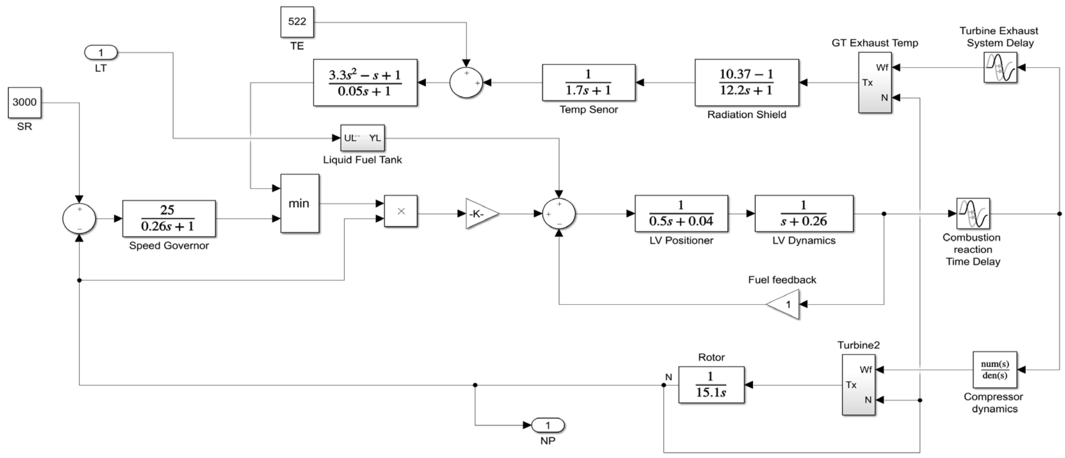

Figure A3.27: Dynamic simulation of integrated liquid-liquid fuel line without controller

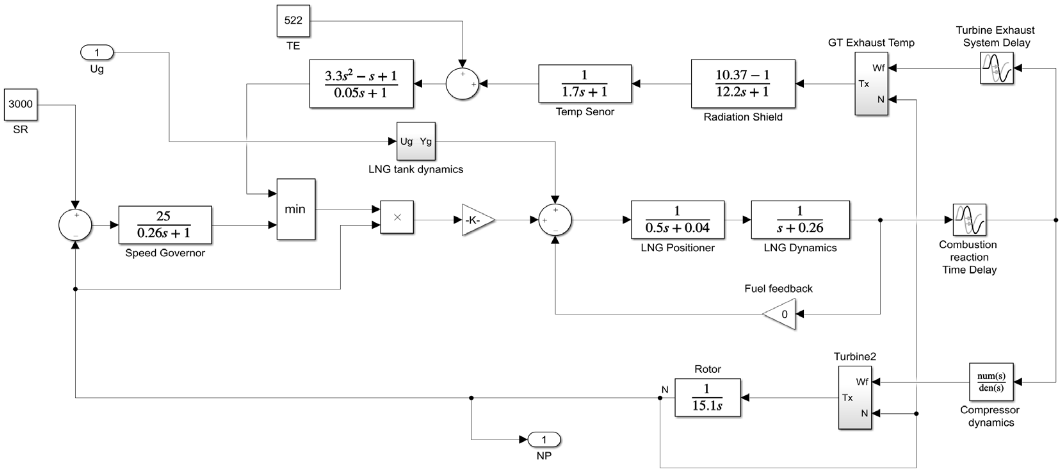

Figure A3.28: Dynamic simulation of integrated LNG – LNG line without controller

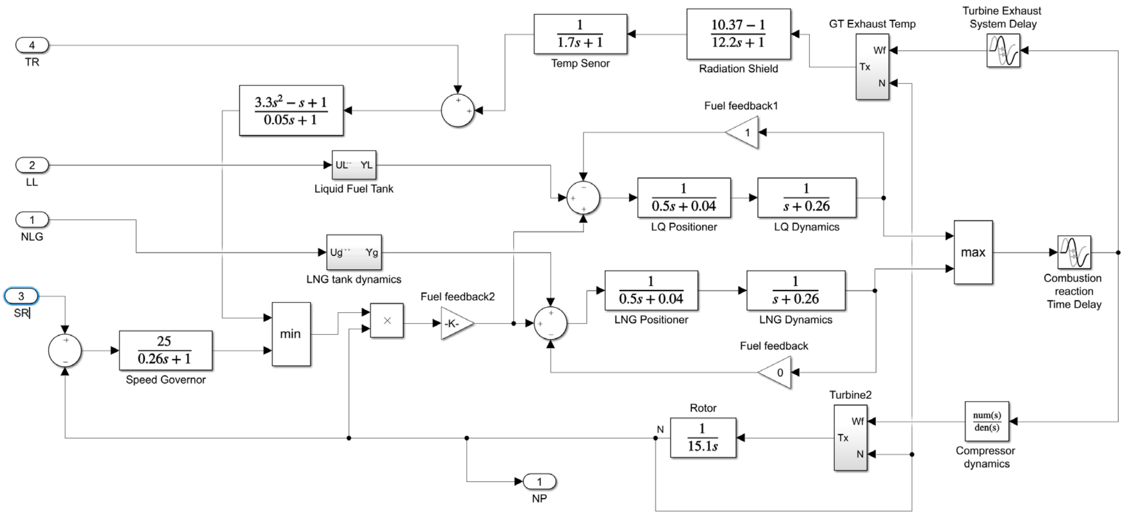

Figure A3.29: Dynamic simulation of integrated synchronized GT LNG – LNG line without controller

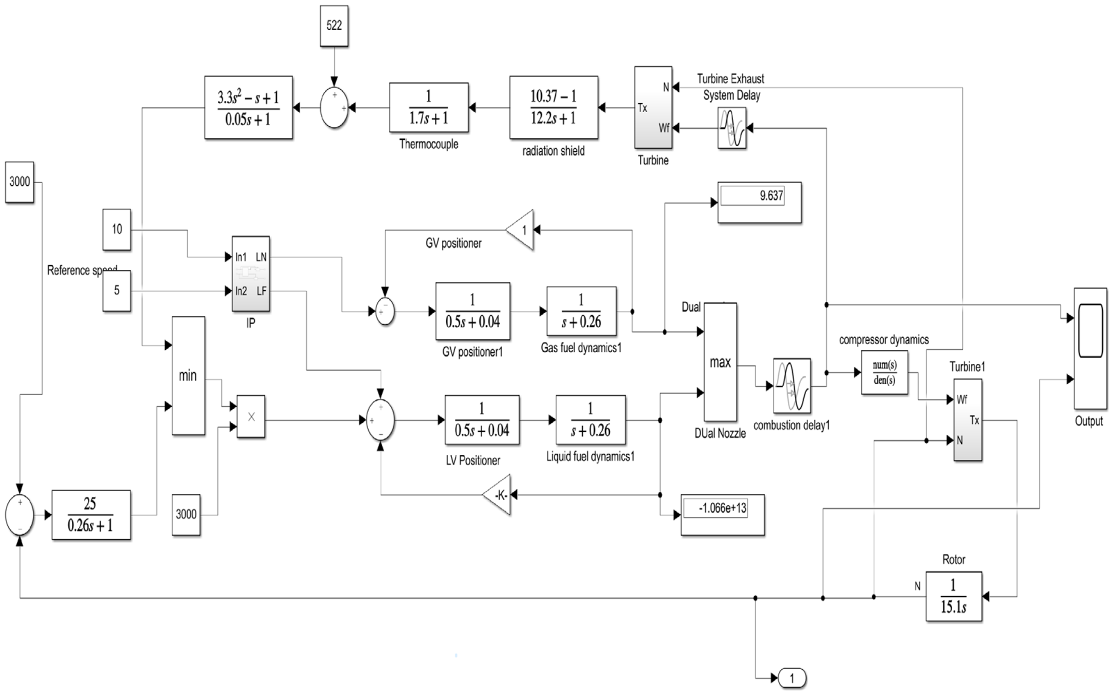

Figure A4.10: Simulink block diagram of integrated dual nozzle GT fuel Control

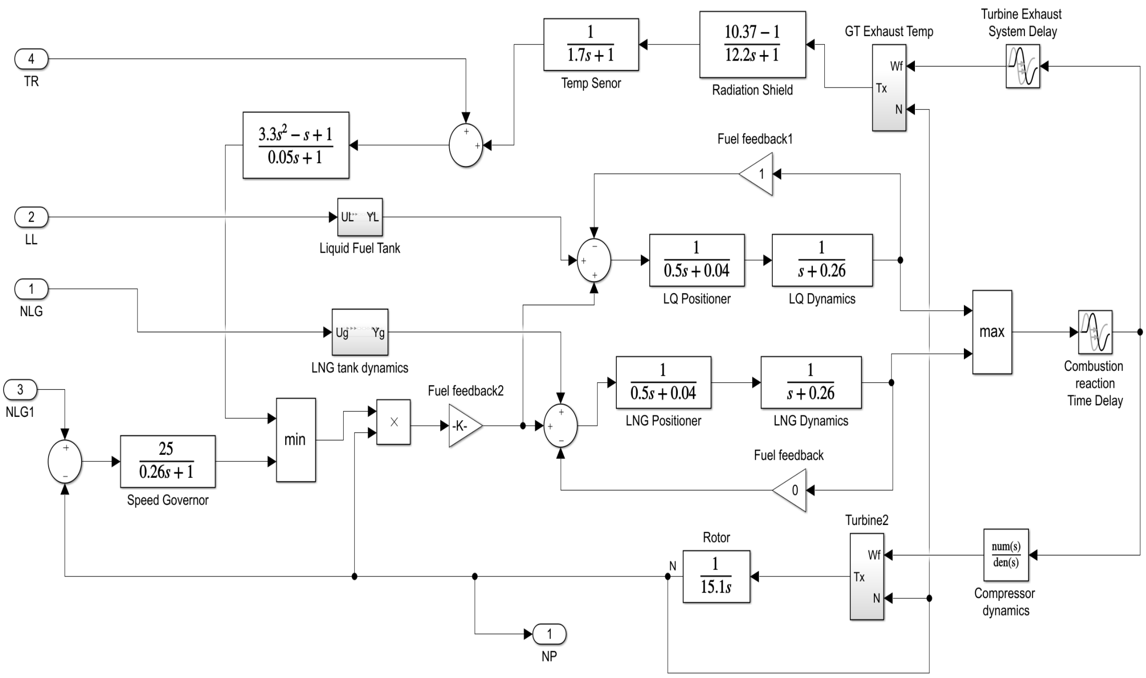

Figure A 5.9: Modify GT model with dual fuel arrangement

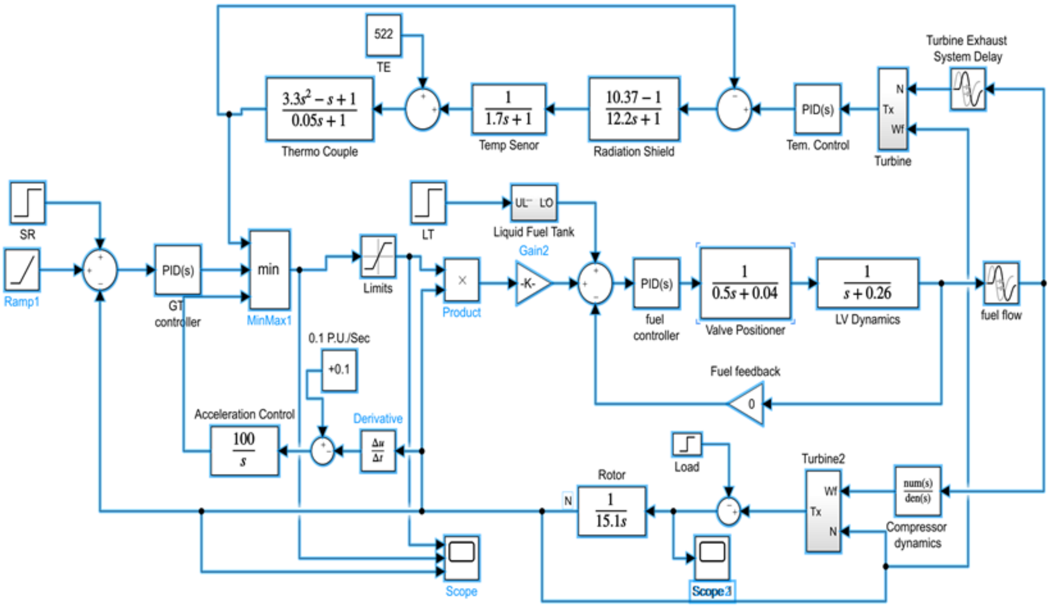

Figure A 5.10: GT Simulink model with Liquid fuel system without PID controller

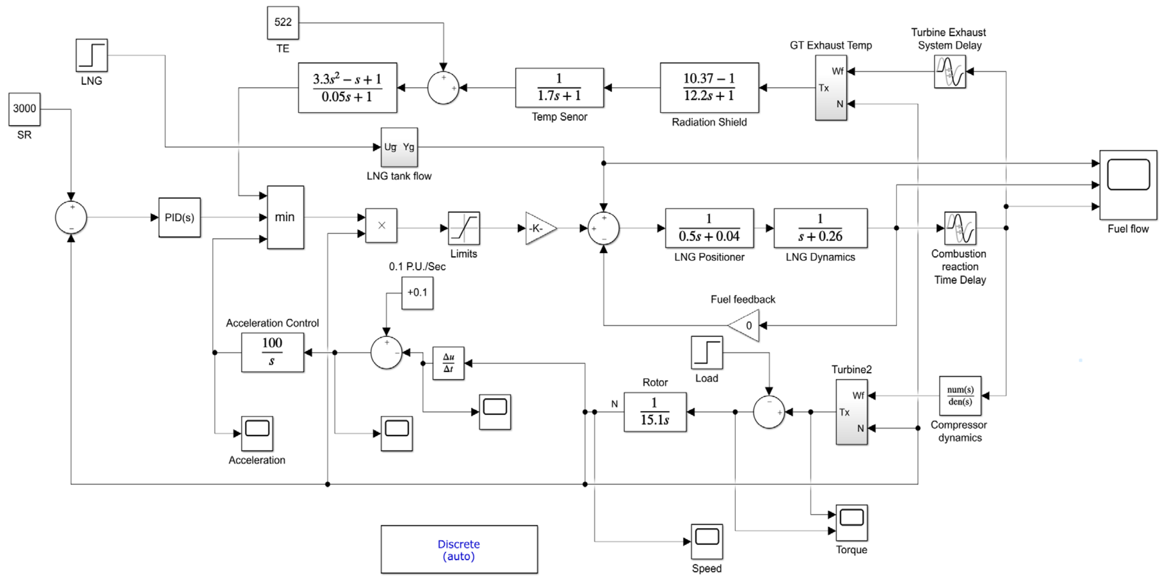

Figure A5.11: GT Simulink model with LNG fuel system with PID controller

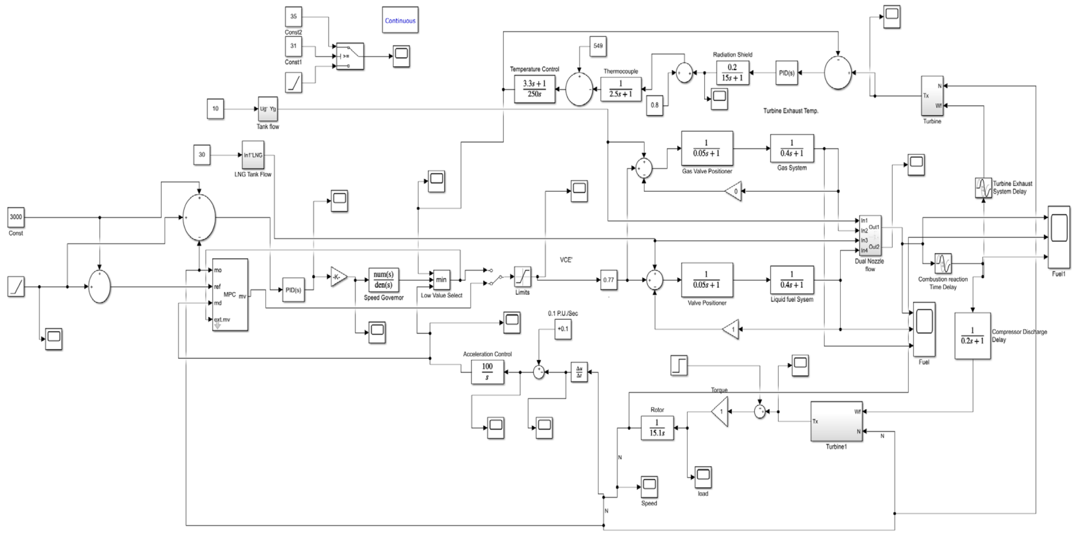

Figure A6.10: MPC -PID block diagram for complete GT system fuel control

APPENDIX B: EDITING CERTIFICATE

NERESHNEE GOVENDER COMMUNICATIONS (PTY) LTD

REGISTRATION NUMBER: 2016/369223/07
DR NERESHNEE GOVENDER (PhD)
neresh@ngcommunications.co.za
0847022553
WRITING PRACTITIONER • EDITOR • COPYWRITER • TRAINER

PhD-Management Sciences: Marketing (gender and media); *PG DIP - Higher Education - Academic Developers (Cum laude;)* M-Tech Public Relations; B-Tech Public Relations *(Cum laude);* B-Tech Journalism *(Cum laude); N-Dip Journalism*

25/04/2022

FRANK KULOR
Central University of Technology
Free State
Bloemfontein

RE: EDITING CERTIFICATE

FOCUS AREA: OPTIMAL OPERATION AND CONTROL FOR A HYBRID HFO-DLCO GAS TURBINE POWER GENERATING PLANT

Thesis submitted in fulfilment of the requirements for the degree Doctor of Engineering in Electrical Engineering in the Department of Electrical, Electronic and Computer Engineering, Faculty of Engineering, Built Environment and Information Technology.

This serves to confirm that this research has been edited for clarity, language and layout.

Kind regards,

Nereshnee Govender (PhD)